Thesis for the Degree of Doctor of Philosophy

Cooperative Diversity Techniques for High-Throughput Wireless Relay Networks

Quoc-Tuan Vien

School of Engineering and Built Environment

Glasgow Caledonian University

United Kingdom

July 2012

Declaration

Name of the student: Quoc-Tuan Vien

Name of degree applied for: Doctor of Philosophy

Title of dissertation: Cooperative Diversity Techniques for High-Throughput Wireless Relay Networks

I declare that I have fully understood the research policies and regulation. The work submitted is my own and expressed in my own words. Any work used by any other author(s) in any form has been properly acknowledged. A list of all the references used has also been included. This work has not already been submitted for any degree and is not being submitted concurrently for any degree.

Name: Quoc-Tuan Vien

Signed: 

Date: 30-July-2012

Abstract

Relay communications has attracted a growing interest in wireless communications with application to various enhanced technologies. This thesis considers a number of issues related to data throughput in various wireless relay network models. Particularly, new implementations of network coding (NC) and space-time coding (STC) techniques are investigated to offer various means of achieving high-throughput relay communications.

Firstly, this thesis investigates different practical automatic repeat request (ARQ) retransmission protocols based on NC for two-way wireless relay networks to improve throughput efficiency. Two improved NC-based ARQ schemes are designed based on go-back-N and selective-repeat (SR) protocols. Addressing ARQ issues in multisource multidestination relay networks, a new NC-based ARQ protocol is proposed and two packet-combination algorithms are developed for retransmissions at relay and sources to significantly improve the throughput.

In relation to the concept of channel quality indicator (CQI) reporting in two-way relay networks, two new efficient CQI reporting schemes are designed based on NC to improve the system throughput by allowing two terminals to simultaneously estimate the CQI of the distant terminal-relay link without incurring additional overhead. The transmission time for CQI feedback at the relays is reduced by half while the increase in complexity and the loss of performance are shown to be negligible. Furthermore, a low-complexity relay selection scheme is suggested to reduce the relay searching complexity.

For the acknowledgment (ACK) process, this thesis proposes a new block ACK scheme based on NC to significantly reduce the ACK overheads and

therefore produce an enhanced throughput. The proposed scheme is also shown to improve the reliability of block ACK transmission and reduce the number of data retransmissions for a higher system throughput. Additionally, this thesis presents a new cooperative retransmission scheme based on relay cooperation and NC to considerably reduce the number of retransmission packets and improve the reliability of retransmissions for a more power efficient and higher throughput system with non-overlapped retransmissions. Moreover, two relay selection schemes are recommended to determine the optimised number of relays for the retransmission.

Finally, with respect to cognitive wireless relay networks (CWRNs), this thesis proposes a new cooperative spectrum sensing (CSS) scheme to improve the spectrum sensing performance and design a new CSS scheme based on NC for three-hop CWRNs to improve system throughput. Furthermore, a new distributed space-time-frequency block code (DSTFBC) is designed for a two-hop nonregenerative CWRN over frequency-selective fading channels. The proposed DSTFBC design achieves higher data rate, spatial diversity gain, and decoupling detection of data blocks at all destination nodes with a low-complexity receiver structure.

Acknowledgements

This dissertation work is dedicated to my family and my friends.

First of all, I would like to express my special thanks to my advisors, Prof. Brian G. Stewart, Prof. Huaglory Tianfield, Dr. Huan Xuan Nguyen, and Prof. Jinho Choi, for their invaluable guidance, advice, and encouragement throughout my research. I have been lucky to work with them over the period of the PhD degree. Their kindly willingness in providing technical support and feedback were most important for the completion of this research. A kindly thanks goes to Prof. Een-Kee Hong, Dr. Le-Nam Tran, and Mr. Nguyen-Vu Le, who recommended me to continue my research in Glasgow Caledonian University. I am also profoundly grateful to Glasgow Caledonian University for funding my research.

I wish to acknowledge my school department for assisting me to conduct my research. A warm appreciation is given to all my colleagues for providing a friendly research environment and for helping me in daily life in Glasgow.

I wish to express my deep gratitude to my family, my parents Tung and Ngoc, my mother-in-law Lien, my aunt Xuan, and my uncle Dung for their permanent and unconditional love and encouragement. Thinking back, it must have been a difficult decision for my parents to allow their only son to study in a Western country which is quite far from home.

Last but certainly not least, I wish to thank my lovely wife Bich Tram and my cute daughter Gia Han for their endless love, patience, and understanding. They have always been my best cheerleaders throughout this PhD journey.

Quoc-Tuan Vien

Glasgow, July 2012

Publication List

Journals

1. Quoc-Tuan Vien, Brian G. Stewart, Huaglory Tianfield, and Huan X. Nguyen, "Efficient cooperative spectrum sensing for three-hop cognitive wireless relay networks," to appear in *IET Communications*, Nov. 2012.

2. Quoc-Tuan Vien, Brian G. Stewart, Huaglory Tianfield, and Huan X. Nguyen, "Cooperative retransmission for wireless regenerative multirelay networks," *IEEE Transactions on Vehicular Technology*, Oct. 2012, DOI 10.1109/TVT.2012.2224393.

3. Quoc-Tuan Vien, Huan X. Nguyen, Jinho Choi, Brian G. Stewart, and Huaglory Tianfield, "Network coding-based block acknowledgement scheme for wireless regenerative relay networks," *IET Communications*, Sep. 2012, DOI 10.1049/iet-com.2011.0681.

4. Quoc-Tuan Vien, Brian G. Stewart, Huaglory Tianfield, Huan X. Nguyen, and Jinho Choi, "An efficient network coded ARQ for multisource multidestination relay networks over mixed flat fading channels," *Elsevier AEU International Journal of Electronics and Communications*, Sep. 2012, DOI 10.1016/j.aeue.2012.08.013.

5. Quoc-Tuan Vien and Huan X. Nguyen, "Network coding-based channel quality indicator reporting for two-way multi-relay networks," *Wiley Journal on Wireless Communications and Mobile Computing*, Sep. 2012, DOI 10.1002/wcm.2296.

6. Quoc-Tuan Vien, Brian G. Stewart, and Huan X. Nguyen, "Outage probability of regenerative protocols for two-source two-destination networks," *Springer Journal on Wireless Personal Communications*, May 2012, DOI 10.1007/s11277-012-0673-8.

7. Quoc-Tuan Vien, Le-Nam Tran, and Huan X. Nguyen, "Efficient ARQ retransmission schemes for two-way relay networks," *Journal of Communications Software and Systems*, vol. 7, no. 1, pp. 9–15, Mar. 2011 (*invited paper*).

Conferences

1. Quoc-Tuan Vien, Brian G. Stewart, Huaglory Tianfield, and Huan X. Nguyen, "An efficient cooperative retransmission for wireless regenerative relay networks," in *Proceedings IEEE Global Communications Conference (GLOBECOM 2012)*, Anaheim, California, USA, Dec. 2012, pp. 4622–4627.

2. Quoc-Tuan Vien, Huaglory Tianfield, and Brian G. Stewart, "Efficient cooperative spectrum sensing for cognitive wireless relay networks over Rayleigh flat fading channels," in *Proceedings IEEE Vehicular Technology Conference (VTC 2012-Spring)*, Yokohama, Japan, May. 2012, pp. 1–5.

3. Quoc-Tuan Vien and Huan X. Nguyen, "CQI reporting strategies for nonregenerative two-way relay networks," in *Proceedings IEEE Wireless Communications and Networking Conference (WCNC 2012)*, Paris, France, Apr. 2012, pp. 974–979.

4. Quoc-Tuan Vien, Huaglory Tianfield, Brian G. Stewart, Huan X. Nguyen, and Jinho Choi, "An efficient retransmission strategy for multisource multidestination relay networks over Rayleigh flat fading channels," in *Proceedings IEEE International Symposium on Wireless Personal Multimedia Communications (WPMC 2011)*, Brest, France, Oct. 2011, pp. 171–175.

5. Quoc-Tuan Vien, Huan X. Nguyen, Jinho Choi, Brian G. Stewart, and Huaglory Tianfield, "Network coding-based block ACK for wireless relay networks," in *Proceedings IEEE Vehicular Technology Conference (VTC 2011-Spring)*, Budapest, Hungary, May. 2011, pp. 1–5.

6. Quoc-Tuan Vien, Le-Nam Tran, and Huan X. Nguyen, "Network coding-based ARQ retransmission strategies for two-way wireless relay networks," in *Proceedings IEEE International Conference on Software, Telecommunications and Computer Networks (SoftCOM 2010)*, Split, Croatia, Sep. 2010, pp. 180–184.

Contents

List of Figures

List of Tables

Abbreviations

4G	Fourth Generation
ACK	Acknowledgement
AF	Amplify-and-Forward
AMC	Adaptive Modulation and Coding
ANC	Analog Network Coding
ANR	Average Number of Retransmission
ARQ	Automatic Repeat reQuest
BC	Broadcast
BCR	Best-relaying Cooperative Retransmission
BER	Bit Error Rate
BPSK	Binary Phase Shift Keying
BS	Base Station
CDMA	Code Division Multiple Access
CF	Compress-and-Forward
CQI	Channel Quality Indicator
CR	Cooperative Retransmission
CROC	Complementary Receiver Operating Characteristic

CSCG	Circularly Symmetric Complex Gaussian
CSI	Channel State Information
CSS	Cooperative Spectrum Sensing
CU	Cognitive User
CWRN	Cognitive Wireless Relay Network
DF	Decode-and-Forward
DFT	Discrete Fourier Transform
DSTBC	Distributed Space-Time Block Code
DSTC	Distributed Space-Time Code
DSTFBC	Distributed Space-Time-Frequency Block Code
DT	Direct Transmission
EX	Exchange
FAP	False Alarm Probability
FC	Fusion Centre
FFT	Fast Fourier Transform
FW	Forward
GBN	Go-Back-N
GCR	Group-relaying Cooperative Retransmission
ICR	Interference Cancellation at Relay
IMT	International Mobile Telecommunications
ISI	Inter-Symbol Interference
LOS	Line-Of-Sight

LSS	Local Spectrum Sensing
LTE	Long Term Evolution
MA	Multiple Access
MAC	Medium Access Control
MCS	Modulation and Coding Scheme
MDP	Missed Detection Probability
MIMO	Multiple-Input Multiple-Output
ML	Maximum Likelihood
MMSRN	Multisource Multidestination Single-Relay Network
MS	Mobile Station
MSE	Mean Square Error
MUD	Multi-User Detection
NACK	Non-Acknowledgement
NC	Network Coding
NLOS	Non-Line-Of-Sight
OFDM	Orthogonal Frequency-Division Multiplexing
OFDMA	Orthogonal Frequency-Division Multiple Access
ORS	Optimal Relay Selection
OSTBC	Orthogonal Space-Time Block Code
PER	Packet Error Rate
PLNC	Physical Layer Network Coding
PU	Primary User

QOSTBC	Quasi-Orthogonal Space-Time Block Code
QPSK	Quadrature Phase Shift Keying
RC	Relay Cooperation
RDEP	Retransmission Decision Error Probability
RET	Retransmission
RIP	Retransmission Indication Packet
ROC	Receiver Operating Characteristic
RP	Reporting
RS	Relay Selection
RT	Relaying Transmission
SBBRS	Suboptimal Bound-Based Relay Selection
SFC	Space-Frequency Code
SISO	Single-Input Single-Output
SIV	Spectrum Indicator Vector
SNR	Signal-to-Noise Ratio
SR	Selective-Repeat
SRS	Suboptimal Relay Selection
SS	Sensing
STC	Space-Time Code
STFC	Space-Time-Frequency Code
STTC	Space-Time Trellis Code
SW	Stop-and-Wait

TDD	Time Division Duplex
TDMA	Time-Domain Division Multiple Access
TR	Time Reversal
TWMRN	Two-Way Multi-Relay Network
TWSRN	Two-Way Single-Relay Network
WiMAX	Worldwide Interoperability for Microwave Access
XRGCR	XOR and Relay Cooperation based Group-relaying Cooperative Retransmission

Notation

$\mathbf{A}^T$	transpose of matrix $\mathbf{A}$
$\mathbf{A}^*$	complex conjugate of matrix $\mathbf{A}$
$\mathbf{A}^{\mathcal{H}}$	Hermitian transpose of matrix $\mathbf{A}$
$\mathbf{F}_M$	normalised $M \times M$ discrete Fourier transform matrix
$\mathbf{0}_{M \times N}$	all-zero matrix of size $M \times N$
$\mathbf{I}_N$	identity matrix of size $N \times N$
$\|\mathbf{x}\|$	Euclidean norm of vector $\mathbf{x}$
$\mathbf{x} \oplus \mathbf{y}$	bitwise XOR operator of two bit vectors $\mathbf{x}$ and $\mathbf{y}$
$\mathbf{x} \otimes \mathbf{y}$	bitwise AND operator of two bit vectors $\mathbf{x}$ and $\mathbf{y}$
$\bar{\mathbf{x}}$	bitwise NOT or complement operator of a bit vector $\mathbf{x}$
$E(\cdot)$	expectation function
$\Phi(\cdot)$	moment generating function
$f(\cdot)$	probability density function
$F(\cdot)$	cumulative density function
$\exp(\cdot)$	exponential function
$E_i(\cdot)$	exponential integral
$\lceil \cdot \rceil$	ceiling function of a real number
C_k^N	number of k-element subsets of an N-element set
$\Gamma(a)$	Gamma function
$\Gamma(a, b)$	incomplete Gamma function
$I_\alpha(\beta)$	modified Bessel function of the first kind
$\mathfrak{G}_{p,q}^{m,n}\left(\begin{smallmatrix} a_1,\ldots,a_p \\ b_1,\ldots,b_q \end{smallmatrix} \middle\| z\right)$	Meijer G function
${}_1\tilde{F}_1(a; b; z)$	regularized hypergeometric function

Chapter 1

Introduction

As wireless communications continues to grow with various enhanced technologies, the broadcast nature of the wireless medium has been exploited to achieve better performance for data transmission. One specific aspect is that multiple nodes in a network can help each other to forward information to a desired destination. The energy waste and the unwanted interference that have been normally considered as drawbacks of the shared media now become a potential resource in assisting the communication between nodes. The attenuation in signal strength caused by severe fading of the source-destination link could be solved with the help of intermediate nodes whose channels are independent of the channel between source node and destination node. Therefore, the probability of successful transmission may be improved for a more reliable communication if these issues are addressed.

The key to developing cooperative schemes for an improved performance lies in multiple-input multiple-output (MIMO) technology which is the deployment of multiple antennas at both the source node and destination node [1, 2]. Recently, MIMO technology has gained attention in Long Term Evolution (LTE) Advanced and Worldwide Interoperability for Microwave Access (WiMAX) wireless network standards [3] since it offers significant increases in data throughput and link range without additional bandwidth or transmit power. With these properties, MIMO is a widely researched theme in wireless communications. However, in practical wireless cellular networks, the instal-

lation of multiple antennas maybe impossible in the uplink transmission due to the inherent hardware limitation of mobile handsets. Also, the requirement of a propagation environment that can support MIMO techniques restricts the use of MIMO in practice. Fortunately, mobile users can cooperate to form a virtual multi-antenna system, and this is known as *cooperative diversity* or *user cooperation* [4,5]. The communication between a source node and a destination node is now realized in a cooperative manner with cooperating nodes acting as relay nodes for a source node.

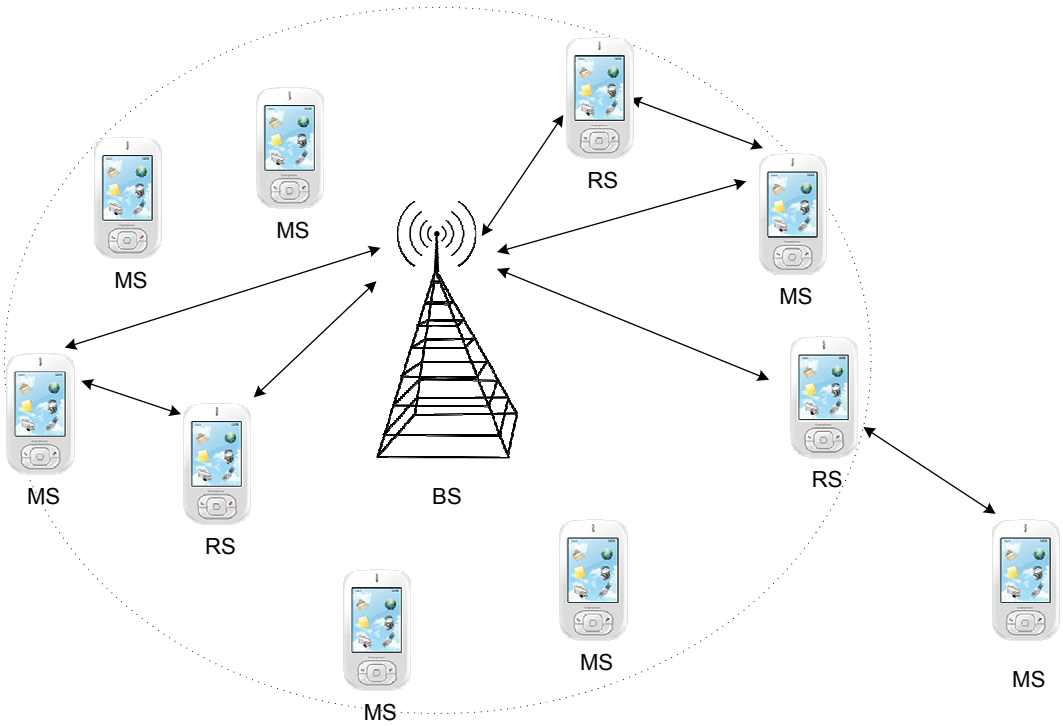

Figure 1.1: Relay communications in cellular network.

In fact, cooperative communications has attracted an increasing interest in wireless communications with the aim of throughput enhancement and quality improvement by exploiting spatial diversity gains [6,7]. The relays can be used not only to improve service quality and link capacity for local users which are located near the source but also to enhance coverage and throughput for remote users. Inspired by the benefits of relays, relay-assisted communications is incorporated in various types of wireless systems such as cellular [8–11], ad hoc [12,13], sensor [14,15], ultra-wideband body area [16,17] and storage [18,19]

networks. An example of applying relay communications in a cellular network is shown in Fig. 1.1 where the transmission between base station (BS) and mobile stations (MSs) is realised with the assistance of various relay stations (RSs). In this figure, RSs are exploited to improve the reliability for near-end MSs with diversity gain and to enhance the coverage of the BS to support far-end MSs.

Relay communications has been investigated and included in LTE Advanced and WiMAX protocols for 4G wireless networks [8, 9]. Data transmission from a source node to a destination node through a relay node in wireless relay networks can be classified into two categories, namely one-way and two-way relay networks. One-way relay networks consider unidirectional communications where a source sends data to a destination through a relay. On the other hand, two-way relay networks refer to a scenario where two parties want to exchange information with each other through a relay. Moreover, depending on the number of relays in the cooperation, the relay networks can be further categorised into single-relay networks and multi-relay networks.

Conventionally, data traverses along the relays in a store-and-forward manner, and thus the use of relays does not immediately increase network throughput. Recently, the idea of *network coding*, which was initially proposed to increase the system throughput in lossless networks [20, 21], has been applied at the relays to dramatically improve the throughput of wireless relay networks [22–27]. By employing NC at the relay nodes to coordinate the transmission among nodes in an efficient way, the optimality of the bandwidth could be achieved. Many NC-based protocols have been proposed for some particular relay channel topologies such as relay-assisted bidirectional channels [28, 29], broadcast channels [30, 31], multicast channels [32, 33] and unicast channels [34, 35].

Most of the recent work has investigated the data transmission in wireless relay networks, where various NC-based techniques and diversity techniques were proposed to improve the throughput and reliability of the data communication channels. The design of signalling and feedback mechanisms that

can achieve high throughput efficiency and reduced retransmission packet latency has received little attention in the previous literature. Specifically, in this thesis, automatic repeat request protocols, channel quality indicator reporting schemes and acknowledgement mechanisms for retransmission will be investigated for various relay channel models. In addition, the scarcity of spectrum resources has motivated to investigate spectrum sensing techniques for wireless relay networks. Furthermore, to deal with the frequency selectivity of fading channels in wide-band communication standards, diversity coding schemes will be investigated to facilitate the data transmission of all licensed and non-licensed users in wireless cooperative networks. In the scope of the thesis, solutions to these problems will be investigated and provided.

The structure of the rest of this chapter is as follows: The main contributions of the thesis are first summarised in Section 1.1. Cooperative communications is then introduced starting from its foundation including the concepts of diversity and MIMO techniques, which are presented in Section 1.2. Basic principles and specific protocols of cooperative communications are then presented in Section 1.3 to point out several physical layer issues and aspects of various relaying techniques. One of the techniques to improve bandwidth efficiency in cooperative communications, namely distributed space-time coding, is discussed in detail. Then, Section 1.4 presents the application of physical layer network coding to improve the throughput of wireless relay networks in which different relay network models are taken into consideration; various physical layer network coding techniques are also briefly introduced. Finally, Section 1.5 outlines the structure of thesis.

1.1 Thesis Contributions

In this thesis, the emphasis of the work is to improving data throughput in various wireless relay network models. Network coding (NC) and space-time coding (STC) techniques are investigated and exploited to offer various means of achieving high-throughput relay communications. Dealing with this prob-

lem statement, this thesis aims to investigate automatic repeat request (ARQ), channel quality indicator (CQI) reporting, acknowledgement (ACK), retransmission, spectrum sensing and diversity coding schemes in the context of wireless relay channels. The main contributions in the thesis can be summarised chapter by chapter as follows:

1.1.1 Chapter 2: NC Based ARQ Retransmission

Generally, the transmission of information over wireless medium suffers from fading and background noise, and thus requires a retransmission mechanism for a reliable communication. The standard ARQ protocol has been proposed as an effective method to improve the reliability of data transmission. Considering the retransmission schemes for two-way wireless relay networks, this chapter proposes different practical ARQ retransmission protocols based on NC to significantly improve throughput efficiency due to the reduction of the number of retransmissions with the NC technique. Additionally, two improved NC-based ARQ schemes are designed based on go-back-N and selective-repeat (SR) protocols. The best retransmission strategy for different scenarios is evaluated through the analysis of throughput efficiency. The combination of an improved NC-based SR ARQ scheme in the broadcast phase and the traditional SR ARQ scheme in the multiple access phase is shown to achieve the highest throughput efficiency compared to the other combinations of ARQ schemes.

Extending these principles to multicast or broadcast networks, lost packets required to be retransmitted with ARQ protocols may introduce significant packet latency since each packet is retransmitted individually and retransmissions are repeated until all packets are received correctly. For wireless relay networks, the design of reliable transmissions over multisource multidestination single-relay networks (MMSRNs) for high network throughput efficiency has received little attention. Addressing the ARQ issue in MMSRNs, this chapter proposes a new ARQ protocol based on NC to improve the throughput by reducing the packets to be retransmitted. Two packet-combination algorithms for the retransmissions at the relay and sources are proposed to

efficiently retransmit all lost packets. Mathematical formulation of the transmission bandwidth for this new NC-based ARQ protocol is derived and compared with some other ARQ protocols over both mixed Rayleigh and Rician flat fading channels. The mixed fading model permits investigation of two typical fading scenarios where the relay is located in the neighbourhood of either the sources or the destinations. The transmission bandwidth results show that the proposed NC-based ARQ protocol achieves superior performance over other existing ARQ schemes.

1.1.2 Chapter 3: NC Based CQI Reporting

In practical wireless communication systems, channel state information (CSI) available at the transmitter side is helpful for a number of designs including optimal beamforming and adaptive modulation and coding schemes. The CSI feedback schemes are commonly realised via CQI reporting. Most of the recent work has investigated CQI reporting in one-way relay networks. Extending these CQI feedback schemes to two-way single-relay networks (TWSRNs) results in doubling the signaling overhead and requiring two time slots at each relay node to forward these overheads to both terminal nodes. To cope with this throughput degradation, this chapter proposes two new efficient CQI reporting schemes based on the XOR operator and superposition coding to improve the system throughput by 16.7%. The proposed schemes allow two terminals to simultaneously estimate the CQI of the distant terminal-relay link without incurring additional overhead. Also, the transmission time for CQI feedback at the relays is reduced by half while the increase in complexity and the loss of performance are negligible. Upper and lower bounds of the mean square error of the estimated CQI are derived to study performance behaviour of the proposed scheme. Furthermore, based on the derived bounds, a low-complexity relay selection scheme is proposed to reduce the searching complexity by at least three times in the case of a large number of relays.

1.1.3 Chapter 4: NC Based Block ACK and Cooperative Retransmission

Over wireless fading and noisy channels, positive ACK with retransmission is a communication protocol designed to assure the reliability of data packet transmission. Due to the frequent transmissions of small-sized ACK packets, a block ACK mechanism has been proposed to reduce the overhead required at each node. Generally, block ACK schemes are restricted to one-to-one communications. Taking into account the circumstance of multi-relay networks, a total of $(2N + 1)$ block ACK packets is required to acknowledge the data transmission between source and destination nodes via the N relay nodes, which may degrade the network throughput. Thus, as an effective means of throughput enhancement, this chapter proposes a new block ACK scheme based on NC to significantly reduce the acknowledgement overheads by N block ACK packets. The proposed scheme also achieves a reduction of $N(N - 1)$ computational operations. Additionally, this chapter derives the error probability of the determination of the packets to be retransmitted at the source and relays. The results show that the NC-based block ACK scheme also improves the reliability of block ACK transmission and reduces the number of data retransmissions for a higher system throughput.

Within relay networks, the retransmission can be realised in a cooperative manner with the assistance of all available relays. This may result in a low network throughput and high overall power consumption due to the retransmission of the same packets across the nodes, especially when the number of relays is large. These performance deteriorations have motivated a new proposed cooperative retransmission (CR) scheme based on relay cooperation and binary XOR operations. The proposed scheme significantly reduces the number of retransmission packets to produce a more power efficient and higher throughput system with non-overlapped retransmissions. Significantly, this chapter derives the error probability of retransmission decisions and average number of packets to be retransmitted at the source and relays. The proposed

CR scheme is shown to improve the reliability of the retransmissions, reduce the number of retransmissions and remove overlapped (or repeated) retransmitted packets. Moreover, two relay selection schemes are proposed to identify the optimised number of relays for the retransmission phase.

1.1.4 Chapter 5: NC Based Spectrum Sensing

Recently, to tackle the scarcity of spectrum resources in wireless communications, cognitive radio has been proposed as a promising technology to improve spectrum efficiency by providing dynamic spectrum access with various spectrum sensing techniques. Inspired by relaying techniques, cooperative spectrum sensing (CSS) was proposed not only to help shadowed cognitive users detect primary users but also to improve detection reliability. With respect to cognitive wireless relay networks (CWRNs), this chapter first proposes a new CSS scheme to improve the spectrum sensing performance by exploiting both local decisions at individual cognitive users and global decisions at the fusion centre. In particular, taking into consideration a practical scenario where all sensing, reporting and backward channels suffer from Rayleigh fading, this chapter derives the probabilities of missed detection and false alarm, which show that the proposed CSS scheme gains a better sensing performance than the conventional scheme. The effects of the fading channels on the sensing reliability are also characterised through the derived expressions. Furthermore, developing a three-hop CWRN consisting of two cognitive radio layers, a new CSS scheme is proposed based on a binary XOR operator to help in reducing one phase of sensing for a higher system throughput compared to the conventional scheme which requires eight phases in total.

1.1.5 Chapter 6: Distributed Space-Time-Frequency Block Coding

This chapter investigates the cooperative transmission in CWRNs over frequency-selective fading channels. A new distributed space-time-frequency block code

(DSTFBC) for a two-hop nonregenerative CWRN is proposed to convey information data from a primary source node and N secondary source nodes to their desired primary destination node and N secondary destination nodes via two relay nodes. The proposed DSTFBC design achieves higher data rate, spatial diversity gain and decoupling detection of data blocks at all destination nodes with a low-complexity receiver structure. In the proposed DSTFBC, before forwarding the data received from various sources to the destination nodes, the relay nodes precode the received signals with a proper precoding matrix. The pairwise error probability is analysed to demonstrate the achievable diversity gain of the proposed DSTFBC for two channel models where the links from the sources to the relays and from the relays to the destinations suffer from either mixed Rayleigh-Rician fading or only Rician fading. These two specific channel models allow to analyse three typical scenarios where the relays are in the neighbourhood of either the sources or the destinations or the midpoint.

Parts of the work in this thesis have appeared in [36, 37] on the NC-based ARQ mechanism for TWSRNs; [38–40] on the NC-based ARQ mechanism for MMSRNs; [41,42] on the NC-based CQI reporting for TWSRNs; [43–46] on the NC-based block ACK and CR schemes for multi-relay networks; and [47, 48] on the NC-based CSS scheme for CWRNs. The rest of this chapter will focus on background material for the thesis.

1.2 Diversity Techniques and Related Work

In this section, the basic concepts of diversity techniques are first described, including temporal diversity, frequency diversity and spatial diversity. MIMO systems are then presented along with different space-time, space-frequency and space-time-frequency coding schemes. The section concludes by introducing the limitations of MIMO techniques in practical wireless networks, and thus motivates the concept of cooperative diversity which is regarded as a new communication paradigm. For brevity, in Fig. 1.2, various basic diversity and

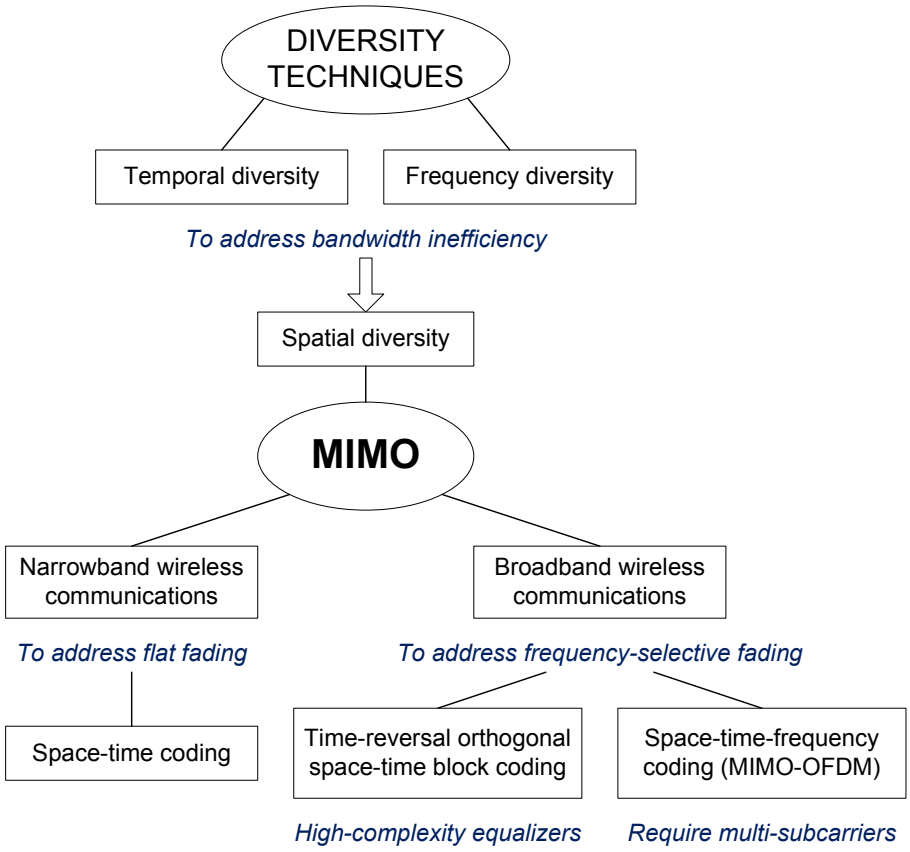

Figure 1.2: Flowchart of diversity and MIMO techniques.

MIMO techniques are presented to address different issues in different wireless communications environments. These techniques can be summarised in the following subsections.

1.2.1 Diversity Techniques

In a communication system consisting of a source node and a destination node, the reliability of the communications link can be improved by providing more than one path between them. This technique is the main idea behind the term *diversity*. In fact, by providing multiple replicas or copies of the transmitted signals over independent channels, the destination can more reliably decode the transmitted signal by either combining all the received signal, namely a maximal ratio combiner, or selecting the best signal with the highest signal-to-noise ratio (SNR), namely a selection combiner, or choosing the signal with an SNR exceeding a threshold, namely a threshold combiner. In order to define

the diversity quantitatively, the relationship between the error probability P_e and the received SNR, γ, is used to define the formula of diversity gain as [49]

$$G_d \triangleq -\lim_{\gamma \to \infty} \frac{\log P_e}{\log \gamma}. \tag{1.1}$$

It can be seen that the diversity gain G_d is the slope of the P_e curve in terms of γ in a log-log scale. This means that a large diversity gain is preferred to achieve a reduced P_e at a higher data rate. The problems are how to provide various copies of the transmitted signal to the destination node in an efficient way in terms of power, time, bandwidth and complexity, and, how to take advantage of these copies at the destination node to achieve the lowest P_e. To cope with these two problems, various diversity methods are implemented as follows:

Temporal Diversity

In temporal diversity, copies of the transmitted signal are sent at different time intervals [50]. The time interval between two transmitted replicas should be longer than the coherence time of the channel to make the fading channels uncorrelated and thus the temporal diversity can be obtained. However, the temporal diversity is bandwidth inefficient due to the delay that may be suffered at the destination node in the case of a slow fading channel, i.e. a large coherence time of the channel.

Frequency Diversity

Instead of using temporal separation between different replicas of the transmitted signal, the transmission of these copies can be carried out over different carrier frequencies to achieve frequency diversity [51]. Similar to temporal diversity, frequency diversity can be achieved when there exists a necessary separation between two carrier frequencies which should be larger than the coherence bandwidth of the channel. It can be seen that the frequency diversity is also bandwidth inefficient and the capability of frequency tuning is required at the destination node.

Spatial Diversity

In spatial diversity, multiple antennas are employed at the source node and/or destination node to transmit and receive different copies of the signal. Thus, it is also called antenna diversity [52]. Spatial diversity does not suffer from bandwidth inefficiency which is the major drawback of temporal and frequency diversity. In order to achieve spatial diversity, the antennas at the source node and destination node are normally separated by at least half a wave length of the transmission frequency to guarantee that the fading channels are low-correlated or independent. Obviously, the condition of antenna separation could be easily satisfied at large base stations, but may not be applicable for small handheld devices.

1.2.2 MIMO Techniques

In radio communications, the negative effects of fading phenomena on quality and data rate in wireless communications can be combated with diversity in the spatial domain. The concept of MIMO systems is defined for systems where multiple antennas are deployed at the source node and destination node to achieve diversity and multiplexing. However, this thesis will focus on diversity MIMO only. Work in [1, 2] on various MIMO techniques is regarded as the first studies of MIMO systems. These two pioneering publications showed that a large capacity gain could be achieved with MIMO systems compared to single-input single-output (SISO) systems. Also, these publications motivated a large number of improvements on MIMO systems in terms of capacity and diversity. In what follows, several well-known MIMO techniques that have been used to achieve spatial diversity gain will will be presented and compared. The comparisons of MIMO techniques for flat and frequency-selective fading channels are briefly summarized in Table 1.1 and Table 1.2, respectively, where the properties of different coding techniques are presented in terms of diversity gain, data rate and decoding complexity.

Table 1.1: Comparison of MIMO techniques for flat fading channels

Coding technique	**Properties**
STTC [55, 56]	Full diversity, full rate, high-complexity decoding
Alamouti code [57] for 2 transmit antennas	Full diversity, full rate, simple decoding
OSTBC [58–60] for more than 2 transmit antennas	Full diversity, simple decoding, rate of 3/4 for 3 and 4 transmit antennas, half rate for any over 4 transmit antennas
QOSTBC [61, 62] for 4 transmit antennas	Half diversity, full rate, simple decoding
Rotated QOSTBC [63] for 4 transmit antennas	Full diversity, full rate, pairwise decoding

Table 1.2: Comparison of MIMO techniques for frequency-selective fading channels

Coding technique	**Properties**
TR-OSTBC [73–75] for single-carrier MIMO	Full rate, full diversity in space and frequency, no ISI, high-complexity equaliser
SFC [76, 78, 79] for MIMO-OFDM	Full rate, spatial diversity, no ISI, low-complexity decoding
SFC [81] for MIMO-OFDM	Full rate, full diversity in space and frequency, no ISI, high-complexity decoding
STFC [82–85] for MIMO-OFDM	Full rate, full diversity in space, time and frequency, no ISI, high-complexity decoding

Space-Time Coding for Flat Fading Channels

In [53, 54], two space-time coding (STC) design criteria were derived based on the upper bound of pairwise error probability. One is rank criterion or diversity criterion in which an STC is said to achieve full diversity if the code difference matrix is of full rank. The other is the product criterion or determinant

criterion in which the coding gain of an STC is determined by the product of eigenvalues of the code difference matrix, and thus it should be large to obtain a high coding gain.

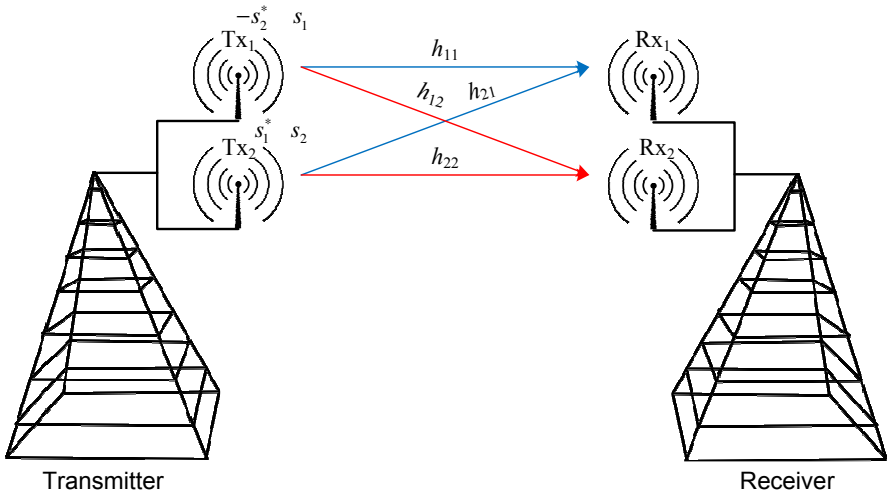

Figure 1.3: 2x2 MIMO with Alamouti scheme.

One important means of achieving spatial diversity is by deployment of multiple antennas at the transmitter, which is known as transmit diversity. Space-time trellis coding (STTC) in [55, 56] can effectively exploit transmit diversity but its decoding complexity increases exponentially with the transmission rate. Thus different transmit diversity schemes should be proposed to avoid the complicated decoding algorithm in STTC. Dealing with this issue, a new orthogonal transmit diversity scheme was proposed in [57] using two transmit antennas. This scheme is well-known as the Alamouti code or Alamouti scheme in honour of its inventor. As shown in Fig. 1.3, the Alamouti code is designed for a two-antenna system with the following coding matrix:

$$\begin{pmatrix} s_1 & -s_2^* \\ s_2 & s_1^* \end{pmatrix} \tag{1.2}$$

The Alamouti scheme possesses very desirable properties including full diversity, full rate (i.e. rate = 1) and simple decoding (i.e. symbol-wise maximum likelihood (ML) decoding).

The Alamouti scheme was later generalized in [58–60] for more than two transmit antennas, and characterised as orthogonal space-time block coding

(OSTBC) for MIMO systems. OSTBC designs can achieve full diversity and simple decoding. However, the rate is limited to a maximum of 3/4 for three and four transmit antennas, and 1/2 for five or more transmit antennas. For a particular case of 4 transmit antennas, a quasi-orthogonal space-time block code (QOSTBC) was proposed in [61, 62] to achieve a rate of 1 and the capability of symbol-wise ML decoding, but the diversity of QOSTBC is 2 which is less than the maximum possible diversity of 4 when using OSTBC. To improve the diversity of QOSTBC, rotated QOSTBC was proposed in [63] to achieve both full rate and full diversity, but with a requirement of pairwise ML decoding. In parallel with OSTBC and QOSTBC, other STCs were designed using some specific matrix structures, such as cyclic STC in [64, 65], unitary STC in [66, 67], diagonal algebraic STC in [68, 69] and groupwise STC in [70–72].

Space-Time-Frequency Coding for Frequency-Selective Fading Channels

Various STCs discussed above for MIMO systems were devised only for narrowband wireless communications with flat fading channels. This means there exists only one propagation path between a pair of transmit and receive antennas. This situation occurs in low data rate transmissions when the channel delay spread is relatively small compared to the symbol duration. In some wireless communication standards, the system is required to operate at a high data rate, and thus the communications channels become frequency-selective fading. The frequency-selective or multipath fading channels cause not only severe attenuation in signal strength, but also a large amount of inter-symbol interference (ISI), which makes the signal detection unreliable. However, multipath fading channels can offer multipath diversity or frequency diversity. Many studies were then dedicated to extend OSTBCs to frequency-selective fading channels [73–75]. Extending from the Alamouti code for two transmit antennas, the proposed coding schemes in [73–75] can be viewed as a block implementation of the Alamouti scheme for frequency-selective fading channels where the transmission is performed at block level instead of symbol level and

the time reversal (TR) operation is additionally carried out on the conjugated version of the data block. Thus, these coding schemes were also known as time reversal OSTBCs (TR-OSTBCs). With TR-OSTBCs, ISI is removed by using only one carrier but a high-complexity equalisation is required.

Another method to mitigate the frequency selectivity of frequency-selective fading channels is orthogonal frequency-division multiplexing (OFDM) . OFDM is effective in reducing the high-complexity equalisation and offering high spectral efficiency. However, multi subcarriers are required to mitigate the fading effects. For wideband MIMO-OFDM systems, space-frequency coding (SFC) was first proposed in [76] by converting the time domain in the proposed STC to the frequency domain. In [77], the performance criteria for SFC were derived and the maximum achievable diversity was shown to be the product of the number of transmit antennas, the number of receive antennas and the number of delay paths. Similarly, different versions of SFC were proposed in [78, 79]. However, these SFCs could achieve only spatial diversity and could not be assured to achieve full diversity in terms of both spatial and frequency diversity. Later, full-diversity SFCs were proposed in [80] based on the mapping from STCs, and then full-rate full-diversity SFCs were proposed in [81] based on diagonal algebraic STCs. Considering SFCs over several consecutive OFDM blocks, space-time-frequency coding (STFC) was first proposed in [82] for two transmit antennas and then extended in [83–85] for multiple transmit antennas. The design of STFCs for MIMO-OFDM systems that could achieve the maximum achievable diversity or full diversity was proposed in [80]. It was shown that the maximum achievable diversity is the product of the number of transmit antennas, the number of receive antennas, the number of delay paths and the number of independent fading blocks.

1.2.3 Motivation of Cooperative Diversity

As presented above, various coding schemes were designed for co-located antennas in MIMO systems to greatly improve the performance of wireless communications due to the capability of achieving spatial diversity. However, more

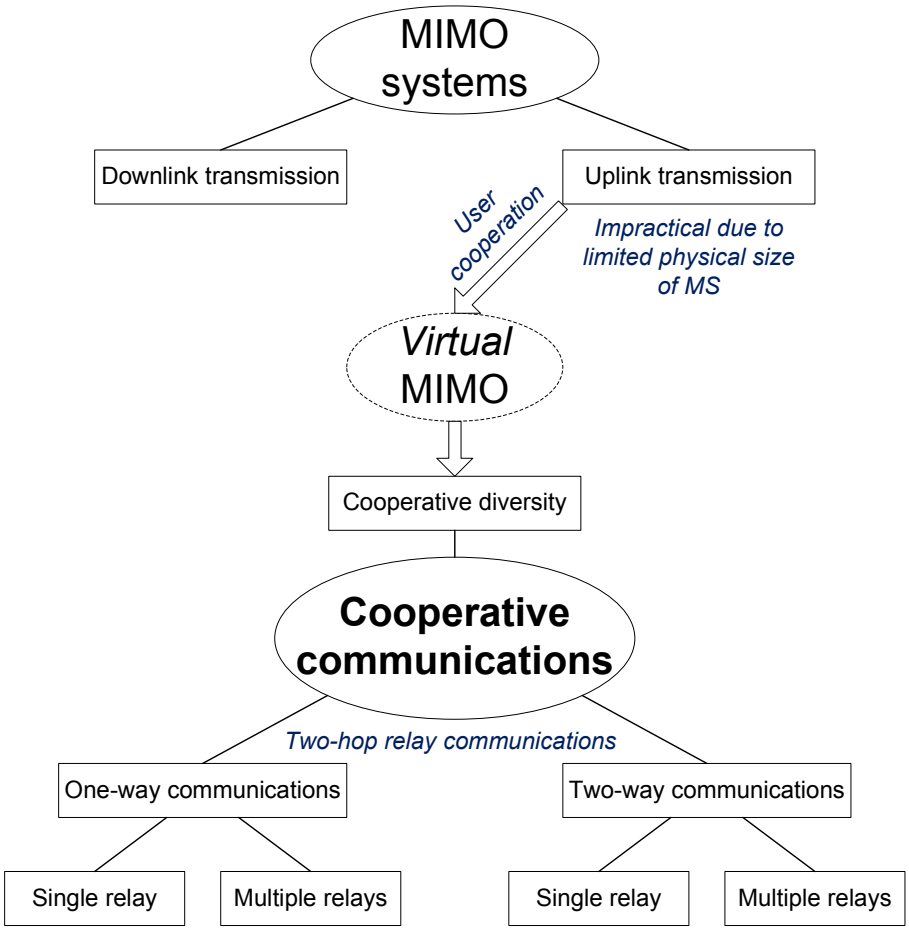

Figure 1.4: Flowchart of cooperative communications.

than one co-located antenna is required at the source node. In wireless cellular networks, these coding schemes can be easily implemented at the base station to improve the reliability and capacity of the downlink transmission. For the uplink transmission, the deployment of multiple antennas is, however, impractical due to the limitation in physical size of many current mobile handsets. Recently, the problem of exploiting spatial diversity for the uplink transmission of wireless cellular networks or more general ad-hoc networks has been solved if various single-antenna terminals could assist the others to transmit data using an efficient protocol. This is equivalent to creating virtual MIMO systems where each single-antenna terminal acts as an antenna element in the MIMO systems. Drawing from user cooperation to achieve some of the benefits of MIMO systems, this form of diversity is well known as cooperative diversity or

user cooperation diversity [4,5]. For brevity, the motivation and the taxonomy of cooperative communications are summarised in Fig. 1.4, where the limitation of MIMO techniques for uplink transmission are shown as a motivation for the proposal of cooperative communications and where different two-hop relay communication models under investigation are outlined.

1.3 Cooperative Diversity and Related Work

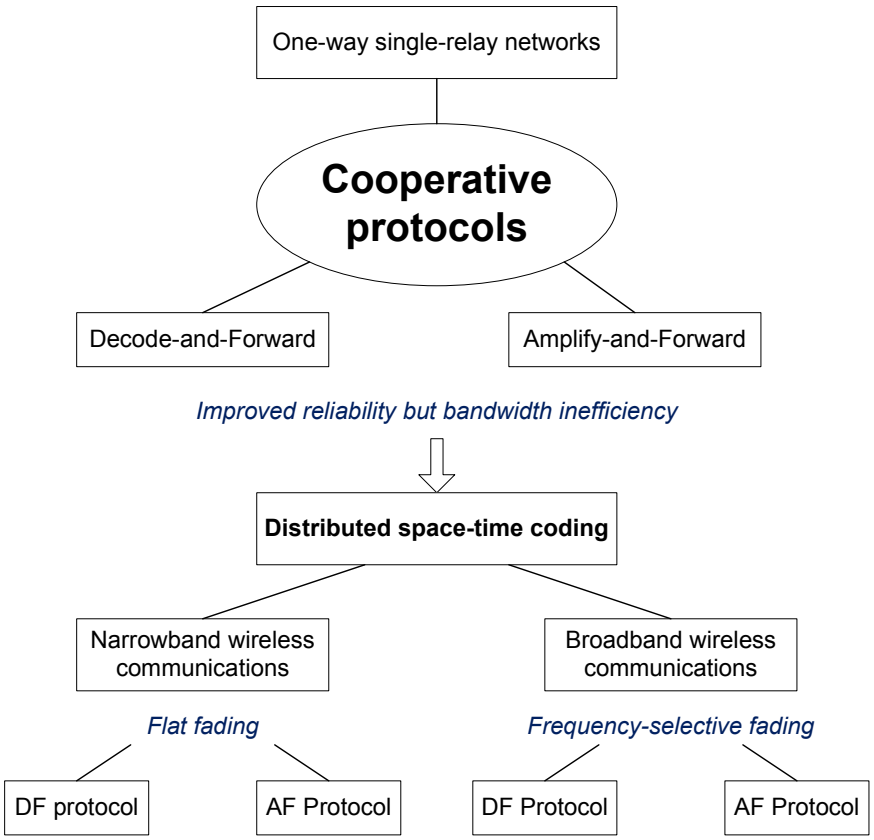

Figure 1.5: Flowchart of cooperative protocols and distributed space-time coding.

In this section, several cooperative protocols in wireless relay networks are briefly presented with a summary comparison of their performance. Specifically, distributed STC is presented as a means to improve the bandwidth efficiency of cooperative communications by implementing the STC in a cooperative manner with the assistance of relays. In Fig. 1.5, different cooperative

protocols and distributed STC for different fading channels are classified depending on the operation at the relays, which can be clarified in the following subsections.

1.3.1 Cooperative Protocols

The very classical relay channel including three terminals was initially defined in [86] where a relay terminal simply listens to the transmitted signal from a source terminal, processes it and then sends it to a destination terminal. For this relay channel model, the capacity was first investigated in [87] where lower and upper bounds of the channel capacity are provided. The ergodic capacity of the relay channel with different coding strategies was then analysed in [88].

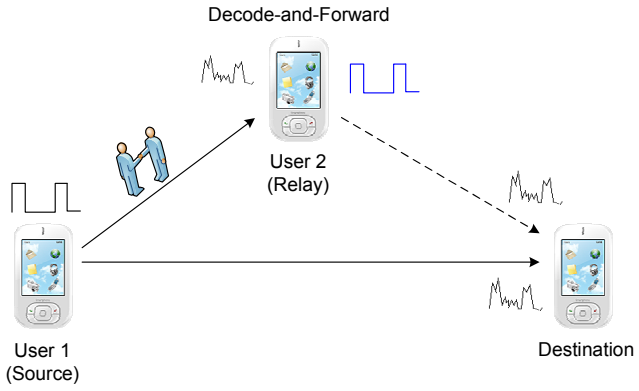

(a)

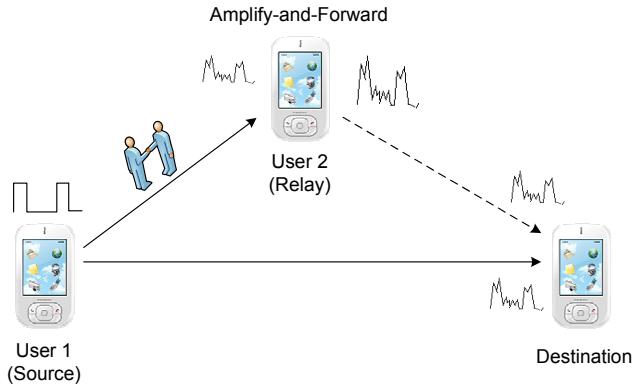

(b)

Figure 1.6: Cooperative protocols: (a) Decode-and-forward and (b) amplify-and-forward.

Motivated by the three-terminal channel model in [86, 87], low-complexity

cooperative protocols were proposed and analysed in [6] considering a more general system model with practical aspects. The protocols in [6] were developed in the context of time-domain division multiple access (TDMA) systems and terminals are assumed to operate in half-duplex. Specifically, two notable cooperative protocols, namely *amplify-and-forward* (AF) and *decode-and-forward* (DF), were defined and investigated for two types of relaying techniques, i.e. fixed and adaptive relaying. These two basic protocols are correspondingly illustrated in Fig. 1.6. While fixed relaying was shown to be easy in implementation at the cost of low bandwidth efficiency, adaptive relaying, including selective and incremental relaying, could increase the rate at the expense of high complexity. In fact, the overall rate using fixed relaying schemes is reduced by half for two transmissions from the source and relay, and thus results in low bandwidth efficiency. Instead of simply processing and forwarding the data to the destination, the relay in the selective relaying scheme has the capability of deciding when to transmit based on a certain threshold of quality of the received signal, e.g. SNR. If the SNR of received signal at the relay is lower than the threshold, i.e. the channel from the source to the relay suffers from severe fading, the relay does not carry out any processing. A relaying scheme known as incremental relaying could improve the performance further if the source knows when to repeat the transmission and the relay knows when the destination needs help. It can be appreciated that adaptive relaying schemes require high-complexity processing and a feedback channel from the destination to both the source and relay is specifically required for incremental relaying. In the scope of this work, fixed relaying techniques will be focused on.

Decode-and-Forward Protocol

In the DF protocol [6], the relay tries to decode the signal from the source and then transmits the decoded signal to the destination. However, the signal detected at the relay is possibly corrupted, and thus might cause the cooperation to be meaningless to the eventual decision at the destination. In order to

achieve optimal detection, the destination needs to know the error statistics of the inter-user link. This method was also mentioned in [4, 5] for code division multiple access (CDMA) in cellular networks. The diversity of the DF protocol was shown to be limited to one due to the worst link from the source to the relay and from the source to the destination [6].

Amplify-and-Forward Protocol

In the AF protocol, the relay only amplifies what it receives from the source and then transmits the amplified version to the destination [6]. The destination combines the information sent by the source and relay, and makes a final decision on the transmitted signal. Although noise at the relay in the AF protocol is amplified by cooperation, the destination can make a better decision with two independently faded versions of the transmitted signal. Thus, the AF protocol achieves the full diversity, i.e. two.

Other Protocols

Besides DF and AF protocols, the compress-and-forward (CF) protocol also attracted much attention in [87,88]. In the CF protocol, the relay transmits to the destination a quantized and compressed version of the signal received from the source. At the destination, the signal received from the source is used as side information to decode the information from the relay. Another cooperative protocol that was studied with the consideration of channel coding is coded cooperation [89,90] where error-control coding is included into the cooperation. In coded cooperation, the relay transmits incremental redundancy to help the destination recover the original data more reliably by combining the codewords with redundancy from the source and relay.

1.3.2 Distributed Space-Time Coding

The above mentioned protocols are in fact repetition-based cooperative diversity schemes designed to achieve spatial diversity gain as a virtual MIMO

system. However, the benefit of these cooperative protocols is achieved at the price of decreasing bandwidth efficiency with the number of cooperating terminals, i.e. number of relays, because each relay requires its own subchannel for repetition [7]. Inspired by the work on STCs for MIMO systems, distributed space-time coding (DSTC) was proposed in [7] to improve the bandwidth efficiency of cooperative communications. The basic idea of DSTCs is that each single-antenna terminal in the relay network transmits a column of the original OSTBCs that were designed for multiple co-located antennas in MIMO systems. In a distributed fashion with the assumption of perfect synchronisation, multiple columns of the original OSTBCs can be transmitted by the source and relays to indirectly generate coding matrices, called distributed space-time block codes (DSTBCs), which are of the same form as OSTBCs. Similar to MIMO techniques, various DSTBCs were proposed for either flat or frequency-selective fading channels. The comparison of various DSTBC techniques for flat and frequency-selective fading channels is summarized in Table 1.3 where the properties of different DSTBC designs are presented in terms of diversity gain and processing complexity at the relay and destination nodes.

DSTBCs for Flat Fading Channels

The relays in [7] operate under the DF protocol, and thus they need to decode their received signals. In [91, 92], different DSTBCs were analysed for AF relay networks. The original design criteria for conventional STC [53] was shown to be able to apply to the DSTBCs. In [7], in order to guarantee full diversity, the number of relay nodes should be less than the number of columns in the conventional OSTBC matrix. The limit on the number of relays was then solved by a new class of DSTBCs in [93] for multiple relays. In this scheme, the signal transmitted by an active relay node is the product of an information-carrying code matrix and a unique node signature vector to ensure that no active node transmits data using the same coding vector. However, this method operates under the DF protocol and requires high-complexity processing at the relay nodes.

Table 1.3: Comparison of DSTBC techniques

DSTBC for flat fading channels	**Properties**
DSTBC for DF protocol [7, 93]	Full diversity, high-complexity relay, low-complexity receiver
DSTBC for AF protocol [91, 92, 95–97]	Full diversity, low-complexity relay, high-complexity receiver
DSTBC for frequency-selective fading channels	**Properties**
DSTBC for DF protocol [98]	*Model*: multiple hops, multiple relays. High-complexity relay, low-complexity receiver
DSTBC with OFDM for DF protocol [99]	*Model*: two hops, multiple relays. High-complexity relay, high-complexity receiver
DSTBC for AF protocol [100]	*Model*: two hops, single relay. Maximal diversity gain, low-complexity relay, high-complexity receiver

For the AF protocol, the idea of linear dispersion space-time coding in [94] was applied to construct a new DSTBC for relaying systems [95, 96] in which the transmitted signal at each relay is a linear function of its received signal. Each relay carries out only simple processing and does not need to decode its received signal. However, these DSTBCs, in general, cannot offer a simple decoding mechanism at the destination. To address this problem, a new class of DSTBCs was proposed in [97] to obtain symbol-wise ML decodability. Moreover, the data rate of these schemes could be designed to be as large as possible.

DSTBCs for Frequency-Selective Fading Channels

Most of related work on cooperative wireless communication systems assume flat fading channels. They ignore the fact that practical transmission through wireless channels would suffer from inherent frequency-selective fading phenomena, especially in networks supporting high data rate transmission as in many current standards. For such cases, all the above mentioned designs are not directly applicable. Considering frequency-selective fading channels, the authors in [98] proposed DSTBCs for multi-hop transmission with the DF protocol. For optimal detection, the error statistics at the relays must be known at the destination. However, this cannot be easily implemented in many current wireless systems. Focused on the uplink communications system with fixed wireless relay stations, the combination of DSTBC and OFDM signaling was introduced in [99].

More recently, DSTBC for frequency-selective fading channels has been studied in [100] where traditional equalisation techniques were extended to DSTBC in cooperative communications with the AF protocol. The transmission scheme presented in [100] is still a repetition algorithm and the full rate is impossible to achieve. Additionally, the DSTBCs in [100] were devised for relay networks where there exists one active relay node and a direct communication link between the source and the destination.

1.4 Network Coding and Related Work

As a well known technique to improve the throughput of wireless relay networks, physical layer NC (PLNC) has recently attracted much attention. In this section, NC and the application of NC at the physical layer will be first presented. Different PLNC techniques for wireless two-way single-relay networks (TWSRNs) are then introduced and compared to show the advantages and disadvantages of each technique. For brevity, in Fig. 1.7, different PLNC techniques for TWSRNs are illustrated along with the summary of the operations at the relay and their characteristics.

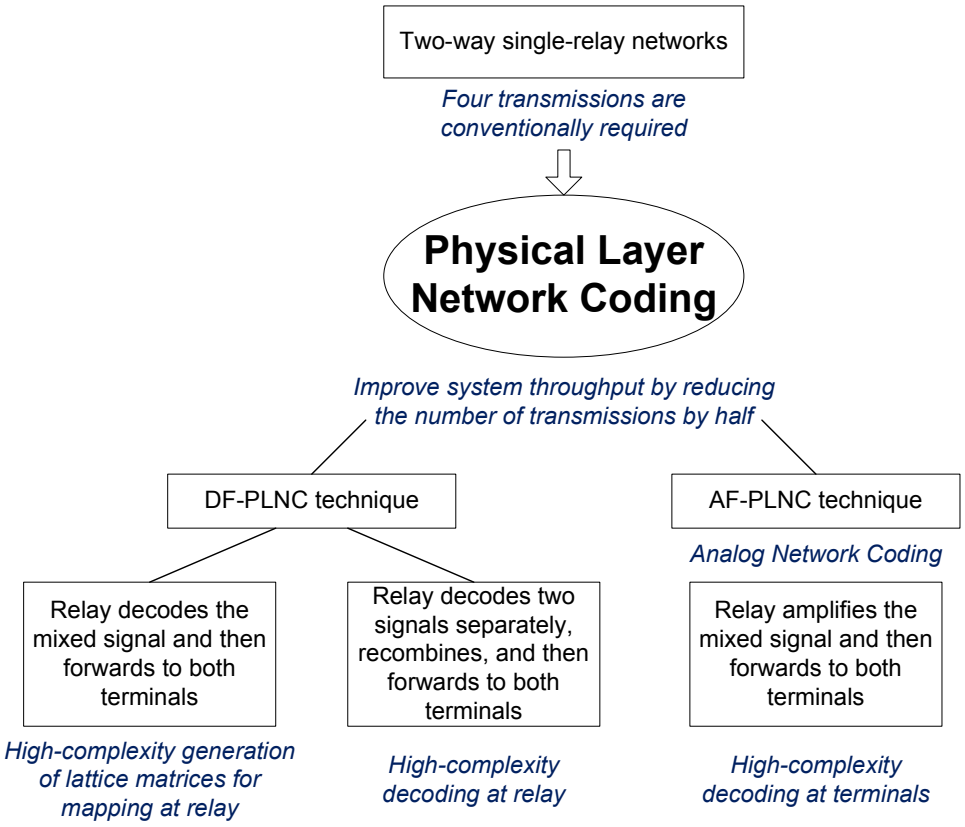

Figure 1.7: Flowchart of physical layer network coding.

1.4.1 Network Coding and Physical Layer Network Coding

NC was first proposed in 2000 by [20] to increase system throughput in lossless networks. This work was regarded as a seminal publication on NC and has motivated a vast amount of related work on NC. The principle of NC is that intermediate nodes are allowed to mix signals received from multiple links for subsequent transmissions, e.g. using XOR operations to mix two signals from two terminals.

In a typical TWSRN with no direct link between two transmitting terminals, as shown in Fig. 1.8(a), four transmissions are conventionally required to exchange the data from two terminals through a relay. By applying NC, the number of transmissions could be reduced to three, including two transmissions from two terminals to the relay and one broadcast transmission of mixed data from the relay to both terminals (see Fig. 1.8(b)). Basically, the relay

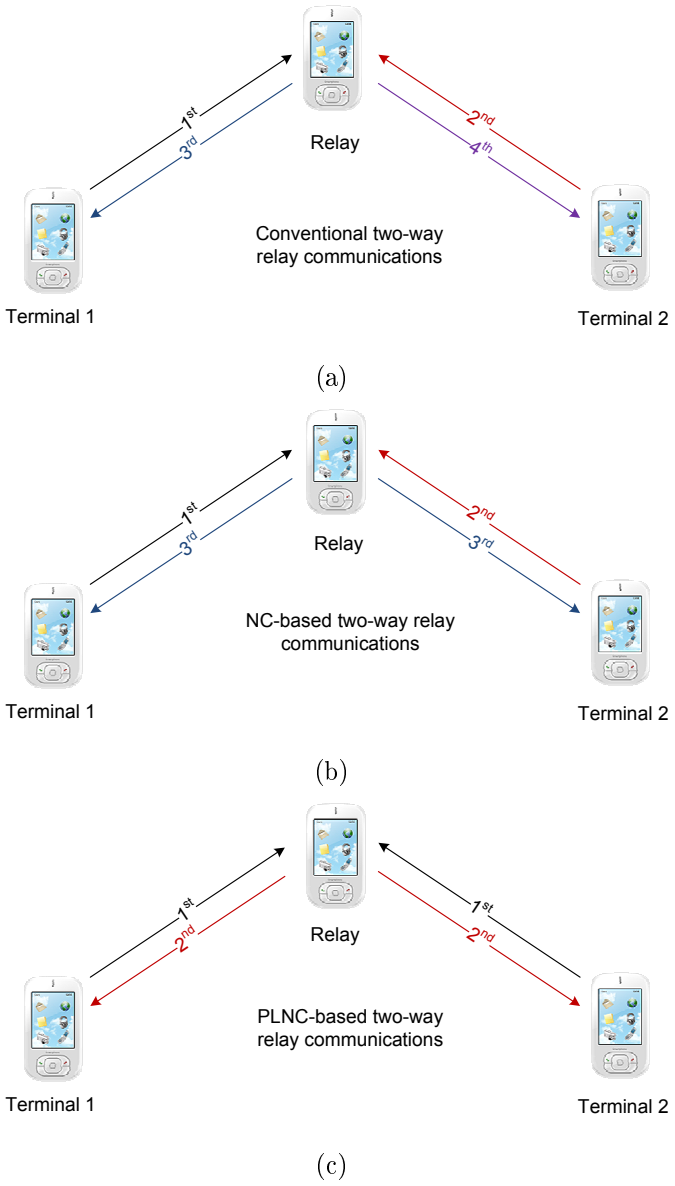

Figure 1.8: Two-way single-relay network with: (a) Conventional relaying, (b) network coding and (c) physical layer network coding.

in an NC-based TWSRN mixes the signals received from two terminals, and then forwards the combined signal to both terminals. An end terminal can extract from the combined signal the data sent by another terminal based on its known signal. However, the relay in the NC-based TWSRN has to avoid the collision of data packets to detect the data from two terminals separately.

Considering the application of NC at the physical layer of TWSRNs, the number of transmissions could be reduced to two due to the fact that two termi-

nals can transmit simultaneously (see Fig. 1.8(c)). Accordingly, the PLNC can improve the throughput in TWSRNs by up to 100 % and 50 % over the conventional relaying and the NC-based relaying, respectively. Several studies have been dedicated to investigating the application of PLNC to TWSRNs [22–27]. In [22–25], PLNC was practically applied to the wireless environment using DF and AF relaying protocols. The scheduling in PLNC-based relay networks was investigated in [26]. In [27], the performance of different PLNC-based protocols was analysed and compared in terms of bit error rate and data rate.

Basically, the processing at the relay in PLNC-based TWSRNs could be carried out with either DF protocol [23] or AF protocol [24]. Thus, in general, PLNC techniques for TWSRNs could be categorised into DF-PLNC and AF-PLNC. The following presents these two typical PLNC techniques that were first investigated in [23–25, 101]. Other related work on PLNC techniques can be found in [27, 28, 102–110], where different PLNC-based approaches were investigated and evaluated, such as performance analysis of DF-PLNC and AF-PLNC protocols for TWSRN in [27, 28, 102, 108], DF-PLNC for multiple-access channels in [103], channel coding and decoding for PLNC-based relay networks in [104], beamforming for AF-PLNC-based TWSRNs in [105], differential modulation for AF-PLNC-based TWSRNs in [106], symbol mapping for AF-PLNC-based Gaussian multiple-access relay channels in [107], AF-PLNC for asynchronous TWSRNs in [109] and convolutional codes for PLNC-based TWSRNs in [110].

1.4.2 Decode-and-Forward Physical Layer Network Coding

In the one-way relay network operated under the DF protocol, the relay simply decodes the signal received from the source before forwarding to the destination. However, the relay in PLNC-based TWSRNs receives two data sequences simultaneously from two terminals. The challenging problem is how the relay decodes this mixed signal. Dealing with this problem, the first strategy was

proposed in [23]. In this approach, the relay decodes the sum of two signals instead of decoding each signal individually. Thus, it was known as the DF-PLNC technique. The sum of any two signals was characterised by a point in a lattice. Based on this lattice, the relay can decode its received mixed signal and then forward it to both terminals. Using the DF protocol, this scheme does not suffer from noise amplification at the relay, and thus a higher data rate is expected. However, the generation of the lattice for mapping seems to be quite complicated for a general scenario where the signals transmitted from two terminals use different modulation and coding schemes. Also, this strategy requires synchronisation at the relay in both time and carrier when receiving signals from two terminals.

Another approach to DF-PLNC was proposed in [101] where the relay separately decodes two signals from the mixed signal received from two terminals, then combines and forwards them to both terminals. The decoding of two signals from the mixed signal could be implemented as multiuser detection [111]. Similar to the proposed DF-PLNC in [23], the error amplification at the relay does not have any effects on this strategy. As an advantage of this scheme, the generation of lattice matrices for mapping is not necessary, which was a difficult problem in the previous DF-PLNC for various modulation and coding techniques. However, decoding at the relay requires a higher complexity and produces a lower data rate.

1.4.3 Amplify-and-Forward Physical Layer Network Coding

Using the AF protocol, the operation at the relay in PLNC-based TWSRNs is much simpler. The relay only amplifies the mix of two signals received from two terminals, and then forwards this amplified version to both terminals. In the AF-PLNC technique, the relay performs processing upon the analog signals received from two terminals, and thus it was also known as analog network coding (ANC) [24]. Similar to the AF protocol for one-way relay

networks, ANC has some advantages and disadvantages. The complexity at the relay using ANC is significantly reduced compared to DF-PLNC techniques. However, the performance and data rate could be affected since the noise at the relay is also amplified and forwarded to both terminals. Additionally, in order to extract the interested signal sent by another terminal from the mixed signal, channel information has to be estimated at both terminals to remove its own signal which is regarded as an interference to the interested signal.

As briefly summarised above, PLNC and DSTC have recently emerged as highly promising techniques to improve either the throughput or the reliability of wireless relay communications. Various cooperative transmission protocols have been designed for a variety of relay channel models based on these two techniques. Inspired by this work, the PLNC and DSTC techniques provide an underlying theory for the research in this thesis. In fact, these two techniques provide the background for the research interest on the improvement of data throughput in wireless relay networks. Specifically, taking into account various relay channel models, ARQ, CQI reporting, ACK, spectrum sensing and diversity coding mechanisms will be designed based on the PLNC and DSTC techniques.

1.5 Thesis Outline

The rest of this thesis is organised as follows. Firstly, Chapter 2 presents the proposed NC-based ARQ retransmission strategies for two-way relay networks and multisource multidestination relay networks to enhance the throughput efficiency and transmission bandwidth of relay communications compared to the non-NC-based schemes. Chapter 3 proposes NC-based CQI reporting schemes for high-throughput two-way relay networks with a reduction of CQI overheads and transmission time slots. In Chapter 4, various block ACK and CR schemes are proposed for relay networks based on NC to achieve a lower error probability of block ACK transmission and reduced number of packets in retransmission for a higher system throughput. Taking into account spec-

trum efficiency in relay networks, CSS schemes are proposed in Chapter 5 to enhance the reliability of spectrum sensing and NC is applied to CSS for a higher system throughput. Furthermore, dealing with the data transmission in cognitive relay networks, Chapter 6 presents the proposed DSTFBC for frequency-selective fading channels to achieve higher data rate, spatial diversity gain and decoupling capability of data blocks with a low-complexity receiver. Finally, Chapter 7 draws conclusions from the thesis and provides discussions for further work.

Chapter 2

NC Based ARQ Retransmission

This chapter investigates various automatic repeat request (ARQ) retransmission protocols for wireless two-way single-relay networks (TWSRNs) and multisource multidestination single-relay networks (MMSRNs) based on implementing network coding (NC).

Firstly, different practical ARQ retransmission protocols are effectively proposed for TWSRNs. The concept of NC is applied to increase the achievable throughput for the exchange of information between two terminals through one relay. Using NC, throughput efficiency is significantly improved due to the reduction of the number of retransmissions. Particularly, two improved NC-based ARQ schemes are designed based on go-back-N and selective-repeat (SR) protocols. The analysis of throughput efficiency is carried out to find the best retransmission strategy for different scenarios. Simulation results are then provided to verify the theoretical analysis.

Secondly, this chapter proposes a new reliable ARQ transmission protocol for MMSRNs over mixed fading channels. Conventional application of ARQ protocols to retransmit lost or erroneous packets in relay networks can cause considerable delay latency with a significant increase in the number of retransmissions when networks consist of multiple sources and multiple destinations. To address this issue, a new efficient ARQ protocol is proposed based on NC, where the relay detects packets from different transmission sources, then uses NC to combine and forward lost packets to their destinations. An effi-

cient means for the retransmission of all lost packets is proposed through two packet-combination algorithms for retransmissions at the relay and sources. Particularly, the chapter derives the mathematical formulation of transmission bandwidth for this new NC-based ARQ protocol and compares analytical and simulation results with some other ARQ protocols over both mixed Rayleigh and Rician flat fading channels. The mixed fading model permits investigation of two typical fading scenarios where the relay is located in the neighbourhood of either the sources or the destinations.

2.1 Introduction

An TWSRN refers to a scenario where two parties want to exchange information with each other with the assistance of a relay. The relay can be used to improve the performance of both transmissions simultaneously. The two-way communications channel was first investigated by Shannon with the derivation of inner and outer bounds on the capacity region [112]. The application of NC to TWSRNs has recently spawned a number of studies, e.g. [22–27]. Specifically, NC was practically applied to TWSRNs using either decode-and-forward or amplify-and-forward relaying protocols [22–25]. The scheduling in NC-based relay networks was then investigated in [26] and the performance of different NC-based protocols was analysed and compared in terms of bit error rate and data rate in [27]. An end node in TWSRNs can decode the signals from another node by XORing its known signal with the combined signals received from the relay.

In addition to the improvement of throughput of relay communications using NC techniques, the reliability of data transmission should be taken into consideration, especially in wireless environments with deep fading and background noise. Basically, reliable information transmission over error-prone channels such as a wireless medium employs a retransmission mechanism via a standard ARQ protocol [113], where, if a packet cannot be decoded, it is discarded and retransmitted. The theoretical limits of ARQ systems in two-way

communications were first investigated by Shannon [112], who demonstrated that acknowledgement feedback could improve the reliability of a memoryless channel at all rates below its capacity although it could not increase the channel capacity. The most common basic schemes of ARQ include stop-and-wait (SW), go-back-N (GBN) and selective repeat (SR). This chapter considers the retransmission schemes for two-way wireless relay networks based on NC. ARQ protocols with NC have been generally studied in [114] and applied to other system models such as broadcast channels in [30] and multicast transmissions in [33]. The principle of NC applied to ARQ schemes is that the sender may XOR the disjoint corrupted packets at different receivers together and retransmit them to all the involving receivers.

ARQ techniques permit information to be reliably delivered over multicast or broadcast networks by repeating the retransmission of the lost packets until all packets are received correctly at each reception node. For relay networks, the design of reliable transmissions over MMSRNs [115] has received little attention in the previous literature. Applying conventional ARQ protocols to MMSRNs may introduce significant packet latency since each packet is retransmitted individually. This motivates to design an efficient ARQ protocol for MMSRNs to achieve high network throughput efficiency and reduced retransmission packet latency, which, to the best of the author's knowledge, has not been investigated.

This chapter firstly considers the retransmission protocol of TWSRNs including two end nodes and a relay node. Different ARQ strategies are evaluated for the comparison between non-NC based schemes and NC-based schemes. The applicability of traditional ARQ protocols such as SW, GBN and SR is also discussed in the context of NC-based two-way relay channel. The information exchange between two end nodes can be divided into two distinct phases: multiple access (MA) phase when two nodes send their data to the relay, and broadcast (BC) phase when the relay broadcasts the combined packet to both nodes. The traditional ARQ approaches can be easily applied to the MA phase because the relay receives signals from end nodes independently.

In the BC phase, the relay XORs the erroneous packets and broadcasts the combined packets to both end nodes. In this phase, the NC-based SW ARQ scheme is firstly studied as the simplest form of ARQ retransmission. Then, in order to obtain the benefits of NC, two improved schemes, namely NC-based GBN ARQ and NC-based SR ARQ, are designed and explained in detail. For comparison purposes, this chapter also analyses the performance of these ARQ systems for NC-based two-way wireless relay networks in terms of throughput efficiency. The simulation results show that improved performance is achieved with the proposed schemes compared with the traditional non-NC retransmission schemes. The theoretical analysis is also shown to be consistent with the numerical throughput efficiency.

Secondly, as an improved solution to the issues of ARQ for MMSRNs, this chapter proposes a new ARQ protocol based on NC for MMSRNs. In this new protocol, the relay detects packets, combines information through NC, and transmits the lost packets from different sources to the destinations. Additionally, to achieve an optimal performance, multi-user detection (MUD) techniques, such as optimum detector, linear decorrelating detector, decision-feedback detector, successive interference cancellation, etc [111, 116–119], are employed at the relay and destinations. Thus along with MUD, lost packets can be combined and retransmitted to achieve an improved ARQ mechanism.

The representation of lost packets in MMSRNs may be categorised into two classification types: Type-I - packets that are successfully received at the relay but lost at the destinations, and Type-II - packets that are lost at both the relay and destinations. Retransmission of Type-II packets is undertaken by the source, but the issue of how the relay retransmits Type-I packets with the lowest number of retransmissions requires to be addressed. To solve this retransmission problem, a relay algorithm and also a source algorithm are proposed to enable retransmission of Type-I and Type-II packets, respectively. As an example of the protocol implementation, a two source, relay, two destination configuration is considered. Specifically, for this scenario, the proposed algorithm employed for retransmission at the relay is based on a combination

of NC and packet detection from the two different sources.

A further contribution of this chapter involves a performance comparison between the proposed NC-based ARQ protocol and other ARQ protocols for MMSRNs. The other protocols considered are the direct transmission (DT)[1] and the relaying transmission (RT)[2] protocols. The performance comparison is achieved through deriving principally the complex analytical expressions of the transmission bandwidth for the new NC-based ARQ protocol and comparing it with the general analytical formulations for the other two protocols. The chapter also extends the analytical performance analysis to include channel fading for the situations when the sources and destinations are located near to, or distant, from the relay. In these scenarios, the links from the sources to the relay, or the links from the relay to the destinations are line-of-sight (LOS) transmissions (close by, Rician fading), or non-line-of-sight (NLOS) transmissions (distant, Rayleigh fading). Accordingly, the considered fading channels are modelled as a mix of both Rayleigh and Rician fading, or are both Rayleigh or Rician fading. It is shown through appropriate analytical and simulation examples, that the proposed ARQ protocol when applied to a two-source two-destination single-relay network, significantly reduces the number of retransmissions for all fading situations and when compared with the DT and RT protocols.

The rest of the chapter is organized as follows: Section 2.2 describes various ARQ strategies of TWSRNs, derives the throughput efficiency for each ARQ retransmission scheme, and presents the numerical results; Section 2.3 describes different retransmission protocols of MMSRNs, derives the transmission bandwidths, and presents the numerical evaluation results; Section 2.4 concludes the chapter.

[1]The DT protocol refers to the model in which multiple sources simultaneously transmit information to the destinations without using the relaying technique.

[2]The RT protocol refers to the model in which the relay participates in the transmission but NC is not employed at the relay.

2.2 ARQ Strategies for Two-Way Single-Relay Networks

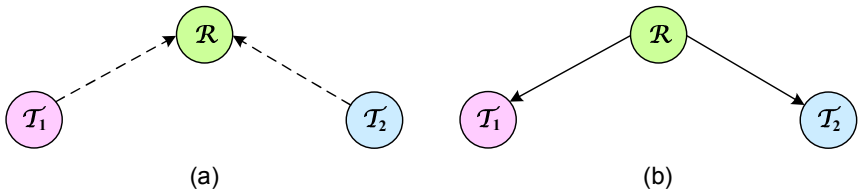

Figure 2.1: Two-way relay channel: (a) MA phase and (b) BC phase.

This section considers a topology with two terminal nodes $\mathcal{T}_i$, $i = 1, 2$, and one relay node $\mathcal{R}$ as shown in Fig. 2.1. The exchange of information between $\mathcal{T}_1$ and $\mathcal{T}_2$ is assisted by applying the conventional NC at $\mathcal{R}$ with the assumption that $\mathcal{T}_1$ cannot communicate directly with $\mathcal{T}_2$. The nodes are assumed to operate in half-duplex mode, i.e. they cannot transmit and receive simultaneously. In NC-based two-way relay networks, the data exchange consists of two consecutive phases: MA phase and BC phase.

First, in the MA phase, $\mathcal{T}_1$ and $\mathcal{T}_2$ send their own packets to $\mathcal{R}$ until the packets are received successfully (at $\mathcal{R}$). When $\mathcal{R}$ detects errors in a packet using error-detecting code (e.g. parity check or cyclic redundancy check), $\mathcal{R}$ requests the corresponding node to retransmit the erroneous packet. In reality, several ARQ retransmission mechanisms were developed for lossy channels such as SW, GBN and SR. The choice of an ARQ scheme depends on the deployment scenario and application. In order to apply NC, the relay has to wait until it receives two correct packets from both nodes $\mathcal{T}_1$ and $\mathcal{T}_2$. Without loss of generality, it is assumed that $\mathcal{T}_1$ and $\mathcal{T}_2$ wish to exchange K packets, denoted by $s_1[i]$ and $s_2[i]$, $i = 0, ..., K-1$, respectively. Two-way relay communications using NC is illustrated in Fig. 2.2. When $\mathcal{R}$ receives and decodes two packets from $\mathcal{T}_1$ and $\mathcal{T}_2$ successfully and separately, it forms a new packet $r[i]$ by XORing the bits of the received packets[3], i.e.

$$r[i] = s_1[i] \oplus s_2[i], i = 0, ..., K-1, \tag{2.1}$$

[3]The packets received at $\mathcal{R}$ are assumed to be perfectly synchronised and scheduled.

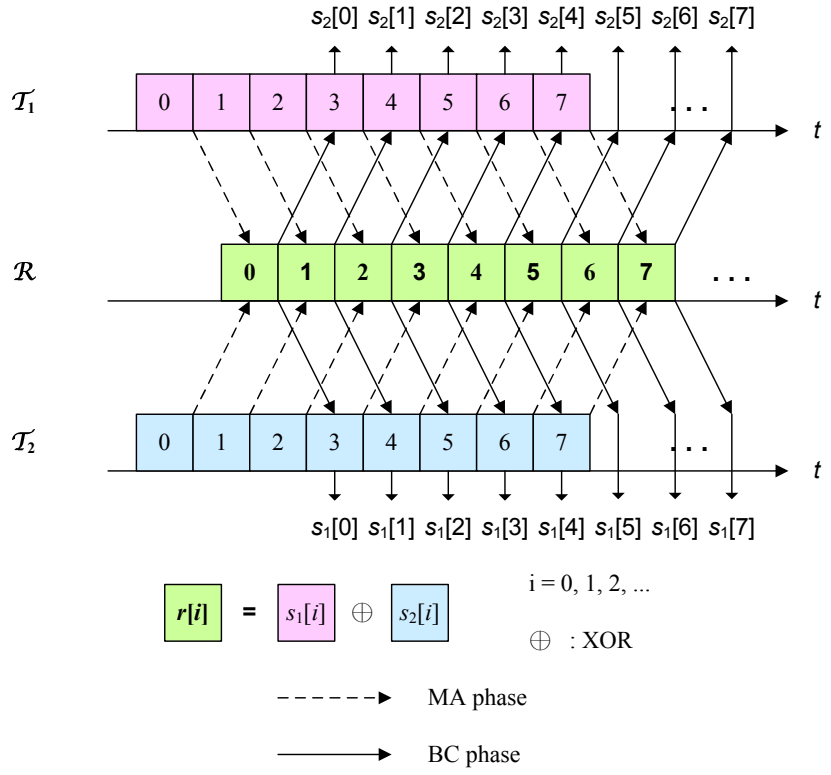

Figure 2.2: Two-way relay channel with NC.

where $\oplus$ denotes the XOR operator.

Then, in the BC phase, the packets $r[i]$, $i = 0, ..., K-1$, are broadcast to both terminal nodes. Assuming successful transmissions in the BC phase, each node extracts its interested packets by XORing $r[i]$ with its own packets, i.e.

$$\hat{s}_2[i] = r[i] \oplus s_1[i], i = 0, ..., K-1, \tag{2.2}$$

$$\hat{s}_1[i] = r[i] \oplus s_2[i], i = 0, ..., K-1. \tag{2.3}$$

When a packet is found to contain errors or is lost at $\mathcal{T}_i$, $\mathcal{R}$ is forced to resend the packet. Suppose $r[0]$ and $r[2]$ are erroneously detected at $\mathcal{T}_1$ and $\mathcal{T}_2$, respectively. The packet number is assumed to be known at all nodes. Without NC, the relay retransmits $r[0]$ to $\mathcal{T}_1$ and $r[2]$ to $\mathcal{T}_2$, one after the other. Thus, the number of retransmissions for $\mathcal{R}$ is two. With NC-based ARQ, $\mathcal{R}$ broadcasts a new packet $r[0] \oplus r[2]$. As a result, it reduces the number of retransmissions to one. The above example demonstrates how NC can increase the bandwidth efficiency. Suppose that the packets with a crossthrough are

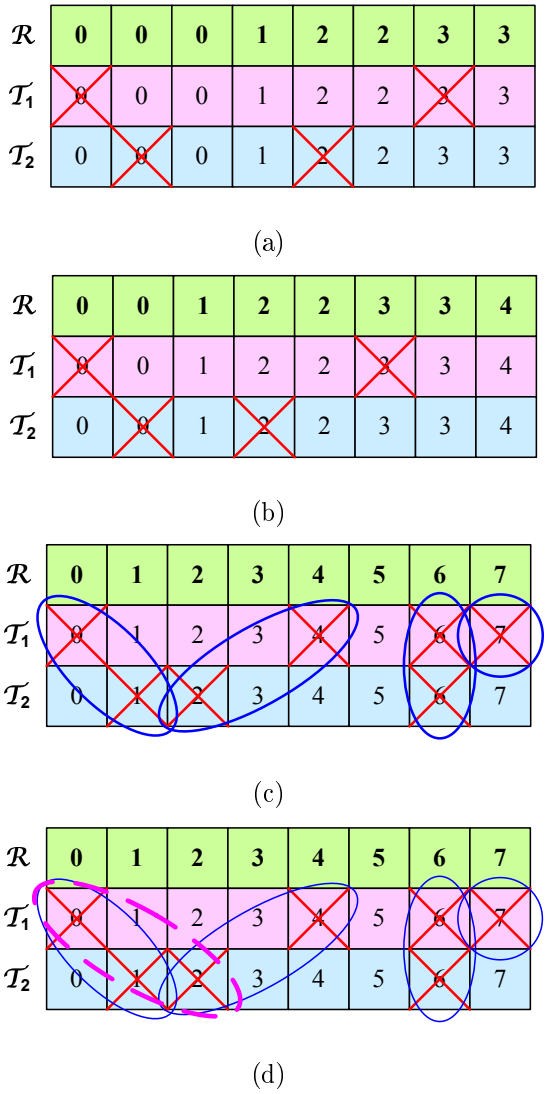

Figure 2.3: BC phase with: (a) Memoryless ARQ, (b) typical ARQ, (c) NC-based ARQ and (d) improved NC-based ARQ.

lost or erroneous. For the comparison of different ARQ protocols with or without NC which can be applied to the BC phase, an example is considered as illustrated in Fig. 2.3 where the lost or erroneous packet is denoted with a crossthrough and four different ARQ schemes are as follows:

- *Memoryless ARQ*: As shown in Fig. 2.3(a), this is the simplest scheme where the relay merely retransmits the combined packet until it receives acknowledgements (ACKs) from two terminals.

- *Typical ARQ*: In this scheme, the relay only retransmits the lost packet

which has not been correctly received in any previous time slot of both terminals. As illustrated in Fig. 2.3(b), this scheme is better than memoryless ARQ scheme in terms of bandwidth usage in the scenario the packet is lost in the current time slot, but it was received correctly in the previous time slot.

- *NC-based ARQ*: Instead of sending immediately the lost packet, the relay in this scheme maintains a list of lost packets and waits until K packets have been received. After that, the relay forms new packets by XORing the lost packets from two terminals and broadcasts these combined packets. Based on the correctly decoded packet, the terminal can recover the lost packet by XORing this correct packet with the XOR packet. If the combined packet is lost, it will be retransmitted until two terminals receive this packet with no error. Fig. 2.3(c) shows an example of this scheme. The lost packets of $\mathcal{T}_1$ and $\mathcal{T}_2$ are $\{r[0], r[4], r[6], r[7]\}$ and $\{r[1], r[2], r[6]\}$, respectively. In the retransmission phase, the combined packets for retransmission are $r[0] \oplus r[1]$, $r[2] \oplus r[4]$, $r[6]$ and $r[7]$. Hence, only 4 packets need to be retransmitted, compared to 5 retransmissions without NC.

- *Improved NC-based ARQ*: A dynamic change of the combined packets based on the correctly received packets at the terminals is considered to improve the throughput efficiency of NC-based ARQ scheme due to the retransmission of the same combined packets. Consider Fig. 2.3(d) with the same lost packets as Fig. 2.3(c) for NC-based retransmission. Suppose that the combined packets $r[0] \oplus r[1]$ and $r[2] \oplus r[4]$ are lost at $\mathcal{T}_1$ and $\mathcal{T}_2$ in the first retransmission, respectively. Thus, $\mathcal{T}_1$ and $\mathcal{T}_2$ cannot recover packet $r[0]$ and $r[2]$, respectively. Instead of retransmitting these two lost combined packets as undertaken by the NC-based ARQ scheme, $\mathcal{R}$ transmits only $r[0] \oplus r[2]$, i.e. 1 retransmission is reduced.

Theoretically, the above ARQ protocols can be applied in the BC phase. However, the latency in the transmission should be considered in practice. In

what follows, different practical ARQ retransmission mechanisms in the BC phase are described in the context of NC.

2.2.1 Scheme A - NC Based Stop-and-Wait ARQ

This is the simplest form of ARQ retransmission strategies. The relay sends one XOR packet at a time and waits for ACKs from both terminals. Scheme A produces a low bandwidth efficiency since the relay does not send any further packets within the waiting period.

2.2.2 Scheme B - Improved NC Based Go-Back-N ARQ

In this scheme, $\mathcal{R}$ maintains a window of N packets (window size) that can be sent continuously without receiving ACKs from $\mathcal{T}_1$ and $\mathcal{T}_2$. With traditional GBN ARQ, the nodes only accept packets in transmission order. If a packet is erroneous at $\mathcal{T}_i$, $\mathcal{T}_i$ will send a non-acknowledgement (NACK) signal to $\mathcal{R}$ and reject all subsequent packets until the missing packet is received. However, in order to get the benefit of NC, an improved NC-based GBN ARQ scheme is developed, where a window is required at both $\mathcal{T}_1$ and $\mathcal{T}_2$. The idea of this window design for both terminals means that if a packet is erroneous at $\mathcal{T}_i$, $\mathcal{T}_i$ will try to receive further packets from $\mathcal{R}$ until it receives a second erroneous packet. When the second error happens, $\mathcal{T}_i$ rejects all subsequent packets. Upon receiving NACKs from $\mathcal{T}_1$ and/or $\mathcal{T}_2$, the relay creates new packets by XORing the erroneous packets and broadcasts these XOR packets. The operation of an NC-Based GBN ARQ is illustrated in Fig. 2.4(a) with a window size of 8 packets. In this example, suppose the packets $\{r[1], r[3], r[6], r[7]\}$ and $\{r[2], r[5], r[6]\}$ are not successfully decoded at $\mathcal{T}_1$ and $\mathcal{T}_2$, respectively. At first, $\mathcal{T}_1$ receives packet $r[1]$ with error, but $\mathcal{T}_2$ receives this packet with no error. Next, $\mathcal{T}_1$ successfully receives $r[2]$ and saves this in its buffer. Since $\mathcal{T}_1$ receives $r[3]$ with error, it ignores all the subsequent packets. At $\mathcal{T}_2$, it receives erroneous $r[2]$. It also tries to receive $r[3]$ and $r[4]$. After that, it ignores all following packets received from $\mathcal{R}$ since $r[5]$ has error. Thus, in the retransmission phase, the

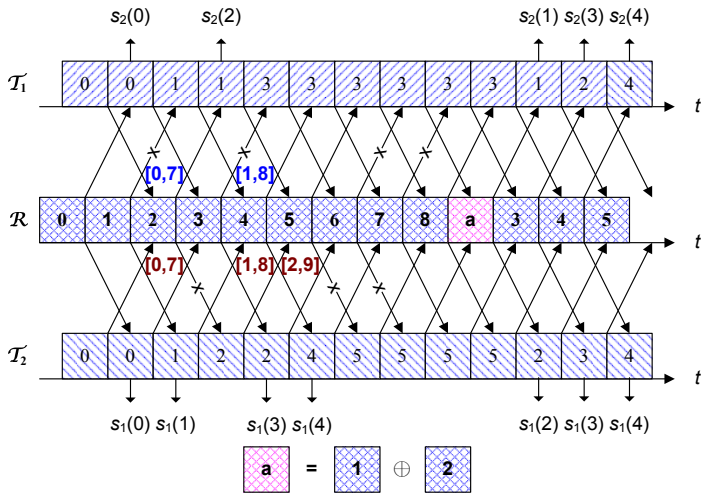

(a)

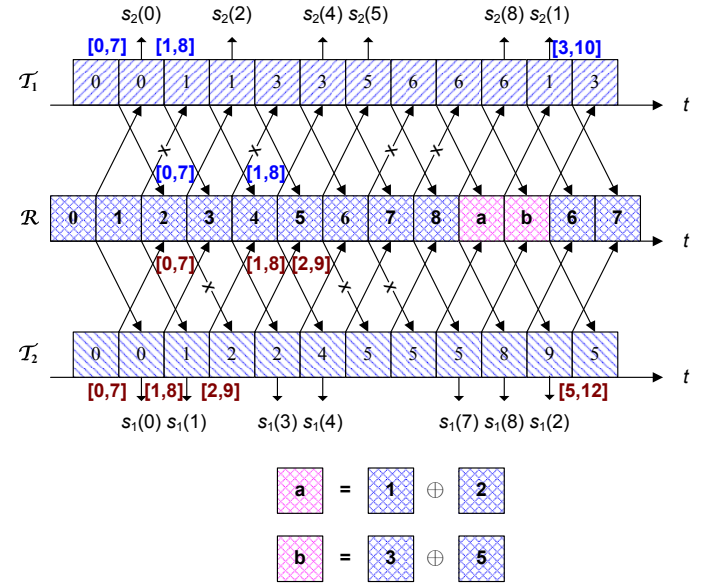

(b)

Figure 2.4: BC phase with: (a) Improved NC-based GBN ARQ and (b) improved NC-based SR ARQ.

sequence of retransmitted packets is $\{a = r[1] \oplus r[2], r[3], r[4], r[5], ...\}$.

2.2.3 Scheme C - Improved NC Based Selective Repeat ARQ

The relay in scheme B re-sends multiple packets when errors or losses occur. Thus, it shows a poor efficiency performance, especially when the packet error

rate (PER) is small. In NC-based SR ARQ, $\mathcal{R}$ continues to send a number of packets in its window even after a packet loss. Each node maintains a receive window of sequence numbers that can be accepted. Only the corrupted packets are retransmitted. Then, the relay continues the transmission sequence where it left off instead of repeating any subsequent correctly received packets. The operation of this scheme is demonstrated in Fig. 2.4(b) by examining a specific example. Similarly, as before, the packets $\{r[1], r[3], r[6], r[7]\}$ and $\{r[2], r[5], r[6]\}$ are assumed to be corrupted at $\mathcal{T}_1$ and $\mathcal{T}_2$, respectively. The window size of all nodes is 8 packets. After the relay empties its window, it re-sends packets $\{a = r[1] \oplus r[2], b = r[3] \oplus r[5], r[6], r[7], r[9], r[10], ...\}$.

2.2.4 Throughput Efficiency Analysis

This subsection studies the throughput efficiency of NC-based two-way relay systems over several ARQ retransmission protocols where throughput efficiency η is defined as the ratio of the total number of data bits to the average number of actual transmitted bits for successful reception.

Scheme A

In the MA phase, the number of transmissions that successfully delivers a packet to the relay $\mathcal{R}$ from the terminal $\mathcal{T}_i$, $i = 1, 2$, follows a geometric distribution with parameter $1 - P_{r_i}$, where P_{r_i} is defined as the PER of the link $\mathcal{T}_i \to \mathcal{R}$. Here, P_{r_i} is calculated by

$$P_{r_i} = 1 - (1 - p_{r_i})^N, \tag{2.4}$$

where p_{r_i} denotes the bit error rate (BER) of the link $\mathcal{T}_i \to \mathcal{R}$ and N is the number of bits in a packet. Thus, the normalised number of transmissions for the MA phase is computed as

$$n_i^{MA} = \frac{1}{1 - P_{r_i}}. \tag{2.5}$$

Define R_{t_i} as the transmission rate in bits-per-second (bps) of each terminal. The required time to transmit one packet of N bits from terminal $\mathcal{T}_i$ to $\mathcal{R}$ using

SW ARQ is given by

$$t_{p_i}^{MA} = \frac{N}{R_{t_i}} + 2(t_{prop} + t_{emis}), \tag{2.6}$$

where t_{prop} [seconds] and t_{emis} [seconds] are defined as propagation and emission delay, respectively, of the transmission from $\mathcal{T}_i$ to $\mathcal{R}$. Thus, the required transmission time of terminal $\mathcal{T}_i$ is

$$t_{r_i}^{MA} = t_{p_i}^{MA} n_i^{MA}. \tag{2.7}$$

In order to apply NC, the relay should wait until it receives successfully data from both terminals, i.e. after $\max\{t_{r_1}^{MA}, t_{r_2}^{MA}\}$. Therefore, the number of bits received at $\mathcal{R}$ is

$$N_{\mathcal{R}} = \max\{R_{t_1} t_{r_1}^{MA}, R_{t_2} t_{r_2}^{MA}\}. \tag{2.8}$$

In the BC phase using scheme A, the number of required transmissions that both terminals simultaneously receive a packet with no error follows a geometric distribution with parameter $(1 - P_{t_1})(1 - P_{t_2})$, where P_{t_i} is defined as the PER of the link $\mathcal{R} \to \mathcal{T}_i$ and is calculated by

$$P_{t_i} = 1 - (1 - p_{t_i})^N, \tag{2.9}$$

where p_{t_i} denotes the BER of the link $\mathcal{R} \to \mathcal{T}_i$. Thus, the normalised number of required transmissions to transmit a correct packet from $\mathcal{R}$ to both $\mathcal{T}_1$ and $\mathcal{T}_2$ is given by

$$n_A^{BC} = \frac{1}{(1 - P_{t_1})(1 - P_{t_2})}. \tag{2.10}$$

With the SW ARQ protocol, the required time to transmit one packet from $\mathcal{R}$ to $\mathcal{T}_i$, $i = 1, 2$, is similarly given by

$$t_{p_A}^{BC} = \frac{N}{R_r} + 2(t_{prop} + t_{emis}), \tag{2.11}$$

where R_r [bps] is the transmission rate of the relay. Thus, the required transmission time of $\mathcal{R}$ is

$$t_{r_A}^{BC} = t_{p_A}^{BC} n_A^{BC}, \tag{2.12}$$

and the number of transmitted bits at $\mathcal{R}$ is

$$N_{\mathcal{T}} = R_r t_{r_A}^{BC}. \tag{2.13}$$

Therefore, the throughput efficiency when using SW ARQ in MA phase and scheme A in BC phase is computed as

$$\begin{aligned}\eta_A &= \frac{2M}{N_{\mathcal{R}} + N_{\mathcal{T}}} \\ &= \frac{2M}{\max\{R_{t_1} t_{p_1}^{MA} n_1^{MA}, R_{t_2} t_{p_2}^{MA} n_2^{MA}\} + R_r t_{p_A}^{BC} n_A^{BC}} \\ &= \frac{2M}{N \max\{\frac{1+\frac{2(t_{prop}+t_{emis})R_{t_1}}{N}}{1-P_{r_1}}, \frac{1+\frac{2(t_{prop}+t_{emis})R_{t_2}}{N}}{1-P_{r_2}}\} + N\frac{1+\frac{2(t_{prop}+t_{emis})R_r}{N}}{(1-P_{t_1})(1-P_{t_2})}},\end{aligned} \tag{2.14}$$

where M is the number of data bits each terminal wants to exchange.

From now on, (2.14) will be used as a general formula of throughput efficiency for other schemes outlined below. It can be observed that M, R_{t_i}, n_i^{MA}, $i = 1, 2$, and R_r are unchanged. Thus, the analysis is simplified to determine $t_{p_i}^{MA}$, n_X^{BC}, and $t_{p_X}^{BC}$ depending on the type of ARQ retransmission protocol X, where $X \in \{A, B, C\}$, in the BC phase.

Scheme B

In the MA phase, when using GBN ARQ, the average time to transmit one packet from terminal $\mathcal{T}_i$ to $\mathcal{R}$ is given by

$$t_{p_i}^{MA} = \frac{N\left(1 + (W_s - 1)P_{r_i}\right)}{R_{t_i}}, \tag{2.15}$$

where W_s denotes the window size indicating the range of packets that the terminal is allowed to transmit.

In the BC phase using improved NC-based ARQ, with sufficiently large buffer size, the normalised number of transmissions to transmit a packet to both terminals can be approximated to the normalised number of transmissions to transmit a packet to the terminal with larger packet error probability [30]. Thus,

$$n_B^{BC} = \frac{1}{1 - \max\{P_{t_1}, P_{t_2}\}}. \tag{2.16}$$

Using GBN ARQ, the average time to transmit one packet from $\mathcal{R}$ to $\mathcal{T}_i$, $i = 1, 2$, is given by

$$t_{p_{B_i}}^{BC} = \frac{N\left(1 + (W_s - 1)P_{t_i}\right)}{R_r}, \tag{2.17}$$

and the average time to transmit one packet from the relay to both terminals is

$$t_{p_B}^{BC} = \max\{t_{p_{B_1}}^{BC}, t_{p_{B_2}}^{BC}\}. \tag{2.18}$$

Therefore, the throughput efficiency is computed as

$$\eta_B = \frac{2M}{N\max\{\frac{1+(W_s-1)P_{r_1}}{1-P_{r_1}}, \frac{1+(W_s-1)P_{r_2}}{1-P_{r_2}}\} + N\frac{1+(W_s-1)\max\{P_{t_1},P_{t_2}\}}{1-\max\{P_{t_1},P_{t_2}\}}}. \tag{2.19}$$

Scheme C

In the MA phase, when using SR ARQ, the average time to transmit one packet from terminal $\mathcal{T}_i$ to $\mathcal{R}$ is given by

$$t_{p_i}^{MA} = \frac{N}{R_{t_i}}. \tag{2.20}$$

In the BC phase, with improved NC-based ARQ protocol, n_C^{BC} is similarly given by (2.16).

Using SR ARQ, the average time $t_{p_{C_i}}^{BC}$ to transmit one packet from $\mathcal{R}$ to $\mathcal{T}_i$, $i = 1, 2$, is given by

$$t_{p_{C_i}}^{BC} = \frac{N}{R_r}, \tag{2.21}$$

with the average time to transmit one packet from the relay to both terminals given by

$$t_{p_C}^{BC} = t_{p_{C_i}}^{BC}, i = 1, 2. \tag{2.22}$$

Therefore, the throughput efficiency is computed as

$$\eta_C = \frac{2M}{N\max\{\frac{1}{1-P_{r_1}}, \frac{1}{1-P_{r_2}}\} + \frac{N}{1-\max\{P_{t_1},P_{t_2}\}}}. \tag{2.23}$$

Remark 2.1. *Scheme C achieves the highest throughput efficiency whilst that of scheme A is the lowest. For the comparison, it is assumed that*

$$\begin{aligned}\frac{2(t_{prop} + t_{emis})R_{t_1}}{N} &\approx \frac{2(t_{prop} + t_{emis})R_{t_2}}{N} \\ &\approx \frac{2(t_{prop} + t_{emis})R_r}{N} \approx W_s - 1.\end{aligned}$$

From (2.14) *and* (2.19), *it can be seen that* $\eta_B > \eta_A$ *since* $(W_s - 1)P_{r_i} < \frac{2(t_{prop}+t_{emis})R_{t_i}}{N}, i = 1, 2$, $(W_s - 1)\max\{P_{t_1}, P_{t_2}\} < W_s - 1 = \frac{2(t_{prop}+t_{emis})R_r}{N}$, *and* $1 - \max\{P_{t_1}, P_{t_2}\} > (1 - P_{t_1})(1 - P_{t_2})$. *Similarly, from* (2.23) *and* (2.19), *it can also be observed that* $\eta_C > \eta_B$ *since* $W_s > 1$. *Thus,*

$$\eta_C > \eta_B > \eta_A. \tag{2.24}$$

Remark 2.2. *While schemes B and C require a higher computational complexity at the relay node due to NC operation in the retransmission and a buffer window of size* W_s *at all nodes, scheme A is the simplest ARQ strategy with no computation at the relay and only one packet in the buffer of all nodes. Specifically,* N *additional XOR operations are required for each combination in schemes B and C since each packet includes* N *bits.*

2.2.5 Numerical and Simulation Results

In this subsection, simulation results of throughput efficiency for different ARQ schemes in different phases - MA phase, BC phase and the whole system - are shown in Figs. 2.5, 2.6 and 2.7, respectively. The results are obtained by using Monte Carlo simulation in MATLAB. The packet size is assumed to be 1024 bits, including 1000 data bits and 24 error checking bits, i.e. $N = 1024$ and $M = 1000$. For simplicity, uncoded signal transmissions are considered[4]. The expression $[2(t_{prop} + t_{emis})R_{t_i}]/N$, $i = 1, 2$, is assumed to be equal to $(W_s - 1)$. The maximum number of packets that a terminal is allowed to transmit (i.e. window size W_s) is set to be 10 packets.

Fig. 2.5 shows the simulation and theoretical results of throughput efficiency as a function of BER in the MA phase with SW, GBN and SR ARQ retransmission schemes. In this phase, NC is not applied in the retransmission. The BERs of the MA links from the source to the relay are set to be equal to each other, i.e. $p_{r_1} = p_{r_2} = \text{BER}$. It can be observed that with the same parameters in good channel conditions (i.e. low BER), the throughput

[4]Note that channel coding with hybrid ARQ can be adapted for reliable data packet transmissions, which would result in different forms of the throughput efficiency.

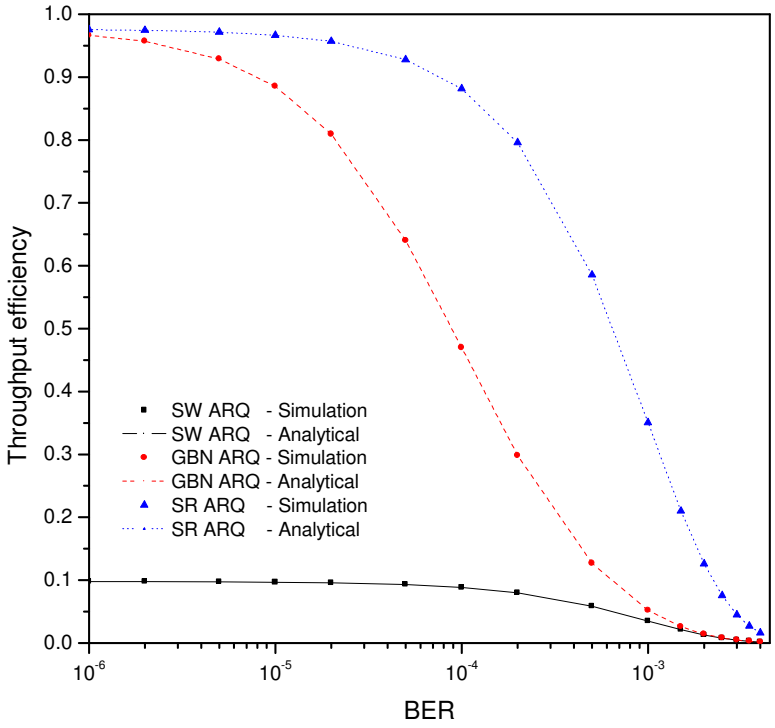

Figure 2.5: Throughput efficiency of MA phase.

efficiency of the SR ARQ protocol is always higher than that of the GBN ARQ protocol. Further, both protocols outperform the SW ARQ protocol. For example, when BER $= 10^{-4}$, the throughput efficiency achieved with SR, GBN and SW ARQ protocols are 0.9, 0.45 and 0.1, respectively. Additionally, the simulation results show that they are consistent with the theoretical analysis.

Fig. 2.6 shows the results of throughput efficiency in the BC phase of the proposed schemes and traditional non-NC schemes. For convenience, the BERs of the two terminal nodes are set to be equal to each other, i.e. $p_{t_1} = p_{t_2} = \text{BER}$. It can be observed that the throughput efficiency of the improved NC-based SR ARQ is higher than that of the improved NC-based GBN ARQ and again these two protocols outperform the SW ARQ protocol. With NC, the proposed schemes are shown to be better than the traditional non-NC schemes for all ARQ retransmission protocols in terms of throughput efficiency due to the reduction in the number of retransmissions. For example, when BER $= 10^{-4}$, 0.02, 0.05 and 0.1 of throughput efficiency are improved with the proposed schemes A, B and C, respectively. The simulation and theoretical results again

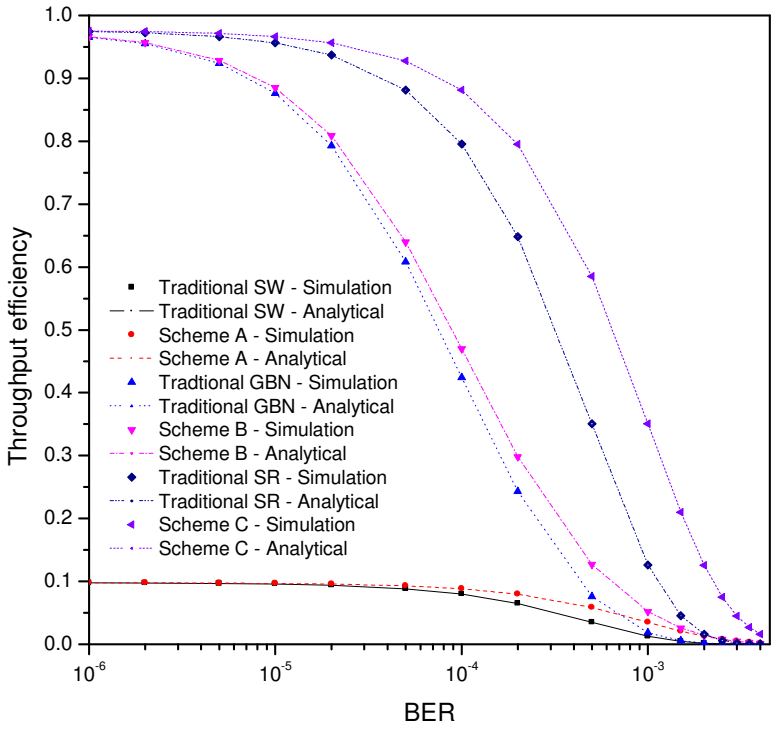

Figure 2.6: Throughput efficiency of BC phase.

prove to be consistently matched.

Fig. 2.7 shows the results of throughput efficiency when considering the whole system (i.e. including both MA and BC phases). The observation is quite similar to the scenario of the BC phase when the retransmission techniques and ARQ protocols in the BC phase are combined with ARQ protocols in the MA phase. This also confirms the relationship (2.24) in Remark 2.1.

In summary, through theoretical and simulation results, it can be observed that higher throughput efficiency is achieved with improved techniques based on NC. However, there is a trade-off between the throughput efficiency and the complexity due to the requirement of buffer size and the NC process.

2.3 ARQ Strategies for Multisource Multidestination Single-Relay Networks

Consider the MMSRN displayed in Fig. 2.8 where data transmitted from two sources $\mathcal{S}_1$ and $\mathcal{S}_2$ to two destinations $\mathcal{D}_1$ and $\mathcal{D}_2$ is assisted by one relay $\mathcal{R}$.

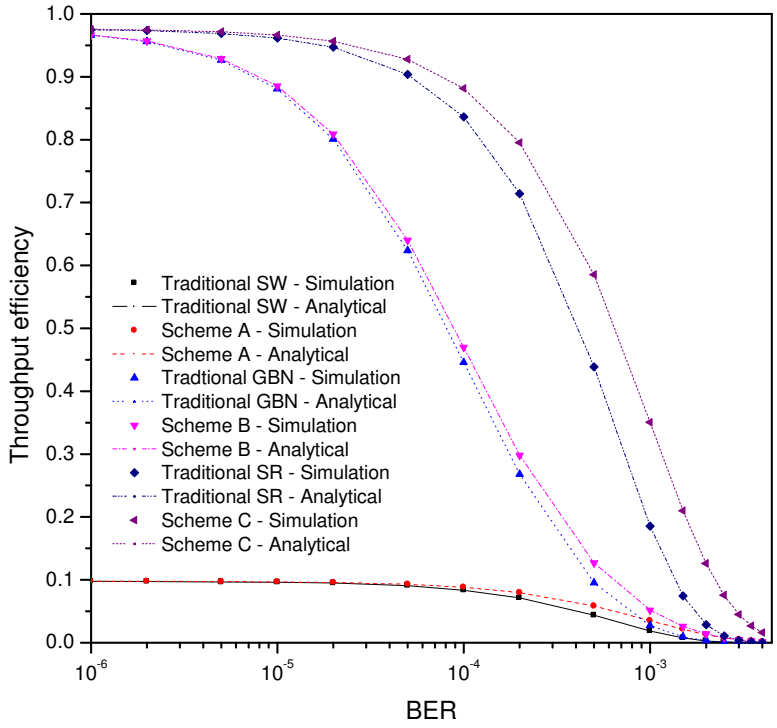

Figure 2.7: Throughput efficiency of two-way relay network considering both MA and BC phase.

Increasing the number of sources and destinations to the model is straightforward. The sources are able to send data packets which must be received without error after a number of transmissions and retransmissions. It is also assumed that the channel link $\mathcal{A} \rightarrow \mathcal{B}$ (where $\mathcal{A} \in \{\mathcal{S}_1, \mathcal{S}_2, \mathcal{R}\}$, $\mathcal{B} \in \{\mathcal{R}, \mathcal{D}_1, \mathcal{D}_2\}$, $\mathcal{A} \neq \mathcal{B}$) is characterised by either Rayleigh or Rician flat fading with a channel gain of $h_{\mathcal{AB}}$.

$\mathcal{R}$ receives data packets from $\mathcal{S}_1$ and $\mathcal{S}_2$ in addition to feedback from $\mathcal{D}_1$ and $\mathcal{D}_2$, thus $\mathcal{R}$ has knowledge of the destinations still waiting for retransmission of lost packets. $\mathcal{R}$ then decides how to combine and forward the data to the intended destinations. The purpose of any retransmission protocol is to facilitate $\mathcal{R}$ in resending the lost packets to $\mathcal{D}_1$ and $\mathcal{D}_2$.

The three retransmission protocols considered for MMSRNs will now be described.

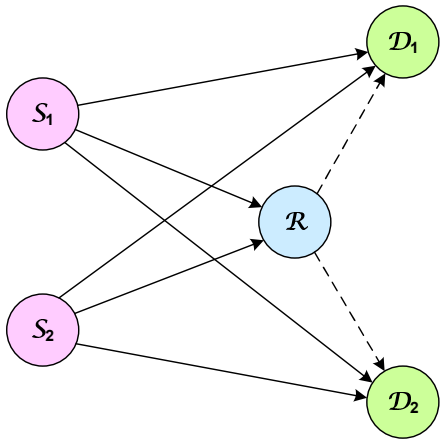

Figure 2.8: Multisource multidestination single-relay network model.

2.3.1 DT Protocol

In the DT protocol, $\mathcal{S}_1$ and $\mathcal{S}_2$ transmit data directly to $\mathcal{D}_1$ and $\mathcal{D}_2$. The transmission employs ARQ and is completed when both $\mathcal{D}_1$ and $\mathcal{D}_2$ receive correctly the data packets from both $\mathcal{S}_1$ and $\mathcal{S}_2$.

2.3.2 RT Protocol

The RT protocol differs from the DT protocol because $\mathcal{R}$ now participates in the transmission process. When $\mathcal{D}_j$, $j = 1, 2$, does not receive a packet from $\mathcal{S}_i$, $i = 1, 2$, but $\mathcal{R}$ successfully receives the packet, $\mathcal{R}$ can assist $\mathcal{S}_i$ by forwarding the correctly received packet to $\mathcal{D}_j$ in the next transmission time slot. Using ARQ, retransmissions at $\mathcal{R}$ continue until the transmitted packet is correctly received by $\mathcal{D}_j$. If $\mathcal{D}_j$ and $\mathcal{R}$ do not receive the same packet from $\mathcal{S}_i$, then $\mathcal{S}_i$ resends the lost packet.

2.3.3 NC-based Protocol

Rather than resending the lost packet when $\mathcal{D}_j$, $j = 1, 2$, fails to receive it, the retransmission in the proposed NC-based ARQ protocol will retransmit after N received packets. A buffer length of N packets is necessary at $\mathcal{S}_i$, $i = 1, 2$, whilst buffers of size $2N$ are required at $\mathcal{R}$ and $\mathcal{D}_j$ since packets are received from two different sources. To improve network throughput, $\mathcal{R}$ retransmits

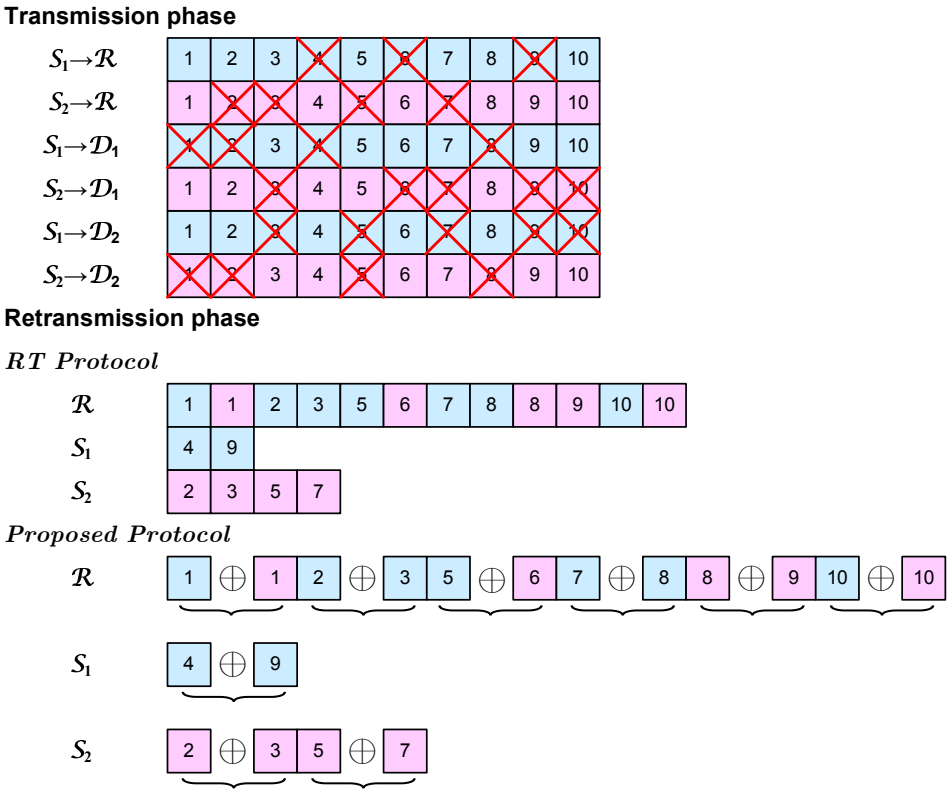

Figure 2.9: Retransmission packets with RT and the new NC-based ARQ protocol.

packets of Type-I, and $\mathcal{S}_i$ organises retransmission of Type-II packets. The distinctiveness and novelty in the proposed ARQ protocol is that $\mathcal{R}$ can mix information from packets received through the two network data flows.

The following packet transmission example outlines the principles of the protocol (see Fig. 2.9). $\mathcal{S}_i$ delivers $N = 10$ packets $\{s_i[1], s_i[2], \ldots, s_i[10]\}$ to both $\mathcal{D}_1$ and $\mathcal{D}_2$. In Fig. 2.9, the packets which are crossed through are considered lost or erroneously received packets. For data flow from $\mathcal{S}_1$, consider the received packets in error at $\mathcal{R}$, $\mathcal{D}_1$ and $\mathcal{D}_2$ as $\{s_1[4], s_1[6], s_1[9]\}$, $\{s_1[1], s_1[2], s_1[4], s_1[8]\}$ and $\{s_1[3], s_1[5], s_1[7], s_1[9], s_1[10]\}$, respectively. Similarly, assume that the received packets which are in error at $\mathcal{R}$, $\mathcal{D}_1$ and $\mathcal{D}_2$ arriving from $\mathcal{S}_2$ are $\{s_2[2], s_2[3], s_2[5], s_2[7]\}$, $\{s_2[3], s_2[6], s_2[7], s_2[9], s_2[10]\}$ and $\{s_2[1], s_2[2], s_2[5], s_2[8]\}$, respectively.

As shown in Fig. 2.9, $\mathcal{R}$ will retransmit 12 packets using the RT protocol. For packets lost at $\mathcal{R}$ and also lost at $\mathcal{D}_1$ and/or $\mathcal{D}_2$, i.e. $\{s_1[4], s_1[9], s_2[2],$

$s_2[3]$, $s_2[5]$, $s_2[7]\}$, $\mathcal{S}_1$ and $\mathcal{S}_2$ will retransmit $\{s_1[4]$, $s_1[9]\}$ and $\{s_2[2]$, $s_2[3]$, $s_2[5]$, $s_2[7]\}$, respectively. In total 18 retransmissions are required for the RT protocol.

Now compare the NC-based ARQ protocol. In this case, a significant reduction in retransmission of lost packets is possible. For example, packets $\{s_1[1]$, $s_2[1]$, $s_1[2]$, $s_1[3]$, $s_1[5]$, $s_2[6]$, $s_1[7]$, $s_1[8]$, $s_2[8]$, $s_2[9]$, $s_1[10]$, $s_2[10]\}$ are classed as Type-I packets and $\{s_1[4]$, $s_1[9]$, $s_2[2]$, $s_2[3]$, $s_2[5]$, $s_2[7]\}$ are Type-II packets. In this scheme, to improve network throughput, in the retransmission phase, $\mathcal{R}$ forwards $\{s_1[1] \oplus s_2[1]$, $s_1[2] \oplus s_1[3]$, $s_1[5] \oplus s_2[6]$, $s_1[7] \oplus s_1[8]$, $s_2[8] \oplus s_2[9]$, $s_1[10] \oplus s_2[10]\}$, whilst, $\mathcal{S}_1$ and $\mathcal{S}_2$ retransmit $\{s_1[4] \oplus s_1[9]\}$ and $\{s_2[2] \oplus s_2[3]$, $s_2[5] \oplus s_2[7]\}$, respectively, where $\oplus$ denotes the bitwise XOR operator.

In total, the proposed NC-based ARQ scheme requires only 9 retransmissions, compared to 18 when deploying the RT scheme. $\mathcal{R}$, $\mathcal{S}_1$ and $\mathcal{S}_2$ will retransmit these 9 packets until all are successfully received at both $\mathcal{D}_1$ and $\mathcal{D}_2$. The lost packets at $\mathcal{D}_j$, $j = 1, 2$, may be recovered through the standard method of XORing the correctly received packets located at $\mathcal{D}_j$ with the XORed packets received from either $\mathcal{R}$ or $\mathcal{S}_i$.

The generalization of the above example for an arbitrary buffer size is summarized in Fig. 2.10. A summary of the NC combination algorithms at $\mathcal{R}$ and $\mathcal{S}_i$, $i = 1, 2$, are described in Tables 2.1 and 2.2, respectively.

2.3.4 Transmission Bandwidth Analysis

In this subsection, the transmission bandwidth[5] of the three protocols discussed above is derived for the scenarios of mixed Rayleigh and Rician flat fading channels for the MMSRNs as described in Fig. 2.8.

When a channel is affected by fading, the signal $\mathbf{y}_{\mathcal{AB}}$ received at any node $\mathcal{B}$ when transmitted from any node $\mathcal{A}$, where $\{\mathcal{A}, \mathcal{B}\} \in \{\mathcal{S}_1, \mathcal{S}_2, \mathcal{R}, \mathcal{D}_1, \mathcal{D}_2\}$,

[5]Transmission bandwidth is defined as the normalised number of transmissions to successfully transmit two packets from two sources to two destinations.

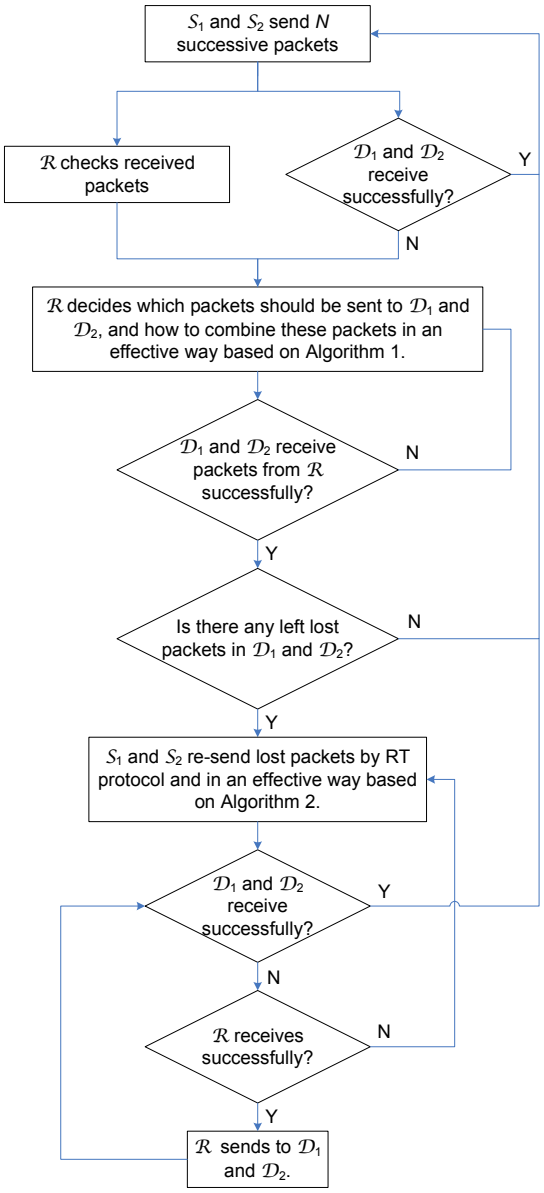

Figure 2.10: Block diagram of proposed protocol.

$\mathcal{A} \neq \mathcal{B}$, can be expressed through

$$\mathbf{y}_{\mathcal{AB}} = \sqrt{\Gamma_{\mathcal{AB}}} h_{\mathcal{AB}} \mathbf{x}_{\mathcal{AB}} + \mathbf{n}_{\mathcal{AB}}, \tag{2.25}$$

where $\Gamma_{\mathcal{AB}}$ describes the long-term fading (i.e. path loss and shadowing) within the transmission link $\mathcal{A} \rightarrow \mathcal{B}$, $h_{\mathcal{AB}}$ is the fading channel, $\mathbf{x}_{\mathcal{AB}}$ is the binary phase shift keying (BPSK) modulated signal of the transmitted packet, and $\mathbf{n}_{\mathcal{AB}}$ is the channel noise. This noise can be considered as an independent circularly symmetric complex Gaussian (CSCG) noise vector with each entry having zero mean and noise variance denoted by N_0. For the situation where

Table 2.1: Combination algorithm at $\mathcal{R}$ to retransmit Type-I packets

1. Let $\mathfrak{G}_1$ and $\mathfrak{G}_2$ denote the ordered sets of correctly received packets at $\mathcal{R}$ transmitted from $\mathcal{S}_1$ and $\mathcal{S}_2$, respectively:
$\mathfrak{G}_1 = \{s_1[i_1], s_1[i_2], \ldots, s_1[i_m]\}$, where $i_1 < i_2 < \cdots < i_m \in \{1, 2, \ldots, N\}$,
$\mathfrak{G}_2 = \{s_2[j_1], s_2[j_2], \ldots, s_2[j_n]\}$, where $j_1 < j_2 < \cdots < j_n \in \{1, 2, \ldots, N\}$.
Define $\Omega = \mathfrak{G}_1 \cup \mathfrak{G}_2$ and divide Ω into 3 groups as follows:
- Group Ω_1 includes packets that $\mathcal{R}$ receives successfully from both $\mathcal{S}_1$ and $\mathcal{S}_2$.
- Group Ω_2 includes packets that $\mathcal{R}$ receives successfully from $\mathcal{S}_1$ but fails to receive from $\mathcal{S}_2$.
- Group Ω_3 includes packets that $\mathcal{R}$ receives successfully from $\mathcal{S}_2$ but fails to receive from $\mathcal{S}_1$.
2. For packets in Ω_1, if one packet is received correctly at $\mathcal{D}_1$ but lost at $\mathcal{D}_2$, while another packet is received correctly at $\mathcal{D}_2$ but lost at $\mathcal{D}_1$, these two packets can be combined. Start from left to right in the group of packets in Ω_1, and choose the suitable XOR combination of packets.
3. For packets in Ω_2 and Ω_3, similarly if one packet is received correctly at $\mathcal{D}_1$ but lost at $\mathcal{D}_2$, while another packet is received correctly at $\mathcal{D}_2$ but lost at $\mathcal{D}_1$, these two packets can be combined.
4. For the remaining lost packets at $\mathcal{D}_1$ and $\mathcal{D}_2$ that $\mathcal{R}$ receives successfully but cannot perform the combination, these are normally resent without using NC.

Rayleigh fading is considered, the BER of the signal transmission through link $\mathcal{A} \to \mathcal{B}$ is expressed by [120]

$$P_b^{(\text{Rayleigh})}(E_{\mathcal{AB}}) = \frac{1}{2}\left(1 - \sqrt{\frac{\gamma_{\mathcal{AB}}}{1+\gamma_{\mathcal{AB}}}}\right), \tag{2.26}$$

where $\gamma_{\mathcal{AB}}$ is the average signal-to-noise ratio (SNR) defined through $\gamma_{\mathcal{AB}} = \Gamma_{\mathcal{AB}}/N_0$.

For the case of Rician fading channels with Rician fading parameter $\mathcal{K}_{AB}$,

Table 2.2: Combination algorithm at $\mathcal{S}_i$ to retransmit Type-II packets

1. Through feedback from $\mathcal{D}_1$, $\mathcal{D}_2$ and $\mathcal{R}$, $\mathcal{S}_i$ determines the number and the position of the remaining lost packets at destinations that $\mathcal{R}$ also fails to receive the packets.
2. Combine the packets for retransmission by NC with the condition that only one packet in the combined packet should be received correctly by only one destination, similar to the combination performed for packets in Ω_2 and Ω_3 as explained in Table 2.1.
3. For the remaining lost packets at $\mathcal{D}_1$ and $\mathcal{D}_2$ that $\mathcal{S}_i$ cannot perform the combination, these are resent without NC.

the BER of the transmission through link $\mathcal{A} \rightarrow \mathcal{B}$ is expressed through [120]

$$P_b^{(\text{Rician})}(E_{\mathcal{AB}}) = \frac{1}{\pi}\int_0^{\frac{\pi}{2}} \frac{(1+\mathcal{K}_{AB})\sin^2\theta}{(1+\mathcal{K}_{AB})\sin^2\theta + \gamma_{\mathcal{AB}}} \times \exp\left(-\frac{\mathcal{K}_{AB}\gamma_{\mathcal{AB}}}{(1+\mathcal{K}_{AB})\sin^2\theta + \gamma_{\mathcal{AB}}}\right) d\theta. \tag{2.27}$$

Thus, for any specified SNR, the packet loss of the transmission link $\mathcal{A} \rightarrow \mathcal{B}$ can be calculated by

$$P_{\mathcal{AB}} = 1 - [1 - P_b(E_{\mathcal{AB}})]^{N_b}, \tag{2.28}$$

where N_b is the number of bits in a packet and $P_b(E_{\mathcal{AB}})$ is denoted either by Eq. (2.26) or (2.27) depending on the fading channel model adopted.

The transmission bandwidth will now be evaluated for each of the three protocols.

DT Protocol

When $\mathcal{R}$ is omitted from the network and NC not considered, the DT protocol transmission bandwidth, n_{DT}, may be expressed by

$$n_{DT} = \max\{n_{DT}^{(\mathcal{S}_1)}, n_{DT}^{(\mathcal{S}_2)}\}, \tag{2.29}$$

where $n_{DT}^{(\mathcal{S}_i)}$, $i = 1, 2$, denotes the transmission bandwidth required for $\mathcal{S}_i$ to send a packet to both $\mathcal{D}_1$ and $\mathcal{D}_2$, and is easily evaluated as

$$n_{DT}^{(\mathcal{S}_i)} = \frac{1}{1 - P_{\mathcal{S}_i\mathcal{D}_1}} + \frac{1}{1 - P_{\mathcal{S}_i\mathcal{D}_2}} - \frac{1}{1 - P_{\mathcal{S}_i\mathcal{D}_1}P_{\mathcal{S}_i\mathcal{D}_2}}. \tag{2.30}$$

RT Protocol

Including $\mathcal{R}$ in the network and still omitting NC, transmission bandwidth for successfully transmitting two packets from $\mathcal{S}_1$ and $\mathcal{S}_2$ to $\mathcal{D}_i$, $i = 1, 2$, is given by

$$\begin{aligned} n_{RT}^{(\mathcal{D}_i)} =& \frac{1}{1 - P_{\mathcal{S}_1\mathcal{R}}P_{\mathcal{S}_2\mathcal{R}}P_{\mathcal{S}_1\mathcal{D}_i}P_{\mathcal{S}_2\mathcal{D}_i}}[1 + P_{\mathcal{S}_1\mathcal{R}}P_{\mathcal{S}_1\mathcal{D}_i}(1 - P_{\mathcal{S}_2\mathcal{D}_i})n_{RT}^{(\mathcal{S}_1,\mathcal{D}_i)} \\ &+ P_{\mathcal{S}_2\mathcal{R}}(1 - P_{\mathcal{S}_1\mathcal{D}_i})P_{\mathcal{S}_2\mathcal{D}_i}n_{RT}^{(\mathcal{S}_2,\mathcal{D}_i)} \\ &+ (1 - P_{\mathcal{S}_1\mathcal{R}})P_{\mathcal{S}_1\mathcal{D}_i}(1 - P_{\mathcal{S}_2\mathcal{D}_i})n_{\mathcal{R}\mathcal{D}_i} \\ &+ (1 - P_{\mathcal{S}_2\mathcal{R}})(1 - P_{\mathcal{S}_1\mathcal{D}_i})P_{\mathcal{S}_2\mathcal{D}_i}n_{\mathcal{R}\mathcal{D}_i} \\ &+ 2(1 - P_{\mathcal{S}_1\mathcal{R}})(1 - P_{\mathcal{S}_2\mathcal{R}})P_{\mathcal{S}_1\mathcal{D}_i}P_{\mathcal{S}_2\mathcal{D}_i}n_{\mathcal{R}\mathcal{D}_i} \\ &+ (1 - P_{\mathcal{S}_1\mathcal{R}})P_{\mathcal{S}_2\mathcal{R}}P_{\mathcal{S}_1\mathcal{D}_i}P_{\mathcal{S}_2\mathcal{D}_i}(n_{\mathcal{R}\mathcal{D}_i} + n_{RT}^{(\mathcal{S}_2,\mathcal{D}_i)}) \\ &+ P_{\mathcal{S}_1\mathcal{R}}(1 - P_{\mathcal{S}_2\mathcal{R}})P_{\mathcal{S}_1\mathcal{D}_i}P_{\mathcal{S}_2\mathcal{D}_i}(n_{\mathcal{R}\mathcal{D}_i} + n_{RT}^{(\mathcal{S}_1,\mathcal{D}_i)})], \end{aligned} \tag{2.31}$$

where $n_{\mathcal{R}\mathcal{D}_i}$ and $n_{RT}^{(\mathcal{S}_i,\mathcal{D}_j)}$ denote the transmission bandwidths of a packet from $\mathcal{R}$ to $\mathcal{D}_i$ and from $\mathcal{S}_i$ to $\mathcal{D}_j$ with the assistance of $\mathcal{R}$, respectively. Thus, $n_{\mathcal{R}\mathcal{D}_i}$ and $n_{RT}^{(\mathcal{S}_i,\mathcal{D}_j)}$ may be computed respectively through

$$n_{\mathcal{R}\mathcal{D}_i} = \frac{1}{1 - P_{\mathcal{R}\mathcal{D}_i}}, \tag{2.32}$$

$$n_{RT}^{(\mathcal{S}_i,\mathcal{D}_j)} = \frac{1 + P_{\mathcal{R}\mathcal{D}_j} + P_{\mathcal{S}_i\mathcal{D}_j}(1 - P_{\mathcal{S}_i\mathcal{R}})}{(1 - P_{\mathcal{S}_i\mathcal{R}}P_{\mathcal{S}_i\mathcal{D}_j})(1 - P_{\mathcal{R}\mathcal{D}_j})}. \tag{2.33}$$

The transmission bandwidth of the RT protocol is therefore given by

$$n_{RT} = \max\{n_{RT}^{(\mathcal{D}_1)}, n_{RT}^{(\mathcal{D}_2)}\}. \tag{2.34}$$

Proposed NC Based Protocol

In the proposed NC-based protocol, $\mathcal{R}$ combines lost packets from the two different packet flows. Since a total of $2N$ packets are transmitted from $\mathcal{S}_1$

and $\mathcal{S}_2$, the transmission bandwidth n_{NC} is expressed as

$$n_{NC} = \frac{n^{(1)} + n^{(2)} + n^{(3)}}{2N}, \tag{2.35}$$

where $n^{(i)}$, $i = 1, 2, 3$, denotes the transmission bandwidth in the i-th step of the proposed protocol. These steps include the following:

- Step 1. Both $\mathcal{S}_1$ and $\mathcal{S}_2$ transmit N packets.
- Step 2. $\mathcal{R}$ retransmits Type-I packets.
- Step 3. $\mathcal{S}_1$ and/or $\mathcal{S}_2$ retransmit Type-II packets.

It is obvious that $n^{(1)} = 2N$. Following the proposed algorithms in Tables 2.1 and 2.2 for the retransmissions at $\mathcal{R}$ and $\mathcal{S}_i$, $i = 1, 2$, $n^{(2)}$ and $n^{(3)}$ can be computed by

$$\begin{aligned} n^{(2)} =& \sum_{k=0}^{N} \{C_k^N P_{\mathcal{S}_1\mathcal{R}}^{N-k} (1 - P_{\mathcal{S}_1\mathcal{R}})^k P_{\mathcal{S}_2\mathcal{R}}^{N-k} (1 - P_{\mathcal{S}_2\mathcal{R}})^k E[n^{(2)}|K = k] \\ &+ \sum_{l=0}^{N-k} \{C_l^{N-k} P_{\mathcal{S}_1\mathcal{R}}^{N-k-l} (1-P_{\mathcal{S}_1\mathcal{R}})^l P_{\mathcal{S}_2\mathcal{R}}^{l} (1-P_{\mathcal{S}_2\mathcal{R}})^{N-k-l} E[n^{(2)}|L = l] \\ &+ \sum_{m=0}^{N-k-l} \{C_m^{N-k-l} P_{\mathcal{S}_1\mathcal{R}}^{m} (1 - P_{\mathcal{S}_1\mathcal{R}})^{N-k-l-m} \\ &\quad \times P_{\mathcal{S}_2\mathcal{R}}^{N-k-l-m} (1 - P_{\mathcal{S}_2\mathcal{R}})^m E[n^{(2)}|M = m]\}\}, \end{aligned} \tag{2.36}$$

$$\begin{aligned} n^{(3)} =& \sum_{k=0}^{N} \{C_k^N P_{\mathcal{S}_1\mathcal{R}}^{N-k} (1 - P_{\mathcal{S}_1\mathcal{R}})^k P_{\mathcal{S}_2\mathcal{R}}^{N-k} (1 - P_{\mathcal{S}_2\mathcal{R}})^k E[n^{(3)}|K = k] \\ &+ \sum_{l=0}^{N-k} \{C_l^{N-k} P_{\mathcal{S}_1\mathcal{R}}^{N-k-l} (1-P_{\mathcal{S}_1\mathcal{R}})^l P_{\mathcal{S}_2\mathcal{R}}^{l} (1-P_{\mathcal{S}_2\mathcal{R}})^{N-k-l} E[n^{(3)}|L = l] \\ &+ \sum_{m=0}^{N-k-l} \{C_m^{N-k-l} P_{\mathcal{S}_1\mathcal{R}}^{m} (1 - P_{\mathcal{S}_1\mathcal{R}})^{N-k-l-m} \\ &\quad \times P_{\mathcal{S}_2\mathcal{R}}^{N-k-l-m} (1 - P_{\mathcal{S}_2\mathcal{R}})^m E[n^{(3)}|M = m]\}\}, \end{aligned} \tag{2.37}$$

where $E[.]$ denotes the expectation value and $C_k^N = N!/k!/(N-k)!$ represents the total number of subsets consisting of k elements in a set of N elements. Here, K, L and M denote three random variables used to represent the numbers of packets that $\mathcal{R}$ successfully receives in groups Ω_1, Ω_2 and Ω_3, respectively.

Given that $K = k$ packets are received successfully at $\mathcal{R}$ in Ω_1, the average number of transmissions at $\mathcal{R}$ based on the proposed algorithm (i.e. algorithm in Table 2.1) in the second step can be computed through

$$\begin{aligned} E[n^{(2)}|K=k] = & \sum_{i=0}^{k}\sum_{j=0}^{k}\sum_{u=0}^{k}\sum_{v=0}^{k} C_i^k P_{\mathcal{S}_1\mathcal{D}_1}^i (1-P_{\mathcal{S}_1\mathcal{D}_1})^{k-i} C_j^k P_{\mathcal{S}_2\mathcal{D}_1}^j (1-P_{\mathcal{S}_2\mathcal{D}_1})^{k-j} \\ & \times C_u^k P_{\mathcal{S}_1\mathcal{D}_2}^u (1-P_{\mathcal{S}_1\mathcal{D}_2})^{k-u} C_v^k P_{\mathcal{S}_2\mathcal{D}_2}^v (1-P_{\mathcal{S}_2\mathcal{D}_2})^{k-v} \\ & \times [\min\{i+j, u+v\} n_{DT}^{(\mathcal{R})} + |(i+j)-(u+v)| n_{\mathcal{R}\mathcal{D}_a}], \end{aligned} \tag{2.38}$$

where $n_{DT}^{(\mathcal{R})}$ is the transmission bandwidth required at $\mathcal{R}$ to send a packet to both $\mathcal{D}_1$ and $\mathcal{D}_2$, and $n_{\mathcal{R}\mathcal{D}_a}$ is given by (2.32) with $a = 1$ if $i + j > u + v$ and $a = 2$ otherwise. Here, $n_{DT}^{(\mathcal{R})}$ can be similarly obtained as (2.30), i.e.

$$n_{DT}^{(\mathcal{R})} = \frac{1}{1-P_{\mathcal{R}\mathcal{D}_1}} + \frac{1}{1-P_{\mathcal{R}\mathcal{D}_2}} - \frac{1}{1-P_{\mathcal{R}\mathcal{D}_1}P_{\mathcal{R}\mathcal{D}_2}}. \tag{2.39}$$

For packets in groups Ω_2 and Ω_3 within the second step of the retransmission at $\mathcal{R}$, the average number of transmissions may be calculated by

$$\begin{aligned} E[n^{(2)}|L=l] = & \sum_{i=0}^{l}\sum_{j=0}^{l} C_i^l P_{\mathcal{S}_1\mathcal{D}_1}^i (1-P_{\mathcal{S}_1\mathcal{D}_1})^{l-i} C_j^l P_{\mathcal{S}_1\mathcal{D}_2}^j (1-P_{\mathcal{S}_1\mathcal{D}_2})^{l-j} \\ & \times [\min\{i,j\} n_{DT}^{(\mathcal{R})} + |i-j| n_{\mathcal{R}\mathcal{D}_a}], \end{aligned} \tag{2.40}$$

$$\begin{aligned} E[n^{(2)}|M=m] = & \sum_{i=0}^{m}\sum_{j=0}^{m} C_i^m P_{\mathcal{S}_2\mathcal{D}_1}^i (1-P_{\mathcal{S}_2\mathcal{D}_1})^{m-i} C_j^m P_{\mathcal{S}_2\mathcal{D}_2}^j (1-P_{\mathcal{S}_2\mathcal{D}_2})^{m-j} \\ & \times [\min\{i,j\} n_{DT}^{(\mathcal{R})} + |i-j| n_{\mathcal{R}\mathcal{D}_a}], \end{aligned} \tag{2.41}$$

where $a = 1$ if $i > j$ and $a = 2$ otherwise.

In the third step where $\mathcal{R}$ fails to receive packets of the first group in the first step, $\mathcal{S}_1$ and $\mathcal{S}_2$ are required to retransmit the remaining lost packets with the average number of transmissions given by

$$\begin{aligned} E[n^{(3)}|K=k] = & \sum_{i=0}^{N-k}\sum_{j=0}^{N-k}\sum_{u=0}^{N-k}\sum_{v=0}^{N-k} C_i^{N-k} P_{\mathcal{S}_1\mathcal{D}_1}^i (1-P_{\mathcal{S}_1\mathcal{D}_1})^{N-k-i} \\ & \times C_j^{N-k} P_{\mathcal{S}_2\mathcal{D}_1}^j (1-P_{\mathcal{S}_2\mathcal{D}_1})^{N-k-j} \\ & \times C_u^{N-k} P_{\mathcal{S}_1\mathcal{D}_2}^u (1-P_{\mathcal{S}_1\mathcal{D}_2})^{N-k-u} \\ & \times C_v^{N-k} P_{\mathcal{S}_2\mathcal{D}_2}^v (1-P_{\mathcal{S}_2\mathcal{D}_2})^{N-k-v} \\ & \times [\min\{i+j, u+v\} n_{RT} + |(i+j)-(u+v)| n_{RT}^{(\mathcal{D}_a)}], \end{aligned} \tag{2.42}$$

where $a = 1$ if $i + j > u + v$ and $a = 2$ otherwise. For the second group and the third group in the third step, the average numbers of transmissions are computed, respectively, through

$$\begin{aligned} E[n^{(3)}|L=l] = & \sum_{i=0}^{N-k-l} \sum_{j=0}^{N-k-l} C_i^{N-k-l} P_{\mathcal{S}_1\mathcal{D}_1}^i (1-P_{\mathcal{S}_1\mathcal{D}_1})^{N-k-l-i} \\ & \times C_j^{N-k-l} P_{\mathcal{S}_1\mathcal{D}_2}^i (1-P_{\mathcal{S}_1\mathcal{D}_2})^{N-k-l-j} \\ & \times [\min\{i,j\} n_{RT}^{(\mathcal{S}_1)} + |i-j| n_{RT}^{(\mathcal{S}_1,\mathcal{D}_a)}], \end{aligned} \tag{2.43}$$

$$\begin{aligned} E[n^{(3)}|M=m] = & \sum_{i=0}^{N-k-l-m} \sum_{j=0}^{N-k-l-m} C_i^{N-k-l-m} P_{\mathcal{S}_2\mathcal{D}_1}^i (1-P_{\mathcal{S}_2\mathcal{D}_1})^{N-k-l-m-i} \\ & \times C_j^{N-k-l-m} P_{\mathcal{S}_2\mathcal{D}_2}^j (1-P_{\mathcal{S}_2\mathcal{D}_2})^{N-k-l-m-j} \\ & \times [\min\{i,j\} n_{RT}^{(\mathcal{S}_2)} + |i-j| n_{RT}^{(\mathcal{S}_2,\mathcal{D}_a)}], \end{aligned} \tag{2.44}$$

where $a = 1$ if $i > j$ and $a = 2$ otherwise. In (2.43) and (2.44), $n_{RT}^{(\mathcal{S}_i)}$, $i = 1, 2$, denotes the normalised number of transmissions to transmit packets from $\mathcal{S}_i$ to both $\mathcal{D}_1$ and $\mathcal{D}_2$ through $\mathcal{R}$ and can be computed by

$$\begin{aligned} n_{RT}^{(\mathcal{S}_i)} = & \frac{1}{1 - P_{\mathcal{S}_i\mathcal{R}} P_{\mathcal{S}_i\mathcal{D}_1} P_{\mathcal{S}_i\mathcal{D}_2}} [1 + P_{\mathcal{S}_i\mathcal{R}} P_{\mathcal{S}_i\mathcal{D}_1} (1 - P_{\mathcal{S}_i\mathcal{D}_2}) n_{RT}^{(\mathcal{S}_i,\mathcal{D}_1)} \\ & + P_{\mathcal{S}_i\mathcal{R}} (1 - P_{\mathcal{S}_i\mathcal{D}_1}) P_{\mathcal{S}_i\mathcal{D}_2} n_{RT}^{(\mathcal{S}_i,\mathcal{D}_2)} + (1 - P_{\mathcal{S}_i\mathcal{R}}) P_{\mathcal{S}_i\mathcal{D}_1} (1 - P_{\mathcal{S}_i\mathcal{D}_2}) n_{\mathcal{R}\mathcal{D}_1} \\ & + (1 - P_{\mathcal{S}_i\mathcal{R}})(1 - P_{\mathcal{S}_i\mathcal{D}_1}) P_{\mathcal{S}_i\mathcal{D}_2} n_{\mathcal{R}\mathcal{D}_2} + (1 - P_{\mathcal{S}_i\mathcal{R}}) P_{\mathcal{S}_i\mathcal{D}_1} P_{\mathcal{S}_i\mathcal{D}_2} n_{DT}^{(\mathcal{R})}]. \end{aligned} \tag{2.45}$$

2.3.5 Numerical and Simulation Results

In this subsection, the transmission bandwidths of the different protocols are evaluated both from the analytical formulations above and also simulation models over mixed Rayleigh and Rician flat fading channels. The simulation results are obtained in MATLAB based on Monte Carlo methods. Rayleigh flat fading channels are considered NLOS transmissions reflecting more distant locations, whilst Rician flat fading channels are considered LOS transmissions representing closer proximities. Four scenarios representing typical fading situations are now considered.

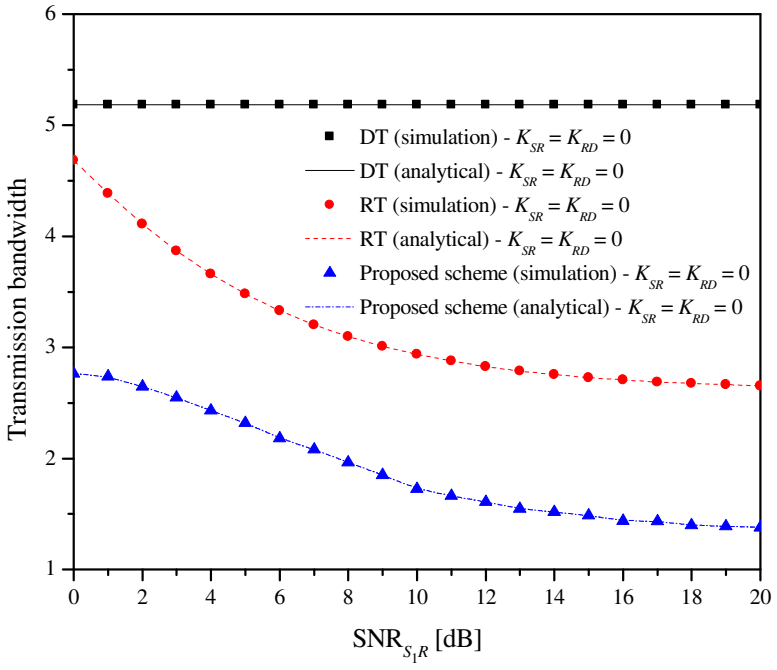

Figure 2.11: Transmission bandwidth of different protocols over Rayleigh fading channels with various SNR$_{\mathcal{S}_1\mathcal{R}}$.

Scenario (a): $\mathcal{S}_i \rightarrow \mathcal{R}$ and $\mathcal{R} \rightarrow \mathcal{D}_i$, $i = 1, 2$, are both NLOS

In this case the channels $\mathcal{S}_i \rightarrow \mathcal{R}$ and $\mathcal{R} \rightarrow \mathcal{D}_i$, $i = 1, 2$, are both Rayleigh fading channels, i.e. $\mathcal{K}_{S_iR} = \mathcal{K}_{SR} = 0$ and $\mathcal{K}_{RD_i} = \mathcal{K}_{RD} = 0$. The range of $\gamma_{\mathcal{S}_1\mathcal{R}}$ was selected to cover 0 to 20 dB in order to characterise the performance over a wide range of SNR conditions. Fig. 2.11 shows the transmission bandwidth of the three ARQ protocols as a function of $\gamma_{\mathcal{S}_1\mathcal{R}}$, i.e. the SNR of the wireless link $\mathcal{S}_1 \rightarrow \mathcal{R}$.

In order to evaluate the influence on the transmission bandwidth performance of the channels between the sources and relay, it is initially assumed that $\gamma_{\mathcal{S}_1\mathcal{R}} = \gamma_{\mathcal{S}_2\mathcal{R}}$. The other channel SNRs may be arbitrarily set to $\gamma_{\mathcal{S}_1\mathcal{D}_1} = \gamma_{\mathcal{S}_2\mathcal{D}_2} = 5$ dB, $\gamma_{\mathcal{S}_1\mathcal{D}_2} = \gamma_{\mathcal{S}_2\mathcal{D}_1} = 0$ dB and $\gamma_{\mathcal{R}\mathcal{D}_1} = \gamma_{\mathcal{R}\mathcal{D}_2} = 10$ dB. It is also assumed that the packet size (i.e. N_b) is 10 bits and the buffer length at the sources (i.e. N) is 10 packets. Fig. 2.11 demonstrates that the proposed NC-based ARQ protocol outperforms the other two ARQ schemes as it is capable of combining the lost packets from different transmission flows within the retransmission phase. It may also be observed that the proposed

NC scheme shows significant transmission bandwidth gain over the other ARQ methods. For example, when $\text{SNR}_{S_1R} = 10$ dB, the proposed protocol achieves a transmission bandwidth of 1.7 while a higher transmission bandwidth of 2.9 and 5.2 is required for the DT and RT protocols, respectively. For packets in the Ω_1 grouping, the proposed scheme significantly reduces the number of retransmissions simply through the process of mixing packets from the two different flows. Importantly, the simulation results match exactly the analytical results demonstrating the validity of the derived analytical expressions.

Scenario (b): $\mathcal{S}_i \to \mathcal{R}$, $i = 1, 2$, is LOS and $\mathcal{R} \to \mathcal{D}_i$, $i = 1, 2$, is NLOS

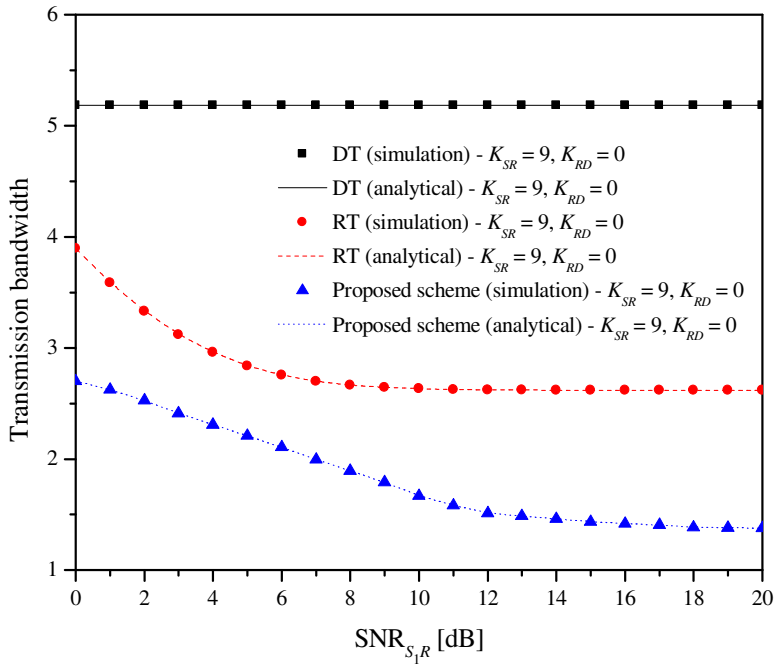

Figure 2.12: Transmission bandwidth of different protocols over Rician fading channels $\mathcal{S}_i \to \mathcal{R}$ and Rayleigh fading channels $\mathcal{R} \to \mathcal{D}_i$, $i = 1, 2$, as a function of $\text{SNR}_{\mathcal{S}_1\mathcal{R}}$.

For this situation, $\mathcal{S}_i \to \mathcal{R}$, $i = 1, 2$, is considered as a Rician channel and $\mathcal{R} \to \mathcal{D}_i$, $i = 1, 2$, as a Rayleigh channel. Fig. 2.12 provides an example of the transmission bandwidth performance for all three protocols as a function of $\gamma_{\mathcal{S}_1\mathcal{R}}$. The fading parameters for the results in Fig. 2.12 are $\mathcal{K}_{S_iR} = \mathcal{K}_{SR} = 9$ and $\mathcal{K}_{RD_i} = \mathcal{K}_{RD} = 0$. The SNRs of the other links are set similar to those in

Fig. 2.11.

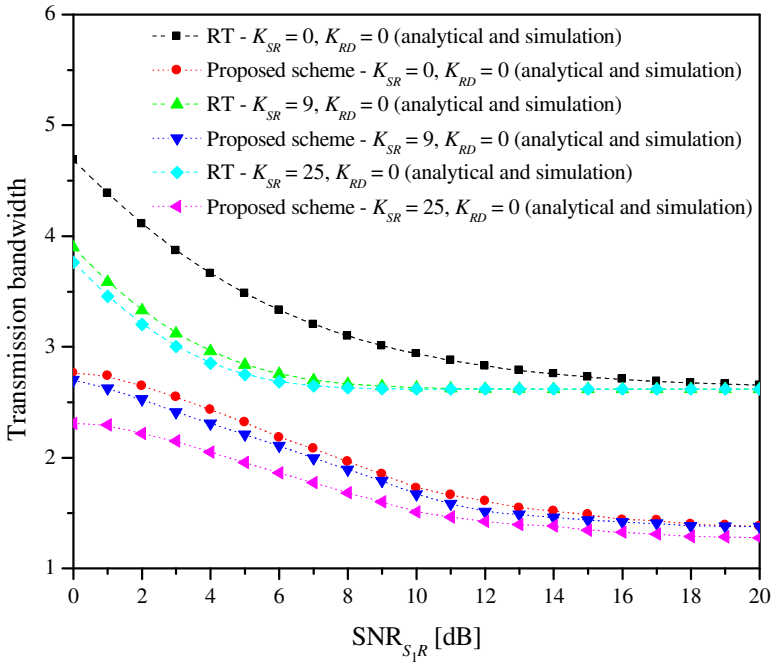

Figure 2.13: Transmission bandwidth of different protocols over Rician fading channels $\mathcal{S}_i \to \mathcal{R}$ and Rayleigh fading channels $\mathcal{R} \to \mathcal{D}_i$, $i = 1, 2$, with various $\mathcal{K}$ factors as a function of $\text{SNR}_{\mathcal{S}_1\mathcal{R}}$.

As the performance of the DT protocol is clearly not as good as the other two protocols, a further comparison specifically between the RT protocol and the proposed NC protocol for scenario (b) is shown in Fig. 2.13 for the situations of $\mathcal{K}_{SR} = \{0, 9, 25\}$ and $\mathcal{K}_{RD} = 0$.

Scenario (c): $\mathcal{S}_i \to \mathcal{R}$, $i = 1, 2$, is NLOS and $\mathcal{R} \to \mathcal{D}_i$, $i = 1, 2$, is LOS

In a similar fashion, $\mathcal{S}_i \to \mathcal{R}$, $i = 1, 2$, is considered now as a Rayleigh fading channel and $\mathcal{R} \to \mathcal{D}_i$, $i = 1, 2$, as a Rician fading channel. Fig. 2.14 provides an example of the transmission bandwidth performance for all three protocols again as a function of $\gamma_{\mathcal{S}_1\mathcal{R}}$. The $\mathcal{K}$ factors for Fig. 2.14 are the same as scenario (b), i.e. $\mathcal{K}_{S_iR} = \mathcal{K}_{SR} = 0$ and $\mathcal{K}_{RD_i} = \mathcal{K}_{RD} = 9$. The comparison between the RT and the proposed NC-based protocol for scenario (c) with the same $\mathcal{K}$ factors used in Fig. 2.13 can be similarly considered. The additional results show that they are identical, and thus they are omitted for brevity.

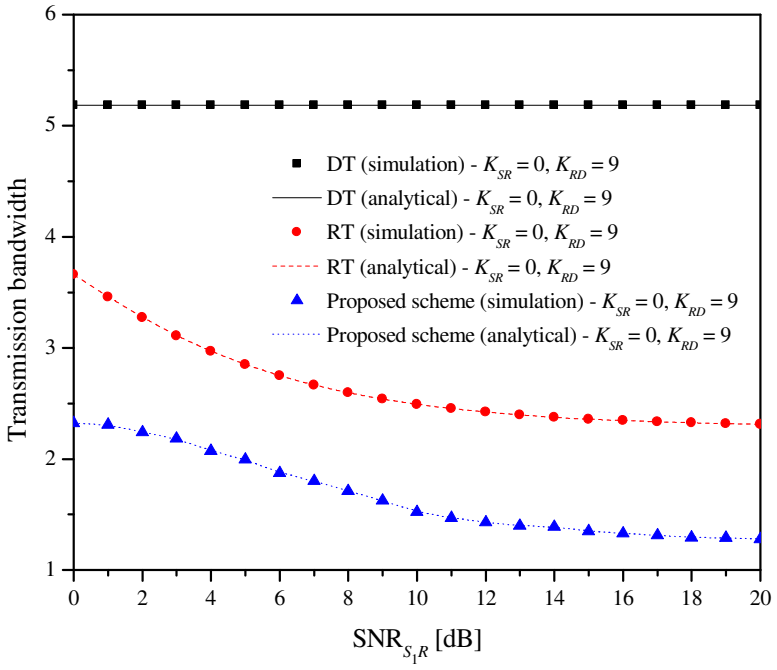

Figure 2.14: Transmission bandwidth of different protocols over Rayleigh fading channels $\mathcal{S}_i \rightarrow \mathcal{R}$ and Rician fading channels $\mathcal{R} \rightarrow \mathcal{D}_i$, $i = 1, 2$, as a function of $\text{SNR}_{\mathcal{S}_1\mathcal{R}}$.

In scenarios (b) and (c), the results again demonstrate that the proposed NC-based ARQ protocol achieves better transmission bandwidth performance when compared with other two schemes for both scenarios of mixed fading channel models. Again, the analytical results in all Figs. are shown to match precisely with the simulation results. It can also be observed that the transmission bandwidth curves show reduced transmission bandwidth performance as $\mathcal{K}_{SR}$ increases. For example, as shown in Fig. 2.14, at $\text{SNR}_{S_1R} = 10$ dB, the transmission bandwidth achieved with our proposed scheme is 1.8, 1.75 and 1.5 corresponding to $\mathcal{K}_{SR} = 0, 9, 25$, respectively. This can be explained as the influence of the LOS component on the BER gain through all ranges of SNR, which accordingly results in the reduction of the transmission bandwidth.

Scenario (d): $\mathcal{S}_i \rightarrow \mathcal{R}$ and $\mathcal{R} \rightarrow \mathcal{D}_i$, $i = 1, 2$, are both LOS

The final scenario is a general scenario where all fading channels $\mathcal{S}_i \rightarrow \mathcal{R}$ and $\mathcal{R} \rightarrow \mathcal{D}_i$, $i = 1, 2$, are characterised by Rician fading alone. Fig. 2.15

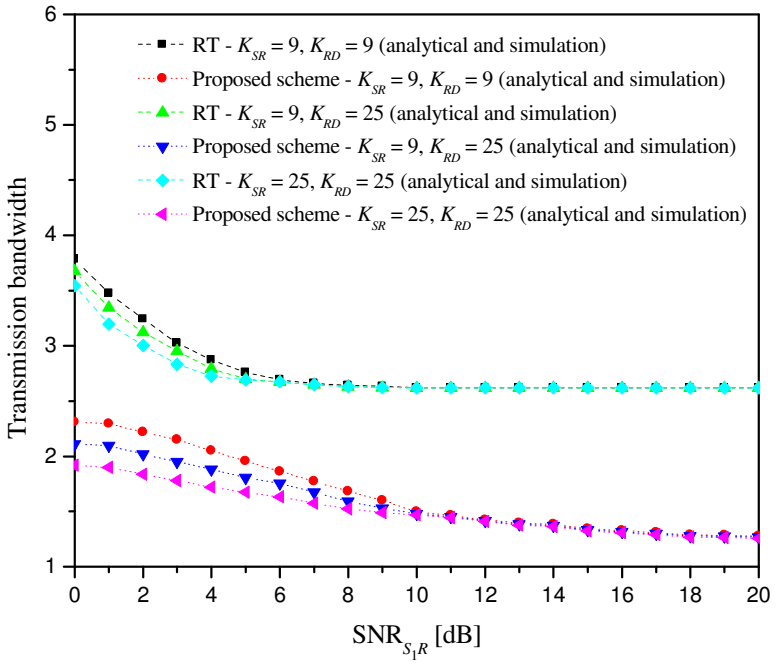

Figure 2.15: Transmission bandwidth of different protocols over Rician fading channels $\mathcal{S}_i \rightarrow \mathcal{R}$ and Rician fading channels $\mathcal{R} \rightarrow \mathcal{D}_i$, $i = 1, 2$, with various $\mathcal{K}$ factors as a function of $\text{SNR}_{\mathcal{S}_1\mathcal{R}}$.

shows the comparison of transmission bandwidths specifically between the RT protocol and the proposed NC-based ARQ protocol against $\gamma_{\mathcal{S}_1\mathcal{R}}$ with respect to various $\mathcal{K}$ factor fading values and with the same assumptions of SNR values as in Fig. 2.11.

Specifically, in Fig. 2.15, three cases $\{\mathcal{K}_{SR} = 9, \mathcal{K}_{RD} = 9\}$, $\{\mathcal{K}_{SR} = 9, \mathcal{K}_{RD} = 25\}$ and $\{\mathcal{K}_{SR} = 25, \mathcal{K}_{RD} = 25\}$ have been considered. Similarly, it can be observed that a reduced transmission bandwidth performance is always achieved when either $\mathcal{K}_{SR}$ or $\mathcal{K}_{RD}$ increases. This again reflects the influence of the LOS components on the BER gain which is helpful in reducing the transmission bandwidth. It is important to note that at small SNR levels the proposed scheme has a much increased performance over the other protocols. As the SNR increases, the improvement in the new protocol is still evident, though as expected, the improvement is smaller due to the improved SNR.

2.4 Conclusions

This chapter has first designed ARQ retransmission strategies for NC based TWSRNs. Different retransmission techniques with three basic ARQ protocols have been studied through the comparison of throughput efficiency. It was found that the best strategy in the sense of throughput efficiency is the scheme where the improved NC-based SR ARQ is applied in the BC phase and the SR ARQ protocol is used in the MA phase. With this combination, better throughput efficiency is obtained when compared with the traditional non-NC schemes. However, this is achieved at the expense of higher complexity due to additional signal processing required for NC and the requirement of buffering at the transmitter/receiver.

As a second contribution of this chapter, a new improved and reliable retransmission scheme for MMSRNs based on NC has been proposed. It has been shown that the new protocol significantly reduces the number of retransmissions. The performance of the proposed retransmission scheme was investigated for the specific case with two sources and two destinations. It was shown to be superior in terms of transmission bandwidth improvement when compared with RT and DT protocols even over mixed Rayleigh and Rician flat fading channels. Specifically, two packet-combination algorithms have been developed to retransmit lost packets. The efficiency of retransmission is improved since the algorithms are able to differentiate between different types of retransmission situations. Further, simulation results of the transmission bandwidth for RT and DT protocols over different Rician and Rayleigh fading factors have validated the theoretically derived analytical expressions. This indicates that any evaluation assessment of transmission bandwidth for the topology presented in this chapter can be determined accurately without the requirement of a simulation model.

Chapter 3

NC Based CQI Reporting

This chapter considers channel quality indicator (CQI) reporting for data exchange in two-way multi-relay networks. Two new efficient CQI reporting schemes are first proposed based on network coding (NC) via XOR computation and superposition coding. These NC-based schemes allow two terminals to simultaneously estimate the CQI of the distant terminal-relay link without incurring additional overhead. In addition, it is shown for the new schemes that the transmission time for CQI feedback at the relays is reduced by half while the increase in complexity and the loss of performance are negligible. This results in a system throughput improvement of 16.7% with the proposed CQI reporting. Upper and lower bounds of the mean square error (MSE) of the estimated CQI are also derived to study the performance behaviour. It is found that the MSE of the estimated CQI increases proportionally with the square of the cardinality of CQI level sets, though an increased number of CQI levels would eventually lead to a higher data-rate transmission. Based on the derived bounds, a low-complexity relay selection (RS) scheme is then proposed. Simulation results show that, in comparison with optimal methods, the suboptimal bound-based RS scheme achieves satisfactory performance while reducing the complexity by at least a factor of three for large numbers of relays.

3.1 Introduction

In a network coding (NC) based two-way single-relay network (TWSRN), the relay node mixes the signals received from two terminal nodes before broadcasting it. From this combined signal, each terminal node can extract the data sent by the other terminal node using network decoding mechanisms. In real-time applications, e.g. in wireless ad-hoc or sensor networks, strict complexity and time delay constraints are generally required, especially when there are multiple intermediate relay nodes. This stimulates to consider a nonregenerative two-way multi-relay network (TWMRN) model that includes two terminal nodes and multiple relay nodes. Under a nonregenerative protocol, the relay nodes simply combine the received data signal and forward this combined signal to both terminal nodes.

In general, channel state information (CSI) available at the transmitter is helpful for a number of designs including optimal beamforming and adaptive modulation and coding (AMC) schemes. In nonregenerative TWMRNs, CSI is required for the detection of the data sent by the other terminal node when NC is used at the relay [29, 121]. There are several approaches to make CSI available at each terminal node. Pilot-based channel estimation can be utilised to obtain the CSI under the assumption of ideal feedback [122] or even without feedback [123]. However, the latter case is carried out under the assumption that the channel does not change over two time slots. In the case of this assumption being not satisfied, practical CSI feedback mechanisms may have to be sought. While ideal feedback is practically difficult, common mechanisms for CSI feedback are via channel quality indicator (CQI) reporting [124, 125], in which CQI is a discrete representation of the CSI.

Most of the recent work investigating CQI reporting or feedback in one-way relay networks have considered only some applications such as adaptive non-orthogonal cooperation [126], user selection with multiple destination nodes [127], adaptive resource scheduling in multihop orthogonal frequency-division multiple access (OFDMA) systems [125] and adaptive utilisation of

time-varying channels [128]. Extending these CQI feedback schemes to TWS-RNs obviously results in doubling the signaling overhead and requiring two time slots at each relay node to forward these overheads to both terminal nodes.

In this chapter, an efficient CQI reporting scheme is proposed for TWM-RNs so as to reduce the number of transmissions at the relays and to avoid the additional overhead. The idea of the proposed scheme is originated from an NC concept and can be summarized by the following steps: i) each terminal node and relay send pilot signals to each other to estimate the link quality of associated channels (i.e. signal-to-noise ratio (SNR)); ii) each relay node combines the estimated CQIs of the two terminal-relay channels using either bitwise XOR or symbol-level superposition coding; iii) the relay node then broadcasts the combined signal to both terminal nodes; and iv) based on the received combined signal, two terminal nodes can simultaneously estimate the CQI of the distant links. With the proposed CQI reporting scheme, the CQIs of the terminal-relay channel are conveyed to the other terminal at no additional cost in terms of bandwidth or energy. It can be seen that N signalling overheads and N transmission time slots are reduced for an N-relay network when compared with the conventional schemes, which accordingly results in a system throughput improvement of 16.7%. Although the advantages of the proposed CQI reporting scheme are considerable, the major novelty of this chapter is the analysis of the mean square error (MSE) of the estimated CQI and the subsequently proposed bound-based relay selection scheme. This is summarised as follows:

- *The upper and lower bounds of the mean square error (MSE) of the estimated CQI over a Rayleigh flat fading channel are derived.* To the best of the author's knowledge, these bounds have not been derived previously. The tight bounds reflect well the behaviour of the numerical MSE. It is found that while the MSE of the estimated CQI increases proportionally with the square of the number of CQI levels, a higher data rate could be achieved with an increased number of CQI levels by using various

AMC schemes. It is also shown that the loss of performance and the increase of complexity of the proposed scheme are negligible compared with conventional CQI reporting schemes.

- *A complexity-reduced relay selection scheme is proposed based on the derived MSE bounds.* Since the data exchange between two terminals in TWMRNs can be assisted by all available relay nodes, relay selection (RS) should be considered. In particular, an opportunistic RS scheme has been generally investigated, where the best relay is chosen based on a specific selection criterion, e.g. minimising the sum of bit error rates (BERs) or maximizing the sum-rate [27]. It is observed that RS can also be simply realized by maximizing the sum of channel gains of both terminal users. However, this work considers a system where CQI is required at the transmitter and therefore CQI reporting is an important performance metric for the system. This motivates to design an efficient RS scheme based on the previously determined MSE of the estimated CQI at the two terminals, where the best relay is chosen such that the sum of the MSE (sum-MSE) of the estimated CQI is minimised. The RS is carried out by a scheduler of a coordinator node in a centralized manner [129,130], i.e. each relay informs the coordinator of its sum-MSE through a specific feedback channel and then the coordinator selects the best relay based on this information. The optimal RS scheme requires a full search of available relays, which results in high complexity. This motivates to propose a suboptimal bound-based RS scheme where the searching process will stop whenever the maximum of MSE (max-MSE) is smaller than the upper bound. The resulting complexity is reduced by a factor of at least three compared with the optimal RS scheme if the number of relays is sufficiently large while its performance is still satisfactory.

The rest of the chapter is organized as follows: Section 3.2 describes the proposed CQI reporting schemes, related algorithms and complexity analysis.

Section 3.3 provides the analysis of the MSE of the estimated CQI. Then, different opportunistic RS schemes are proposed and analysed in Section 3.4. Numerical results are discussed in Section 3.5, and Section 3.6 concludes the chapter.

3.2 Proposed CQI Reporting Scheme

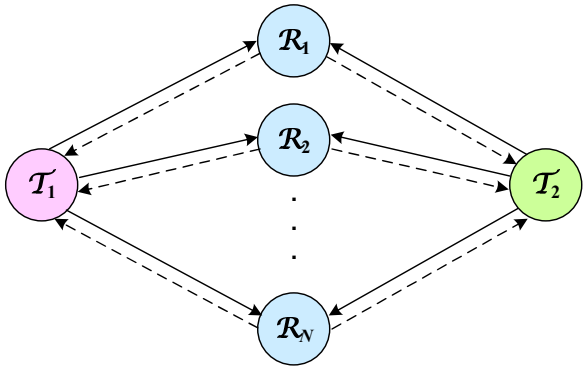

Figure 3.1: System model of two-way multi-relay network.

The system model of a general TWMRN under investigation is shown in Fig. 3.1 where the data exchange between two terminals $\mathcal{T}_1$ and $\mathcal{T}_2$ is assisted by a group of N relays $\mathcal{R}^{(N)} = \{\mathcal{R}_1, \mathcal{R}_2, \ldots, \mathcal{R}_N\}$. The channel quality reporting at these relays is assumed to be concurrently carried out. For convenience, the channel quality reporting for branch $\mathcal{T}_1 - \mathcal{R}_1 - \mathcal{T}_2$ is considered only. Let h_{AB} denote the channel coefficient of the $A \to B$ link where $A, B \in \{\mathcal{T}_1, \mathcal{T}_2, \mathcal{R}_1\}$. The following assumptions are made: i) there is no direct link between the terminal nodes due to power limit in each node; ii) time division duplex (TDD) signalling is employed in the considered system; iii) the channel in each link is reciprocal, i.e. $h_{\mathcal{T}_i\mathcal{R}_1} = h_{\mathcal{R}_1\mathcal{T}_i} = h_i$, $i = 1, 2$; iv) the channel in each link is Rayleigh flat fading; and v) pilot signals are used to initially estimate the link quality of all channels (i.e. instantaneous SNR at the receiver) (see [122, 123] for more details).

It is noteworthy that for various signal processing mechanisms in TWSRNs such as data detection or adaptive modulation [29], each terminal node $\mathcal{T}_i$

requires the channel quality information of not only its associated link $\mathcal{T}_i - \mathcal{R}_1$ but also that of the distant link $\mathcal{T}_j - \mathcal{R}_1, j \neq i$. In order to reduce the amount of feedback information, the value of channel quality, SNR, should be quantized into a finite bit sequence called CQI with different levels. The CQI reporting in TWSRNs can be divided into two phases as follows: In the first phase, $\mathcal{T}_i, i = 1, 2$, and $\mathcal{R}_1$ transmit pilot signals to each other to estimate the CQI of the associated link $\mathcal{T}_i - \mathcal{R}_1$ in two time slots. In the second phase, $\mathcal{R}_1$ helps $\mathcal{T}_i$ estimate the CQI of the distant link $\mathcal{T}_j - \mathcal{R}_1, j = 1, 2, j \neq i$, which is not directly available at $\mathcal{T}_i$. It can be observed that the CQI estimation in the first phase can straightforwardly follow conventional pilot-based approaches. This chapter therefore focuses on the CQI reporting in the second phase. Conventionally, the doubling of signaling overhead should be required at $\mathcal{R}_1$ to consecutively forward the CQIs of the links $\mathcal{T}_1 - \mathcal{R}_1$ and $\mathcal{T}_2 - \mathcal{R}_1$ to $\mathcal{T}_2$ and $\mathcal{T}_1$, respectively, in two time slots. This considerably reduces the network throughput. Therefore, a new efficient CQI reporting scheme is proposed based on NC to eliminate the additional overhead as well as reduce the number of time slots by half. By using NC, $\mathcal{R}_1$ can combine the estimated CQIs of two links $\mathcal{T}_1 - \mathcal{R}_1$ and $\mathcal{T}_2 - \mathcal{R}_1$ before broadcasting it to allow each terminal $\mathcal{T}_i$ to simultaneously estimate the CQI of the distant link $\mathcal{T}_j - \mathcal{R}_1$ $(j \neq i)$.

Let γ_i and ρ_i denote the SNR and CQI, respectively, of link h_i, $i = 1, 2$. Assume that $\rho_i \in \mathcal{C}_i$ where $\mathcal{C}_i$ is the set of all possible CQI levels of link h_i. Let Q_i denote the cardinality of $\mathcal{C}_i$. Thus, it requires $L_i = \lceil \log_2 Q_i \rceil$ bits to represent a ρ_i level, where $\lceil . \rceil$ denotes the ceiling function of a real number. The lists of ρ_1 and ρ_2 levels are assumed to be available at $\mathcal{R}_1$, $\mathcal{T}_1$ and $\mathcal{T}_2$. Practically, there are multiple ways to map SNR to CQI [131, 132]. One of the common ways is that CQI can be approximated by a linear function of SNR as follows

$$\rho_i = \lceil a\gamma_i[\text{dB}] + b \rceil, \tag{3.1}$$

where a and b are constants and γ_i [dB] is calculated as the power ratio between the signal and the background noise over a complex baseband channel. Assume that the range of SNR for CQI mapping is from 0 to γ_{mdB} [dB], where γ_{mdB}

is positive and measured in dB. Following the above approach, the range $[0 : \gamma_{mdB}]$ is divided into Q_i levels $(1, 2, \ldots, Q_i)$ by setting $a = Q_i/\gamma_{mdB}$ and $b = 0$. As a result, ρ_i can be obtained as

$$\rho_i = \left\lceil \frac{Q_i}{\gamma_{mdB}} \gamma_i[\text{dB}] \right\rceil = \left\lceil \frac{10 Q_i \log_{10} \gamma_i}{\gamma_{mdB}} \right\rceil. \tag{3.2}$$

Let $\rho_{i,\mathcal{T}}$ and $\rho_{i,\mathcal{R}}$ denote the estimated values of ρ_i at $\mathcal{T}_i$ and $\mathcal{R}_1$, respectively, in the first phase. It can be seen that $\rho_{i,\mathcal{T}}, \rho_{i,\mathcal{R}} \in \mathcal{C}_i$. The proposed CQI reporting scheme is carried out in the second phase. $\mathcal{R}_1$ combines two estimated CQIs, i.e. $\rho_{1,\mathcal{R}}$ and $\rho_{2,\mathcal{R}}$, using either a bit-level XOR operation or symbol-level superposition as follows:

Scheme A – Bit-level XOR

The bit sequences of $\rho_{1,\mathcal{R}}$ and $\rho_{2,\mathcal{R}}$ are XORed together as

$$\mathbf{b}^{(A)} \triangleq \mathbf{b}_{\rho_{1,\mathcal{R}}} \oplus \mathbf{b}_{\rho_{2,\mathcal{R}}}, \tag{3.3}$$

where $\oplus$ denotes the bitwise XOR operator and $\mathbf{b}_{\rho_{i,\mathcal{R}}}, i = 1, 2$, denotes the bit-level format of $\rho_{i,\mathcal{R}}$. It is noticed that the terms within XOR operations in (3.3) must have the same length. Thus, zero-padding is used to match the length of CQIs, i.e. the length of $\mathbf{b}^{(A)}$ is $\max\{L_1, L_2\} \triangleq L_m$.

Scheme B – Symbol-level superposition

The bit sequences $\mathbf{b}_{\rho_{1,\mathcal{R}}}$ and $\mathbf{b}_{\rho_{2,\mathcal{R}}}$ are encoded into baseband signal sequences $\mathbf{b'}_{\rho_{1,\mathcal{R}}}$ and $\mathbf{b'}_{\rho_{2,\mathcal{R}}}$, respectively. Then, they are superimposed together as

$$\mathbf{b}^{(B)} = \sqrt{\theta_{\rho_1}} \mathbf{b'}_{\rho_{1,\mathcal{R}}} + \sqrt{\theta_{\rho_2}} \mathbf{b'}_{\rho_{2,\mathcal{R}}}, \tag{3.4}$$

where θ_{ρ_1} and θ_{ρ_2} are power allocation coefficients such that $\theta_{\rho_1} + \theta_{\rho_2} = 1$ and optimised as in [101].

For the CQI estimation at $\mathcal{T}_1$ and $\mathcal{T}_2$, $\mathcal{R}$ then broadcasts $\mathbf{b}^{(M)}$, $M \in \{A, B\}$, to $\mathcal{T}_1$ and $\mathcal{T}_2$. The received signal at $\mathcal{T}_i, i = 1, 2$, can be written by

$$\mathbf{y}_i^{(M)} = \sqrt{P} h_i \mathbf{x}^{(M)} + \mathbf{n}_i, \tag{3.5}$$

where P is the transmission power of $\mathcal{R}$, $\mathbf{x}^{(M)}$ is the modulated version of $\mathbf{b}^{(M)}$, and $\mathbf{n}_i$ is the white Gaussian noise vector with each entry having zero mean and variance of σ_i^2.

At $\mathcal{T}_i$, $i = 1, 2$, the question is how to estimate $\rho_{j,\mathcal{R}}$, $j \neq i$ of the distant link $\mathcal{T}_j - \mathcal{R}_1$. Based on the estimated CQI of the link $\mathcal{T}_i - \mathcal{R}_1$ at $\mathcal{T}_i$ (i.e. $\rho_{i,\mathcal{T}}$) in the first phase, $\mathcal{T}_i$ can create a list of all possible NC-based combinations of $\rho_{i,\mathcal{T}}$ and ρ_j using either scheme A or B as follows

Scheme A

$$\mathbf{b}'^{(A)}_{\rho_j} = \mathbf{b}_{\rho_{i,\mathcal{T}}} \oplus \mathbf{b}_{\rho_j}, \tag{3.6}$$

where $\mathbf{b}_{\rho_{i,\mathcal{T}}}$, $\mathbf{b}_{\rho_j}$ and $\mathbf{b}'^{(A)}_{\rho_j}$ denote the bit-level formats of $\rho_{i,\mathcal{T}}$, ρ_j and the NC-based combination of $\rho_{i,\mathcal{T}}$ and ρ_j using the XOR operation, respectively.

Scheme B

$$\mathbf{b}'^{(B)}_{\rho_j} = \sqrt{\theta_{\rho_i}}\mathbf{b}'_{\rho_{i,\mathcal{T}}} + \sqrt{\theta_{\rho_j}}\mathbf{b}'_{\rho_j}, \tag{3.7}$$

where $\mathbf{b}'_{\rho_{i,\mathcal{T}}}$, $\mathbf{b}'_{\rho_j}$ and $\mathbf{b}'^{(B)}_{\rho_j}$ denote the encoded baseband signal sequences of $\mathbf{b}_{\rho_{i,\mathcal{T}}}$, $\mathbf{b}_{\rho_j}$ and the NC-based combination of $\rho_{i,\mathcal{T}}$ and ρ_j using superposition coding, respectively.

Note that $\rho_j \in \mathcal{C}_j$ and therefore there are Q_j possible candidates of $\mathbf{b}_{\rho_j}$. $\mathcal{T}_i$ then compares the received signal $\mathbf{y}_i^{(M)}$, $M \in \{A, B\}$ given in (3.5) with all possible $\mathbf{b}'_{\rho_j}$'s in order to choose the matched $\mathbf{b}_{\rho_j}$. Correspondingly, the matched $\rho_j \in \mathcal{C}_j$ can be found. This matched ρ_j is the estimated value of $\rho_{j,\mathcal{R}}$, which is denoted by $\hat{\rho}_{j,\mathcal{R}}$. It can be observed that finding $\hat{\rho}_{j,R}$ can be carried out by using an exhaustive search method, where the correlation-based decision is based on the received signal $\mathbf{y}_i^{(M)}$ and the NC-based combination sample $\mathbf{b}'^{(M)}_{\rho_j}$. This correlation-based decision is represented by the following correlation value:

$$\vartheta^{(M)}_{\rho_j} = \sum_{l=1}^{L_m} \mathbf{y}_i^{(M)}[l] \frac{\mathbf{x}^{(M)}_{\rho_j}[l]}{|\mathbf{x}^{(M)}_{\rho_j}[l]|^2}, \tag{3.8}$$

where $\mathbf{x}_{\rho_j}^{(M)}$ denotes the modulated version of $\mathbf{b}_{\rho_j}^{\prime(M)}$. Here, $\mathbf{y}_i^{(M)}[l]$ and $\mathbf{x}_{\rho_j}^{(M)}[l]$ denote the l-th element of vectors $\mathbf{y}_i^{(M)}$ and $\mathbf{x}_{\rho_j}^{(M)}$, respectively.

Theorem 3.1. *$\vartheta_{\rho_j}^{(M)}$ is almost surely upper bounded by $(\sqrt{P}h_iL_m+\sqrt{L_m}\sigma_iN_{\rho_j})$ when $\rho_{i,\mathcal{R}} = \rho_{i,\mathcal{T}}$ and $\rho_j = \rho_{j,\mathcal{R}}$, where N_{ρ_j} is an independent complex-valued random number.*

Proof. From (3.5), (3.8) can be rewritten as

$$\vartheta_{\rho_j} = \sqrt{P}h_i \sum_{l=1}^{L_m} \mathbf{x}[l] \frac{\mathbf{x}_{\rho_j}[l]}{|\mathbf{x}_{\rho_j}[l]|^2} + \sum_{l=1}^{L_m} \mathbf{n}_i[l] \frac{\mathbf{x}_{\rho_j}[l]}{|\mathbf{x}_{\rho_j}[l]|^2}. \tag{3.9}$$

The first term in (3.9) can be expressed by [133]

$$\sqrt{P}h_i \sum_{l=1}^{L_m} \mathbf{x}[l] \frac{\mathbf{x}_{\rho_j}[l]}{|\mathbf{x}_{\rho_j}[l]|^2} = \begin{cases} \sqrt{P}h_iL_m, \text{ if } \rho_{i,\mathcal{R}} = \rho_{i,\mathcal{T}} \text{ and } \rho_j = \rho_{j,\mathcal{R}}, \\ \sqrt{P}h_i \left(\sqrt{\frac{L_m}{2}}\omega_1 + \sqrt{-\frac{L_m}{2}}\omega_2 \right), \text{otherwise}, \end{cases} \tag{3.10}$$

where ω_1 and ω_2 are independent Gaussian random numbers with zero mean and unit variance. Additionally, the second term in (3.9) can be expressed as

$$\sum_{l=1}^{L_m} \mathbf{n}_i[l] \frac{\mathbf{x}_{\rho_j}[l]}{|\mathbf{x}_{\rho_j}[l]|^2} = \sqrt{L_m}\sigma_iN_{\rho_j}, \tag{3.11}$$

where N_{ρ_j} is an independent complex-valued random number [133]. Thus, (3.9) can be written as

$$\vartheta_{\rho_j} = \begin{cases} \sqrt{P}h_iL_m + \sqrt{L_m}\sigma_iN_{\rho_j}, \text{if } \rho_{i,\mathcal{R}} = \rho_{i,\mathcal{T}} \text{ and } \rho_j = \rho_{j,\mathcal{R}}, \\ \sqrt{P}h_i \left(\sqrt{\frac{L_m}{2}}\omega_1 + \sqrt{-\frac{L_m}{2}}\omega_2 \right) + \sqrt{L_m}\sigma_iN_{\rho_j}, \text{otherwise}. \end{cases} \tag{3.12}$$

It can be seen that $\left(\sqrt{\frac{L_m}{2}}\omega_1 + \sqrt{-\frac{L_m}{2}}\omega_2 \right)$ is almost surely smaller than L_m when $L_m \geqslant 2$. Therefore, it can be concluded that ϑ_{ρ_j} is almost surely upper bounded by $(\sqrt{P}h_iL_m + \sqrt{L_m}\sigma_iN_{\rho_j})$ when $\rho_{i,\mathcal{R}} = \rho_{i,\mathcal{T}}$ and $\rho_j = \rho_{j,\mathcal{R}}$. □

In Theorem 3.1, two conditions to maximize $\vartheta_{\rho_j}^{(M)}$ mean that the estimated ρ_i and ρ_j at $\mathcal{R}_1$ in the first phase should be equal to the estimated ρ_i in the first phase and the required ρ_j in the second phase at $\mathcal{T}_i$, respectively. Thus, the estimated value of $\rho_{j,\mathcal{R}}$ in the second phase is chosen from $\mathcal{C}_j$ to maximize $\vartheta_{\rho_j}^{(M)}$, i.e.

$$\hat{\rho}_{j,\mathcal{R}} = \arg\max_{\rho_j \in \mathcal{C}_j} \vartheta_{\rho_j}^{(M)}. \tag{3.13}$$

Note that the estimation of $\rho_{2,\mathcal{R}}$ at $\mathcal{T}_1$ and the estimation of $\rho_{1,\mathcal{R}}$ at $\mathcal{T}_2$ are carried out simultaneously.

Remark 3.1 (*Imperfect CQI Estimation*). *The required condition $\rho_{i,\mathcal{R}} = \rho_{i,\mathcal{T}}$ in order to maximize $\vartheta_{\rho_j}^{(M)}$ causes a loss in the performance of the proposed scheme when compared with the conventional scheme*[6] *in terms of the MSE of the estimated $\rho_{j,\mathcal{R}}$ at $\mathcal{T}_i$. This condition may not be achieved due to the imperfect estimation of ρ_i at $\mathcal{R}_1$ and $\mathcal{T}_i$. Thus, the overall performance of the proposed CQI reporting scheme depends on that of the pilot-based CQI estimation in the first phase.*

Remark 3.2 (*Higher Reliability in Asymmetric Broadcast Channel with Scheme B*). *Scheme B would be preferable if an asymmetric broadcast channel is considered, e.g. the SNR of $\mathcal{R} \to \mathcal{T}_i$ link is much higher than the SNR of $\mathcal{R} \to \mathcal{T}_j$, $j \neq i$, link. In this case, the reliability of the estimation of ρ_i at $\mathcal{T}_j$ is significantly reduced while the estimation of ρ_j at $\mathcal{T}_i$ can be carried out with an insignificant error. However, using scheme B, the estimation of ρ_i at $\mathcal{T}_j$ can be improved with an increased θ_{ρ_i} and a reduced θ_{ρ_j}. Note that the loss in the performance of the estimation of ρ_j at $\mathcal{T}_i$ caused by the reduced θ_{ρ_j} is not significant since the $\mathcal{R} \to \mathcal{T}_i$ link is of high quality.*

Remark 3.3 (*Throughput Improvement*). *It can be seen that the proposed CQI reporting scheme for the one-relay system needs five transmissions of five signalling overheads while the traditional scheme requires six transmissions. This means that one transmission and one overhead are reduced with the proposed scheme for the one-relay system. Extending to N-relay networks, N transmission time slots and N signalling overheads are reduced. In general, a system throughput improvement of 16.7% is obtained from the proposed design.*

Remark 3.4 (*Complexity*). *For complexity analysis, the proposed scheme is compared with the conventional scheme. First, the complexity of the exhaustive search for $\hat{\rho}_{j,\mathcal{R}}$ at $\mathcal{T}_i$, $i = 1, 2$, $j \neq i$ is discussed. Second, the computation*

[6]The conventional scheme is referred to as a scheme where $\mathcal{R}$ sequentially transmits $\rho_{i,\mathcal{R}}$ and $\rho_{j,\mathcal{R}}$ to $\mathcal{T}_j$ and $\mathcal{T}_i$, respectively, in two separate time slots.

complexity at $\mathcal{R}_1$ and $\mathcal{T}_i$ is studied. For the first comparison, the complexity is measured by the number of searches to find the desired CQI. In the proposed scheme, at $\mathcal{T}_i$, ρ_j is chosen in $\mathcal{C}_j$ to maximize the correlation value ϑ_{ρ_j} given by (3.8)*. Thus, Q_j searches are required. In the conventional scheme where an exhaustive search is also used, the same number of searches is required at $\mathcal{T}_i$ to find the desired ρ_j. However, the proposed scheme has a slightly higher computation complexity compared to the conventional scheme. The XOR operation is required for the generation of $\mathbf{b}$ in* (3.3)*. Thus, the complexity at $\mathcal{R}_1$ in the proposed scheme increases by L_m XOR operations. At $\mathcal{T}_i$, the difference between the proposed scheme and the conventional scheme is the generation of $\mathbf{b}'_{\rho_j}$ defined in* (3.6)*. The XOR operation in* (3.6) *results in L_m more computations at $\mathcal{T}_i$. Similarly, L_m more computations are required at $\mathcal{T}_j$. If letting L_T denote the total number of computations in the whole system using the conventional scheme, then the proposed scheme would require $(L_T + 3L_m)$ computations. However, it can be seen that $L_T \gg L_m$, and thus this increase in complexity of the proposed scheme is insignificant.*

3.3 Analysis of MSE of Estimated CQI

This section derives the MSE expression of the estimated CQI of scheme B. The MSE analysis of scheme A can be similarly carried out. For simplicity, this section studies the CQI estimation at $\mathcal{T}_2$ only. The analysis of the CQI estimation at $\mathcal{T}_1$ can be similarly obtained. The estimation error occurs if the estimated $\rho_{1,\mathcal{R}}$ at $\mathcal{T}_2$ in the second phase (i.e. $\hat{\rho}_{1,\mathcal{R}}$) is different from the value of ρ_1 estimated at $\mathcal{R}$ in the first phase (i.e. $\rho_{1,\mathcal{R}}$). Thus, the MSE of the estimated CQI can be computed by

$$\text{MSE} = E\left\{\left[\rho_{1,\mathcal{R}} - \hat{\rho}_{1,\mathcal{R}}\right]^2\right\}, \tag{3.14}$$

where $E\{.\}$ denotes the expectation.

As it is difficult to derive $\hat{\rho}_{1,\mathcal{R}}$ and $\rho_{1,\mathcal{R}}$ for any arbitrary characteristics of two links $\mathcal{T}_1 \to \mathcal{R}_1$ and $\mathcal{R}_1 \to \mathcal{T}_2$ simultaneously, it is observed to be still useful

to understand the behaviour of the MSE in (3.14) in an asymptotic case and gain some insights from it. Thus, for simple analysis, it is assumed that the link $\mathcal{T}_1 \rightarrow \mathcal{R}_1$ is at a high SNR[7], i.e. $\gamma_1[dB] = \gamma_{mdB}$, and thus from (3.2), $\rho_{1,\mathcal{R}}$ can be approximated by Q_1.

Now $\hat{\rho}_{1,\mathcal{R}}$ is derived. From (3.5), the SNR γ_2 of $\mathcal{R}_1 \rightarrow \mathcal{T}_2$ link can be expressed as

$$\gamma_2 = \frac{P_R \theta_{\rho_1} |h_2|^2}{\sigma_2^2}. \tag{3.15}$$

Note that, in the second phase, $\mathbf{x}$ in (3.5) is constructed by both $\rho_{1,R}$ and $\rho_{2,R}$. It is assumed that $\rho_{2,R} \approx \rho_{2,T}$ in the first phase. Since $\rho_{2,T}$ is known at $\mathcal{T}_2$, it can be removed from the received signal. Thus, it can be approximated that γ_2 determines the mapping of $\rho_{1,R}$, i.e.

$$\hat{\rho}_{1,R} \approx \left\lceil \frac{10 \log_{10}(\gamma_2)}{\gamma_{mdB}/Q_1} \right\rceil. \tag{3.16}$$

Substituting (3.16) into (3.14) with the assumption that the $\mathcal{T}_1 \rightarrow \mathcal{R}_1$ link is at a high SNR, then (3.14) can be approximated as

$$\text{MSE} \approx E\left\{ \left(Q_1 - \left\lceil \frac{10 \log_{10}(\gamma_2)}{\gamma_{mdB}/Q_1} \right\rceil \right)^2 \right\}. \tag{3.17}$$

Let $\alpha = e^{-\gamma_m/\bar{\gamma}}$, $\beta = e^{-1/\bar{\gamma}}$, $\gamma_m = 10^{\gamma_{mdB}/10}$, $Q_1' = 10Q_1/(\gamma_{mdB}\ln 10)$, $Q_1'' = Q_1 - Q_1' \ln \theta_{\rho_1}$ where $\bar{\gamma}$ is average SNR, $\ln x$ is the natural logarithm of x, $E_i(\cdot)$ is the exponential integral, and $\mathfrak{G}_{p,q}^{m,n}\left(\begin{smallmatrix} a_1,\ldots,a_p \\ b_1,\ldots,b_q \end{smallmatrix} | z \right)$ is the Meijer G function [134]. The following theorem can be then derived:

Theorem 3.2. *The MSE given by* (3.17) *is upper-bounded and lower-bounded by MSE_u and MSE_l, respectively, where*

$$MSE_u = \lambda_1 + \lambda_2 A + \lambda_3 B, \tag{3.18}$$

$$MSE_l = \lambda_1' + \lambda_2' A + \lambda_3 B, \tag{3.19}$$

and

$$\lambda_1 = (Q_1'' - Q_1' ln\bar{\gamma})^2(\beta - \alpha), \lambda_2 = -2Q_1'(Q_1'' - Q_1' ln\bar{\gamma}), \lambda_3 = Q_1'^2,$$

[7]This assumption of high SNR is for analysis purpose only. The proposed CQI reporting algorithm is actually for a general case and valid for any SNR value of the uplink.

$$\lambda_1' = (Q_1'' - 1 - Q_1' ln\bar{\gamma})^2(\beta - \alpha), \lambda_2' = -2Q_1'(Q_1'' - 1 - Q_1' ln\bar{\gamma}),$$
$$A = \beta ln(-ln\beta) - \alpha ln(-ln\alpha) + E_i(ln\alpha) - E_i(ln\beta),$$
$$B = \beta ln^2(-ln\beta) - \alpha ln^2(-ln\alpha)$$
$$- 2ln(-ln\alpha)\mathfrak{G}_{1,2}^{2,0}\left(\begin{smallmatrix}1\\0,0\end{smallmatrix}\middle| - ln\alpha\right) + 2ln(-ln\beta)\mathfrak{G}_{1,2}^{2,0}\left(\begin{smallmatrix}1\\0,0\end{smallmatrix}\middle| - ln\beta\right)$$
$$- 2\mathfrak{G}_{2,3}^{3,0}\left(\begin{smallmatrix}1,1\\0,0,0\end{smallmatrix}\middle| - ln\alpha\right) + 2\mathfrak{G}_{2,3}^{3,0}\left(\begin{smallmatrix}1,1\\0,0,0\end{smallmatrix}\middle| - ln\beta\right).$$

Proof. It is noticed that $\lceil x \rceil \geqslant x \ \forall x$. Thus,

$$Q_1 \geqslant \left\lceil \frac{10\log_{10}(\gamma_2)}{\gamma_{mdB}/Q_1} \right\rceil \geqslant \frac{10\log_{10}(\gamma_2)}{\gamma_{mdB}/Q_1} \geqslant 0. \tag{3.20}$$

Applying the inequality in (3.20) to (3.17), the MSE has an upper bound given by

$$\mathrm{MSE}_u = E\left\{\left(Q_1 - \frac{10\log_{10}(\gamma_2)}{\gamma_{mdB}/Q_1}\right)^2\right\}. \tag{3.21}$$

Denote $Q_1' = 10Q_1/(\gamma_{mdB}\ln 10)$, $Q_1'' = Q_1 - Q_1'\ln\theta_{\rho_1}$, where $\ln x$ is the natural logarithm of x, and denote $\gamma = \gamma_2$. (3.21) can then be rewritten as

$$\mathrm{MSE}_u = E\left\{(Q_1'' - Q_1'\ln\gamma)^2\right\}. \tag{3.22}$$

This expectation can be computed by

$$\mathrm{MSE}_u = \int_1^{\gamma_m} (Q_1'' - Q_1'\ln\gamma)^2 f_\gamma(\gamma) d\gamma, \tag{3.23}$$

where $\gamma_m = 10^{\gamma_{mdB}/10}$ and $f(.)$ is the probability density function (pdf) of a random variable. Since the fading channel $\mathcal{R}_1 \to \mathcal{T}_2$ is Rayleigh flat fading, $f_\gamma(\gamma)$ is given by [120]

$$f_\gamma(\gamma) = \frac{1}{\bar{\gamma}}\exp\left(-\frac{\gamma}{\bar{\gamma}}\right), \tag{3.24}$$

where $\bar{\gamma}$ is the average SNR. Thus,

$$\mathrm{MSE}_u = \int_1^{\gamma_m} (Q_1'' - Q_1'\ln\gamma)^2 \frac{1}{\bar{\gamma}}\exp\left(-\frac{\gamma}{\bar{\gamma}}\right) d\gamma. \tag{3.25}$$

Let $t = \exp(-\gamma/\bar{\gamma})$, $\alpha = e^{-\gamma_m/\bar{\gamma}}$ and $\beta = e^{-1/\bar{\gamma}}$, then (3.25) can be expressed as

$$\begin{aligned}\mathrm{MSE}_u &= \int_\alpha^\beta [(Q_1''{-}Q_1'\ln\bar{\gamma})^2{-}2Q_1'(Q_1''{-}Q_1'\ln\bar{\gamma})\ln(\text{–}\ln t){+}Q_1'^2\ln^2(\text{–}\ln t)]dt \\ &= \lambda_1 + \lambda_2 A + \lambda_3 B,\end{aligned} \tag{3.26}$$

where

$$\lambda_1 = (Q_1'' - Q_1' \ln\bar{\gamma})^2(\beta - \alpha), \tag{3.27}$$

$$\lambda_2 = -2Q_1'(Q_1'' - Q_1' \ln\bar{\gamma}), \tag{3.28}$$

$$\lambda_3 = Q_1'^2, \tag{3.29}$$

$$A = \int_{\alpha}^{\beta} \ln(-\ln t)dt, \tag{3.30}$$

$$B = \int_{\alpha}^{\beta} \ln^2(-\ln t)dt. \tag{3.31}$$

The derivation of MSE_u is simplified to the integral calculus evaluation of A and B. From [134] and some simple algebraic manipulation, A and B can be determined through

$$A = \beta\ln(-\ln\beta) - \alpha\ln(-\ln\alpha) + E_i(\ln\alpha) - E_i(\ln\beta), \tag{3.32}$$

$$\begin{aligned} B = {} & \beta\ln^2(-\ln\beta) - \alpha\ln^2(-\ln\alpha) \\ & - 2\ln(-\ln\alpha)\mathfrak{G}_{1,2}^{2,0}\left(\begin{smallmatrix}1\\0,0\end{smallmatrix}\middle| -\ln\alpha\right) + 2\ln(-\ln\beta)\mathfrak{G}_{1,2}^{2,0}\left(\begin{smallmatrix}1\\0,0\end{smallmatrix}\middle| -\ln\beta\right) \\ & - 2\mathfrak{G}_{2,3}^{3,0}\left(\begin{smallmatrix}1,1\\0,0,0\end{smallmatrix}\middle| -\ln\alpha\right) + 2\mathfrak{G}_{2,3}^{3,0}\left(\begin{smallmatrix}1,1\\0,0,0\end{smallmatrix}\middle| -\ln\beta\right), \end{aligned} \tag{3.33}$$

respectively, where $E_i(.)$ is the exponential integral and $\mathfrak{G}_{p,q}^{m,n}\left(\begin{smallmatrix}a_1,\ldots,a_p\\b_1,\ldots,b_q\end{smallmatrix}\middle|z\right)$ is the Meijer G function.

Another important inequality related to the ceiling function is that $\lceil x \rceil < x + 1 \ \forall x$. Thus,

$$0 \leqslant \left\lceil \frac{10\log_{10}(\gamma_2)}{\gamma_{mdB}/Q_1} \right\rceil < \frac{10\log_{10}(\gamma_2)}{\gamma_{mdB}/Q_1} + 1. \tag{3.34}$$

The lower bound of the MSE is then given by

$$\text{MSE}_l = E\left\{ \left(Q_1 - 1 - \frac{10\log_{10}(\gamma_2)}{\gamma_{mdB}/Q_1} \right)^2 \right\}. \tag{3.35}$$

It is observed that the expression of MSE_l has the same form as MSE_u in (3.21). Thus, MSE_l can be calculated by

$$\text{MSE}_l = \lambda_1' + \lambda_2' A + \lambda_3 B, \tag{3.36}$$

where

$$\lambda_1' = (Q_1'' - 1 - Q_1' \ln\bar{\gamma})^2(\beta - \alpha), \tag{3.37}$$

$$\lambda_2' = -2Q_1'(Q_1'' - 1 - Q_1' \ln\bar{\gamma}). \tag{3.38}$$

□

Corollary 3.1. *MSE bounds in* (3.18) *and* (3.19) *increase as a function of* Q_1^2.

Proof. From Theorem 3.2, λ_1, λ_2, λ_1', λ_2' and λ_3 depend on Q_1, whereas A and B are independent of Q_1. Here, λ_1, λ_2 and λ_3 can be rewritten as

$$\lambda_1 = Q_1^2 \left(1 - \frac{10\ln\theta_{\rho_1}}{\gamma_{mdB}\ln 10} - \frac{10\ln\bar{\gamma}}{\gamma_{mdB}\ln 10}\right)^2 (\beta - \alpha),$$

$$\lambda_2 = Q_1^2 \frac{-20}{\gamma_{mdB}\ln 10} \left(1 - \frac{10\ln\theta_{\rho_1}}{\gamma_{mdB}\ln 10} - \frac{10\ln\bar{\gamma}}{\gamma_{mdB}\ln 10}\right),$$

$$\lambda_3 = Q_1^2 \left(\frac{10}{\gamma_{mdB}\ln 10}\right)^2.$$

Thus, MSE_u can be rewritten as

$$\begin{aligned} \mathrm{MSE}_u = Q_1^2 \Bigg[& \left(1 - \frac{10\ln\theta_{\rho_1}}{\gamma_{mdB}\ln 10} - \frac{10\ln\bar{\gamma}}{\gamma_{mdB}\ln 10}\right)^2 (\beta - \alpha) \\ & + \frac{-20}{\gamma_{mdB}\ln 10} \left(1 - \frac{10\ln\theta_{\rho_1}}{\gamma_{mdB}\ln 10} - \frac{10\ln\bar{\gamma}}{\gamma_{mdB}\ln 10}\right) A + \left(\frac{10}{\gamma_{mdB}\ln 10}\right)^2 B \Bigg]. \end{aligned} \tag{3.39}$$

It is observed that if we change Q_1 and fix the other parameters, MSE_u is a function of Q_1^2, i.e.

$$\mathrm{MSE}_u = \zeta Q_1^2, \tag{3.40}$$

where ζ is a non-negative constant since $\mathrm{MSE}_u \geqslant 0$.

Considering MSE_l, λ_1' and λ_2' can be written as

$$\lambda_1' = Q_1^2 \left(1 - 1/Q_1 - \frac{10\ln\theta_{\rho_1}}{\gamma_{mdB}\ln 10} - \frac{10\ln\bar{\gamma}}{\gamma_{mdB}\ln 10}\right)^2 (\beta - \alpha),$$

$$\lambda_2' = Q_1^2 \frac{-20}{\gamma_{mdB}\ln 10} \left(1 - 1/Q_1 - \frac{10\ln\theta_{\rho_1}}{\gamma_{mdB}\ln 10} - \frac{10\ln\bar{\gamma}}{\gamma_{mdB}\ln 10}\right).$$

When Q_1 is large, the term $1/Q_1$ can be omitted. Thus, MSE_l can also be written by

$$\mathrm{MSE}_l = \zeta' Q_1^2, \tag{3.41}$$

where ζ' is a non-negative constant. □

Remark 3.5 (*Impact of* Q_1). *Although increasing the number of CQI levels (i.e.* Q_1*) would provide a more precise representation of channel quality and add more flexibility to the implementation of various adaptive schemes, from Corollary 3.1 it can be observed that the performance of the CQI reporting scheme is significantly reduced with* Q_1*. Thus, a trade-off between performance of CQI reporting and performance of data transmission should be considered when choosing* Q_1*.*

3.4 Opportunistic CQI Based Relay Selection

In Section 3.2, the proposed CQI reporting scheme was considered for each relay node. This section will consider all the relays and therefore this requires an efficient RS mechanism. Particularly, based on the estimated CQIs at the relays and two terminals, different RS schemes are proposed for TWMRNs where only one best relay is opportunistically selected by a coordinator in the network to exchange data between two terminal nodes. Specifically, an optimal RS (ORS) scheme is proposed where the relay is chosen to minimise the sum-MSE given by

$$\mathrm{SMSE}(n) = \mathrm{MSE}_1(n) + \mathrm{MSE}_2(n), \tag{3.42}$$

where $\mathrm{MSE}_i(n)$ denotes the MSE of the estimated ρ_i at $\mathcal{T}_j$, $i, j \in \{1, 2\}$, $i \neq j$, in a TWSRN using $\mathcal{R}_n$, $n \in \{1, \ldots, N\}$. From the MSE analysis for TWSRNs in Section 3.3, $\mathrm{MSE}_i(n)$ is computed by

$$\mathrm{MSE}_i(n) \approx E\left\{\left(Q_i - \left\lceil \frac{10\log_{10}(\gamma_j(n))}{\gamma_{mdB}/Q_i} \right\rceil\right)^2\right\}. \tag{3.43}$$

Thus, the ORS based on the sum-MSE is represented by

$$n^* = \arg\min_n \mathrm{SMSE}(n). \tag{3.44}$$

However, the computation complexity of this scheme is high. A suboptimal RS (SRS) scheme is considered based on the max-MSE. In fact, it is well-known that minimising the sum can be approximated to minimising the maximum.

Therefore, the relay chosen by SRS scheme may be determined in a centralised mannner by

$$n^*_{sub} = \arg\min_n \max\{\mathrm{MSE}_1(n), \mathrm{MSE}_2(n)\}. \tag{3.45}$$

Due to the quantization carried out in the mapping process as explained for TWSRNs, the upper bound and lower bound of $\mathrm{MSE}(n^*_{sub})$ can be derived. For simple analysis, it is assumed that scheme A is applied at each relay, Q_1 and Q_2 are equal, and $\gamma_1(n)$ and $\gamma_2(n)$ have the same probability density function. Let $\alpha_N = e^{-2\gamma_m/\bar{\gamma}}$, $\beta_N = e^{-2/\bar{\gamma}}$, $Q = Q_1 = Q_2$ and $Q' = 10Q/(\gamma_{mdB}\ln 10)$. The following finding is then obtained:

Theorem 3.3. *$MSE(n^*_{sub})$ is upper-bounded and lower-bounded by $MSE_u(n^*_{sub})$ and $MSE_l(n^*_{sub})$, respectively, where*

$$MSE_u(n^*_{sub}) = \lambda_{1N} + \lambda_{2N}A_N + \lambda_{3N}B_N, \tag{3.46}$$

$$MSE_l(n^*_{sub}) = \lambda'_{1N} + \lambda'_{2N}A_N + \lambda_{3N}B_N, \tag{3.47}$$

and

$$\lambda_{1N} = \left(Q - Q' ln\frac{\bar{\gamma}}{2}\right)^2 \left[(1-\alpha_N)^N - (1-\beta_N)^N\right], \lambda_{2N} = -2Q'\left(Q - Q' ln\frac{\bar{\gamma}}{2}\right), \lambda_{3N} = Q'^2,$$

$$\lambda'_{1N} = \left(Q - 1 - Q' ln\frac{\bar{\gamma}}{2}\right)^2 \left[(1-\alpha_N)^N - (1-\beta_N)^N\right], \lambda'_{2N} = -2Q'\left(Q - 1 - Q' ln\frac{\bar{\gamma}}{2}\right),$$

$$A_N = (-1)^{N-1}\sum_{m=1}^{N}(-1)^{m-1}\frac{\prod_{j=1}^{m-1}(N-j+1)}{(m-1)!} \times \left\{E_i\left[(N-m+1)ln\alpha_N\right] - E_i\left[(N-m+1)ln\beta_N\right] - \alpha_N^{N-m+1}ln(-ln\alpha_N) + \beta_N^{N-m+1}ln(-ln\beta_N)\right\},$$

$$B_N = (-1)^N\sum_{m=1}^{N}(-1)^{m-1}\frac{\prod_{j=1}^{m-1}(N-j+1)}{(m-1)!} \times \left\{\alpha_N^{N-m+1}ln^2(-ln\alpha_N) - \beta_N^{N-m+1}ln^2(-ln\beta_N) + 2ln(-ln\alpha_N)\mathfrak{G}_{1,2}^{2,0}\left(\begin{smallmatrix}1\\0,0\end{smallmatrix}\middle|-(N-m+1)ln\beta_N\right) - 2ln(-ln\beta_N)\mathfrak{G}_{1,2}^{2,0}\left(\begin{smallmatrix}1\\0,0\end{smallmatrix}\middle|-(N-m+1)ln\beta_N\right) + 2\mathfrak{G}_{2,3}^{3,0}\left(\begin{smallmatrix}1,1\\0,0,0\end{smallmatrix}\middle|-(N-m+1)ln\alpha_N\right) - 2\mathfrak{G}_{2,3}^{3,0}\left(\begin{smallmatrix}1,1\\0,0,0\end{smallmatrix}\middle|-(N-m+1)ln\beta_N\right)\right\}.$$

Proof. From (3.43), (3.45), and $Q_1 = Q_2$, n^*_{sub} can be obtained as

$$n^*_{sub} = \arg\max_n \min\{\gamma_1(n), \gamma_2(n)\}. \tag{3.48}$$

Denote $\gamma^* = \max \gamma_{\min}(n)$ where $\gamma_{\min}(n) = \min\{\gamma_1(n), \gamma_2(n)\}$. $\mathrm{MSE}(n^*_{sub})$ can be calculated by

$$\mathrm{MSE}(n^*_{sub}) \approx E\left\{\left(Q - \left\lceil \frac{10\log_{10}\gamma^*}{\gamma_{mdB}/Q}\right\rceil\right)^2\right\}. \tag{3.49}$$

Similarly, applying the inequalities (3.20) and (3.34) to (3.49), $\mathrm{MSE}(n^*_{sub})$ has an upper bound and a lower bound given by

$$\mathrm{MSE}_u(n^*_{sub}) = E\left\{\left(Q - \frac{10\log_{10}\gamma^*}{\gamma_{mdB}/Q}\right)^2\right\}, \tag{3.50}$$

$$\mathrm{MSE}_l(n^*_{sub}) = E\left\{\left(Q - 1 - \frac{10\log_{10}\gamma^*}{\gamma_{mdB}/Q}\right)^2\right\}, \tag{3.51}$$

respectively, where $Q = Q_1 = Q_2$. Observing that (3.50) and (3.51) have the same form, the expression of $\mathrm{MSE}_u(n^*_{sub})$ will be derived. The derivation for $\mathrm{MSE}_l(n^*_{sub})$ can be carried out in a similar fashion.

In order to derive $\mathrm{MSE}_u(n^*_{sub})$, the pdf of γ^* need to be calculated. Note that $\gamma_1(n)$ and $\gamma_2(n)$ have the same pdf given by (3.24) and cumulative density function (cdf) given by

$$F_\gamma(\gamma) = 1 - \exp\left(-\frac{\gamma}{\bar{\gamma}}\right), \tag{3.52}$$

respectively. Applying order statistics [135], the pdf of γ^* can be calculated by

$$f_{\gamma^*}(\gamma) = N f_{\gamma_{\min}}(\gamma) F^{N-1}_{\gamma_{\min}}(\gamma), \tag{3.53}$$

where

$$f_{\gamma_{\min}}(\gamma) = 2 f_\gamma(\gamma)[1 - F_\gamma(\gamma)], \tag{3.54}$$

$$F_{\gamma_{\min}}(\gamma) = 1 - [1 - F_\gamma(\gamma)]^2, \tag{3.55}$$

denote the pdf and cdf of $\gamma_{\min}$, respectively. Thus,

$$f_{\gamma^*}(\gamma) = \frac{2N}{\bar{\gamma}}\exp\left(-\frac{2\gamma}{\bar{\gamma}}\right)\left[1 - \exp\left(-\frac{2\gamma}{\bar{\gamma}}\right)\right]^{N-1}. \tag{3.56}$$

From (3.50), $\mathrm{MSE}_u(n^*_{sub})$ can be computed by

$$\mathrm{MSE}_u(n^*_{sub})=\int_1^{\gamma_m}\left(Q-\frac{10\log_{10}\gamma}{\gamma_{mdB}/Q}\right)^2 2N\exp\left(-\frac{2\gamma}{\bar{\gamma}}\right)\left[1-\exp\left(-\frac{2\gamma}{\bar{\gamma}}\right)\right]^{N-1}d\gamma. \quad (3.57)$$

Let $Q'=10Q/(\gamma_{mdB}\ln 10)$, $t=\exp(-2\gamma/\bar{\gamma})$, $\alpha_N=e^{-2\gamma_m/\bar{\gamma}}$ and $\beta_N=e^{-2/\bar{\gamma}}$, (3.57) can be rewritten as

$$\begin{aligned}\mathrm{MSE}_u(n^*_{sub})=&N\int_{\alpha_N}^{\beta_N}\left[\left(Q-Q'\ln\frac{\bar{\gamma}}{2}\right)^2-2Q'\left(Q-Q'\ln\frac{\bar{\gamma}}{2}\right)\ln(-\ln t)+Q'^2\ln^2(-\ln t)\right]\\&\times(1-t)^{N-1}dt\\=&\lambda_{1N}+\lambda_{2N}A_N+\lambda_{3N}B_N,\end{aligned} \quad (3.58)$$

where

$$\lambda_{1N}=\left(Q-Q'\ln\frac{\bar{\gamma}}{2}\right)^2\left[(1-\alpha_N)^N-(1-\beta_N)^N\right], \quad (3.59)$$

$$\lambda_{2N}=-2Q'\left(Q-Q'\ln\frac{\bar{\gamma}}{2}\right), \quad (3.60)$$

$$\lambda_{3N}=Q'^2, \quad (3.61)$$

$$A_N=N\int_{\alpha_N}^{\beta_N}\ln(-\ln t)(1-t)^{N-1}dt, \quad (3.62)$$

$$B_N=N\int_{\alpha_N}^{\beta_N}\ln^2(-\ln t)(1-t)^{N-1}dt. \quad (3.63)$$

Solving the two integrals A_N and B_N with identities in [134] and some simple algebraic manipulation, A_N and B_N can be obtained as

$$\begin{aligned}A_N=&(-1)^{N-1}\sum_{m=1}^{N}(-1)^{m-1}\frac{\prod_{j=1}^{m-1}(N-j+1)}{(m-1)!}\\&\times\left\{E_i\left[(N-m+1)\ln\alpha_N\right]-E_i\left[(N-m+1)\ln\beta_N\right]\right.\\&\left.-\alpha_N^{N-m+1}\ln(-\ln\alpha_N)+\beta_N^{N-m+1}\ln(-\ln\beta_N)\right\},\end{aligned} \quad (3.64)$$

$$\begin{aligned}B_N=&(-1)^N\sum_{m=1}^{N}(-1)^{m-1}\frac{\prod_{j=1}^{m-1}(N-j+1)}{(m-1)!}\\&\times\left\{\alpha_N^{N-m+1}\ln^2(-\ln\alpha_N)-\beta_N^{N-m+1}\ln^2(-\ln\beta_N)\right.\\&+2\ln(-\ln\alpha_N)\mathfrak{G}_{1,2}^{2,0}\left(\begin{matrix}1\\0,0\end{matrix}\middle|-(N-m+1)\ln\beta_N\right)\\&-2\ln(-\ln\beta_N)\mathfrak{G}_{1,2}^{2,0}\left(\begin{matrix}1\\0,0\end{matrix}\middle|-(N-m+1)\ln\beta_N\right)\\&\left.+2\mathfrak{G}_{2,3}^{3,0}\left(\begin{matrix}1,1\\0,0,0\end{matrix}\middle|-(N-m+1)\ln\alpha_N\right)-2\mathfrak{G}_{2,3}^{3,0}\left(\begin{matrix}1,1\\0,0,0\end{matrix}\middle|-(N-m+1)\ln\beta_N\right)\right\}.\end{aligned} \quad (3.65)$$

Similarly, $\mathrm{MSE}_l(n^*_{sub})$ is given by

$$\mathrm{MSE}_l(n^*_{sub}) = \lambda'_{1N} + \lambda'_{2N} A_N + \lambda_{3N} B_N, \tag{3.66}$$

where

$$\lambda'_{1N} = \left(Q - 1 - Q' \ln \frac{\bar{\gamma}}{2}\right)^2 \left[(1-\alpha_N)^N - (1-\beta_N)^N\right], \tag{3.67}$$

$$\lambda'_{2N} = -2Q' \left(Q - 1 - Q' \ln \frac{\bar{\gamma}}{2}\right). \tag{3.68}$$

□

Remark 3.6 (*Tighter Bounds with Larger N*). *The MSE performance of the SRS scheme converges to zero when the number of relays is large. It can be seen that $\lambda_{1N} \to 0$, $\lambda'_{1N} \to 0$, $A_N \to 0$, and $B_N \to 0$ as $N \to \infty$. Thus, $MSE_u(n^*_{sub}) \to 0$ and $MSE_l(n^*_{sub}) \to 0$. Since $MSE_u(n^*_{sub}) \geqslant MSE(n^*_{sub}) \geqslant MSE_l(n^*_{sub})$, it can be deduced that $MSE(n^*_{sub}) \to 0$ as $N \to \infty$. It can also be deduced that the bounds are tighter as N increases.*

Based on the upper and lower bounds of $\mathrm{MSE}(n^*_{sub})$ given in Theorem 3.3 and their characteristics discussed in Remark 3.6, a so-called suboptimal bound-based RS (SBBRS) scheme is proposed to reduce further the complexity of the searching method in (3.45). Note that if the previously mentioned SRS scheme (i.e. (3.45)) is used, N relays would be exhaustively verified to choose the best one to minimise the max-MSE. Instead, the proposed SBBRS scheme will stop the searching when finding a relay with max-MSE being smaller than $\mathrm{MSE}_u(n^*_{sub})$. As the result, the number of searches is significantly reduced, especially with larger N (i.e. when $\mathrm{MSE}_u(n^*_{sub})$ decreases). The complexity reduction will be shown and further discussed in the simulation results. The algorithm corresponding to the SBBRS scheme is summarized in Table 3.1.

3.5 Numerical and Simulation Results

This section compares the MSE of the estimated CQI for different schemes using Monte Carlo simulation in MATLAB.

Table 3.1: Bound-based relay selection scheme

For $n = 1 : N$

Calculate max-MSE(n).

If max-MSE(n) $\leqslant$ MSE$_u(n^*_{sub})$

$n^*_{bound-based\ sub} = n$

max-MSE($n^*_{bound-based\ sub}$) = max-MSE(n)

Exit For

End If

End For

3.5.1 Performance of CQI reporting in TWSRN

The TWSRNs are first considered where the CQI estimation is carried out at $\mathcal{T}_2$. The estimation error occurs if the estimated $\rho_{1,\mathcal{R}}$ at $\mathcal{T}_2$ (i.e. $\hat{\rho}_{1,\mathcal{R}}$) is different from ρ_1 estimated at $\mathcal{R}_1$ (i.e. $\rho_{1,\mathcal{R}}$). For comparison, the conventional scheme is considered. Using the conventional scheme, ρ_1 of the link $\mathcal{T}_1 - \mathcal{R}_1$ is fed back to $\mathcal{T}_2$ through one feedback link, and ρ_2 is separately fed back to $\mathcal{T}_1$ through another link, which results in double overhead and two time slots. Using the proposed scheme, combined data broadcast from relay $\mathcal{R}_1$ enables each terminal to estimate the required CQI. This process utilizes only one time slot and requires no additional overhead.

As shown in Fig. 3.2, the MSE of the estimated $\rho_{1,\mathcal{R}}$ of various schemes is plotted as a function of the SNR of the $\mathcal{R}_1 \rightarrow \mathcal{T}_2$ link with the assumption that 8 different CQI levels are used, i.e. $Q_1 = Q_2 = 8$. It is also assumed that the length of pilot sequences used for the CQI estimation in the first phase is 8 bits. The range of SNR in CQI mapping is from 0 to 20 dB, i.e. $\gamma_{mdB} = 20$ dB. The SNRs of the $\mathcal{T}_1 \rightarrow \mathcal{R}_1$ link and the $\mathcal{T}_2 \rightarrow \mathcal{R}$ link in the first time slot are assumed to be 20 dB. First, the upper and lower bounds given by (3.18) and (3.19) are shown to be quite tight and reflect well the behaviour of the numerical MSEs. Secondly, it can be observed that the performance of the proposed scheme is close to that of the conventional scheme, especially at a high SNR. The expected small loss, as explained in Remark 3.1, occurs because the

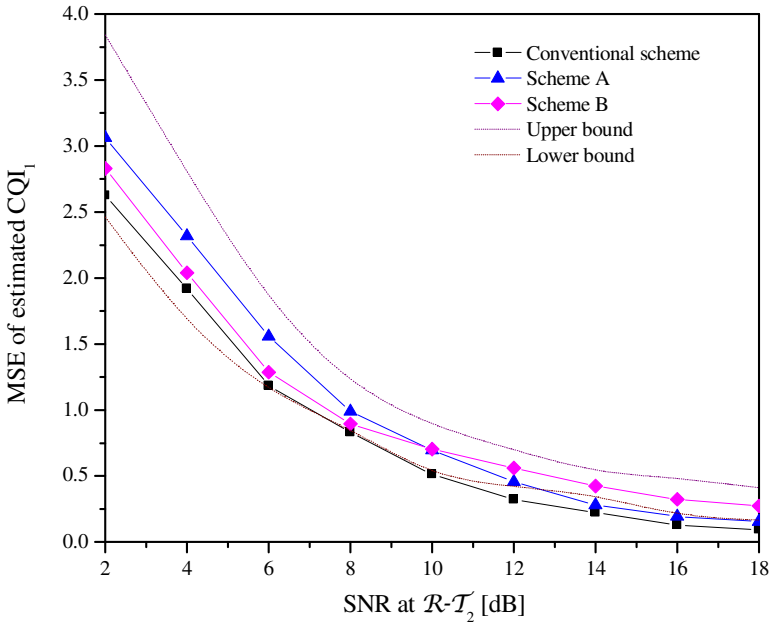

Figure 3.2: MSE of estimated ρ_1 at $\mathcal{T}_2$ versus SNR of $\mathcal{R}_1 - \mathcal{T}_2$ link with different relay schemes.

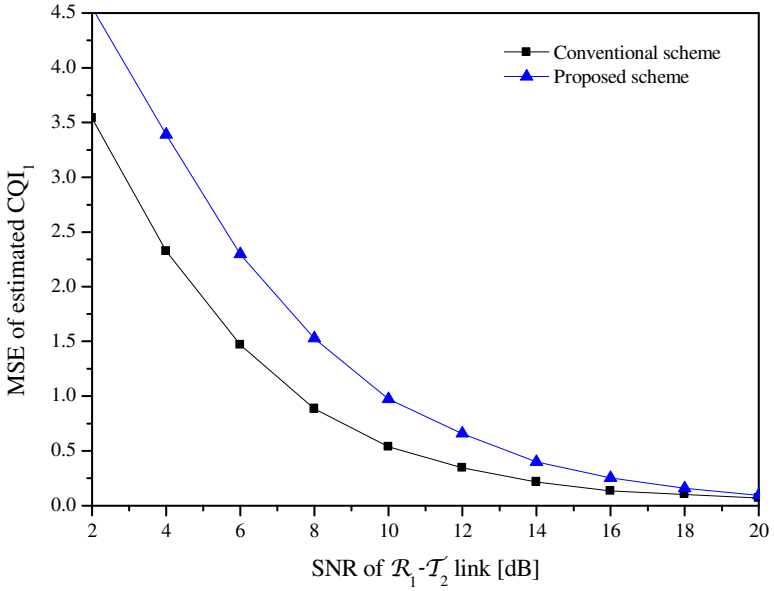

Figure 3.3: MSE of estimated ρ_1 at $\mathcal{T}_2$ versus SNR of $\mathcal{R}_1 - \mathcal{T}_2$ link when the SNRs of $\mathcal{T}_1 - \mathcal{R}_1$ and $\mathcal{R}_1 - \mathcal{T}_2$ links are equal.

perfect condition $\rho_{2,\mathcal{R}} = \rho_{2,\mathcal{T}}$ in Theorem 3.1 could not be satisfied in the first phase of the CQI estimation process. Finally, comparing scheme A and scheme B, it is observed that an improved performance can be achieved with scheme B

when the SNR of $\mathcal{R} \rightarrow \mathcal{T}_2$ link is less than 10 dB. This confirms the explanation in Remark 3.2. Moreover, in order to compare the proposed scheme with the conventional scheme for various SNR values of the transmission link in the first time slot, investigate the case when the $\mathcal{T}_1 \rightarrow \mathcal{R}_1$ transmission has the same SNR as that of the $\mathcal{R}_1 \rightarrow \mathcal{T}_2$ transmission (see Fig. 3.3). It can be observed that the performance of the proposed scheme is still close to that of the conventional scheme, especially when both links are at high SNR. This observation confirms the validity of the proposed CQI reporting scheme for any SNR value of the uplink transmission.

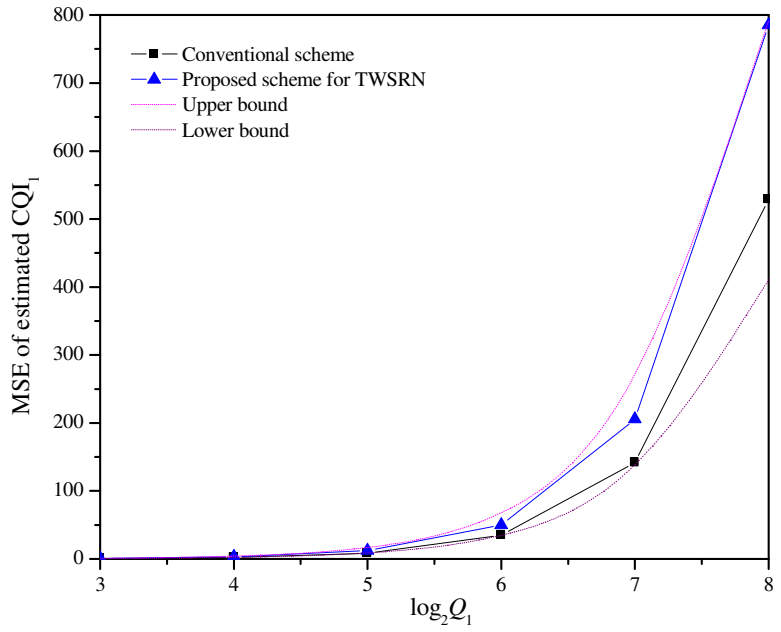

Figure 3.4: MSE of estimated ρ_1 at $\mathcal{T}_2$ versus different CQI levels (Q_1).

The effects of the cardinality of CQI sets are shown in Figs. 3.4, 3.5 and 3.6, where the MSE of the estimated CQI, sum-rate and sum-BER are plotted against the number of CQI levels (i.e. Q_1), respectively. The SNRs of the links in the second phase, i.e. $\mathcal{R}_1 \rightarrow \mathcal{T}_1$ and $\mathcal{R}_1 \rightarrow \mathcal{T}_2$ links, are fixed at 10 dB. The data transmission over TWSRNs in Figs. 3.5 and 3.6 is carried out using various adaptive modulation and coding schemes shown in Table 3.2 which are empirically selected to map the CQI level to MCS level. Specifically, in Table 3.2, for simple simulation, 16 modulation and coding scheme (MCS) levels are selected to map to 16 CQI values using various modulation schemes and coding

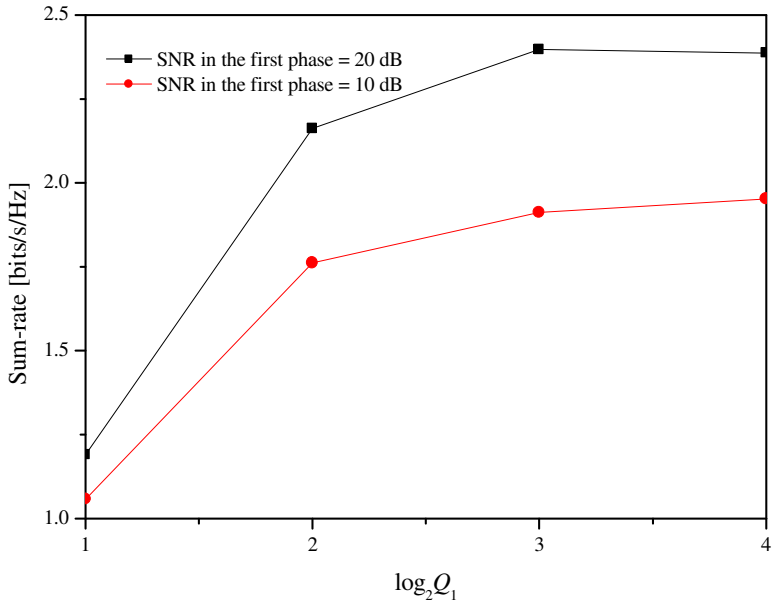

Figure 3.5: Sum-rate versus different CQI levels with adaptive modulation and coding scheme.

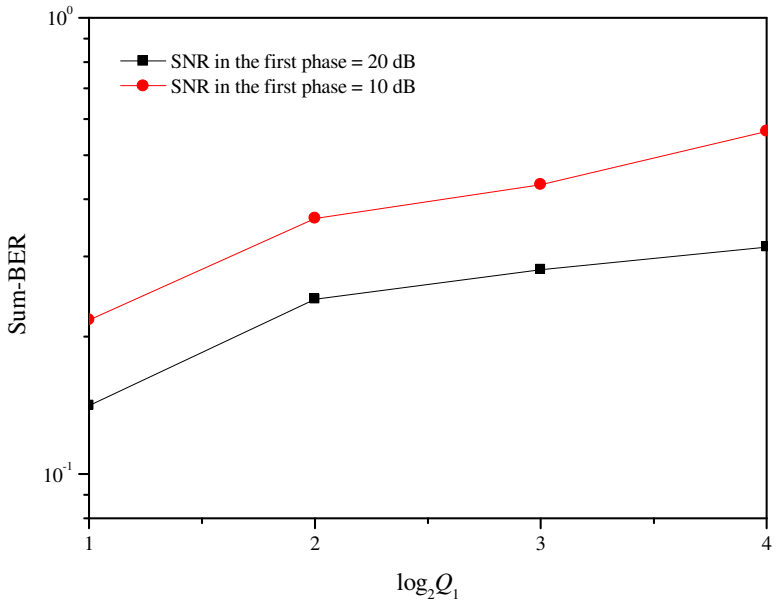

Figure 3.6: Sum-BER versus different CQI levels with adaptive modulation and coding scheme.

rates satisfying the number of bits per symbol increases (e.g. from 0.5 to 5.25 bits/symbol). The SNRs in the first phase are arbitrarily chosen to be 10 dB or 20 dB. It can be seen in Fig. 3.4 that the MSE of the estimated CQI increases as a function of Q_1^2, e.g. MSE increases by 4 times as Q_1 increases by two.

This is further shown in Fig. 3.6 where data transmission is taken into account. The sum-BER performance is reduced as Q_1 increases. However, the increase of CQI levels is helpful in adding more flexibility in selecting a precise MCS level to achieve a higher sum-rate (see Fig. 3.5). These observations confirm the discussion in Remark 3.5 about the trade-off between the performance of CQI reporting and the performance of data transmission.

Table 3.2: CQI mapping table for 16 MCS levels

CQI value	**Modulation**	**Coding rate**	**Bits/Symbol**
0	BPSK	1/2	0.50
1	BPSK	3/4	0.75
2	QPSK	1/2	1.00
3	QPSK	2/3	1.33
4	QPSK	3/4	1.50
5	QPSK	5/6	1.67
6	QPSK	7/8	1.75
7	16 QAM	1/2	2.00
8	16 QAM	2/3	2.67
9	16 QAM	3/4	3.00
10	16 QAM	5/6	3.33
11	16 QAM	7/8	3.50
12	64 QAM	2/3	4.00
13	64 QAM	3/4	4.50
14	64 QAM	5/6	5.00
15	64 QAM	7/8	5.25

3.5.2 Performance of CQI reporting and RS in TWMRN

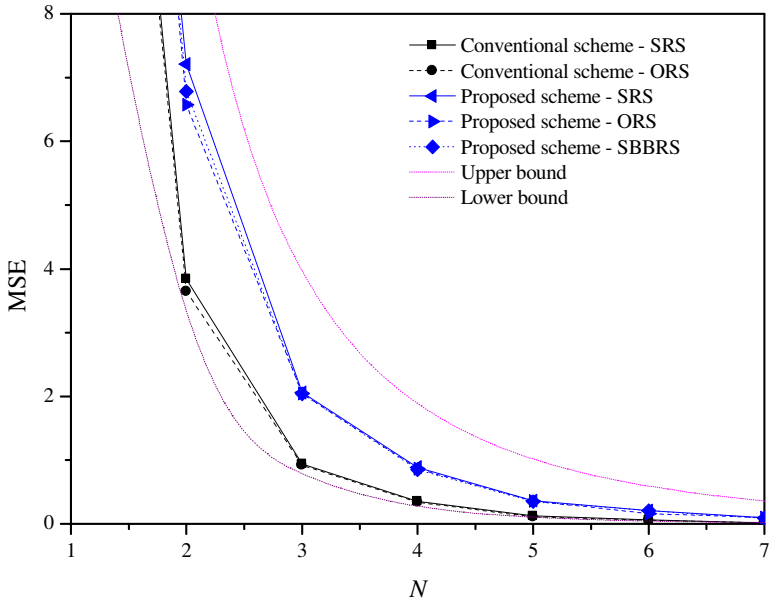

Figure 3.7: MSE versus number of relays (N) with different relay selection schemes.

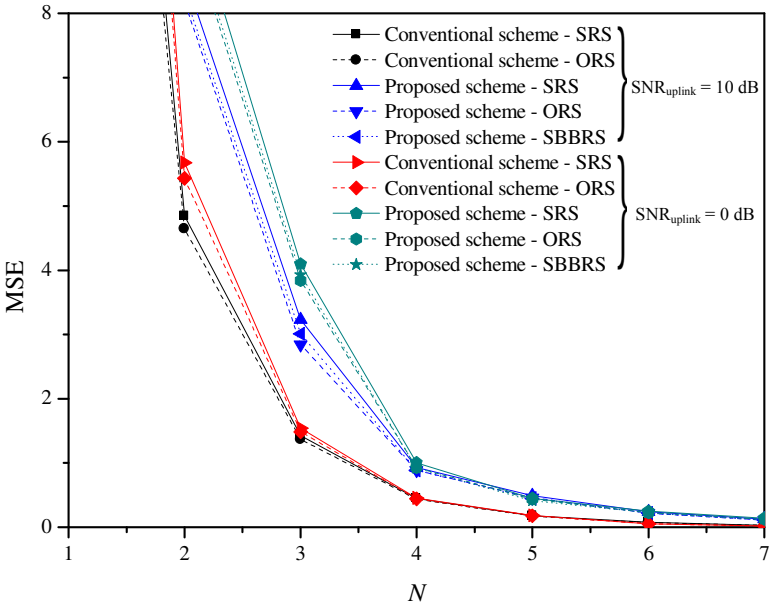

Figure 3.8: MSE versus number of relays (N) with different relay selection schemes and different SNR values of uplink transmission.

Next, the TWMRNs are considered, where multiple relays are taken into account. For RS, the ORS scheme in (3.44), the SRS scheme in (3.45) and

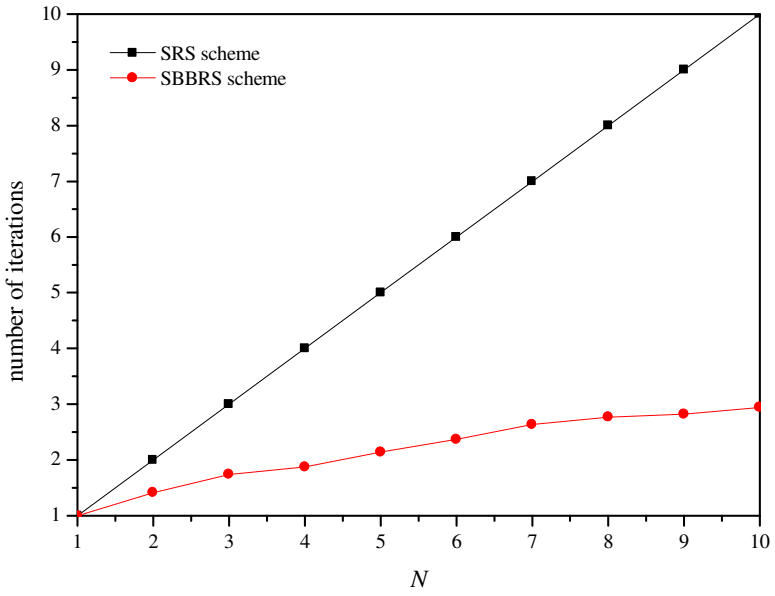

Figure 3.9: Number of iterations versus number of relays (N) with SRS and SBBRS schemes.

the proposed SBBRS scheme are used. For CQI estimation, the conventional scheme is also considered. It is assumed that the number of CQI levels is 16, the length of the pilot sequence is 8, the SNRs of two links from the relay to both terminals are 4 dB, and the SNRs of the uplink transmissions from both terminals to the relay are 20 dB. The assumption of the SNRs in the uplink is to ensure that they are high SNRs, and thus the consistency of the simulation results with analytical results can be confirmed for high-SNR scenarios. As shown in Fig. 3.7, the performance of different RS schemes is close and converges to zero if the number of relays is large. This observation confirms the discussion in Remark 3.6. Furthermore, the effects of different SNR levels in the uplink on the performance of the proposed RS schemes are investigated. Specifically, in Fig. 3.8, the performances of various RS schemes are plotted against the number of relays with respect to various SNR levels in the uplink, including low SNR (0 dB) and medium SNR (10 dB). It can be seen that the performance gap between the proposed schemes and conventional schemes is larger when N is small but still converges to zero if N is large. This observation confirms that the proposed RS schemes work reasonably well with

different SNR levels in the uplink.

Finally, Fig. 3.9 shows the complexity advantage of the proposed SBBRS scheme. The number of iterations is significantly reduced compared to that of the searching algorithm in (3.45), especially when the number of relays in TWMRNs is large. For example, the complexity is reduced by at least a factor of three when the number of relays is larger than five.

3.6 Conclusions

This chapter has proposed and discussed two efficient CQI reporting schemes in nonregenerative TWSRNs based on NC via XOR operation and superposition coding. These schemes reduce the transmission time by half while incurring no additional overhead. Significantly, a system throughput enhancement of 16.7% is obtained at the expense of insignificant increase of complexity and negligible performance loss. In addition, the upper and lower bounds of the MSE of the estimated CQI are derived. The bounds are shown to be quite tight and reflect well the behaviour of the numerical MSEs. Furthermore, a suboptimal CQI-based relay selection scheme has been proposed to reduce the searching complexity of the optimal schemes. The complexity is significantly reduced while the performance is close to that of the optimal ones. For future work, one can investigate the impact of the CQI estimation errors at the relays.

Chapter 4

NC Based Block ACK and Cooperative Retransmission

This chapter is concerned with designing, implementing and evaluating new block acknowledgement (ACK) and retransmission mechanisms in wireless regenerative multi-relay networks through network coding (NC).

In an N-relay network, a total of $(2N+1)$ block ACK packets is required to acknowledge the data transmission between source and destination nodes via the N relay nodes. This chapter first proposes a new block ACK scheme based on NC to significantly reduce the acknowledgement overheads by N block ACK packets. In addition, this new method achieves a reduction of $N(N-1)$ computational operations. Particularly, this chapter derives the error probability of the determination of the packets to be retransmitted at the source and relays, and show that the NC-based scheme also improves the reliability of block ACK transmissions. Furthermore, asymptotic signal-to-noise (SNR) scenarios for forward links are considered and a general expression of error probability in multi-relay networks is derived for each SNR scenario. Simulation results are presented to verify the analytical findings and demonstrate a lower number of data retransmissions for a higher system throughput using NC.

Conventionally, retransmission in an N-relay network can be realised in a cooperative manner with the assistance of all available relays. However, this may result in a high overall power consumption due to the retransmission of the

same packets across the nodes, especially when the number of relays is large. In this chapter, a cooperative retransmission (CR) scheme is further proposed based on relay cooperation and binary XOR operations to significantly reduce the number of packets retransmitted to produce a more power efficient system with non-overlapped (or repeated) retransmissions. Significantly, this chapter also derives the error probability of retransmission decisions at the source and relays and show that the proposed CR scheme improves the reliability of the retransmissions. Furthermore, by deriving the average number of packets to be retransmitted at the source and relays, it is not only shown that the proposed CR scheme reduces the number of retransmissions and removes overlapped retransmitted packets, but also determined the optimised number of relays used for the retransmission phase. Finally, simulation results are presented to demonstrate the validity of the analytical expressions.

4.1 Introduction

Positive acknowledgement (ACK) with retransmission is a communications protocol designed to assure the reliability of data packet transmission over wireless channels that suffer from fading and background noise. This protocol requires the receiver to send an ACK packet to the transmitter to confirm the successful reception of each data packet. Although the transmission reliability is improved by using the ACK protocol, overall throughput is significantly reduced due to frequent transmissions of small-sized ACK packets [136]. To address this issue, a block ACK mechanism is employed for example in the IEEE 802.11e standard to reduce the overhead required at each node [137–140]. A block ACK aggregates multiple ACK packets into a single ACK packet to acknowledge a group of received data packets. This aggregation of block ACK packets improves the overall throughput by reducing the arbitrary inter-frame spacing periods, the backoff counter time and the acknowledgement time. Recently, new medium access control (MAC) amendments based on package aggregation techniques [141] and block ACK mechanisms [142, 143]

have been proposed for the IEEE 802.11n standard [144] to improve further the throughput. However, existing block ACK schemes are generally restricted to one-to-one communications.

In relay-assisted communications (i.e. cooperative communications), the transmission from source node $\mathcal{S}$ to destination node $\mathcal{D}$ is assumed to be carried out with the aid of N relay nodes $\mathcal{R}^{(N)} = \{\mathcal{R}_1, \mathcal{R}_2, \ldots, \mathcal{R}_N\}$ in an orthogonal decode-and-forward manner, where $\mathcal{R}_n$ denotes the nth relay node. While block ACK mechanisms were originally proposed for one-to-one communications, using block ACK in wireless relay networks is more complicated because each relay node in $\mathcal{R}^{(N)}$ has to send block ACK packets for links $\mathcal{S} \rightarrow \mathcal{R}^{(N)}$ to $\mathcal{S}$, and $\mathcal{D}$ has to send block ACK packets for links $\mathcal{R}^{(N)} \rightarrow \mathcal{D}$ to $\mathcal{R}^{(N)}$ and send a block ACK packet for link $\mathcal{S} \rightarrow \mathcal{D}$ to $\mathcal{S}$ [145, 146]. These will result in a total of $(2N+1)$ block ACK packets. Furthermore, the resulting simultaneous retransmissions of the same packets at $\mathcal{S}$ and $\mathcal{R}^{(N)}$ can considerably degrade the network throughput. To solve this problem, a cooperative retransmission scheme was proposed in [147], i.e. $\mathcal{S}$ only retransmits the corrupted packets at both $\mathcal{R}^{(N)}$ and $\mathcal{D}$, and $\mathcal{R}^{(N)}$ helps $\mathcal{S}$ retransmit the rest of the corrupted packets at $\mathcal{D}$. However, the overall throughput of this cooperative network still suffers from having to send and process $(2N + 1)$ block ACK packets at $\mathcal{S}$, $\mathcal{R}^{(N)}$ and $\mathcal{D}$.

In general, within relay networks, data transmission from a source node to a destination node is carried out with the aid of one or multiple relays. The issue of relay selection (RS) is often considered so that only the "best" relay is chosen for forwarding packets according to different selection criterion (e.g. minimizing bit error rate or maximizing throughput) [148–151]. The employment of block ACK packets in wireless multi-relay networks also leads to the issue of simultaneous retransmissions of the same packets, that can considerably degrade the network throughput. To solve this problem, the retransmissions can be carried out in a cooperative manner [147], referred to as cooperative retransmission (CR). In the application of CR, the relays can help the source retransmit the corrupted packets whereas the source retransmits

only the packets corrupted at all the relays and also the destination.

In multi-relay networks, two relaying and retransmission strategies can be considered. Firstly, only the "best" relay is chosen for forwarding the data packets and retransmitting the corrupted packets according to various relay selection criteria. This is referred to as the best-relaying CR (BCR) scheme in this chapter. Secondly, multiple relays, rather than just the best relay, can participate in the retransmission phase. This group-relaying CR (GCR) scheme relies on a group of relays which are able to determine and retransmit the corrupted packets[8]. However, the overall throughput and power consumption of the system using the GCR scheme suffer from the problem of sending the same packets at different relays due to the lack of mutual information shared between the relays.

This chapter first proposes a new block ACK scheme based on network coding (NC) for wireless regenerative relay networks. The proposed NC-based block ACK scheme will not only reduce the number of block ACK packets but also improve the reliability of determination of packets to be retransmitted[9]. This NC-based scheme will thus minimize the number of data retransmissions for an improved system throughput with a lower complexity in comparison with the non-NC-based block ACK scheme[10]. The basic idea of the proposed NC-based scheme is that $\mathcal{D}$ combines all the block ACK packets for links $\mathcal{R}^{(N)} \rightarrow \mathcal{D}$ and $\mathcal{S} \rightarrow \mathcal{D}$ to create a combined block ACK packet. Thus, the total number of block ACK packets decreases to $(N+1)$ through this combination. After this combined block ACK packet is received along with the block ACK packets for links $\mathcal{S} \rightarrow \mathcal{R}^{(N)}$, the question becomes - *How can* $\mathcal{S}$ *and* $\mathcal{R}^{(N)}$ *determine the packets to be retransmitted to* $\mathcal{D}$*?* As it will be shown

[8]Note that the retransmissions at the relays are assumed to be perfectly synchronised and scheduled.

[9]The work in this chapter is limited to the phases of generation and detection of acknowledgement information only. For full MAC protocols, readers are referred to standard references, e.g. [144].

[10]The non-NC-based block ACK scheme is referred to as a scheme where $\mathcal{R}^{(N)}$ sends N block ACK packets to $\mathcal{S}$, and $\mathcal{D}$ sends $(N+1)$ block ACK packets to $\mathcal{R}^{(N)}$ and $\mathcal{S}$.

later, with NC, the packets to be retransmitted can be determined by performing simple bitwise XOR and/or AND operations on the received block ACK packets at $\mathcal{S}$ and $\mathcal{R}^{(N)}$. The analysis will also show that the reduction of the number of block ACK packets not only improves the reliability of the determination of packets to be retransmitted at the source and relay nodes, but also incurs a lower complexity compared to the non-NC-based block ACK scheme by a reduction of $N(N-1)$ computational operations. In addition, this chapter will derive closed-form expressions for the probability of error in the determination of the packets to be retransmitted at $\mathcal{S}$ and $\mathcal{R}_1$ over Rayleigh flat fading channels in a one-relay network. To the best of the author's knowledge, this has not yet been derived in the literature. The error probabilities are derived with respect to the signal-to-noise ratio (SNR) of the forward and backward links. The derived closed-form expressions manifest not only the effect of channel links on the determination of packets to be retransmitted but also the higher reliability of the proposed NC-based block ACK scheme over the non-NC-based scheme. In order to gain insights into the proposed NC-based block ACK scheme, this chapter will consider some extreme scenarios for the forward links at either very low or very high SNRs. For each scenario, an approximate general expression for the error probability will be derived for multi-relay networks. Simulations are then presented to verify the advantages of the proposed NC-based block ACK scheme. The simulation results are shown to be consistent with the numerical results in the three extreme scenarios and reflect the improved reliability in the determination of packets to be retransmitted using the proposed NC-based block ACK scheme compared with the non-NC-based scheme. Furthermore, the higher reliability of the proposed NC-based block ACK scheme results in a significant reduction in the average number of data retransmissions at all nodes, which is verified through the simulation results.

As a second contribution of this chapter, a new GCR scheme is proposed for wireless regenerative multi-relay networks based on relay cooperation (RC) and binary XOR operations, namely an XOR and RC-based GCR (i.e. XRGCR)

scheme. This novel cooperative retransmission mechanism is designed with the incorporation of two key elements: i) *relay cooperation*: the acknowledged information can be shared among the relays to avoid overlapping in retransmissions; and ii) *XOR operations*: the destination combines all acknowledged information to form one single block ACK packet. This novel design will lead to a significantly improved throughput, particularly when the number of relay nodes is large. Using these methods, the smallest number of packets to be retransmitted will be determined in a cooperative way across both the relays and the source itself. Additionally, closed-form expressions for the retransmission decision error probability (RDEP) across the source and relays are derived for Rayleigh flat fading channels. The analysis shows that the XOR combination helps improve the reliability of the determination of packets to be retransmitted at the source and the relays, which leads to a reduced number of overall retransmissions. The average number of packets to be retransmitted (or average number of retransmissions (ANRs)) across the nodes is then derived, which helps to understand and quantify the level of packet retransmission overlapping in any relaying approach. Importantly, the derived ANRs motivate to propose two RS schemes for high power efficient retransmission by determining the optimised number of relays in the XRGCR scheme. The first RS scheme is identified based on the constraint of frame length (i.e. the number of data packets in a data frame) and the second scheme is designed based on the constraint of total power consumption at the relays, respectively.

The rest of this chapter is organized as follows: Section 4.2 presents various block ACK schemes and provides two examples for one-relay and two-relay networks to illustrate the difference between the non-NC-based block ACK scheme and the proposed NC-based block ACK scheme. The error probability in the determination of packets to be retransmitted at $\mathcal{S}$ and $\mathcal{R}$ is analysed and numerical results are presented. Section 4.3 discusses details and examples of various CR schemes, presents the formulation of the mathematical expressions for RDEP and ANR at both sources and relays. Two RS schemes for the retransmission are also presented. Numerical and simulation results to validate

the concepts are also presented. Section 4.4 concludes the chapter.

4.2 Block ACK Schemes

Fig. 4.1 illustrates the system model of a typical two-hop regenerative relay network. The data transmission from source node $\mathcal{S}$ to destination node $\mathcal{D}$ is accomplished by a two-hop protocol with the assistance of a group of N relays $\mathcal{R}^{(N)} = \{\mathcal{R}_1, \mathcal{R}_2, \ldots, \mathcal{R}_N\}$. In this two-hop regenerative cooperation scheme, $\mathcal{S}$ transmits data sequences continuously to $\mathcal{R}^{(N)}$ and $\mathcal{D}$ in the first hop. In the second hop, $\mathcal{R}^{(N)}$ decode and forward the received data sequences to $\mathcal{D}$ (see Fig. 4.1). It is assumed that $\mathcal{S}$ sends data sequences in the form of aggregated frames, each consisting of W data packets. An aggregated ACK packet, i.e. block ACK packet, of length K (in bits) is used to report the status of each frame where bits '0' and '1' represent the data packet being correctly received and the packet being lost or erroneously received, respectively. For the sake of simplicity, the bits used for overhead and other signalling information are omitted in block ACK packets, and it is assumed that the length of each block ACK packet in bits is equal to the number of packets in a data frame, i.e. $K = W$. For convenience, let Θ_{AB} denote the W-bit block ACK packet that is generated at node B and sent to node A to acknowledge a frame of W packets that are sent from A to B, where $A, B \in \{\mathcal{S}, \mathcal{D}, \mathcal{R}_1, \mathcal{R}_2, \ldots, \mathcal{R}_N\}$.

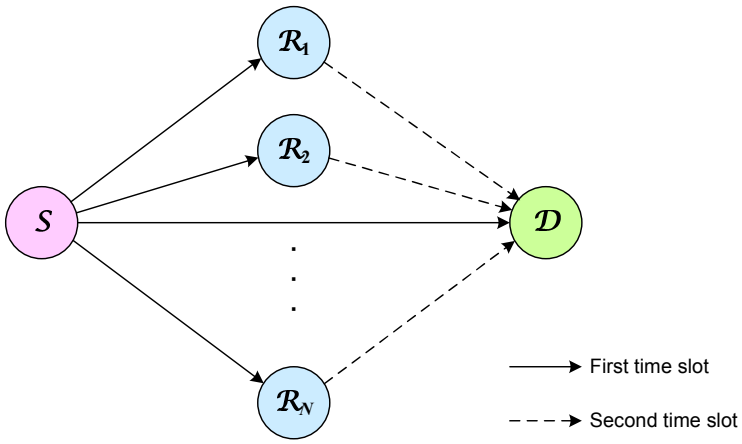

Figure 4.1: System model of two-hop multi-relay network.

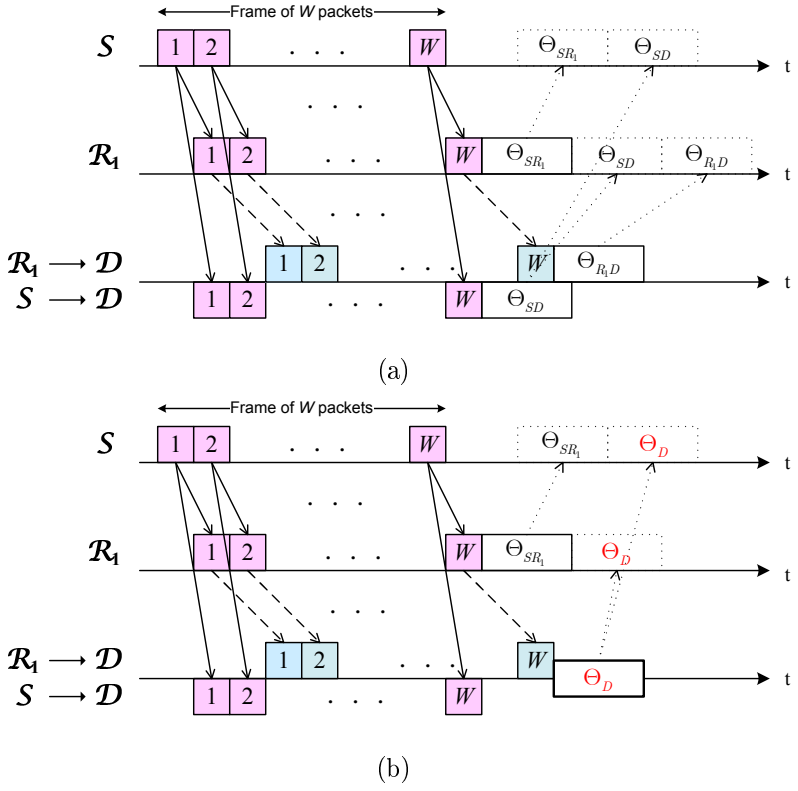

Figure 4.2: Protocol sequence with: (a) non-NC-based block ACK scheme, (b) proposed NC-based block ACK scheme.

Fig. 4.2 illustrates the process of data transmission and block ACK reporting for a one-relay network. The transmission protocol can be readily extended for multi-relay networks. In the first hop, $\mathcal{S}$ transmits W packets sequentially to $\mathcal{R}^{(N)}$ and $\mathcal{D}$. Then, $\mathcal{R}^{(N)}$ forwards the correctly received packet to $\mathcal{D}$ in the second hop. After decoding and error-checking all the W packets received from $\mathcal{S}$, relay nodes $\mathcal{R}_j$, $j \in \{1, 2, \ldots, N\}$, and destination node $\mathcal{D}$ generate block ACK packets Θ_{SR_j} and Θ_{SD}, respectively. Meanwhile, $\mathcal{D}$ also attempts to decode signals forwarded from $\{\mathcal{R}_j\}$ and then generates $\{\Theta_{R_jD}\}$ after checking all the W data packets.

In the non-NC-based block ACK scheme as shown in Fig. 4.2(a), $\mathcal{R}_j$ and $\mathcal{D}$ send the block ACK packets Θ_{SR_j} and Θ_{SD}, respectively, to $\mathcal{S}$ to acknowledge their receipt of the data packets. Similarly, $\mathcal{D}$ sends Θ_{R_jD} to $\mathcal{R}_j$ to acknowledge the receipt of the packets forwarded by $\mathcal{R}_j$. For the purpose of cooperative retransmission, $\mathcal{R}_j$ needs to know which packets $\mathcal{D}$ has received correctly from

$\mathcal{S}$. Thus, Θ_{SD} is additionally sent to all $\{\mathcal{R}_j\}$. In the proposed NC-based block ACK scheme as shown in Fig. 4.2(b), instead of sending Θ_{SD} and Θ_{R_jD} separately, $\mathcal{D}$ generates *only one* combined block ACK packet, denoted as Θ_D, and broadcasts it to $\mathcal{R}_j$ and $\mathcal{S}$. Thus, the number of block ACK packets to be sent from $\mathcal{D}$ decreases.

4.2.1 Non-NC-based and Proposed NC-based Block ACK

The basic principle of NC is that data flows from multiple source nodes are mixed at intermediate nodes before sending to various destination nodes to reduce the number of transmissions and thus the system throughput is improved [20]. This section presents the fundamentals of the proposed NC-based block ACK scheme in contrast with the non-NC-based block ACK scheme.

Non-NC-based Block ACK Scheme

After decoding a frame of W packets, each relay node $\mathcal{R}_j, j = 1, 2, \ldots, N$, generates block ACK packet Θ_{SR_j} while $\mathcal{D}$ generates $(N+1)$ block ACK packets Θ_{R_1D}, Θ_{R_2D}, $\ldots, \Theta_{R_ND}$, and Θ_{SD}. Note that the length of each block ACK packet is W bits. Let Ω_S and Ω_{R_j} denote the W-bit retransmission indication packets (RIPs) generated at $\mathcal{S}$ and $\mathcal{R}_j$, respectively, in which bit '1' indicates that the corresponding data packet needs to be retransmitted while bit '0' indicates otherwise. The RIPs can be obtained as follows:

$$\Omega_S = \Theta_{SR_1} \otimes \Theta_{SR_2} \otimes \cdots \otimes \Theta_{SR_N} \otimes \Theta_{SD}, \tag{4.1a}$$

$$\Omega_{R_j} = \Theta_{R_1D} \otimes \Theta_{R_2D} \otimes \cdots \otimes \Theta_{R_ND} \otimes \Theta_{SD} \otimes \overline{\Theta}_{SR_j}, \tag{4.1b}$$

respectively, where $\otimes$ denotes the bitwise AND operator and $\overline{\Theta}_{AB}$ is the bitwise complement of Θ_{AB}. Note that (4.1a) and (4.1b) are based on the principle of cooperative retransmission, i.e. the source node retransmits the packets that are lost at all the relay and destination nodes, whereas each relay node retransmits only those packets that it correctly decodes but the destination node fails to do so.

The Proposed NC-based Block ACK Scheme

Instead of sending $(2N+1)$ block ACK packets, $\{\Theta_{SR_j}\}$, $\{\Theta_{R_jD}\}$ and Θ_{SD}, as in the non-NC-based block ACK scheme, the proposed NC-based block ACK scheme only needs to send $(N+1)$ block ACK packets, $\{\Theta_{SR_j}\}$ and Θ_D, at $\mathcal{R}^{(N)}$ and $\mathcal{D}$, respectively. While $\{\Theta_{SR_j}\}$ is generated at $\mathcal{R}^{(N)}$ as in the non-NC-based scheme, Θ_D is created at $\mathcal{D}$ as follows:

$$\Theta_D = \Theta_{R_1D} \otimes \Theta_{R_2D} \otimes \cdots \otimes \Theta_{R_ND} \otimes \Theta_{SD}. \tag{4.2}$$

The RIPs, Ω_S and $\Omega_{R_j}, j = 1, 2, \ldots, N$, can be obtained by

$$\Omega_S = \Theta_{SR_1} \otimes \Theta_{SR_2} \otimes \cdots \otimes \Theta_{SR_N} \otimes \Theta_D, \tag{4.3a}$$

$$\Omega_{R_j} = \Theta_D \oplus \left(\Theta_{SR_j} \otimes \Theta_D\right), \tag{4.3b}$$

respectively, where $\oplus$ denotes the bitwise XOR operator. In (4.3a), the determination of packets to be retransmitted at $\mathcal{S}$ follows the principle that the source node retransmits the packets that are lost at all $\mathcal{R}^{(N)}$ and $\mathcal{D}$. Particularly, the idea behind (4.3b) is originated from NC in the sense that $\mathcal{R}_j$ resends those packets that are correctly decoded at $\mathcal{R}_j$ but fails to be decoded at $\mathcal{D}$ and that are not to be resent by $\mathcal{S}$. Thus, the packets that $\mathcal{R}_j$ needs to retransmit are determined by an XOR operation of Θ_D and $\left(\Theta_{SR_j} \otimes \Theta_D\right)$. It is noted that (4.3b) is different from (4.1b).

Remark 4.1 (*Higher Reliability*). *The proposed NC-based scheme can determine the packets to be retransmitted more reliably than the non-NC-based scheme. In the proposed NC-based scheme as shown in* (4.3a)*, to determine* Ω_S*, besides* N *block ACK packets from* $\mathcal{R}^{(N)}$*, i.e.* Θ_{SR_1}*,* Θ_{SR_2}*,* $\ldots, \Theta_{SR_N}$*, a block ACK packet* Θ_D *is required from* $\mathcal{D}$ *instead of* Θ_{SD} *as in the non-NC-based scheme shown in* (4.1a)*. From* (4.2)*,* Θ_D *is determined by combining the block ACK packets of links* $\mathcal{R}^{(N)} \to \mathcal{D}$ *and* $\mathcal{S} \to \mathcal{D}$*. This means that the creation of* Θ_D *depends on decisions of various links, and thus, the decision reliability of the packets to be retransmitted at* $\mathcal{S}$ *can be improved. Additionally, in the non-NC-based scheme as shown in* (4.1b)*, to determine* Ω_{R_j} *at each* $\mathcal{R}_j$*,*

a total of $(N+1)$ *block ACK packets,* Θ_{R_1D}, Θ_{R_2D}, $\ldots, \Theta_{R_ND}$ *and* Θ_{SD}, *are required. Contrastingly, in the proposed NC-based scheme as shown in* (4.3b), *only one packet,* Θ_D, *needs to be known to determine* Ω_{R_j} *at* $\mathcal{R}_j$. *Therefore, the proposed NC-based scheme has a lower probability of error in the determination of packets to be retransmitted at* $\mathcal{R}_j$ *since only one packet,* Θ_D, *has to be detected correctly. Furthermore, it can be seen that the number of packets to be retransmitted depends on the quality of backward links and block ACK schemes. Compared with the non-NC-based block ACK scheme over the same backward environment, the proposed NC-based scheme achieves a higher reliability in the determination of packets to be retransmitted, and thus less data retransmissions are needed.*

Remark 4.2 (*Lower Complexity*). *If the computational complexity is measured by the number of binary operations (e.g. XOR, AND and complement) to determine the packets to be retransmitted at the relays and the source, i.e. the number of required operations to compute* Ω_S *and* Ω_{R_j}, $j \in \{1, 2, \ldots, N\}$, *the proposed NC-based scheme has lower complexity than the non-NC-based scheme. It can be seen from* (4.1a) *and* (4.1b) *that the number of operations performed at* $\mathcal{S}$ *and* $\mathcal{R}_j$ *are* N *and* $(N+2)$, *respectively. Thus, a total of* (N^2+3N) *operations is required in the non-NC-based block ACK scheme. In the proposed NC-based scheme,* N *operations are required at* $\mathcal{D}$, *while no operation is performed at* $\mathcal{D}$ *in the non-NC-based scheme. However, in the proposed NC-based scheme, the complexity at* $\mathcal{R}_j$ *is significantly low since only* 2 *operations are required at* $\mathcal{R}_j$ *(see* (4.3b)*). In addition,* N *operations are required at* $\mathcal{S}$ *according to* (4.3a). *Thus, a total of* $4N$ *operations is required in the proposed NC-based scheme, which results in a quadratic reduction of* (N^2-N) *operations compared to the non-NC-based block ACK scheme. This reduction is substantial when* N *increases. For example, only 20 operations are required when* $N=5$ *(i.e. 50% reduced), while only 8 operations are required when* $N=2$ *(i.e. 20% reduced).*

In order to see the difference between the non-NC-based and the proposed NC-based schemes in generating the block ACK packets and determining the

RIPs, two examples are considered, i.e. a one-relay and a two-relay network, as illustrated in Fig. 4.3 and Fig. 4.4, respectively.

Example 1: One-Relay Network

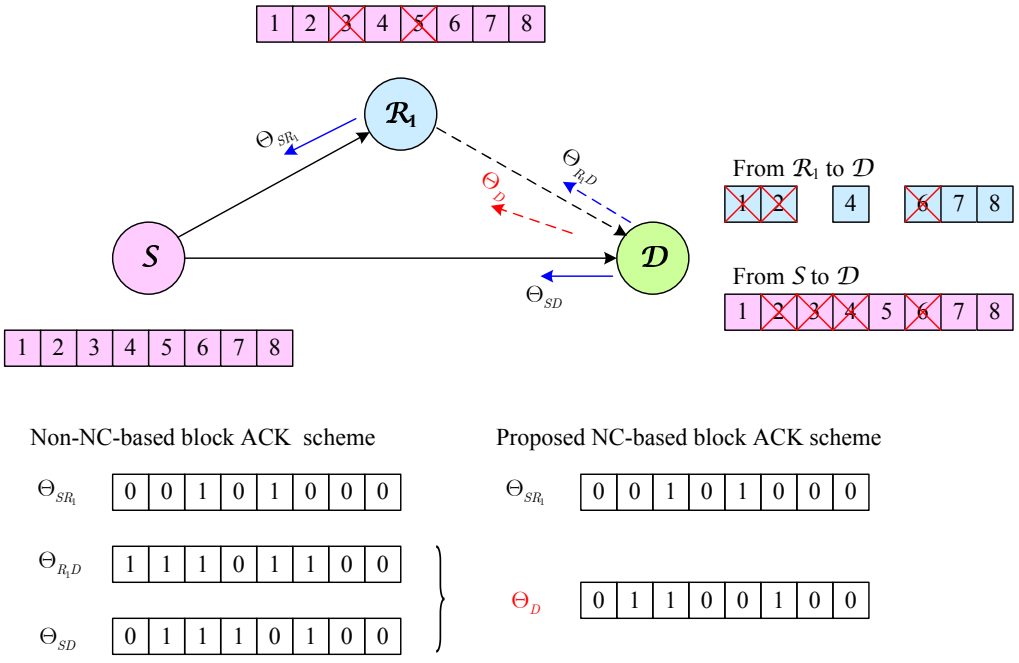

Figure 4.3: Example for block ACK schemes in one-relay network.

An example is considered as depicted in Fig. 4.3 where $\mathcal{S}$ wishes to deliver a data frame of $W = 8$ packets $\{s[1], s[2],...,s[8]\}$ to $\mathcal{D}$ with the aid of $\mathcal{R}_1$. Suppose that the packets with a crossthrough are lost or erroneous. In this example, it is assumed that the erroneous packets received at $\mathcal{R}_1$ and $\mathcal{D}$ in the first hop are $\{s[3], s[5]\}$ and $\{s[2], s[3], s[4], s[6]\}$, respectively. Then, $\mathcal{R}_1$ forwards its correctly decoded packets $\{s[1], s[2], s[4], s[6], s[7], s[8]\}$ to $\mathcal{D}$ in the second hop. Assume that the erroneous packets of link $\mathcal{R}_1 \rightarrow \mathcal{D}$ are $\{s[1], s[2], s[6]\}$. Since the data frame contains 8 packets, the block ACK packet for acknowledgement is 8 bits in length.

Non-NC-based Block ACK Scheme

Based on the received data packets, $\mathcal{R}_1$ generates Θ_{SR_1} = '00101000' while $\mathcal{D}$ generates Θ_{SD} = '01110100' and Θ_{R_1D} = '11101100'. The RIPs can then be

obtained using (4.1a) and (4.1b) as follows: $\Omega_S = \Theta_{SR_1} \otimes \Theta_{SD}$ = '00100000' and $\Omega_{R_1} = \Theta_{R_1D} \otimes \Theta_{SD} \otimes \overline{\Theta}_{SR_1}$ = '01000100'. In this case, $\mathcal{S}$ and $\mathcal{R}_1$ need to retransmit $\{s[3]\}$ and $\{s[2], s[6]\}$, respectively. Obviously, $\mathcal{R}_1$ helps resend the packets (i.e. $\{s[2], s[6]\}$) that $\mathcal{D}$ fails to decode while $\mathcal{S}$ resends the packets that are lost at both $\mathcal{R}_1$ and $\mathcal{D}$ (i.e. $\{s[3]\}$). Note that three block ACK packets in total are required for $\mathcal{S}$ and $\mathcal{R}_1$ to determine the packets to be retransmitted to $\mathcal{D}$.

The Proposed NC-based Block ACK Scheme

The difference in the proposed NC-based scheme is that instead of two separate packets Θ_{R_1D} and Θ_{SD}, only one combined block ACK packet Θ_D is generated and sent from $\mathcal{D}$. In particular, $\Theta_D = \Theta_{R_1D} \otimes \Theta_{SD}$ = '01100100'. The RIPs are obtained as $\Omega_S = \Theta_{SR_1} \otimes \Theta_D$ = '00100000' and $\Omega_{R_1} = \Theta_D \oplus (\Theta_{SR_1} \otimes \Theta_D)$ = '01000100', respectively. This means that $\mathcal{S}$ and $\mathcal{R}_1$ need to retransmit $\{s[3]\}$ and $\{s[2], s[6]\}$, respectively, which is the same as in the non-NC-based scheme.

Example 2: Two-Relay Network

The example depicted in Fig. 4.4 contains two relays. Suppose the erroneous packets received at $\mathcal{R}_1$, $\mathcal{R}_2$ and $\mathcal{D}$ in the first hop are $\{s[3], s[5]\}$, $\{s[2], s[5], s[7]\}$ and $\{s[2], s[3], s[5], s[6]\}$, respectively. Then, $\mathcal{R}_1$ and $\mathcal{R}_2$ forward their correctly decoded packets $\{s[1], s[2], s[4], s[6], s[7], s[8]\}$ and $\{s[1], s[3], s[4], s[6], s[8]\}$, respectively, to $\mathcal{D}$ in the second hop. Assume that the erroneous packets received at $\mathcal{D}$ from $\mathcal{R}_1$ and $\mathcal{R}_2$ are $\{s[1], s[2], s[6]\}$ and $\{s[3], s[6], s[8]\}$, respectively.

Non-NC-based Block ACK Scheme

In order to acknowledge the received data packets, $\mathcal{R}_1$ generates Θ_{SR_1} = '00101000' while $\mathcal{R}_2$ generates Θ_{SR_2} = '01001010'. Similarly, $\mathcal{D}$ generates Θ_{SD} = '01101100', Θ_{R_1D} = '11101100' and Θ_{R_2D} = '01101111'. Based on these block ACK packets, the RIPs can be obtained (using (4.1a) and (4.1b)) as $\Omega_S = \Theta_{SR_1} \otimes \Theta_{SR_2} \otimes \Theta_{SD}$ = '00001000', $\Omega_{R_1} = \Theta_{R_1D} \otimes \Theta_{R_2D} \otimes \Theta_{SD} \otimes \overline{\Theta}_{SR_1}$ =

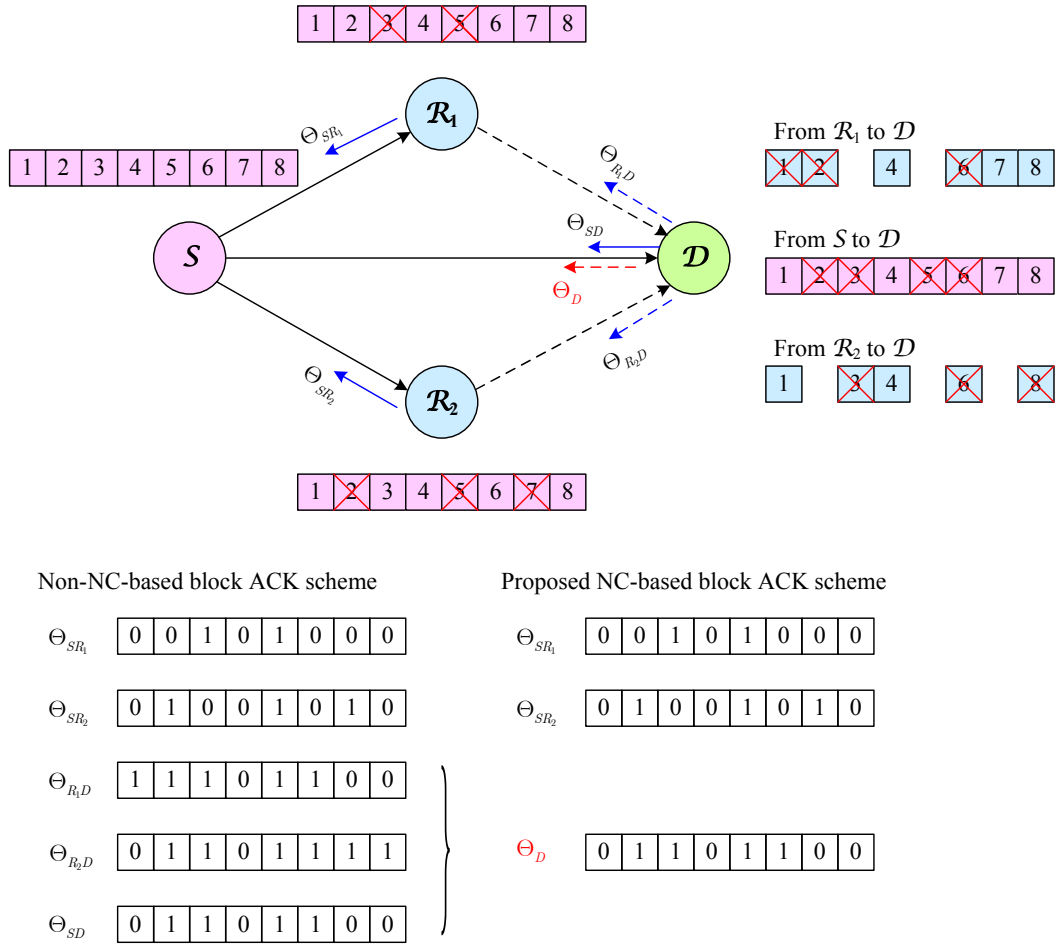

Figure 4.4: Example for block ACK schemes in two-relay network.

'01000100' and $\Omega_{R_2} = \Theta_{R_1D} \otimes \Theta_{R_2D} \otimes \Theta_{SD} \otimes \overline{\Theta}_{SR_2}$ = '00100100'. As a result, $\mathcal{S}$ has to retransmit $\{s[5]\}$ while $\mathcal{R}_1$ has to retransmit $\{s[2], s[6]\}$, and $\mathcal{R}_2$ has to retransmit $\{s[3], s[6]\}$. In this two-relay scenario, five block ACK packets are required in total for $\mathcal{S}$, $\mathcal{R}_1$ and $\mathcal{R}_2$ to be able to determine the packets for retransmission.

The Proposed NC-based Block ACK Scheme

Instead of sending three separate block ACK packets Θ_{R_1D}, Θ_{R_2D} and Θ_{SD}, one combined block ACK is created and sent from $\mathcal{D}$ as $\Theta_D = \Theta_{R_1D} \otimes \Theta_{R_2D} \otimes \Theta_{SD}$ = '01101100'. The RIPs are then obtained as follows: $\Omega_S = \Theta_{SR_1} \otimes \Theta_{SR_2} \otimes \Theta_D$ = '00001000', $\Omega_{R_1} = \Theta_D \oplus (\Theta_{SR_1} \otimes \Theta_D)$ = '01000100', and $\Omega_{R_2} = \Theta_D \oplus (\Theta_{SR_2} \otimes \Theta_D)$ = '00100100'. Thus, $\mathcal{S}$, $\mathcal{R}_1$ and $\mathcal{R}_2$ can determine the

packets to be retransmitted as $\{s[5]\}$, $\{s[2], s[6]\}$ and $\{s[3], s[6]\}$, respectively.

The above examples illustrate how the source and relay nodes in the proposed NC-based block ACK scheme determine the packets to be retransmitted with a reduced number of block ACK packets. For example, in the computation of RIPs, one block ACK packet is saved for a one-relay system and two block ACK packets for a two-relay system. If generalising to networks with N relays, N block ACK packets would be saved using the proposed NC-based block ACK scheme.

4.2.2 Error Probability Analysis of Block ACK Transmission

This subsection first presents signal models for the transmission of block ACK packets through backward links. Then, this subsection will derive the probability of error in the determination of packets to be retransmitted, i.e. the RDEP, at the relay and source nodes in the proposed NC-based scheme.

The channels for all links are assumed to be Rayleigh flat fading channels. The channel gains for forward links $\mathcal{S} \to \mathcal{R}_j$, $\mathcal{R}_j \to \mathcal{D}$, $j \in \{1, 2, \ldots, N\}$, and $\mathcal{S} \to \mathcal{D}$ are denoted by h_{SR_j}, h_{R_jD} and h_{SD}, respectively. Similarly, the channel gains for backward links $\mathcal{R}_j \to \mathcal{S}$, $\mathcal{D} \to \mathcal{R}_j$ and $\mathcal{D} \to \mathcal{S}$ are denoted by h_{R_jS}, h_{DR_j} and h_{DS}, respectively. After receiving a frame of W packets from $\mathcal{S}$ in the first hop of the transmission, each $\mathcal{R}_j$ creates a block ACK packet $\Theta_{SR_j}, j = 1, \ldots, N$, and sends it back to $\mathcal{S}$. The signal received at $\mathcal{S}$ from $\mathcal{R}_j$ can be written as

$$\mathbf{y}_{R_jS} = \sqrt{\Gamma_{R_jS}} h_{R_jS} \mathbf{x}_{SR_j} + \mathbf{n}_{R_jS}, \tag{4.4}$$

where Γ_{R_jS} is the power level for the block ACK signal of link $\mathcal{R}_j \to \mathcal{S}$, $\mathbf{x}_{SR_j}$ is the binary phase shift keying (BPSK) modulated signal[11] of Θ_{SR_j}, and $\mathbf{n}_{R_jS}$ is an independent circularly symmetric complex Gaussian (CSCG) noise vector with each entry having zero mean and variance of N_0. From $\mathbf{y}_{R_jS}$, $\mathcal{S}$ can

[11] BPSK is considered in this thesis for simple analysis. The proposed scheme is applicable for any higher-order modulation schemes.

detect Θ_{SR_j}. Let $\hat{\Theta}_{SR_j}$ denote the detected Θ_{SR_j}. Assume that the channels for the backward links are invariant over the whole transmission of block ACK sequences and known to all the nodes in the network.

At the same time, $\mathcal{D}$ generates Θ_{SD} corresponding to the error of the packets transmitted from $\mathcal{S}$. The data packets forwarded from each $\mathcal{R}_j$ in the second hop of the transmission are acknowledged by packet Θ_{R_jD}. Thus, $(N+1)$ block ACK packets are generated at $\mathcal{D}$, i.e. Θ_{SD} and $\{\Theta_{R_jD}\}$. Then, $\mathcal{D}$ generates a new combined block ACK packet, denoted as Θ_D, as described in (4.2). Θ_D is sent to $\mathcal{S}$ and all $\{\mathcal{R}_j\}$. The received signals at $\mathcal{S}$ and $\mathcal{R}_j, j = 1, \ldots, N$, can be written as

$$\mathbf{y}_{DS} = \sqrt{\Gamma_{DS}} h_{DS} \mathbf{x}_D + \mathbf{n}_{DS}, \tag{4.5}$$

$$\mathbf{y}_{DR_j} = \sqrt{\Gamma_{DR_j}} h_{DR_j} \mathbf{x}_D + \mathbf{n}_{DR_j}, \tag{4.6}$$

respectively. Here, Γ_{DS} and Γ_{DR_j} are the power levels for the block ACK signals of the two links $\mathcal{D} \to \mathcal{S}$ and $\mathcal{D} \to \mathcal{R}_j$, respectively, $\mathbf{x}_D$ is the BPSK modulated signal of Θ_D, and $\mathbf{n}_{DS}$ and $\mathbf{n}_{DR_j}$ are independent CSCG noise vectors with each entry having zero mean and variance of N_0. From (4.5) and (4.6), $\mathcal{S}$ and $\mathcal{R}_j$ can detect Θ_D as $\hat{\Theta}_{D,0}$ and $\hat{\Theta}_{D,j}$, respectively.

The RIPs at $\mathcal{S}$ and $\mathcal{R}_j$ are given, respectively, by

$$\hat{\Omega}_S = \hat{\Theta}_{SR_1} \otimes \hat{\Theta}_{SR_2} \otimes \cdots \otimes \hat{\Theta}_{SR_N} \otimes \hat{\Theta}_{D,0}, \tag{4.7}$$

$$\hat{\Omega}_{R_j} = \hat{\Theta}_{D,j} \oplus \left(\Theta_{SR_j} \otimes \hat{\Theta}_{D,j} \right). \tag{4.8}$$

Next, closed-form expressions for the RDEPs at both $\mathcal{S}$ and $\mathcal{R}_1$ are derived for the proposed NC-based scheme in the one-relay network ($N = 1$). Eqs. (4.7) and (4.8) now become:

$$\hat{\Omega}_S = \hat{\Theta}_{SR_1} \otimes \hat{\Theta}_{D,0}, \tag{4.9}$$

$$\hat{\Omega}_{R_1} = \hat{\Theta}_{D,1} \oplus \left(\Theta_{SR_1} \otimes \hat{\Theta}_{D,1} \right), \tag{4.10}$$

respectively. The RDEP at $\mathcal{S}$ and $\mathcal{R}_1$ can be defined as the bit error rate (BER) of Ω_S given by (4.9) and BER of Ω_{R_1} given by (4.10), respectively.

Without loss of generality, only the first bit in each block ACK and RIP packet is considered. In particular, let a_S and a_{R_1} denote the first bits of Ω_S

and Ω_{R_1}, respectively. Similarly, b_D and b_{SR_1} represent the first bits of Θ_D and Θ_{SR_1}, respectively. From (4.9) and (4.10), the BER of Ω_S and Ω_{R_1} can be obtained as follows:

$$\begin{aligned}
P_b\left(E_{\Omega_S}\right) &= \Pr\left(\hat{a}_S=0|a_S=1\right)\Pr\left(a_S=1\right)+\Pr\left(\hat{a}_S=1|a_S=0\right)\Pr\left(a_S=0\right)\\
&=\Pr\left(\hat{b}_{SR_1}\otimes\hat{b}_{D,0}=0|b_{SR_1}=1,b_D=1\right)\Pr\left(b_{SR_1}=1\right)\Pr\left(b_D=1\right)\\
&+\Pr\left(\hat{b}_{SR_1}\otimes\hat{b}_{D,0}=1|b_{SR_1}=0,b_D=1\right)\Pr\left(b_{SR_1}=0\right)\Pr\left(b_D=1\right)\\
&+\Pr\left(\hat{b}_{SR_1}\otimes\hat{b}_{D,0}=1|b_{SR_1}=1,b_D=0\right)\Pr\left(b_{SR_1}=1\right)\Pr\left(b_D=0\right)\\
&+\Pr\left(\hat{b}_{SR_1}\otimes\hat{b}_{D,0}=1|b_{SR_1}=0,b_D=0\right)\Pr\left(b_{SR_1}=0\right)\Pr\left(b_D=0\right),
\end{aligned} \tag{4.11}$$

$$\begin{aligned}
P_b\left(E_{\Omega_{R_1}}\right) &= \Pr(\hat{a}_{R_1}=0|a_{R_1}=1)\Pr(a_{R_1}=1)+\Pr(\hat{a}_{R_1}=1|a_{R_1}=0)\Pr(a_{R_1}=0)\\
&=\Pr\left(\hat{b}_{D,1}\oplus(b_{SR_1}\otimes\hat{b}_{D,1})=0|b_{SR_1}=0,b_D=1\right)\Pr(b_{SR_1}=0)\Pr(b_D=1)\\
&+\Pr\left(\hat{b}_{D,1}\oplus(b_{SR_1}\otimes\hat{b}_{D,1})=1|b_{SR_1}=0,b_D=0\right)\Pr(b_{SR_1}=0)\Pr(b_D=0)\\
&+\Pr\left(\hat{b}_{D,1}\oplus(b_{SR_1}\otimes\hat{b}_{D,1})=1|b_{SR_1}=1,b_D=0\right)\Pr(b_{SR_1}=1)\Pr(b_D=0)\\
&+\Pr\left(\hat{b}_{D,1}\oplus(b_{SR_1}\otimes\hat{b}_{D,1})=1|b_{SR_1}=1,b_D=1\right)\Pr(b_{SR_1}=1)\Pr(b_D=1),
\end{aligned} \tag{4.12}$$

where $\hat{a}_S$, $\hat{a}_{R_1}$, $\hat{b}_{SR_1}$, $\hat{b}_{D,0}$ and $\hat{b}_{D,1}$ denote the first bit in $\hat{\Omega}_S$, $\hat{\Omega}_{R_1}$, $\hat{\Theta}_{SR_1}$, $\hat{\Theta}_{D,0}$ and $\hat{\Theta}_{D,1}$, respectively. It is observed that $\hat{b}_{D,1}\oplus(b_{SR_1}\otimes\hat{b}_{D,1})=0$ if $b_{SR_1}=1$. Consequently, $\Pr(\hat{b}_{D,1}\oplus(b_{SR_1}\otimes\hat{b}_{D,1})=1|b_{SR_1}=1,b_D=0)=0$ and $\Pr(\hat{b}_{D,1}\oplus(b_{SR_1}\otimes\hat{b}_{D,1})=1|b_{SR_1}=1,b_D=1)=0$. Thus, (4.12) can be rewritten as

$$\begin{aligned}
P_b\left(E_{\Omega_{R_1}}\right) &= \Pr\left(\hat{b}_{D,1}\oplus(b_{SR_1}\otimes\hat{b}_{D,1})=0|b_{SR_1}=0,b_D=1\right)\Pr(b_{SR_1}=0)\Pr(b_D=1)\\
&+\Pr\left(\hat{b}_{D,1}\oplus(b_{SR_1}\otimes\hat{b}_{D,1})=1|b_{SR_1}=0,b_D=0\right)\Pr(b_{SR_1}=0)\Pr(b_D=0).
\end{aligned} \tag{4.13}$$

For simplicity, it is assumed that the channels for both forward and backward links are Rayleigh flat fading. That is, $h_{AB} \sim \mathcal{CN}(0,1)$, $A, B \in \{S, R_1, D\}$, $A \neq B$. In this case, the BER for signal transmission through link $A \to B$, $A, B \in \{S, R_1, D\}$, $A \neq B$, over a Rayleigh flat fading channel is given by [120][12]

$$P_b(E_{AB}) = \phi(\gamma_{AB}), \tag{4.14}$$

where γ_{AB} is the average SNR given by $\gamma_{AB} = \Gamma_{AB}/N_0$, Γ_{AB} is the power level of the signal transmitted through the link $A \to B$, and $\phi(x) \triangleq \frac{1}{2}\left(1 - \sqrt{\frac{x}{1+x}}\right)$.

Theorem 4.1. *The RDEPs at $\mathcal{S}$ and $\mathcal{R}_1$ are given by*

$$P_b(E_{\Omega_S}) = \zeta_{11}\alpha\beta + \zeta_{01}(1-\alpha)\beta + \zeta_{10}\alpha(1-\beta) + \zeta_{00}(1-\alpha)(1-\beta), \tag{4.15a}$$

$$P_b(E_{\Omega_{R_1}}) = \xi(1-\alpha), \tag{4.15b}$$

respectively, where $\alpha = \phi(\gamma_{SR_1})$, $\beta = \phi(\gamma_{R_1D})\phi(\gamma_{SD})$, $\zeta_{00} = \phi(\gamma_{R_1S})\phi(\gamma_{DS})$, $\zeta_{01} = \phi(\gamma_{R_1S})\,[1-\phi(\gamma_{DS})]$, $\zeta_{10} = [1-\phi(\gamma_{R_1S})]\phi(\gamma_{DS})$, $\zeta_{11} = \phi(\gamma_{R_1S}) + \phi(\gamma_{DS}) - \phi(\gamma_{R_1S})\phi(\gamma_{DS})$ and $\xi = \phi(\gamma_{DR_1})$.

Proof. For convenience, let $\alpha' = \Pr(b_{SR_1} = 1)$, $\beta' = \Pr(b_D = 1)$, $\zeta'_{ij} = \Pr(\hat{b}_{SR_1} \otimes \hat{b}_{D,0} = \overline{i \otimes j} | b_{SR_1} = i, b_D = j)$ and $\xi'_i = \Pr(\hat{b}_{D,1} \oplus (b_{SR_1} \otimes \hat{b}_{D,1}) = \bar{i} | b_{SR_1} = 0, b_D = i)$, $\{i, j\} \in \{0, 1\}$. Then, (4.11) and (4.13) can be rewritten as

$$P_b(E_{\Omega_S}) = \zeta'_{11}\alpha'\beta' + \zeta'_{01}(1-\alpha')\beta' + \zeta'_{10}\alpha'(1-\beta') + \zeta'_{00}(1-\alpha')(1-\beta'), \tag{4.16}$$

$$P_b\left(E_{\Omega_{R_1}}\right) = \xi'_1(1-\alpha')\beta' + \xi'_0(1-\alpha')(1-\beta'), \tag{4.17}$$

respectively. Now, α', β', ζ'_{ij} and ξ'_i need to be found.

First, find α' and β'. It is observed that $b_{SR_1} = 1$ if there are errors in the data transmission over forward link $\mathcal{S} \to \mathcal{R}_1$, and $b_D = 1$ if $b_{SD} = 1$ and $b_{R_1D} = 1$, i.e. if the data transmission over both links $\mathcal{S} \to \mathcal{D}$ and $\mathcal{R}_1 \to \mathcal{D}$ has errors. Thus, α' and β' can be given by

$$\alpha' = P_b(E_{SR_1}), \tag{4.18}$$

[12]Note that the channel characteristics of the forward and backward links can be different. In this case, different transmission techniques can be used for each link.

$$\beta' = P_b(E_{R_1D})P_b(E_{SD}), \tag{4.19}$$

where $P_b(E_{SR_1})$, $P_b(E_{R_1D})$ and $P_b(E_{SD})$ denote the BERs of data transmission over forward links $\mathcal{S} \rightarrow \mathcal{R}_1$, $\mathcal{R}_1 \rightarrow \mathcal{D}$ and $\mathcal{S} \rightarrow \mathcal{D}$, respectively. Applying (4.14), α' and β' can be obtained as

$$\alpha' = \phi(\gamma_{SR_1}) = \alpha, \tag{4.20}$$

$$\beta' = \phi(\gamma_{R_1D})\phi(\gamma_{SD}) = \beta. \tag{4.21}$$

In (4.16), ζ'_{ij}, $\{i, j\} \in \{0, 1\}$ can be found as

$$\zeta'_{00} = P_b(E_{\Theta_{SR_1}})P_b(E_{\Theta_{D,0}}), \tag{4.22}$$

$$\zeta'_{01} = P_b(E_{\Theta_{SR_1}})(1 - P_b(E_{\Theta_{D,0}})), \tag{4.23}$$

$$\zeta'_{10} = (1 - P_b(E_{\Theta_{SR_1}}))P_b(E_{\Theta_{D,0}}), \tag{4.24}$$

$$\zeta'_{11} = \zeta'_{00} + \zeta'_{01} + \zeta'_{10} = P_b(E_{\Theta_{SR_1}}) + P_b(E_{\Theta_{D,0}}) - P_b(E_{\Theta_{SR_1}})P_b(E_{\Theta_{D,0}}), \tag{4.25}$$

where $P_b(E_{\Theta_{SR_1}})$ and $P_b(E_{\Theta_{D,0}})$ denote the BERs of Θ_{SR_1} and Θ_D, respectively, at $\mathcal{S}$. Applying (4.14), $P_b(E_{\Theta_{SR_1}})$ and $P_b(E_{\Theta_{D,0}})$ can be given by

$$P_b(E_{\Theta_{SR_1}}) = \phi(\gamma_{R_1S}), \tag{4.26}$$

$$P_b(E_{\Theta_{D,0}}) = \phi(\gamma_{DS}), \tag{4.27}$$

respectively. Substituting (4.26) and (4.27) into (4.22), (4.23), (4.24) and (4.25), ζ'_{ij}, $\{i, j\} \in \{0, 1\}$ can be obtained as

$$\zeta'_{00} = \phi(\gamma_{R_1S})\phi(\gamma_{DS}) = \zeta_{00}, \tag{4.28}$$

$$\zeta'_{01} = \phi(\gamma_{R_1S})[1 - \phi(\gamma_{DS})] = \zeta_{01}, \tag{4.29}$$

$$\zeta'_{10} = [1 - \phi(\gamma_{R_1S})]\phi(\gamma_{DS}) = \zeta_{10}, \tag{4.30}$$

$$\zeta'_{11} = \phi(\gamma_{R_1S}) + \phi(\gamma_{DS}) - \phi(\gamma_{R_1S})\phi(\gamma_{DS}) = \zeta_{11}. \tag{4.31}$$

It is observed that $\xi'_i, i = 0, 1$, in (4.17) depends only on the estimation of Θ_D at $\mathcal{R}_1$. Thus, ξ'_i can be given by

$$\xi'_0 = \xi'_1 = P_b(E_{\Theta_{D,1}}), \tag{4.32}$$

where $P_b(E_{\Theta_{D,1}})$ denotes the BER of Θ_D at $\mathcal{R}_1$. From (4.14), ξ_i', $i = 0, 1$, is obtained as

$$\xi_0' = \xi_1' = \phi(\gamma_{DR_1}) = \xi. \tag{4.33}$$

Finally, closed-form expressions for the RDEPs at $\mathcal{S}$ and $\mathcal{R}_1$ are obtained as

$$P_b(E_{\Omega_S}) = \zeta_{11}\alpha\beta + \zeta_{01}(1-\alpha)\beta + \zeta_{10}\alpha(1-\beta) + \zeta_{00}(1-\alpha)(1-\beta), \tag{4.34a}$$

$$P_b(E_{\Omega_{R_1}}) = \xi(1-\alpha)\beta + \xi(1-\alpha)(1-\beta) = \xi(1-\alpha), \tag{4.34b}$$

respectively, where α, β, ζ_{ij}, $\{i, j\} \in \{0, 1\}$, and ξ are given by (4.20), (4.21), (4.28), (4.29), (4.30), (4.31) and (4.33), respectively.

□

Remark 4.3 (*Impact of Transmission Links on RDEP at $\mathcal{S}$*). *As seen from* (4.15a), *RDEP at $\mathcal{S}$ is influenced by the qualities of all outgoing forward links (i.e. $\mathcal{S} \to \mathcal{R}_1$, $\mathcal{R}_1 \to \mathcal{D}$ and $\mathcal{S} \to \mathcal{D}$) and two incoming backward links (i.e. $\mathcal{R}_1 \to \mathcal{S}$ and $\mathcal{D} \to \mathcal{S}$). Specifically, $P_b(E_{\Omega_S})$ monotonically increases over α, β, $\phi(\gamma_{R_1S})$, or $\phi(\gamma_{DS})$. This can be seen by taking the derivative of $P_b(E_{\Omega_S})$ with respect to α, β, $\phi(\gamma_{R_1S})$ and $\phi(\gamma_{DS})$ as follows:*

$$\frac{\partial P_b(E_{\Omega_S})}{\partial \alpha} = \phi(\gamma_{DS})\beta + \phi(\gamma_{DS})[1 - 2\phi(\gamma_{R_1S})](1-\beta) \geqslant 0, \tag{4.35a}$$

$$\frac{\partial P_b(E_{\Omega_S})}{\partial \beta} = \phi(\gamma_{R_1S})\alpha + \phi(\gamma_{R_1S})[1 - 2\phi(\gamma_{DS})](1-\alpha) \geqslant 0, \tag{4.35b}$$

$$\frac{\partial P_b(E_{\Omega_S})}{\partial \phi(\gamma_{R_1S})} = [1 - \phi(\gamma_{DS})]\beta + \phi(\gamma_{DS})(1-\beta)(1-2\alpha) \geqslant 0, \tag{4.35c}$$

$$\frac{\partial P_b(E_{\Omega_S})}{\partial \phi(\gamma_{DS})} = [1 - \phi(\gamma_{R_1S})]\alpha + \phi(\gamma_{R_1S})(1-\alpha)(1-2\beta) \geqslant 0. \tag{4.35d}$$

This implies that if the quality of any forward and backward links $\mathcal{S} \to \mathcal{R}_1$, $\mathcal{R}_1 \to \mathcal{D}$, $\mathcal{S} \to \mathcal{D}$, $\mathcal{R}_1 \to \mathcal{S}$ and $\mathcal{D} \to \mathcal{S}$ is improved, lower determination error of retransmissions at $\mathcal{S}$ is expected. In fact, it can be drawn from an intuitive observation that the quality of any outgoing and incoming links at $\mathcal{S}$ influences, in a monotonically increasing manner, the RDEP at $\mathcal{S}$.

Remark 4.4 (*Impact of Transmission Links on RDEP at $\mathcal{R}_1$*). *As seen from* (4.15b), *RDEP at $\mathcal{R}_1$ is influenced by the qualities of two incoming links including a forward link $\mathcal{S} \to \mathcal{R}_1$ and a backward link $\mathcal{D} \to \mathcal{R}_1$. However, RDEP*

at $\mathcal{R}_1$ is independent of the outgoing links (i.e. $\mathcal{R}_1 \to \mathcal{S}$ and $\mathcal{R}_1 \to \mathcal{D}$) (see the above derivation of RDEP at $\mathcal{R}_1$). Specifically, $P_b(E_{\Omega_{R_1}})$ monotonically increases over ξ but monotonically decreases over α. This means that the reliability of the determination of packets to be retransmitted at $\mathcal{R}_1$ would be improved if either the quality of the backward link $\mathcal{D} \to \mathcal{R}_1$ increases or that of the forward link $\mathcal{S} \to \mathcal{R}_1$ deteriorates. In fact, it can be intuitively observed that the increase of the quality of backward link $\mathcal{D} \to \mathcal{R}_1$ obviously improves the RDEP at $\mathcal{R}_1$, and $\mathcal{R}_1$ would be released from the responsibility of helping $\mathcal{S}$ retransmit a packet to $\mathcal{D}$ if this packet received from $\mathcal{S}$ is corrupted. Thus, if the number of corrupted packets received at $\mathcal{R}_1$ from $\mathcal{S}$ increases, i.e. α increases, the RDEP at $\mathcal{R}_1$ would decrease. However, it should be noted that if α increases, $P_b(E_{\Omega_S})$ would increase as well, as discussed in Remark 4.3.

Remark 4.5 (*Lower RDEP at $\mathcal{S}$ and $\mathcal{R}_1$*). *The proposed NC-based block ACK scheme has a lower RDEP at $\mathcal{S}$ and $\mathcal{R}_1$ than the non-NC-based scheme. This observation confirms the statement in Remark 4.1. Following the non-NC-based block ACK scheme, the BERs of Ω_S and Ω_{R_1} can be derived as*

$$P_b(E_{\Omega'_S}) = \zeta_{11}\alpha\mu + \zeta_{01}(1-\alpha)\mu + \zeta_{10}\alpha(1-\mu) + \zeta_{00}(1-\alpha)(1-\mu), \quad (4.36a)$$

$$P_b(E_{\Omega'_{R_1}}) = \nu_1(1-\alpha)\beta + \nu_0(1-\alpha)(1-\beta), \quad (4.36b)$$

respectively, where

$$\mu \triangleq Pr(b_{SD} = 1), \quad (4.37)$$

$$\nu_1 \triangleq Pr(\hat{b}_{R_1D} \otimes \hat{b}_{SD} \otimes \bar{b}_{SR_1} = 0 | b_{SR_1} = 0, b_{R_1D} = 1, b_{SD} = 1), \quad (4.38)$$

$$\nu_0 \triangleq Pr(\hat{b}_{R_1D} \otimes \hat{b}_{SD} \otimes \bar{b}_{SR_1} = 1 | b_{SR_1} = 0, b_{R_1D} \otimes b_{SD} = 0). \quad (4.39)$$

Similar to the proof of Theorem 4.1, ν_1 and ν_0 can be found as

$$\begin{aligned}\nu_0 = \nu_1 = \nu &= \phi(\gamma_{DR_1})[1-\phi(\gamma_{DR_1})] + [1-\phi(\gamma_{DR_1})]\phi(\gamma_{DR_1}) + [\phi(\gamma_{DR_1})]^2 \\ &= 2\phi(\gamma_{DR_1}) - [\phi(\gamma_{DR_1})]^2.\end{aligned} \quad (4.40)$$

Thus, (4.36b) *can be rewritten as*

$$P_b(E_{\Omega'_{R_1}}) = \nu(1-\alpha). \quad (4.41)$$

It can be seen that $Pr(b_{SD}=1) > Pr(b_D=1) = Pr(b_{SD}=1)Pr(b_{R_1D}=1)$, *i.e.* $\mu > \beta$, *and* $2\phi(\gamma_{DR_1}) - [\phi(\gamma_{DR_1})]^2 > \phi(\gamma_{DR_1})$, *i.e.* $\nu > \xi$. *Thus,* $P_b(E_{\Omega'_S})$ *and* $P_b(E_{\Omega'_{R_1}})$ *in* (4.36a) *and* (4.36b) *are greater than* $P_b(E_{\Omega_S})$ *and* $P_b(E_{\Omega_{R_1}})$ *in* (4.15a) *and* (4.15b), *respectively.*

To understand further the behaviour of the error probabilities in (4.15a) and (4.15b), some asymptotic scenarios of forward links are considered, where links $\mathcal{S} \to \mathcal{R}_1$ and $\mathcal{R}_1 \to \mathcal{D}$ are at either very low or very high SNR (see Table 4.1)[13]. The direct link, $\mathcal{S} \to \mathcal{D}$, is assumed to have a very low SNR (i.e. $\gamma_{SD} \to 0$) (as this is the main motivation for using relay-assisted cooperative transmissions). These asymptotic scenarios allow to extend the error probability analysis to an N-relay network.

Table 4.1: Specific analysis scenarios

Scenario 1	High-SNR $\mathcal{S} \to \mathcal{R}_1$	High-SNR $\mathcal{R}_1 \to \mathcal{D}$
Scenario 2	High-SNR $\mathcal{S} \to \mathcal{R}_1$	Low-SNR $\mathcal{R}_1 \to \mathcal{D}$
Scenario 3	Low-SNR $\mathcal{S} \to \mathcal{R}_1$	High-SNR $\mathcal{R}_1 \to \mathcal{D}$

Scenario 1: High-SNR $\mathcal{S} \to \mathcal{R}_1$ and high-SNR $\mathcal{R}_1 \to \mathcal{D}$

In this scenario, $\gamma_{SR_1} \to \infty$, $\gamma_{R_1D} \to \infty$ and $\gamma_{SD} \to 0$. From (4.20) and (4.21), $\alpha \approx 0$ and $\beta \approx 0$. Thus, $P_b(E_{\Omega_S})$ and $P_b(E_{\Omega_{R_1}})$ can be approximated as

$$P_b(E_{\Omega_S}) \approx \zeta_{00} = \phi(\gamma_{R_1S})\phi(\gamma_{DS}), \tag{4.42a}$$

$$P_b(E_{\Omega_{R_1}}) \approx \xi = \phi(\gamma_{DR_1}). \tag{4.42b}$$

Extended to an N-relay network, $P_b^{(N)}(E_{\Omega_S})$ can be computed by

$$\begin{aligned} P_b^{(N)}(E_{\Omega_S}) \approx \zeta_{00}^{(N)} &= \Pr\{\hat{a}_S = 1 | b_{SR^{(N)}} = 0, b_D = 0\} \\ &= P_b(E_{\Theta_{SR_1}})P_b(E_{\Theta_{SR_2}}) \cdots P_b(E_{\Theta_{SR_N}})P_b(E_{\Theta_{D,0}}) \\ &= \phi(\gamma_{R_1S})\phi(\gamma_{R_2S}) \cdots \phi(\gamma_{R_NS})\phi(\gamma_{DS}). \end{aligned} \tag{4.43}$$

[13]Note that the scenario where both links $\mathcal{S} \to \mathcal{R}_1$ and $\mathcal{R}_1 \to \mathcal{D}$ are at very low SNR is not considered since it is expected that the relay node is in a reasonable condition for relaying.

Similar to a one-relay network, $P_b^{(N)}(E_{\Omega_{R_j}}), j = 1, 2, \ldots, N$, is given by

$$P_b^{(N)}(E_{\Omega_{R_j}}) \approx \phi(\gamma_{DR_j}). \tag{4.44}$$

Scenario 2: High-SNR $\mathcal{S} \to \mathcal{R}_1$ and low-SNR $\mathcal{R}_1 \to \mathcal{D}$

In this scenario, $\gamma_{SR_1} \to \infty$, $\gamma_{R_1D} \to 0$ and $\gamma_{SD} \to 0$. From (4.20) and (4.21), $\alpha \approx 0$ and $\beta \approx 1/4$. Thus, $P_b(E_{\Omega_S})$ and $P_b(E_{\Omega_{R_1}})$ can be approximated as

$$P_b(E_{\Omega_S}) \approx \frac{1}{4}\zeta_{01} + \frac{3}{4}\zeta_{00} = \frac{1}{4}\phi(\gamma_{R_1S})\left[1 + 2\phi(\gamma_{DS})\right], \tag{4.45a}$$

$$P_b(E_{\Omega_{R_1}}) \approx \xi = \phi(\gamma_{DR_1}). \tag{4.45b}$$

Extended to an N-relay network, $P_b^{(N)}(E_{\Omega_S})$ can be computed by

$$P_b^{(N)}(E_{\Omega_S}) \approx \frac{1}{2^{N+1}}\zeta_{01}^{(N)} + \frac{2^{N+1}-1}{2^{N+1}}\zeta_{00}^{(N)}, \tag{4.46}$$

where $\zeta_{00}^{(N)}$ is given by (4.43) and

$$\begin{aligned}\zeta_{01}^{(N)} &= \Pr\left\{\hat{a}_S = 1 | b_{SR^{(N)}} = 0, b_D = 1\right\} \\ &= P_b(E_{\Theta_{SR_1}})P_b(E_{\Theta_{SR_2}})\cdots P_b(E_{\Theta_{SR_N}})\left[1 - P_b(E_{\Theta_{D,0}})\right] \\ &= \phi(\gamma_{R_1S})\phi(\gamma_{R_2S})\cdots\phi(\gamma_{R_NS})[1 - \phi(\gamma_{DS})].\end{aligned} \tag{4.47}$$

Similar to a one-relay network, $P_b^{(N)}(E_{\Omega_{R_j}}), j = 1, 2, \ldots, N$, is given by

$$P_b^{(N)}(E_{\Omega_{R_j}}) \approx \phi(\gamma_{DR_j}). \tag{4.48}$$

Scenario 3: Low-SNR $\mathcal{S} \to \mathcal{R}_1$ and High-SNR $\mathcal{R}_1 \to \mathcal{D}$

In this scenario, $\gamma_{SR_1} \to 0$, $\gamma_{R_1D} \to \infty$ and $\gamma_{SD} \to 0$. From (4.20) and (4.21), $\alpha \approx 1/2$ and $\beta \approx 0$. Thus, $P_b(E_{\Omega_S})$ and $P_b(E_{\Omega_{R_1}})$ can be approximated as

$$P_b(E_{\Omega_S}) \approx \frac{1}{2}\zeta_{10} + \frac{1}{2}\zeta_{00} = \frac{1}{2}\phi(\gamma_{DS}), \tag{4.49a}$$

$$P_b(E_{\Omega_{R_1}}) \approx \frac{1}{2}\xi = \frac{1}{2}\phi(\gamma_{DR_1}). \tag{4.49b}$$

Extended to an N-relay network, $P_b^{(N)}(E_{\Omega_S})$ can be computed by

$$P_b^{(N)}(E_{\Omega_S}) \approx \frac{1}{2^N}\zeta_{10}^{(N)} + \frac{2^N-1}{2^N}\zeta_{00}^{(N)}, \tag{4.50}$$

where $\zeta_{00}^{(N)}$ is given by (4.43) and

$$\begin{aligned}\zeta_{10}^{(N)} &= \Pr\{\hat{a}_S = 1 | b_{SR^{(N)}} = 1, b_D = 0\} \\ &= \left[1-P_b(E_{\Theta_{SR_1}})\right]\left[1-P_b(E_{\Theta_{SR_2}})\right]\cdots\left[1-P_b(E_{\Theta_{SR_N}})\right]P_b(E_{\Theta_{D,0}}) \\ &= [1-\phi(\gamma_{R_1S})][1-\phi(\gamma_{R_2S})]\cdots[1-\phi(\gamma_{R_NS})]\phi(\gamma_{DS}).\end{aligned} \tag{4.51}$$

Similar to a one-relay network, $P_b^{(N)}(E_{\Omega_{R_j}}), j = 1, 2, \ldots, N$, is given by

$$P_b^{(N)}(E_{\Omega_{R_j}}) \approx \frac{1}{2}\phi(\gamma_{DR_j}). \tag{4.52}$$

Remark 4.6 (*Comparison of Scenarios*). *Investigate the sum-RDEP*[14] *of the whole system defined by* $P_b(E) \triangleq P_b(E_{\Omega_S}) + P_b(E_{\Omega_{R_1}})$. *It can be observed that a high SNR of the forward links in Scenario 1 leads to a lower* $P_b(E)$ *compared to Scenario 2. However, this is not always the case when compared to Scenario 3. For convenience, let* $P_{b,i}(E)$ *denote the* $P_b(E)$ *of Scenario* i *and let* $\delta_{ij} \triangleq P_{b,i}(E) - P_{b,j}(E), i, j \in \{1, 2, 3\}$. δ_{ij} *can be given by*

$$\delta_{12} = P_{b,1}(E) - P_{b,2}(E) = \frac{1}{4}\phi(\gamma_{R_1S})\left[2\phi(\gamma_{DS}) - 1\right], \tag{4.53}$$

$$\delta_{13} = P_{b,1}(E) - P_{b,3}(E) = \frac{1}{2}\phi(\gamma_{DS})[2\phi(\gamma_{R_1S}) - 1] + \frac{1}{2}\phi(\gamma_{DR_1}), \tag{4.54}$$

$$\delta_{23} = P_{b,2}(E) - P_{b,3}(E) = \frac{1}{4}\phi(\gamma_{R_1S})\left[1+2\phi(\gamma_{DS})\right] - \frac{1}{2}\phi(\gamma_{DS}) + \frac{1}{2}\phi(\gamma_{DR_1}). \tag{4.55}$$

It can be seen that $\delta_{12} < 0$ *for all* $\gamma_{R_1S}, \gamma_{DS}, \gamma_{DR_1}$. *On the other hand, the other two functions,* δ_{13} *and* δ_{23}, *can be zero at some values of* γ_{R_1S}, γ_{DR_1} *or* γ_{DS}. *In particular, in these equations,* $\delta_{13} = 0$ *and* $\delta_{23} = 0$ *have only one root with respect to either* γ_{R_1S}, γ_{DR_1} *or* γ_{DS}. *This clearly shows that the sum-RDEP,* $P_b(E)$, *in Scenario 2 can be lower or higher than that in Scenario 3 depending on the values of* γ_{R_1S}, γ_{DR_1} *and* γ_{DS}, *which is understandable. However, the same cannot be said for the result with* δ_{13} *which shows that the sum-RDEP in Scenario 3 can be lower than that in Scenario 1, which is surprising. Actually, this is implied by Remark 4.4, where it is shown that* $P_b(E_{\Omega_{R_1}})$ *can be lower as the SNR of link* $\mathcal{S} \to \mathcal{R}_1$ *is lower. This behaviour will be further confirmed by simulations in subsection 4.2.3.*

[14] The sum-RDEP is defined as the summation of the RDEPs at $\mathcal{S}$ and $\mathcal{R}^{(N)}$ in the RET phase.

4.2.3 Numerical and Simulation Results

This subsection presents simulation results of the RDEP and the average number of packets to be retransmitted at the source and relay nodes for different block ACK schemes when both forward and backward channels experience Rayleigh flat fading. Computer simulations are carried out for a typical one-relay network consisting of three nodes $\mathcal{S}$, $\mathcal{R}_1$ and $\mathcal{D}$ with BPSK for signaling and no channel coding. The results are obtained by using Monte Carlo simulation in MATLAB. At $\mathcal{S}$ and $\mathcal{R}_1$, errors occur if the packets required to be retransmitted are different from the actual retransmitted packets.

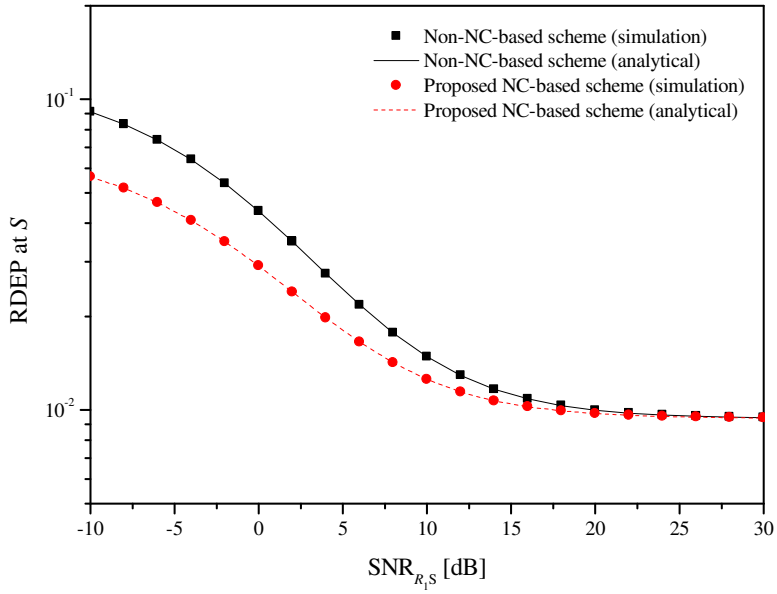

Figure 4.5: RDEP at $\mathcal{S}$ versus SNR_{R_1S}.

The RDEPs at $\mathcal{S}$ and $\mathcal{R}_1$ are first investigated. As shown in Figs. 4.5, 4.6 and 4.7, the RDEP at $\mathcal{S}$ is plotted as a function of various SNR values of links $\mathcal{R}_1 \to \mathcal{S}$ and $\mathcal{D} \to \mathcal{S}$, and the RDEP at $\mathcal{R}_1$ is plotted as a function of the SNR of link $\mathcal{D} \to \mathcal{R}_1$. The SNRs of the forward links $\mathcal{S} \to \mathcal{R}_1$, $\mathcal{R}_1 \to \mathcal{D}$ and $\mathcal{S} \to \mathcal{D}$ are assumed to be 5 dB, 5 dB and 0 dB, respectively. The SNRs of the remaining backward links are assumed as follows:

- Fig. 4.5: $\gamma_{DR_1} = 10$ dB and $\gamma_{DS} = 0$ dB
- Fig. 4.6: $\gamma_{DR_1} = 10$ dB and $\gamma_{R_1S} = 10$ dB

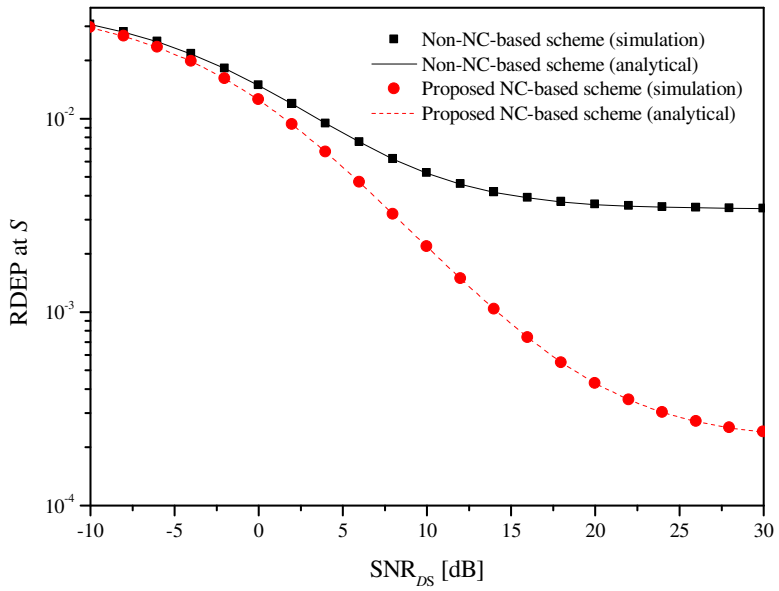

Figure 4.6: RDEP at $\mathcal{S}$ versus SNR_{DS}.

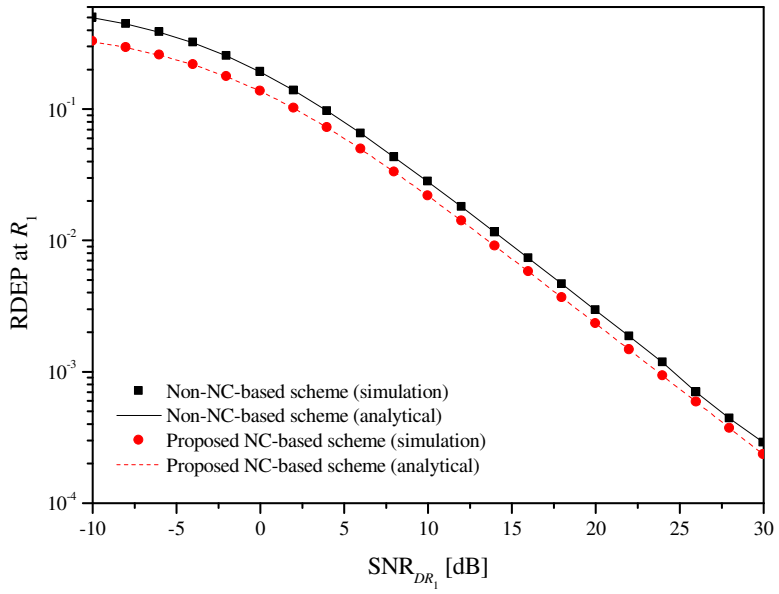

Figure 4.7: RDEP at $\mathcal{R}_1$ versus SNR_{DR_1}.

- Fig. 4.7: $\gamma_{R_1S} = 10$ dB and $\gamma_{DS} = 0$ dB.

It can be seen in Figs. 4.5, 4.6 and 4.7 that the derived RDEPs at $\mathcal{S}$ and $\mathcal{R}_1$ for the proposed NC-based scheme and the non-NC-based scheme given by (4.15a), (4.15b), (4.36a) and (4.41) are consistent with the simulation results. Also, it can be observed that the proposed NC-based block ACK scheme achieves an improved performance over the non-NC-based scheme in terms of both

RDEPs at $\mathcal{S}$ and $\mathcal{R}_1$. For example, to achieve the RDEP at $\mathcal{S}$ and $\mathcal{R}_1$ of 0.02, the proposed scheme improves 3 dB of SNR_{R_1S}, 3 dB of SNR_{DS} and 2 dB of SNR_{DR_1}. This observation confirms the statements in Remarks 4.1 and 4.5 concerning the lower RDEPs at $\mathcal{S}$ and $\mathcal{R}_1$ that can be achieved with the proposed NC-based scheme.

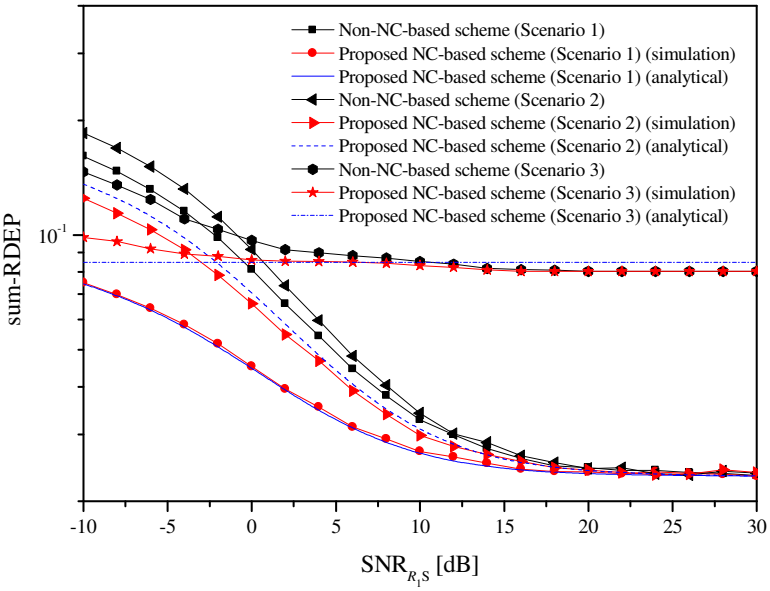

Figure 4.8: Sum-RDEP versus SNR_{R_1S}.

Investigating the whole system, in Fig. 4.8, the sum-RDEP, i.e. the summation of BERs of Ω_S and Ω_{R_1}, is shown for various values of the SNR of link $\mathcal{R}_1 \to \mathcal{S}$ with respect to the following scenarios of the forward links.

- Scenario 1: $\gamma_{SR_1} = 20$ dB, $\gamma_{R_1D} = 20$ dB and $\gamma_{SD} = -20$ dB
- Scenario 2: $\gamma_{SR_1} = 20$ dB, $\gamma_{R_1D} = -20$ dB and $\gamma_{SD} = -20$ dB
- Scenario 3: $\gamma_{SR_1} = -20$ dB, $\gamma_{R_1D} = 20$ dB and $\gamma_{SD} = -20$ dB.

The SNRs of the other backward links $\mathcal{D} \to \mathcal{R}_1$ and $\mathcal{D} \to \mathcal{S}$ are assumed to be 10 dB and 0 dB, respectively. First of all, it can be observed in Fig. 4.8 that the sums of the error probabilities at $\mathcal{S}$ and $\mathcal{R}_1$ given by (4.42a) and (4.42b), (4.45a) and (4.45b), (4.49a) and (4.49b) are consistent with the simulation results. As expected, an improved performance is achieved in Scenario 1 compared to Scenario 2. However, when comparing Scenario 1 and Scenario

2 with Scenario 3, such an explicit conclusion cannot be reached since there are cross-over points among the $P_b(E)$ curves. This observation confirms the statement in Remark 4.6 where the performance of these three scenarios is theoretically compared, i.e. a better performance is always achieved with Scenario 1 when compared to Scenario 2 but the absolute relationship cannot be concluded when comparing Scenario 1 or Scenario 2 with Scenario 3. It can also be seen that $P_b(E)$ in Scenario 3 does not depend on γ_{R_1S} as shown in (4.49a) and (4.49b). Finally, it can be seen that the performance of the proposed NC-based block ACK scheme is better than the non-NC-based scheme for all scenarios. This performance improvement, as explained in Remarks 4.1 and 4.5, is achieved by the reduced number of block ACK transmissions in the proposed NC-based block ACK scheme.

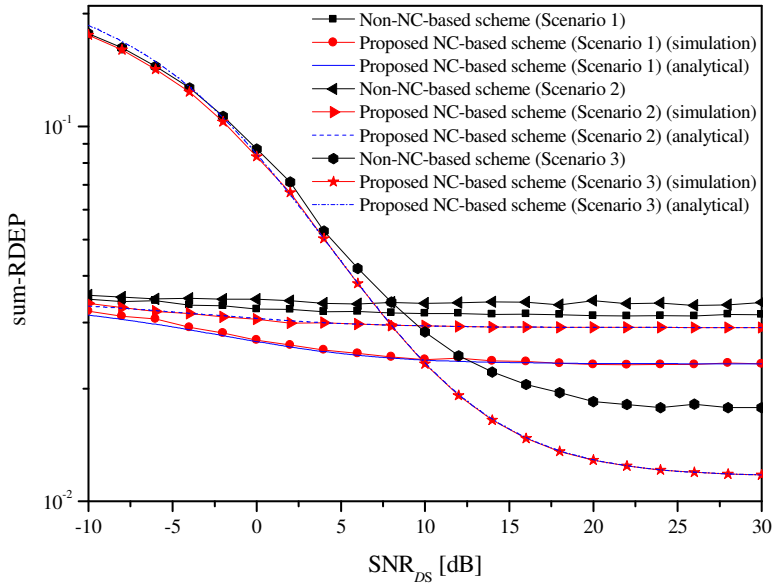

Figure 4.9: Sum-RDEP versus SNR_{DS}.

The impact of SNR of link $\mathcal{D} \rightarrow \mathcal{S}$ on the sum-RDEP is shown in Fig. 4.9, where the SNRs of the other backward links, $\mathcal{R}_1 \rightarrow \mathcal{S}$ and $\mathcal{D} \rightarrow \mathcal{R}_1$, are assumed to be equal to 10 dB. The behaviour which was discussed in Remarks 4.1, 4.5 and 4.6 can be observed, i.e. better performance is achieved with the proposed NC-based scheme for all three scenarios and the relationship between these scenarios is confirmed. In addition, since γ_{R_1S} and γ_{DR_1} are fixed at 10

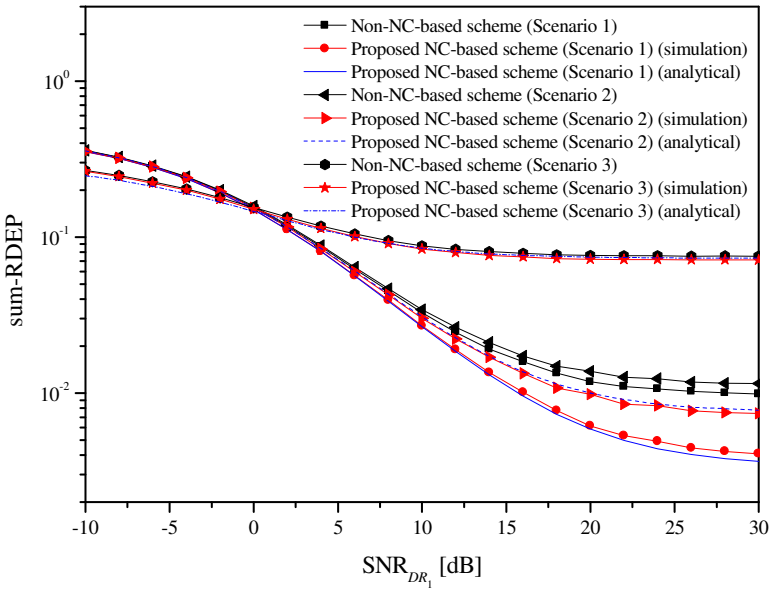

Figure 4.10: Sum-RDEP versus SNR_{DR_1}.

dB which can be assumed to be a high SNR level, the sum-RDEPs in Scenario 1 and Scenario 2 are close to each other and do not depend particularly on γ_{DS}. On the other hand, the sum-RDEP in Scenario 3 depends only on γ_{DS} and γ_{DR_1}, and as such, there is a significant improvement on the sum-RDEP when γ_{DS} increases. The same behaviour can be observed when the RDEP is plotted against the SNR of the link $\mathcal{D} \to \mathcal{R}_1$ as shown in Fig. 4.10 where the reflections in Remarks 4.1, 4.5 and 4.6 can also be realised.

For the comparison of the average number of data retransmissions required for the whole system to transmit one packet from the source to the destination using different block ACK schemes, Scenario 1 is considered with the similar assumption of the SNRs of the forward and backward links. Using the non-NC-based scheme, the packets to be retransmitted at $\mathcal{S}$ and $\mathcal{R}_1$, i.e. the RIPs Ω_S and Ω_{R_1}, are determined by (4.1a) and (4.1b), respectively. Using the proposed NC-based scheme, the RIPs Ω_S and Ω_{R_1} are computed by (4.3a) and (4.3b), respectively. In Figs. 4.11, 4.12 and 4.13, the average number of data retransmissions is plotted as a function of the SNR of backward links $\mathcal{R}_1 \to \mathcal{S}$, $\mathcal{D} \to \mathcal{S}$ and $\mathcal{D} \to \mathcal{R}_1$, respectively. It can be seen that the proposed NC-based block ACK scheme reduces the average number of data retransmissions

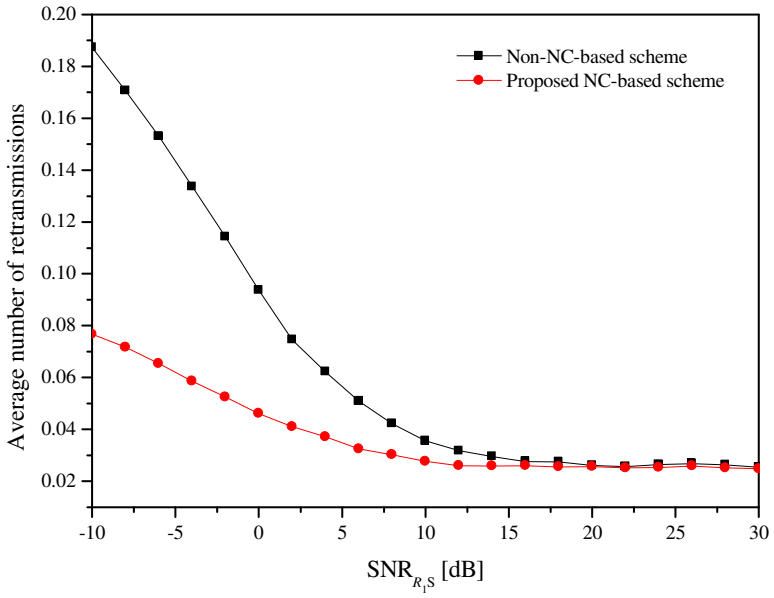

Figure 4.11: Average number of data retransmissions per packet versus SNR_{R_1S} for Scenario 1.

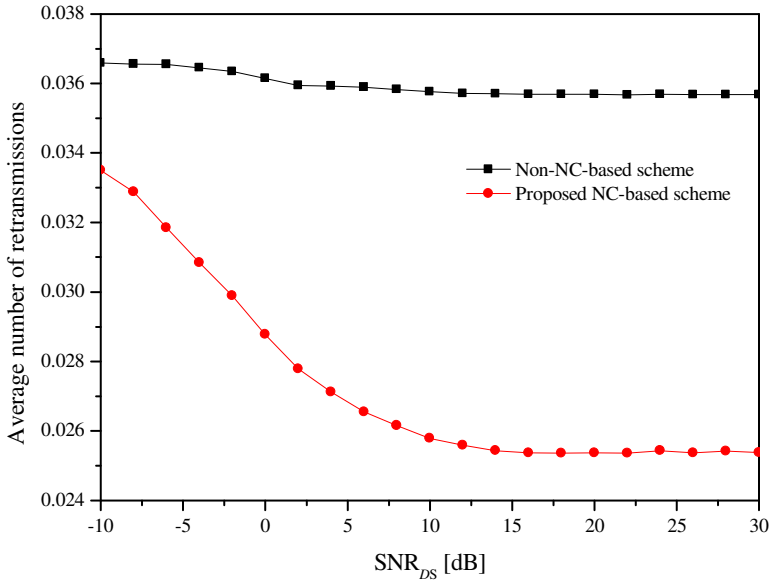

Figure 4.12: Average number of data retransmissions per packet versus SNR_{DS} for Scenario 1.

compared with the non-NC-based scheme over any backward links. It can be observed that the reduction of the number of packets to be retransmitted in Figs. 4.11, 4.12 and 4.13 corresponds to the lower sum-RDEPs achieved with the proposed NC-based scheme for Scenario 1 in Figs. 4.8, 4.9 and 4.10, re-

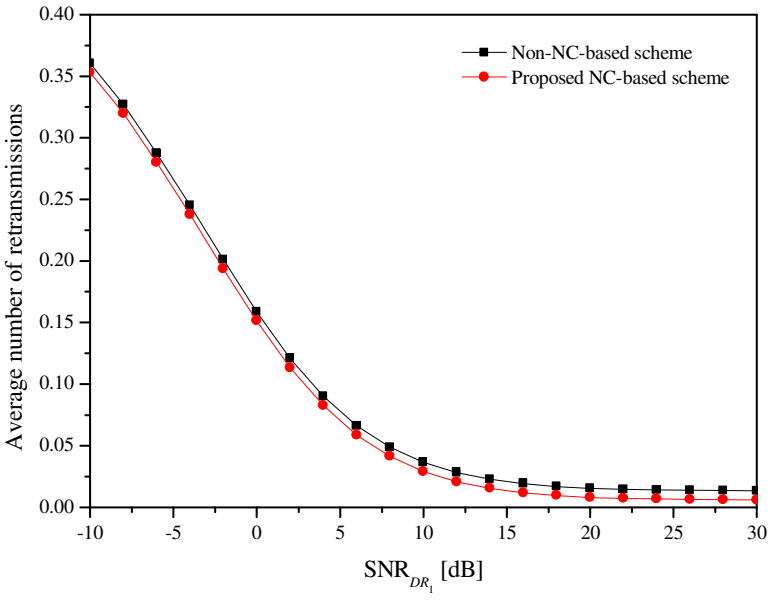

Figure 4.13: Average number of data retransmissions per packet versus SNR_{DR_1} for Scenario 1.

spectively. This significant improvement not only reflects the high reliability of the proposed NC-based scheme in the determination of packets to be retransmitted which is stated in Remarks 4.1 and 4.5, but also substantiates the improvement of system throughput with the proposed NC-based block ACK scheme.

4.3 Cooperative Retransmission Schemes

Fig. 4.14 illustrates a typical regenerative relay system model. The data transmission from a source node $\mathcal{S}$ to a destination node $\mathcal{D}$ is accomplished by a two-hop protocol with the assistance of a best relay in a group of N relays $\mathcal{R}^{(N)} = \{\mathcal{R}_1, \mathcal{R}_2, \ldots, \mathcal{R}_N\}$[15]. There are three phases during the data transmission: broadcast (BC), forward (FW) and retransmission (RET) phases. Source $\mathcal{S}$ transmits data sequences continuously to $\mathcal{R}^{(N)}$ and $\mathcal{D}$ in the BC phase. Then, in the FW phase, all $\mathcal{R}^{(N)}$ decode the received data sequences but only the best relay is selected to forward the decoded data to $\mathcal{D}$ (see

[15]The best relay can be selected by a scheduler of a coordinator node in a centralized manner [129, 130].

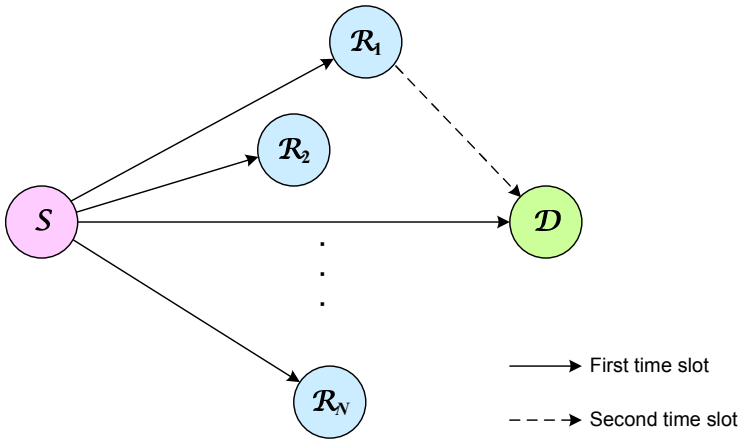

Figure 4.14: System model of two-hop multi-relay network with relay selection.

Fig. 4.14). In the RET phase, only the best relay or group of best relays will carry out retransmissions depending on whether BCR or GCR is used.

The following assumptions are made:

(A1) Without loss of generality, the order of the relays in the group $\mathcal{R}^{(N)}$ is based on the quality of the received signal at the relays, i.e. $\mathcal{R}_1$ denotes the best quality relay while $\mathcal{R}_N$ represents the relay with the lowest signal quality.

(A2) The relays are located within the transmission range of each other in a rather dense network, thus each relay is able to overhear the ACK information from all other relays.

(A3) Source $\mathcal{S}$ sends each data sequence in the form of aggregated frames, with every frame consisting of W data packets.

(A4) An aggregated ACK packet, i.e. block ACK packet, of length K (in bits) is used to report the status of each frame, where bits '0' and '1' represent the data packet being correctly received and the packet being lost or erroneously received, respectively.

(A5) The length of each block ACK packet, in bits, is equal to the number of packets in a data frame, i.e. $K = W$. The bits used for overheads and

other signalling information in block ACK packets are omitted for the sake of simplicity.

For convenience, the notation used in this section is as follows:

(B1) Θ_{AB} denotes the W-bit block ACK packet that is generated at node $\mathcal{B}$ and sent to node $\mathcal{A}$ to acknowledge a frame of W packets that are sent from $\mathcal{A}$ to $\mathcal{B}$, where $\mathcal{A}, \mathcal{B} \in \{\mathcal{S}, \mathcal{D}, \mathcal{R}_1, \mathcal{R}_2, \ldots, \mathcal{R}_N\}$.

(B2) $\Omega_S^{(\mathfrak{X})}$ and $\Omega_{R_j}^{(\mathfrak{X})}$, $\mathfrak{X} \in \{\mathrm{B}, \mathrm{G}, \mathrm{X}\}$[16], denote the W-bit retransmission indication packets (RIPs) generated at $\mathcal{S}$ and $\mathcal{R}_j$, respectively, using various CR schemes in which bit '1' indicates that the corresponding data packet needs to be retransmitted while bit '0' indicates otherwise.

(B3) $\otimes$ and $\oplus$ denote the bitwise AND and XOR operators, respectively.

(B4) $\overline{\Theta}_{AB}$ denotes the bitwise complement of Θ_{AB}.

4.3.1 BCR, GCR and Proposed XRGCR Schemes

The BCR, GCR and XRGCR cooperative schemes may be described as follows:

BCR

Since only $\mathcal{R}_1$ is used in the FW and RET phases, the RIPs at $\mathcal{S}$ and $\mathcal{R}_1$ can be obtained as follows:

$$\Omega_S^{(\mathrm{B})} = \Theta_{SR_1} \otimes \Theta_{SD}, \tag{4.56}$$

$$\Omega_{R_1}^{(\mathrm{B})} = \Theta_{R_1D} \otimes \Theta_{SD} \otimes \overline{\Theta}_{SR_1}. \tag{4.57}$$

Note that (4.56) and (4.57) are based on the principle of CR, i.e. the source node retransmits the packets that are lost at the selected relay and destination nodes, whereas the selected relay node retransmits only those packets that it correctly decodes but the destination node fails to decode.

[16]For simplification, throughout this chapter, the superscript letter in parentheses corresponds to the first letter in the name of CR scheme, e.g. B, G and X represent BCR, GCR and XRGCR, respectively.

GCR

The RIPs at $\mathcal{S}$ and $\mathcal{R}_j$, $j \in \{1, 2, \ldots, N\}$, can be obtained by

$$\Omega_S^{(\mathrm{G})} = \Theta_{SR_1} \otimes \Theta_{SR_2} \otimes \cdots \otimes \Theta_{SR_N} \otimes \Theta_{SD}, \tag{4.58}$$

$$\Omega_{R_j}^{(\mathrm{G})} = \Theta_{R_1D} \otimes \Theta_{SD} \otimes \overline{\Theta}_{SR_j}. \tag{4.59}$$

The principle of CR in (4.58) and (4.59) is that the source node retransmits the packets that are lost at all the relay and destination nodes, whereas each relay node retransmits only those packets that it correctly decodes but the destination node fails to receive.

Proposed XRGCR

Instead of sending 3 block ACK packets Θ_{SR_1}, Θ_{SD} and Θ_{R_1D} as in the BCR and GCR schemes, the proposed XRGCR scheme only requires to send 2 block ACK packet Θ_{SR_1} and Θ_D, at $\mathcal{R}_1$ and $\mathcal{D}$, respectively, where Θ_D is created as follows:

$$\Theta_D = \Theta_{R_1D} \otimes \Theta_{SD}. \tag{4.60}$$

The RIPs at $\mathcal{S}$ and $\mathcal{R}_1$ can be obtained as

$$\Omega_S^{(\mathrm{X})} = \Theta_{SR_1} \otimes \Theta_{SR_2} \otimes \cdots \otimes \Theta_{SR_N} \otimes \Theta_D, \tag{4.61}$$

$$\Omega_{R_1}^{(\mathrm{X})} = \Theta_D \oplus (\Theta_{SR_1} \otimes \Theta_D). \tag{4.62}$$

In (4.61), the determination of packets to be retransmitted at $\mathcal{S}$ follows the principle that $\mathcal{S}$ retransmits the packets that are lost at all the relays $\{\mathcal{R}_1, \mathcal{R}_2, \ldots, \mathcal{R}_N\}$ as well as $\mathcal{D}$. The idea behind (4.62) is originated from the sense that $\mathcal{R}_1$ resends the packets that are correctly decoded at $\mathcal{R}_1$ but $\mathcal{D}$ fails to decode and are not resent by $\mathcal{S}$. Thus, the packets that $\mathcal{R}_1$ needs to retransmit are determined by the XOR operation of Θ_D and $(\Theta_{SR_1} \otimes \Theta_D)$.

Since $\mathcal{R}_2$ can overhear the block ACK Θ_{SR_1} from $\mathcal{R}_1$, the RIPs at $\mathcal{R}_2$ can be obtained by

$$\Omega_{R_2}^{(\mathrm{X})} = \Lambda_{2,1} \oplus \left(\Lambda_{2,1} \otimes \Omega_{R_1}^{(\mathrm{X})}\right), \tag{4.63}$$

where $\Lambda_{2,1} \triangleq \Theta_D \oplus (\Theta_{SR_2} \otimes \Theta_D)$. The idea behind (4.63) is also based on the principle that $\mathcal{R}_2$ resends the packets that are correctly decoded at $\mathcal{R}_2$, but both $\mathcal{R}_1$ and $\mathcal{D}$ fail to decode in both the BC and FW phases, and are not resent by $\mathcal{S}$. Generally, the RIPs at $\mathcal{R}_j$, $j \geq 2$, can be obtained by the inductive method as follows:

$$\Omega_{R_j}^{(\mathrm{X})} = \Lambda_{j,j-1} \oplus \left(\Lambda_{j,j-1} \otimes \Omega_{R_{j-1}}^{(\mathrm{X})}\right), \tag{4.64}$$

where

$$\Lambda_{j,j-1} = \Lambda_{j,j-2} \oplus \left(\Lambda_{j,j-2} \otimes \Omega_{R_{j-2}}^{(\mathrm{X})}\right), \tag{4.65}$$

$$\Lambda_{j,1} = \Theta_D \oplus \left(\Theta_{SR_j} \otimes \Theta_D\right). \tag{4.66}$$

Some Remarks

Remark 4.7 (*Higher Reliability*). *The combination of block ACK packets at the destination in the proposed XRGCR scheme improves the reliability of the determination of the packets to be retransmitted. For convenience, the XRGCR scheme without such combination is referred to as the non-combined XRGCR scheme. The RIPs at $\mathcal{S}$ and $\mathcal{R}_1$ using the non-combined XRGCR scheme can be determined as*

$$\Omega_S^{\prime(X)} = \Theta_{SR_1} \otimes \Theta_{SR_2} \otimes \cdots \otimes \Theta_{SR_N} \otimes \Theta_{SD}, \tag{4.67}$$

$$\Omega_{R_1}^{\prime(X)} = \Theta_{R_1 D} \otimes \Theta_{SD} \otimes \overline{\Theta}_{SR_1}. \tag{4.68}$$

As shown in (4.61)*, besides the requirement of block ACK packets from $\mathcal{R}^{(N)}$, the determination of RIPs at $\mathcal{S}$ requires a combined block ACK packet Θ_D from $\mathcal{D}$ instead of a single block ACK packet Θ_{SD} as shown in* (4.67)*. It can be observed in* (4.60) *that Θ_D is generated by combining the block ACK packets of links $\mathcal{R}_1 \to \mathcal{D}$ and $\mathcal{S} \to \mathcal{D}$. This means that the creation of Θ_D depends on the decisions of these two different links, and thus the decision reliability of the packets to be retransmitted at $\mathcal{S}$ is improved with the proposed XRGCR scheme. Additionally, only one block ACK packet, Θ_D, needs to be known in the proposed XRGCR scheme as shown in* (4.62) *to determine the RIPs at $\mathcal{R}_1$. In the non-combined XRGCR scheme as shown in* (4.68)*, the*

determination of RIPs at $\mathcal{R}_1$ requires two block ACK packets Θ_{R_1D} and Θ_{SD} from $\mathcal{D}$. Therefore, the proposed XRGCR scheme has a lower probability of error in the determination of RIPs at $\mathcal{R}_1$.

Remark 4.8 (*Reduced Number of Retransmissions*). *With the proposed XRGCR scheme, the number of packets to be retransmitted at the source and relay nodes is reduced compared with the non-combined XRGCR scheme. It can be seen that the detection of packets to be retransmitted depends on the quality of the backward links and block ACK schemes. As noted in Remark 4.7, the reliability in the determination of RIPs in the proposed XRGCR scheme is higher than that in the non-combined XRGCR scheme, and thus, over the same backward environment, the proposed XRGCR scheme requires a lower number of data retransmissions.*

Remark 4.9 (*Reduced Number of Retransmissions at $\mathcal{S}$ and Non-Overlapping Retransmissions at $\mathcal{R}_j$*). *The number of packets to be retransmitted at the source is significantly reduced in the GCR and the proposed XRGCR schemes compared to the BCR scheme due to the help of multiple relays in the RET phase. In the GCR scheme, it can be observed that the relays retransmit many overlapped packets due to the lack of cooperation between the relays. Instead, there are no overlapped retransmission packets at the relays in the proposed XRGCR scheme with the RC between the relays. In fact, with binary XOR and AND operations as shown in* (4.64)*, the relays can determine the packets to be retransmitted with no overlap.*

Examples of Cooperative Retransmission Schemes

Examples of retransmission schemes are considered for two-relay and three-relay networks as illustrated in Figs. 4.15 and 4.16, respectively. These will help clarify the generation of block ACK packets along with different CR schemes in determining the RIPs at the source and relays.

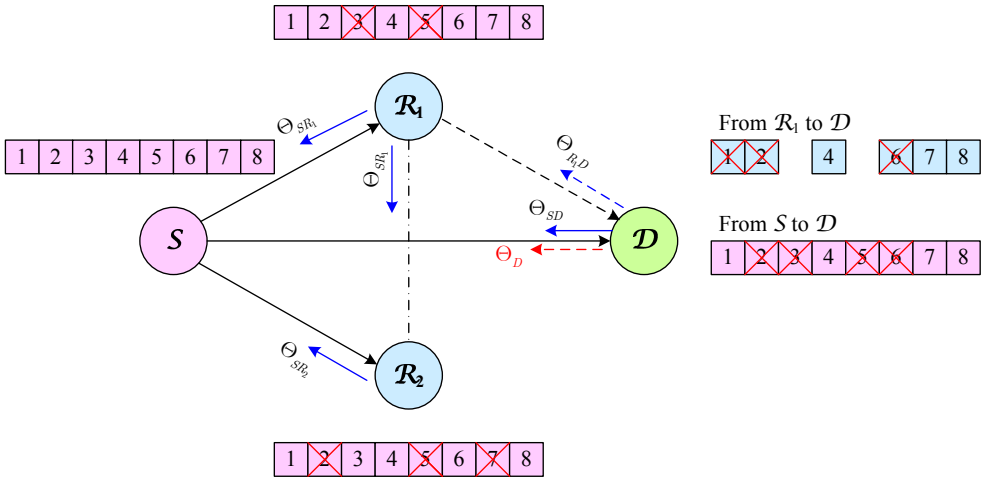

Figure 4.15: Example of proposed XRGCR scheme in two-relay network.

Example 1 - Two-Relay Network

As depicted in Fig. 4.15, an example is considered where $\mathcal{S}$ wishes to deliver a data frame of $W = 8$ packets $\{s[1], s[2], \ldots, s[8]\}$ to $\mathcal{D}$ with the assistance of $\mathcal{R}_1$ and $\mathcal{R}_2$. Suppose that the packets with a crossthrough are lost or have errors. In this example, it is assumed that the erroneous packets received at $\mathcal{R}_1$, $\mathcal{R}_2$ and $\mathcal{D}$ in the BC phase are $\{s[3], s[5]\}$, $\{s[2], s[5], s[7]\}$ and $\{s[2], s[3], s[5], s[6]\}$, respectively. Then, $\mathcal{R}_1$ is selected to forward its correctly decoded packets $\{s[1], s[2], s[4], s[6], s[7], s[8]\}$ to $\mathcal{D}$ in the FW phase. Assume that the erroneous packets of link $\mathcal{R}_1 \rightarrow \mathcal{D}$ are $\{s[1], s[2], s[6]\}$. Since the data frame includes 8 packets, the block ACK packet for the acknowledgement is 8 bits in length. Based on the received data packets, $\mathcal{R}_1$ generates Θ_{SR_1} ='00101000', $\mathcal{R}_2$ generates Θ_{SR_2} ='01001010', and $\mathcal{D}$ generates Θ_{SD} ='01101100' and Θ_{R_1D} ='11101100'.

BCR Scheme

Following the BCR scheme, only the best relay (i.e. $\mathcal{R}_1$), which has most correctly received packets, is used in the FW and RET phases. The RIPs can be obtained using (4.56) and (4.57) as follows: $\Omega_S^{(\mathrm{B})} = \Theta_{SR_1} \otimes \Theta_{SD}$ ='00101000' and $\Omega_{R_1}^{(\mathrm{B})} = \Theta_{R_1D} \otimes \Theta_{SD} \otimes \overline{\Theta}_{SR_1}$ ='01000100'. In this case, $\mathcal{S}$ and $\mathcal{R}_1$ need to retransmit $\{s[3], s[5]\}$ and $\{s[2], s[6]\}$, respectively. It is obvious that $\mathcal{R}_1$ helps

resend the packets (i.e. $\{s[2], s[6]\}$) that $\mathcal{D}$ fails to decode while $\mathcal{S}$ resends the packets that are lost at both $\mathcal{R}_1$ and $\mathcal{D}$ (i.e. $\{s[3], s[5]\}$).

GCR Scheme

In the GCR scheme, $\mathcal{R}_2$ helps $\mathcal{R}_1$ in the RET phase. The RIPs at $\mathcal{S}$, $\mathcal{R}_1$ and $\mathcal{R}_2$ can be obtained using (4.58) and (4.59) as follows: $\Omega_S^{(\mathrm{G})} = \Theta_{SR_1} \otimes \Theta_{SR_2} \otimes \Theta_{SD}$ ='00001000', $\Omega_{R_1}^{(\mathrm{G})} = \Theta_{R_1D} \otimes \Theta_{SD} \otimes \overline{\Theta}_{SR_1}$ ='01000100' and $\Omega_{R_2}^{(\mathrm{G})} = \Theta_{R_1D} \otimes \Theta_{SD} \otimes \overline{\Theta}_{SR_2}$ ='00100100'. In this case, $\mathcal{S}$, $\mathcal{R}_1$ and $\mathcal{R}_2$ retransmit $\{s[5]\}$, $\{s[2], s[6]\}$ and $\{s[3], s[6]\}$, respectively. It can be seen that $\mathcal{S}$ only retransmits one packet $s[5]$ with the help of $\mathcal{R}_2$ in the retransmission of $s[3]$. However, there is one overlapped packet in the RET phase (i.e. $s[6]$).

Proposed XRGCR Scheme

In the proposed XRGCR scheme, only one combined block ACK packet Θ_D is generated by (4.60) and sent from $\mathcal{D}$ instead of two separate packets Θ_{R_1D} and Θ_{SD}. In particular, $\Theta_D = \Theta_{R_1D} \otimes \Theta_{SD}$ ='01101100'. The RIPs at $\mathcal{S}$, $\mathcal{R}_1$ and $\mathcal{R}_2$ can be obtained using (4.61), (4.62) and (4.64) as follows: $\Omega_S^{(\mathrm{X})} = \Theta_{SR_1} \otimes \Theta_{SR_2} \otimes \Theta_D$ ='00001000', $\Omega_{R_1}^{(\mathrm{X})} = \Theta_D \oplus (\Theta_{SR_1} \otimes \Theta_D)$ ='01000100' and $\Omega_{R_2}^{(\mathrm{X})} = \Lambda_{2,1} \oplus (\Lambda_{2,1} \otimes \Omega_{R_1}^{(\mathrm{X})})$ ='00100000', where $\Lambda_{2,1} = \Theta_D \oplus (\Theta_{SR_2} \otimes \Theta_D)$ ='00100100'. Thus, the packets that $\mathcal{S}$, $\mathcal{R}_1$ and $\mathcal{R}_2$ require to retransmit are $\{s[5]\}$, $\{s[2], s[6]\}$ and $\{s[3]\}$, respectively. It can be seen that there is no overlapped packet in the RET phase with the proposed XRGCR scheme.

Example 2 - Three-Relay Network

The example depicted in Fig. 4.16 contains three relays. Let the erroneous packets received at $\mathcal{R}_1$, $\mathcal{R}_2$, $\mathcal{R}_3$ and $\mathcal{D}$ in the BC phase be $\{s[3], s[5]\}$, $\{s[2], s[5], s[7]\}$, $\{s[1], s[4], s[8]\}$ and $\{s[2], s[3], s[5], s[6]\}$, respectively. Similar to the example of the two-relay network, $\mathcal{R}_1$ is selected to forward its correctly decoded packets $\{s[1], s[2], s[4], s[6], s[7], s[8]\}$ to $\mathcal{D}$ in the FW phase and the erroneous packets of link $\mathcal{R}_1 \rightarrow \mathcal{D}$ are $\{s[1], s[2], s[6]\}$. In order to acknowledge the received data packets, $\mathcal{R}_1$ generates Θ_{SR_1} ='00101000', $\mathcal{R}_2$

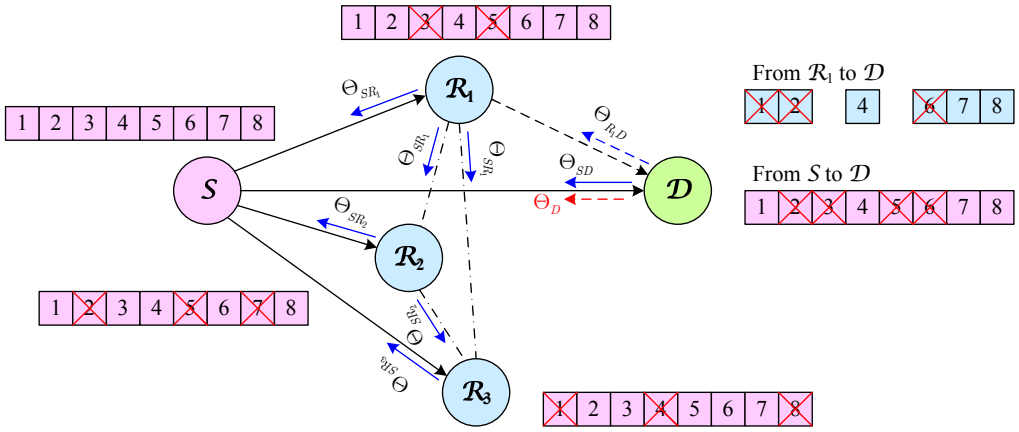

Figure 4.16: Example of proposed XRGCR scheme in three-relay network.

generates Θ_{SR_2} ='01001010', $\mathcal{R}_3$ generates Θ_{SR_3} ='10010001', and $\mathcal{D}$ generates Θ_{SD} ='01101100' and Θ_{R_1D} ='11101100'.

BCR Scheme

Since the BCR scheme does not depend on the number of relays, the determinations of packets to be retransmitted at $\mathcal{S}$ and $\mathcal{R}_1$ are carried out in the same way as the BCR scheme for the two-relay network, and thus the RIPs at $\mathcal{S}$ and $\mathcal{R}_1$ are $\{s[3], s[5]\}$ and $\{s[2], s[6]\}$, respectively.

GCR Scheme

In this scheme, $\mathcal{R}_2$ and $\mathcal{R}_3$ help $\mathcal{R}_1$ in the RET phase. The RIPs at $\mathcal{S}$, $\mathcal{R}_1$, $\mathcal{R}_2$ and $\mathcal{R}_3$ can be obtained using (4.58) and (4.59) as follows: $\Omega_S^{(\mathrm{G})} = \Theta_{SR_1} \otimes \Theta_{SR_2} \otimes \Theta_{SR_3} \otimes \Theta_{SD}$ ='00000000', $\Omega_{R_1}^{(\mathrm{G})} = \Theta_{R_1D} \otimes \Theta_{SD} \otimes \overline{\Theta}_{SR_1}$ ='01000100', $\Omega_{R_2}^{(\mathrm{G})} = \Theta_{R_1D} \otimes \Theta_{SD} \otimes \overline{\Theta}_{SR_2}$ ='00100100' and $\Omega_{R_3}^{(\mathrm{G})} = \Theta_{R_1D} \otimes \Theta_{SD} \otimes \overline{\Theta}_{SR_3}$ = '01101100'. In this case, $\mathcal{S}$ does not require to retransmit any packets while $\mathcal{R}_1$, $\mathcal{R}_2$ and $\mathcal{R}_3$ need to retransmit $\{s[2], s[6]\}$, $\{s[3], s[6]\}$ and $\{s[2], s[3], s[5], s[6]\}$, respectively. It can be seen that $\mathcal{R}_1$, $\mathcal{R}_2$ and $\mathcal{R}_3$ assist $\mathcal{S}$ in the retransmission of lost packets. However, there are four overlapped packets in the RET phase including two $s[6]$ packets, one $s[2]$ packet and one $s[3]$ packet.

Proposed XRGCR Scheme

With only one combined block ACK packet Θ_D ='01101100' at $\mathcal{D}$, the RIPs at $\mathcal{S}$, $\mathcal{R}_1$, $\mathcal{R}_2$ and $\mathcal{R}_3$ can be obtained using (4.61), (4.62) and (4.64) as follows: $\Omega_S^{(\mathrm{X})} = \Theta_{SR_1} \otimes \Theta_{SR_2} \otimes \Theta_{SR_3} \otimes \Theta_D$ ='00000000', $\Omega_{R_1}^{(\mathrm{X})} = \Theta_D \oplus (\Theta_{SR_1} \otimes \Theta_D)$ ='01000100', $\Omega_{R_2}^{(\mathrm{X})} = \Lambda_{2,1} \oplus (\Lambda_{2,1} \otimes \Omega_{R_1}^{(\mathrm{X})})$ ='00100000' and $\Omega_{R_3}^{(\mathrm{X})} = \Lambda_{3,2} \oplus (\Lambda_{3,2} \otimes \Omega_{R_2}^{(\mathrm{X})})$ = '00001000', where $\Lambda_{2,1} = \Theta_D \oplus (\Theta_{SR_2} \otimes \Theta_D)$ ='00100100', $\Lambda_{3,2} = \Lambda_{3,1} \oplus (\Lambda_{3,1} \otimes \Omega_{R_1}^{(\mathrm{X})})$ = '00101000' and $\Lambda_{3,1} = \Theta_D \oplus (\Theta_{SR_3} \otimes \Theta_D)$ ='01101100'. Thus, $\mathcal{S}$ does not require to retransmit any packet and the packets that $\mathcal{R}_1$, $\mathcal{R}_2$ and $\mathcal{R}_3$ need to retransmit are $\{s[2], s[6]\}$, $\{s[3]\}$ and $\{s[5]\}$, respectively. It can also be observed, as in the example for the two-relay network, that there are no overlapped packets in the RET phase with the proposed XRGCR scheme.

4.3.2 Error Probability Analysis of Block ACK Transmission

This subsection first presents signal models for the transmission of block ACK packets through the backward links. Then, this subsection will derive the RDEP, i.e. the probability of error in the determination of packets to be retransmitted, at the relay and source nodes in the proposed XRGCR scheme.

The channel gains for forward links $\mathcal{S} \to \mathcal{R}_j$, $\mathcal{R}_j \to \mathcal{D}$, $j \in \{1, 2, \ldots, N\}$ and $\mathcal{S} \to \mathcal{D}$ are denoted by h_{SR_j},h_{R_jD} and h_{SD}, respectively. Similarly, the channel gains for the backward links $\mathcal{R}_j \to \mathcal{S}$, $\mathcal{D} \to \mathcal{R}_j$ and $\mathcal{D} \to \mathcal{S}$ are denoted by h_{R_jS}, h_{DR_j} and h_{DS}, respectively and the channel gains for cooperation links between relays, i.e. $\mathcal{R}_j \to \mathcal{R}_{j'}$, $j' \in \{2, 3, \ldots, N\}$, $j' > j$, are denoted by $h_{R_jR_{j'}}$. After receiving a frame of W packets from $\mathcal{S}$ in the BC phase, each $\mathcal{R}_j$ creates a block ACK packet Θ_{SR_j}, $j \in \{1, 2, \ldots, N\}$, and sends it back to $\mathcal{S}$. Over the wireless medium, the other relays, i.e. $\mathcal{R}_{j'}$, $j' \in \{2, 3, \ldots, N\}$, $j' > j$, can also receive the block ACK packet from $\mathcal{R}_j$ through the cooperation links $h_{R_jR_{j'}}$. The signals received at $\mathcal{S}$ and $\mathcal{R}_{j'}$ from $\mathcal{R}_j$ can be written as

$$\mathbf{y}_{R_jS} = \sqrt{\Gamma_{R_jS}} h_{R_jS} \mathbf{x}_{SR_j} + \mathbf{n}_{R_jS}, \tag{4.69}$$

$$\mathbf{y}_{R_jR_{j'}} = \sqrt{\Gamma_{R_jR_{j'}}} h_{R_jR_{j'}} \mathbf{x}_{SR_j} + \mathbf{n}_{R_jR_{j'}}, \tag{4.70}$$

respectively, where Γ_{R_jS} and $\Gamma_{R_jR_{j'}}$ are the power levels for the block ACK signals of links $\mathcal{R}_j \to \mathcal{S}$ and $\mathcal{R}_j \to \mathcal{R}_{j'}$, respectively, $\mathbf{x}_{SR_j}$ is BPSK modulated signal of Θ_{SR_j}, and $\mathbf{n}_{R_jS}$ and $\mathbf{n}_{R_jR_{j'}}$ are independent circularly symmetric complex Gaussian (CSCG) noise vectors with each entry having zero mean and variance of N_0. From $\mathbf{y}_{R_jS}$ and $\mathbf{y}_{R_jR_{j'}}$, $\mathcal{S}$ and $\mathcal{R}_{j'}$ can detect Θ_{SR_j}. Let $\hat{\Theta}_{SR_j,0}$ and $\hat{\Theta}_{SR_j,j'}$ denote the detected Θ_{SR_j} at $\mathcal{S}$ and $\mathcal{R}_{j'}$, respectively. It is also assumed that the channels for the backward links and the links between relays are time-invariant over the whole transmission of block ACK sequences and known to all the nodes in the network.

Meanwhile, $\mathcal{D}$ generates Θ_{SD} corresponding to the error of the packets received from $\mathcal{S}$. The data packets forwarded from $\mathcal{R}_1$ in the FW phase are acknowledged by packet Θ_{R_1D}. Then, $\mathcal{D}$ generates a new block ACK packet Θ_D as described in (4.60). This block ACK packet is sent to $\mathcal{S}$ and all $\{\mathcal{R}_j\}$. The received signals at $\mathcal{S}$ and $\mathcal{R}_j, j = 1, \ldots, N$, can be written as

$$\mathbf{y}_{DS} = \sqrt{\Gamma_{DS}} h_{DS} \mathbf{x}_D + \mathbf{n}_{DS}, \tag{4.71}$$

$$\mathbf{y}_{DR_j} = \sqrt{\Gamma_{DR_j}} h_{DR_j} \mathbf{x}_D + \mathbf{n}_{DR_j}, \tag{4.72}$$

respectively. Here, Γ_{DS} and Γ_{DR_j} are the power levels for the block ACK signals of the two links $\mathcal{D} \to \mathcal{S}$ and $\mathcal{D} \to \mathcal{R}_j$, respectively, $\mathbf{x}_D$ is the BPSK modulated signal of Θ_D, and $\mathbf{n}_{DS}$ and $\mathbf{n}_{DR_j}$ are independent CSCG noise vectors with each entry having zero mean and variance of N_0. From (4.71) and (4.72), $\mathcal{S}$ and $\mathcal{R}_j$ can detect Θ_D as $\hat{\Theta}_{D,0}$ and $\hat{\Theta}_{D,j}$, respectively.

The RIPs at $\mathcal{S}$ and $\mathcal{R}_j$ are given by

$$\hat{\Omega}_S = \hat{\Theta}_{SR_1,0} \otimes \hat{\Theta}_{SR_2,0} \otimes \cdots \otimes \hat{\Theta}_{SR_N,0} \otimes \hat{\Theta}_{D,0}, \tag{4.73}$$

$$\hat{\Omega}_{R_1} = \hat{\Theta}_{D,1} \oplus \left(\Theta_{SR_1} \otimes \hat{\Theta}_{D,1} \right), \tag{4.74}$$

$$\hat{\Omega}_{R_j} = \hat{\Lambda}_{j,j-1} \oplus \left(\hat{\Lambda}_{j,j-1} \otimes \hat{\Omega}_{R_{j-1},j} \right), j = 2, 3, \ldots, N, \tag{4.75}$$

where

$$\hat{\Lambda}_{j,j-1} = \hat{\Lambda}_{j,j-2} \oplus \left(\hat{\Lambda}_{j,j-2} \otimes \hat{\Omega}_{R_{j-2},j} \right), \tag{4.76}$$

$$\hat{\Lambda}_{j,1} = \hat{\Theta}_{D,j} \oplus \left(\Theta_{SR_j} \otimes \hat{\Theta}_{D,j}\right), \tag{4.77}$$

$$\hat{\Omega}_{R_{i,j}} = \hat{\Theta}_{D,j} \oplus \left(\hat{\Theta}_{SR_{i,j}} \otimes \hat{\Theta}_{D,j}\right), i = 1, 2, \ldots, N, i < j. \tag{4.78}$$

Next, closed-form expressions for the RDEPs at $\mathcal{S}$ and $\mathcal{R}_j$ are derived for the proposed XRGCR scheme. The RDEP at $\mathcal{S}$ and $\mathcal{R}_j$ can be defined as the BER of Ω_S given by (4.73) and the BER of Ω_{R_j} given by (4.75), respectively.

For simplicity, it is assumed that the channels for all forward, backward and cooperation links are Rayleigh flat fading channels. That is, $h_{AB} \sim \mathcal{CN}(0,1)$ $(A, B \in \{S, R_j, D\}, A \neq B)$, where $\mathcal{CN}(a,b)$ represents the distribution of an CSCG random variable with mean a and variance b. Over a Rayleigh flat fading channel, the BER for signal transmission through link $A \to B$ is similarly calculated as (4.14).

Theorem 4.2. *The RDEPs at $\mathcal{S}$ and $\mathcal{R}_j$, $j = 1, 2, \ldots, N$, in the proposed XRGCR scheme are given by*

$$P_b(E_{\Omega_S}) = \left[1 - \prod_{i=0}^{N}(1-\beta_i)\right]\prod_{i=0}^{N}\alpha_i + \sum_{\mathbb{P}}\prod_{i=0}^{N}\delta_i\epsilon_i, \tag{4.79}$$

$$\begin{aligned} P_b(E_{\Omega_{R_j}}) = {} & (1-\alpha_j)\left[1 - (1-\zeta_j)\prod_{i=1}^{j-1}(1-\eta_{ij})\right]\prod_{i=0}^{j-1}\alpha_i \\ & + (1-\alpha_j)\left[\zeta_j(1-\alpha_0) + (1-\zeta_j)\alpha_0\right]\sum_{\mathbb{P}'}\prod_{i=1}^{j-1}\delta_i'\epsilon_i', \end{aligned} \tag{4.80}$$

where $\alpha_i = \phi(\gamma_{SR_i})$, $\beta_i = \phi(\gamma_{R_iS})$, $\zeta_i = \phi(\gamma_{DR_i})$, $\eta_{ij} = \phi(\gamma_{R_iR_j})$, $\{i,j\} \in \{1,2,\ldots,N\}$, $i < j$, $\alpha_0 = \alpha_{00}\alpha_{01}$, $\alpha_{00} = \phi(\gamma_{SD})$, $\alpha_{01} = \phi(\gamma_{R_1D})$, $\beta_0 = \phi(\gamma_{DS})$, $\mathbb{P} = \{(\delta,\epsilon)|\delta_i = \beta_i$ or $1-\beta_i, \epsilon_i = 1-\alpha_i$ if $\delta_i = \beta_i$ and $\epsilon_i = \alpha_i$ if $\delta_i = 1-\beta_i\}$ and $\mathbb{P}' = \{(\delta',\epsilon')|\delta_i' = \eta_{ij}$ or $1-\eta_{ij}, \epsilon_i' = 1-\alpha_i$ if $\delta_i' = \eta_{ij}$ and $\epsilon_i' = \alpha_i$ if $\delta_i' = 1-\eta_{ij}\}$.

Proof. Without loss of generality, only the first bit in each block ACK and RIP packet is considered. For mathematical convenience, let a_S, $\hat{a}_S$, a_{R_j} and $\hat{a}_{R_j}$, $j = 1, \ldots, N$, denote the first bits of Ω_S, $\hat{\Omega}_S$, Ω_{R_j} and $\hat{\Omega}_{R_j}$, respectively. Similarly, b_D, $\hat{b}_{D,0}$, $\hat{b}_{D,j}$, b_{SR_j}, $\hat{b}_{SR_{j,0}}$, $\hat{b}_{SR_{i,j}}$, b_{SD} and b_{R_1D} represent the first bits of Θ_D, $\hat{\Theta}_{D,0}$, $\hat{\Theta}_{D,j}$, Θ_{SR_j}, $\hat{\Theta}_{SR_{j,0}}$, $\hat{\Theta}_{SR_{i,j}}$, $\{i,j\} \in \{1,\ldots,N\}$, $i < j$, Θ_{SD}

and Θ_{R_1D}, respectively. Then, the BERs of Ω_S and Ω_{R_j} can be obtained as

$$P_b(E_{\Omega_S}) = \Pr(\hat{a}_S = 0|a_S = 1)\Pr(a_S = 1) + \Pr(\hat{a}_S = 1|a_S = 0)\Pr(a_S = 0)\,, \quad (4.81)$$

$$P_b\left(E_{\Omega_{R_j}}\right) = \Pr\left(\hat{a}_{R_j} = 0|a_{R_j} = 1\right)\Pr\left(a_{R_j} = 1\right) + \Pr\left(\hat{a}_{R_j} = 1|a_{R_j} = 0\right)\Pr\left(a_{R_j} = 0\right). \quad (4.82)$$

For convenience, let $\alpha'_0 = \Pr(b_D = 1)$, $\alpha'_{00} = \Pr(b_{SD} = 1)$, $\alpha'_{01} = \Pr(b_{R_1D} = 1)$ and $\alpha'_j = \Pr\left(b_{SR_j} = 1\right)$, $j = 1, 2, \ldots, N$.

First, proceed with the calculation of $P_b(E_{\Omega_S})$. It is observed that $b_{SR_j} = 1$ if there are errors in the data transmission over forward link $\mathcal{S} \to \mathcal{R}_j$ and $b_D = 1$ if $b_{SD} = 1$ and $b_{R_1D} = 1$ (see (4.60)), i.e. if the data transmission over both links $\mathcal{S} \to \mathcal{D}$ and $\mathcal{R}_1 \to \mathcal{D}$ has errors. Thus, α'_j and α'_0 can be given by

$$\alpha'_j = P_b\left(E_{SR_j}\right), \quad (4.83)$$

$$\alpha'_0 = \alpha'_{00}\alpha'_{01} = P_b(E_{SD})\,P_b(E_{R_1D})\,. \quad (4.84)$$

Applying (4.14), α'_j and α'_0 can be obtained as

$$\alpha'_j = \phi\left(\gamma_{SR_j}\right) = \alpha_j, \quad (4.85)$$

$$\alpha'_0 = \phi(\gamma_{SD})\,\phi(\gamma_{R_1D}) = \alpha_{00}\alpha_{01} = \alpha_0. \quad (4.86)$$

From (4.73), (4.81) can be rewritten as

$$\begin{aligned} P_b(E_{\Omega_S}) = {} & \Pr\left(\hat{b}_{SR_{1,0}}\hat{b}_{SR_{2,0}}\ldots\hat{b}_{SR_{N,0}}\hat{b}_{D,0} = 0|b_{SR_1}b_{SR_2}\ldots b_{SR_N}b_D = 1\right) \\ & \times \Pr(b_{SR_1}b_{SR_2}\ldots b_{SR_N}b_D = 1) \\ & + \Pr\left(\hat{b}_{SR_{1,0}}\hat{b}_{SR_{2,0}}\ldots\hat{b}_{SR_{N,0}}\hat{b}_{D,0} = 1|b_{SR_1}b_{SR_2}\ldots b_{SR_N}b_D = 0\right) \\ & \times \Pr(b_{SR_1}b_{SR_2}\ldots b_{SR_N}b_D = 0)\,. \end{aligned} \quad (4.87)$$

Note that

$$\Pr\left(\hat{b}_{SR_{j,0}} = 0|b_{SR_j} = 1\right) = \Pr\left(\hat{b}_{SR_{j,0}} = 1|b_{SR_j} = 0\right) = P_b\left(E_{\Theta_{SR_{j,0}}}\right) = \phi\left(\gamma_{R_jS}\right) = \beta_j, \quad (4.88)$$

$$\Pr\left(\hat{b}_{D,0} = 0|b_D = 1\right) = \Pr\left(\hat{b}_{D,0} = 1|b_D = 0\right) = P_b(E_{\Theta_{DS}}) = \phi(\gamma_{DS}) = \beta_0. \quad (4.89)$$

Substituting α_0, α_j, β_0 and β_j into (4.87), the closed-form expression of $P_b(E_{\Omega_S})$ is obtained as

$$P_b(E_{\Omega_S}) = \left[1 - \prod_{i=0}^{N}(1-\beta_i)\right]\prod_{i=0}^{N}\alpha_i + \sum_{\mathbb{P}}\prod_{i=0}^{N}\delta_i\epsilon_i, \quad (4.90)$$

where $\mathbb{P}$ denotes a set of $\{\beta_i, \alpha_i\}$ satisfying the condition that if one term is β_i then there is another term $(1-\alpha_i)$, and if one term is $(1-\beta_i)$ then there is another term α_i. In other words, $\mathbb{P}$ can be represented as

$$\mathbb{P}=\{(\delta,\epsilon)|\delta_i=\beta_i \text{ or } 1-\beta_i, \epsilon_i=1-\alpha_i \text{ if } \delta_i=\beta_i \text{ and } \epsilon_i=\alpha_i \text{ if } \delta_i=1-\beta_i\}. \quad (4.91)$$

Next, the RDEP at $\mathcal{R}_j$, $j=1,2,\ldots,N$ (i.e. $P_b(E_{\Omega_{R_j}})$) given by (4.82) is calculated. It is observed that $\mathcal{R}_j$ only retransmits the correctly received packets, thus b_{SR_j} should be equal to zero. Otherwise, $\Omega_{R_j}=\hat{\Omega}_{R_j}=0$. From (4.74), (4.75), (4.77), (4.76) and (4.78), (4.82) is rewritten as

$$\begin{aligned} P_b\left(E_{\Omega_{R_j}}\right)=&\Pr\left(\hat{b}_{SR_{j-1},j}\hat{b}_{SR_{j-2},j}\ldots\hat{b}_{SR_1,j}\hat{b}_{D,j}=0|b_{SR_{j-1}}b_{SR_{j-2}}\ldots b_{SR_1}b_D=1\right)\\ &\times\Pr\left(b_{SR_j}=0 \text{ and } b_{SR_{j-1}}b_{SR_{j-2}}\ldots b_{SR_1}b_D=1\right)\\ &+\Pr\left(\hat{b}_{SR_{j-1},j}\hat{b}_{SR_{j-2},j}\ldots\hat{b}_{SR_1,j}\hat{b}_{D,j}=1|b_{SR_{j-1}}b_{SR_{j-2}}\ldots b_{SR_1}b_D=0\right)\\ &\times\Pr\left(b_{SR_j}=0 \text{ and } b_{SR_{j-1}}b_{SR_{j-2}}\ldots b_{SR_1}b_D=0\right). \end{aligned} \quad (4.92)$$

Note that

$$\Pr\left(\hat{b}_{SR_{i,j}}=0|b_{SR_i}=1\right)=\Pr\left(\hat{b}_{SR_{i,j}}=1|b_{SR_i}=0\right)=P_b\left(E_{\Theta_{SR_{i,j}}}\right)=\phi\left(\gamma_{R_iR_j}\right)=\eta_{ij}, \quad (4.93)$$

$$\Pr\left(\hat{b}_{D,j}=0|b_D=1\right)=\Pr\left(\hat{b}_{D,j}=1|b_D=0\right)=P_b\left(E_{\Theta_{DR_j}}\right)=\phi\left(\gamma_{DR_j}\right)=\zeta_j, \quad (4.94)$$

where $\{i,j\}\in\{1,2,\ldots,N\}$ and $i<j$. Substituting α_0, α_j, ζ_j and η_{ij} into (4.92), the closed-form expression of $P_b(E_{\Omega_{R_j}})$ is obtained as

$$\begin{aligned} P_b(E_{\Omega_{R_j}})=&(1-\alpha_j)\left[1-(1-\zeta_j)\prod_{i=1}^{j-1}(1-\eta_{ij})\right]\prod_{i=0}^{j-1}\alpha_i\\ &+(1-\alpha_j)\left[\zeta_j(1-\alpha_0)+(1-\zeta_j)\alpha_0\right]\sum_{\mathbb{P}'}\prod_{i=1}^{j-1}\delta_i'\epsilon_i', \end{aligned} \quad (4.95)$$

where $\mathbb{P}'$ denotes a set of $\{\eta_{ij},\alpha_i\}$ satisfying the condition that if one term is η_{ij} then there is another term $(1-\alpha_i)$, and if one term is $(1-\eta_{ij})$ then there is another term α_i. Similarly, $\mathbb{P}'$ can be represented as

$$\mathbb{P}'=\{(\delta',\epsilon')|\delta_i'=\eta_{ij} \text{ or } 1-\eta_{ij}, \epsilon_i'=1-\alpha_i \text{ if } \delta_i'=\eta_{ij} \text{ and } \epsilon_i'=\alpha_i \text{ if } \delta_i'=1-\eta_{ij}\}. \quad (4.96)$$

□

Lemma 4.1. *The RDEPs at $\mathcal{S}$ and $\mathcal{R}_j$, $j = 1, 2, \ldots, N$, in the non-combined XRGCR scheme can be similarly derived as*

$$P_b(E_{\Omega'_S}) = \left[1 - \prod_{i=0}^{N}(1-\beta_i)\right]\alpha_{00}\prod_{i=1}^{N}\alpha_i + \left[\beta_0(1-\alpha_{00}) + (1-\beta_0)\alpha_{00}\right]\sum_{\mathbb{P}}\prod_{i=1}^{N}\delta_i\epsilon_i, \quad (4.97)$$

$$\begin{aligned} P_b(E_{\Omega'_{R_j}}) &= (1-\alpha_j)\left[1 - (1-\zeta_j)^2\prod_{i=1}^{j-1}(1-\eta_{ij})\right]\prod_{i=0}^{j-1}\alpha_i \\ &\quad + (1-\alpha_j)\left[\zeta_j(1-\alpha_{01}) + (1-\zeta_j)\alpha_{01}\right]\sum_{\mathbb{P}'}\prod_{i=1}^{j-1}\delta'_i\epsilon'_i. \end{aligned} \quad (4.98)$$

The following remark is made in relation to (4.79), (4.80), (4.97) and (4.98):

Remark 4.10 (*Lower RDEPs*). *The proposed XRGCR scheme has lower $P_b(E_{\Omega_S})$ and $P_b(E_{\Omega_{R_j}})$, $j = 1, 2, \ldots, N$, than the non-combined XRGCR scheme. This confirms the statement in Remark 4.7. It is noted that $0 < \phi(x) \leqslant 1/2$ $\forall x$. Thus, $0 < \alpha_{00} \leqslant 1/2$, $0 < \alpha_{01} \leqslant 1/2$, $0 < \beta_0 \leqslant 1/2$, $0 < \zeta_j \leqslant 1/2$, $\alpha_0 < \alpha_{00}$, $\alpha_0 < \alpha_{01}$ and $(1-\zeta_j)^2 < (1-\zeta_j)$. Also, it can be deduced that $\beta_0(1-\alpha_{00}) + (1-\beta_0)\alpha_{00} > \beta_0(1-\alpha_0) + (1-\beta_0)\alpha_0$ and $\zeta_j(1-\alpha_{01}) + (1-\zeta_j)\alpha_{01} > \zeta_j(1-\alpha_0) + (1-\zeta_j)\alpha_0$. Thus, $P_b(E_{\Omega'_S})$ and $P_b(E_{\Omega'_{R_j}})$ in (4.97) and (4.98) are greater than $P_b(E_{\Omega_S})$ and $P_b(E_{\Omega_{R_j}})$ in (4.79) and (4.80), respectively.*

4.3.3 Average Number of Packets in Retransmission

This subsection derives the ANR at $\mathcal{S}$ and $\mathcal{R}_j$, $j = 1, 2, \ldots, N$, in the proposed XRGCR scheme, i.e. the average number of data retransmissions required to transmit one packet from $\mathcal{S}$ to $\mathcal{D}$ and from $\mathcal{R}_j$ to $\mathcal{D}$, respectively.

At first, the expression of ANRs is derived over error-free backward links. In this error-free environment, the RDEPs are omitted, i.e. $P_b(E_{\Omega_S}) = 0$ and $P_b(E_{\Omega_{R_j}}) = 0$, $j = 1, 2, \ldots, N$.

Theorem 4.3. *Over error-free backward links, the ANRs at $\mathcal{S}$ and $\mathcal{R}_j$, $j = 1, 2, \ldots, N$, in the XRGCR scheme are given by*

$$\lambda_S^{(free)} = \alpha_{00}\prod_{j=1}^{N}\alpha_j, \quad (4.99)$$

$$\lambda_{R_j}^{(free)} = (1-\alpha_j)\alpha_{01}\alpha_{00}\prod_{i=1}^{j-1}\alpha_i\prod_{i=1}^{j-1}(1-\eta_{ij}), \tag{4.100}$$

where $\lambda_A^{(free)}$, $A \in \{S, R_j\}$, *denotes the ANR at node* A. *Here,* α_{00}, α_{01}, α_i *and* η_{ij}, $\{i,j\} \in \{1,2,\ldots,N\}$, *are defined as in Theorem 4.2.*

Proof. It is noted that the ANR is corresponding to the error probability of the data transmission. It is observed that $\mathcal{S}$, in the proposed XRGCR scheme, only retransmits the packet which is not correctly received by all $\{\mathcal{R}_j\}$ and $\mathcal{D}$, i.e. $b_{SD} = 1$ and $b_{SR_j} = 1$ $\forall j \in \{1,2,\ldots,N\}$. Thus, the ANR at $\mathcal{S}$ can be determined by

$$\lambda_S^{(free)} = \Pr(b_{SD}=1)\prod_{j=1}^{N}\Pr\left(b_{SR_j}=1\right). \tag{4.101}$$

Substituting $\Pr(b_{SD}=1) = P_b(E_{SD}) = \alpha_{00}$ and $\Pr\left(b_{SR_j}=1\right) = P_b\left(E_{SR_j}\right) = \alpha_j$, $j = 1,2,\ldots,N$, (see Theorem 4.2) into (4.101), $\lambda_S^{(free)}$ can be obtained as

$$\lambda_S^{(free)} = \alpha_{00}\prod_{j=1}^{N}\alpha_j, \tag{4.102}$$

In the proposed XRGCR scheme, $\mathcal{R}_j$, $j = 1,2,\ldots,N$, retransmits a packet when the following conditions are satisfied:

- The packet is correctly received at $\mathcal{R}_j$,
- The packet fails to be received at $\mathcal{R}_1$ and $\mathcal{D}$ in both BC and FW phases,
- The packet fails to be received at $\mathcal{R}_i$, $i = 1,2,\ldots,N$, $i < j$,
- The block ACK packets from $\mathcal{R}_i$ to $\mathcal{R}_j$ are correct.

Taking all these conditions into account, the ANR at $\mathcal{R}_j$ can be obtained by

$$\lambda_{R_j}^{(free)} = \Pr\left(b_{SR_j}=0\right)\Pr(b_{SD}=1)\Pr(b_{R_1D}=1)\prod_{i=1}^{j-1}\Pr(b_{SR_i}=1)\prod_{i=1}^{j-1}\left[1-P_b\left(E_{\Theta_{SR_{i,j}}}\right)\right]. \tag{4.103}$$

Substituting $P_b\left(E_{\Theta_{SR_{i,j}}}\right) = \phi\left(\gamma_{R_iR_j}\right) = \eta_{ij}$, $\Pr(b_{R_1D}=1) = P_b(E_{R_1D}) = \alpha_{01}$, $\Pr(b_{SD}=1) = \alpha_{00}$ and $\Pr\left(b_{SR_j}=1\right) = \alpha_j$, $j = 1,2,\ldots,N$, into (4.103), $\lambda_{R_j}^{(free)}$ can be obtained as

$$\lambda_{R_j}^{(free)} = (1-\alpha_j)\alpha_{01}\alpha_{00}\prod_{i=1}^{j-1}\alpha_i\prod_{i=1}^{j-1}(1-\eta_{ij}). \tag{4.104}$$

□

Some important points may be observed in relation to (4.99) and (4.100):

Remark 4.11 (*Reduced ANR at $\mathcal{S}$*). *The ANR at $\mathcal{S}$ in the GCR and the proposed XRGCR schemes is significantly reduced compared to the BCR scheme when the number of relays is larger than one. This confirms the statement in Remark 4.9. In fact, following the BCR scheme, the ANR at $\mathcal{S}$ depends only on the links $\mathcal{S} \to \mathcal{R}_1$ and $\mathcal{S} \to \mathcal{D}$, and thus can be derived easily as*

$$\lambda_S^{(B,free)} = \alpha_{00}\alpha_1. \tag{4.105}$$

Similar to the proposed XRGCR scheme, the ANR at $\mathcal{S}$ in the GCR scheme is given by

$$\lambda_S^{(G,free)} = \alpha_{00}\prod_{j=1}^{N}\alpha_j. \tag{4.106}$$

From (4.99), (4.105) and (4.106), it can be seen that $\lambda_S^{(free)} = \lambda_S^{(G,free)} < \lambda_S^{(B,free)}$ when $N > 1$.

Remark 4.12 (*Reduced ANR at $\mathcal{R}_j$*). *The ANR at $\mathcal{R}_j$, $j > 1$, in the XRGCR scheme is lower than that in the GCR scheme. Following the GCR scheme, the ANR at $\mathcal{R}_j$, $j = 1, 2, \ldots, N$, depends only on the links $\mathcal{S} \to \mathcal{R}_j$, $\mathcal{S} \to \mathcal{D}$ and $\mathcal{R}_1 \to \mathcal{D}$. Thus, its ANR is simply given by*

$$\lambda_{R_j}^{(G,free)} = (1-\alpha_j)\alpha_{01}\alpha_{00}. \tag{4.107}$$

Comparing (4.100) and (4.107), it can be observed that $\lambda_{R_j}^{(free)} < \lambda_{R_j}^{(G,free)}$. In fact, in the GCR scheme, there is lack of cooperation between the relays and thus there are various overlapped packets in the RET phase compared with the proposed XRGCR scheme which has non-overlapped packets. The overlapped packets at $\mathcal{R}_j$, $j > 1$, in the GCR scheme can be quantified as

$$\Delta_j = \lambda_{R_j}^{(G,free)} - \lambda_{R_j}^{(free)} = (1-\alpha_j)\alpha_{01}\alpha_{00}\left[1 - \prod_{i=1}^{j-1}\alpha_i \prod_{i=1}^{j-1}(1-\eta_{ij})\right]. \tag{4.108}$$

This confirms the statement in Remark 4.9 concerning the overlapped packets at the relays in the RET phase.

Lemma 4.2. *Over erroneous backward links, the ANRs at $\mathcal{S}$ and $\mathcal{R}_j$, $j = 1, 2, \ldots, N$, in the XRGCR scheme are given by*

$$\lambda_S = \lambda_S^{(free)} + P_b(E_{\Omega_S}), \tag{4.109}$$

$$\lambda_{R_j} = \lambda_{R_j}^{(free)} + P_b(E_{\Omega_{R_j}}), \tag{4.110}$$

where $P_b(E_{\Omega_S})$ and $P_b(E_{\Omega_{R_j}})$ are given by (4.79) *and* (4.80)*, respectively.*

Remark 4.13 (*Lower ANRs*)**.** *Over unreliable backward links, the ANRs at $\mathcal{S}$ and $\mathcal{R}_j$, $j = 1, 2, \ldots, N$, in the proposed XRGCR scheme are reduced compared to that in the non-combined XRGCR scheme due to the improved RDEPs (see Remarks 4.7 and 4.10). This confirms the statement in Remark 4.8 regarding the reduced number of retransmissions. In fact, the ANRs at $\mathcal{S}$ and $\mathcal{R}_j$ in the non-combined XRGCR scheme can be similarly derived as*

$$\lambda'_S = \lambda_S^{(free)} + P_b(E_{\Omega'_S}), \tag{4.111}$$

$$\lambda'_{R_j} = \lambda_{R_j}^{(free)} + P_b(E_{\Omega'_{R_j}}), \tag{4.112}$$

where $P_b(E_{\Omega'_S})$ and $P_b(E_{\Omega'_{R_j}})$ are the RDEPs at $\mathcal{S}$ and $\mathcal{R}_j$ in the non-combined XRGCR scheme given by (4.97) *and* (4.98)*, respectively. Thus, from* (4.109)*,* (4.110)*,* (4.111)*,* (4.112) *and Remark 4.10, it can be deduced that $\lambda_S < \lambda'_S$ and $\lambda_{R_j} < \lambda'_{R_j}$.*

4.3.4 Relay Selection for Retransmission

In multi-relay networks, various RS schemes are considered in the FW phase to help the source forward data to the destination [148–151]. In the work, various CR schemes have been investigated, where multiple relays are used to help the source retransmit the corrupted packets to the destination. This naturally requires an efficient RS mechanism in the RET phase[17].

In this subsection, based on the derived ANR at the relays in subsection 4.3.3, two RS schemes are proposed for the RET phase. The first is based

[17]Note that the best relay in the FW phase is also used as the best relay in the RET phase. The RS in the RET phase is to select the remaining relays to support the best relay in the retransmission.

on the constraint of the total number of packets in a frame and the second is based on the constraint of the total power consumption at the relays. The RS process can be carried out by a scheduler of a coordinator node in a centralized manner [129, 130], i.e. each relay informs the coordinator its ANR through a specific feedback channel and then the coordinator selects the relays for the retransmission based on this information.

Let N_1^* and N_2^* denote the number of relays required for the RET phase using the first and second RS schemes, respectively. Regarding the frame length (i.e. W), the first RS scheme is defined through

$$N_1^* = \arg \max_{j=1,2,\ldots,N} \left\{ \lambda_{R_j} \geqslant \lambda_{\text{threshold}} \triangleq \frac{1}{W} \right\}. \tag{4.113}$$

With limited total power consumption at the relays for the RET phase, the second RS scheme is determined by

$$N_2^* = \arg \max_{j=1,2,\ldots,N} \left\{ \sum_{i=1}^{j} W \lambda_{R_j} P_R \leqslant P_{R,\text{tot}} \right\}, \tag{4.114}$$

where P_R and $P_{R,\text{tot}}$ are the power required at each relay node to retransmit a packet and the total power constraint at the relays for the retransmission, respectively. The algorithms corresponding to the two RS schemes are summarized in Tables 4.2 and 4.3.

Table 4.2: RS based on frame length

Step 1. Calculate ANR at relay $\mathcal{R}_j$, $j = 1, 2, \ldots, N$ (i.e. λ_{R_j}).
Step 2. Compare λ_{R_j} with $\lambda_{\text{threshold}}$:
. If λ_{R_j} is larger than or equal to $\lambda_{\text{threshold}}$, then assign N_1^* as j.
. Back to Step 1 with the next relay $\mathcal{R}_{j+1}$.
. Otherwise, stop the RS process.

Remark 4.14 (*High Power Efficiency*). *The first RS scheme is helpful for the proposed XRGCR scheme to reduce the power consumption in the RET phase since the ANR of $\mathcal{R}_j$ decreases as j increases. Specifically, when W is small, the proposed XRGCR scheme requires a lower number of relays in the*

Table 4.3: RS based on power constraint

Step 1. Calculate ANR at relay $\mathcal{R}_j$, $j = 1, 2, \ldots, N$ (i.e. λ_{R_j}).
Step 2. Compare the total power consumption for retransmission (i.e.$\sum_{i=1}^{j} W\lambda_{R_j} P_R$) with the total power constraint (i.e. $P_{R,\text{tot}}$):
. If $\sum_{i=1}^{j} W\lambda_{R_j} P_R$ is smaller than or equal to $P_{R,\text{tot}}$, then assign N_2^* as j.
. Back to Step 1 with the next relay $\mathcal{R}_{j+1}$.
. Otherwise, stop the RS process.

RET phase compared to the GCR scheme. With the second RS scheme, it can be seen that the proposed XRGCR scheme is preferred for a limited $P_{R,tot}$ while the GCR scheme is beneficial to achieve a higher diversity gain in the RET phase if $P_{R,tot}$ is large enough. In fact, the proposed XRGCR scheme can exploit all the relays to help the source in the RET phase even with a low $P_{R,tot}$ since the relays can help each other to retransmit the corrupted packets without any packet overlapping. In other words, the proposed XRGCR scheme is more power efficient than the GCR scheme.

4.3.5 Numerical and Simulation Results

This subsection presents both analytical evaluation and simulation results of the RDEP and the ANR at the source and relay nodes using different CR schemes. The Monte Carlo simulations are carried out in MATLAB for a network consisting of a source node $\mathcal{S}$, five relay nodes $\{\mathcal{R}_1, \mathcal{R}_2, \mathcal{R}_3, \mathcal{R}_4, \mathcal{R}_5\}$ and a destination node $\mathcal{D}$. All forward and backward channels experience Rayleigh fading, BPSK is used for signalling, and no channel coding is employed[18]. Without any loss of generality, the SNRs of the forward links $\mathcal{S} \to \mathcal{R}_i$, $i = 1, \ldots, 5$, are assumed to be 5 dB, 2 dB, -1 dB, -4 dB and -7 dB, respectively. Thus, $\mathcal{R}_1$ is selected as the best relay to forward the data in the FW phase. In the RET phase, $\mathcal{R}_1$, $\mathcal{R}_2$, $\mathcal{R}_3$, $\mathcal{R}_4$ and $\mathcal{R}_5$ sequentially help $\mathcal{S}$ retransmit the lost packets to $\mathcal{D}$. The SNRs of the remaining forward

[18]For simplicity, uncoded BPSK is considered in the simulation. Channel coding with higher-order modulation schemes can be applied, which results in different performance.

inks $\mathcal{S} \to \mathcal{D}$ and $\mathcal{R}_i \to \mathcal{D}$, $i = 1, \ldots, 5$, are assumed to be -20 dB and 0 dB, respectively. At the source and relay nodes, errors occur if the packets required to be retransmitted are different from the actual retransmitted packets.

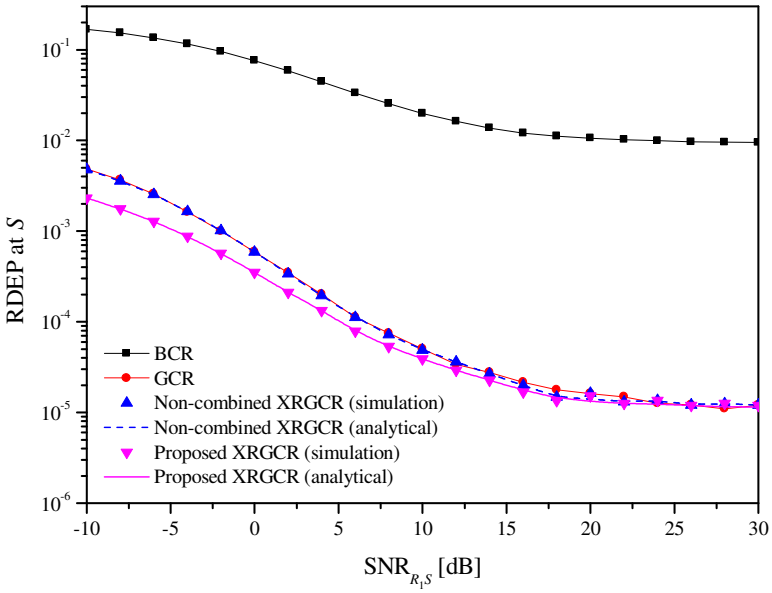

Figure 4.17: RDEP at $\mathcal{S}$ versus SNR_{R_1S}.

The RDEPs with various CR schemes are first investigated for both analytical expression and simulation results. As shown in Fig. 4.17, the RDEP at $\mathcal{S}$ is plotted as a function of the SNR of the backward link $\mathcal{R}_1 \to \mathcal{S}$. The SNRs of the remaining backward links $\mathcal{R}_j \to \mathcal{S}$, $j = 2, \ldots, 5$, $\mathcal{D} \to \mathcal{S}$ and $\mathcal{D} \to \mathcal{R}_i$, $i = 1, \ldots, 5$, are assumed as follows: $\gamma_{R_jS} = \gamma_{R_1S}$, $\gamma_{DS} = 0$ dB and $\gamma_{DR_i} = 10$ dB. It can be seen that the proposed XRGCR scheme achieves better performance than the non-combined XRGCR scheme in terms of RDEP. This confirms the statement in Remarks 4.7 and 4.10 regarding the higher reliability in the determination of packets to be retransmitted with the combination of block ACK packets at the destination. With the GCR and the proposed XRGCR schemes, the RDEPs at $\mathcal{S}$ are shown to be significantly improved due to the combination of various block ACK packets from various relays in the RET phase. Also, the derived analytical RDEPs at $\mathcal{S}$ for the proposed XRGCR and the non-combined XRGCR schemes given by (4.79) and (4.97) are consistent with the simulation results.

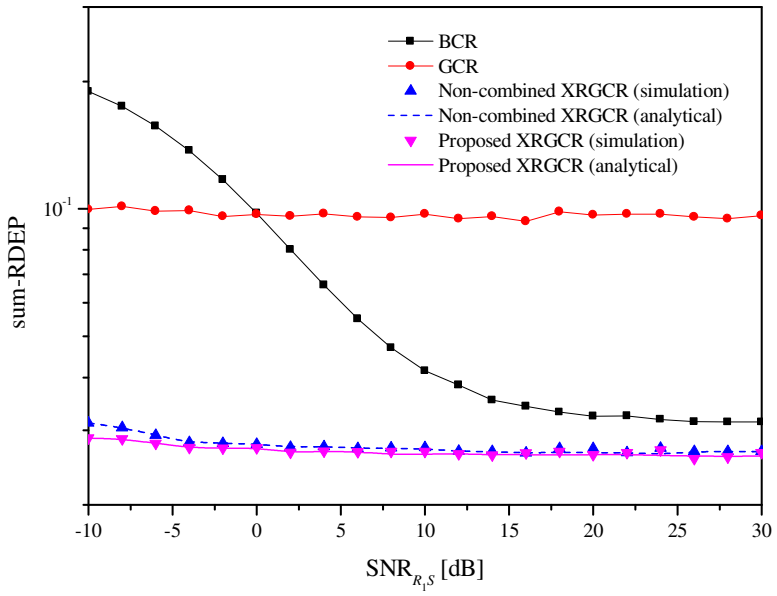

Figure 4.18: Sum-RDEP versus SNR_{R_1S}.

Considering the reliability of the retransmissions in the whole system, Fig. 4.18 shows the sum-RDEP against various values of the SNR of the backward link $\mathcal{R}_1 \rightarrow \mathcal{S}$. It can be observed that the summations of the derived RDEPs at $\mathcal{S}$ and $\mathcal{R}^{(N)}$ for the proposed XRGCR and the non-combined XRGCR schemes given by the analytical expressions (4.79), (4.80), (4.97) and (4.98) are consistent with the simulation results. Also, it can be seen that the proposed XRGCR scheme achieves the best performance in terms of sum-RDEP. In fact, with the cooperation between the relays, the RDEPs at the relays are considerably improved and this results in the improvement of the sum-RDEP for the whole system. This can be easily seen when comparing the sum-RDEPs of the XRGCR scheme with the GCR scheme.

For the comparison of ANRs with various CR schemes, Figs. 4.19, 4.20 and 4.21 show the ANRs at the source, relays and for the whole system (in terms of sum-ANR[19]), respectively. The ANRs are also plotted as a function of the backward link $\mathcal{R}_1 \rightarrow \mathcal{S}$ with respect to various CR schemes. As shown in Fig. 4.19, it is observed that the ANR at $\mathcal{S}$ in the proposed XRGCR scheme is

[19]The sum-ANR is defined as the summation of the ANRs at $\mathcal{S}$ and $\mathcal{R}^{(N)}$ required for the RET phase.

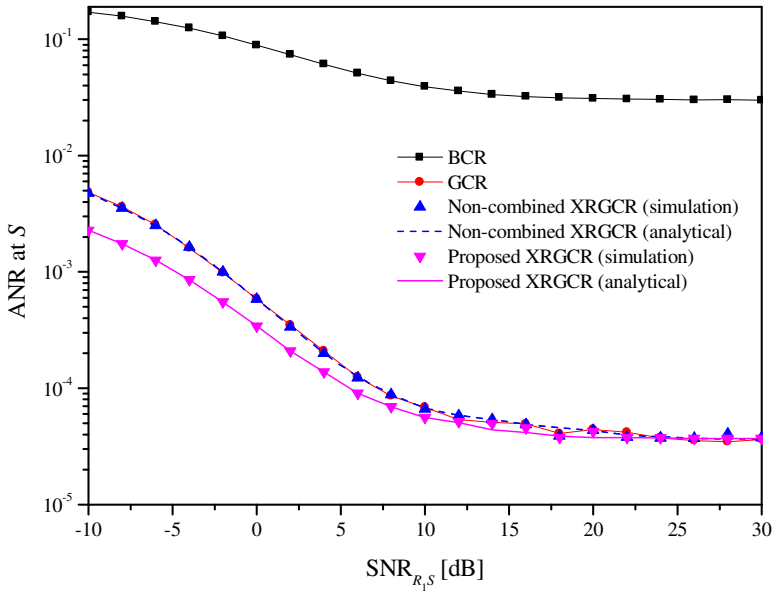

Figure 4.19: ANR at $\mathcal{S}$ versus SNR$_{R_1S}$.

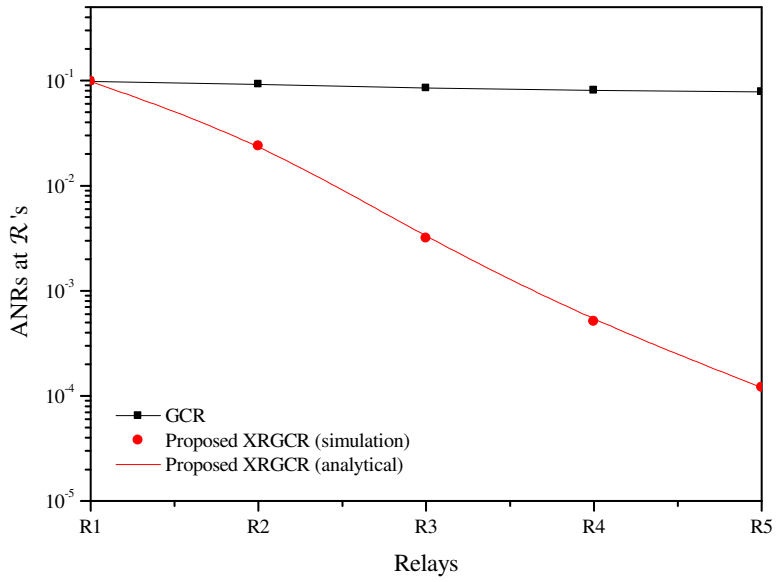

Figure 4.20: ANRs at the 5 relays.

lower than the non-combined XRGCR scheme. In addition, the GCR and the proposed XRGCR schemes significantly reduce the ANR at $\mathcal{S}$ due to the help of all the relays in the RET phase. This confirms the statements in Remarks 4.8, 4.9, 4.11 and 4.13 regarding the lower ANRs at $\mathcal{S}$. In Fig. 4.20, it can be seen that the proposed XRGCR scheme significantly reduces the ANRs at $\mathcal{R}_2$, $\mathcal{R}_3$, $\mathcal{R}_4$ and $\mathcal{R}_5$ compared to the GCR scheme. The reduced ANRs at

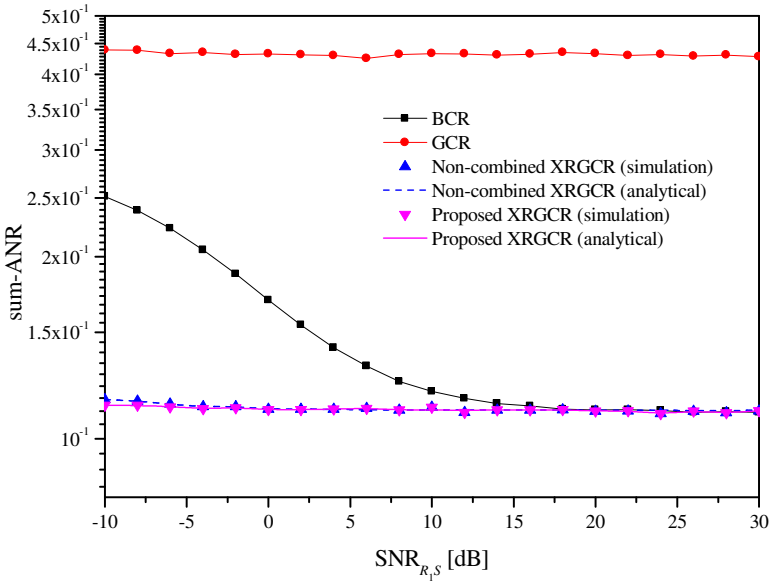

Figure 4.21: Sum-ANR versus SNR_{R_1S}.

the relays confirm the statements in Remarks 4.9 and 4.12 in relation to the non-overlapped packets in the RET phase with the proposed XRGCR scheme. Therefore, summarising the ANRs at all the source and relay nodes for the evaluation of the whole system, Fig. 4.21 shows that the proposed XRGCR scheme achieves the best performance in terms of sum-ANR while a larger sum-ANR is required in the GCR scheme as a consequence of the overlapping packets in the RET phase. Also, in Figs. 4.19, 4.20 and 4.21, the derived expressions of ANRs at $\mathcal{S}$ and $\mathcal{R}^{(N)}$ for the proposed XRGCR and the non-combined XRGCR schemes given by (4.109), (4.110), (4.111) and (4.112) are consistent with the simulation results.

Taking the RS for the RET phase into consideration, Figs. 4.22 and 4.23 show the number of relays selected for the RET phase versus the frame length (i.e. W [packets]) and total power constraint of the relays (i.e. $P_{R,\mathrm{tot}}$ [Watts]), respectively, for both the GCR and the proposed XRGCR schemes. As shown in Fig. 4.22, if W is smaller than 10000 packets, the proposed XRGCR scheme requires a lower number of relays for the RET phase compared to the GCR scheme. This arises since the relays in the XRGCR scheme can share the packets with each other in the RET phase without any overlapping packets. In

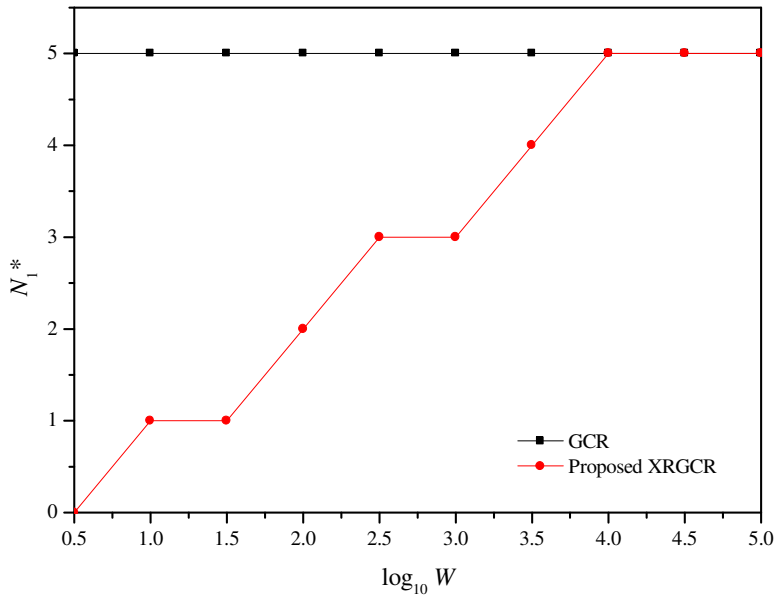

Figure 4.22: Number of relays selected for the RET phase versus frame length ($\log_{10} W$).

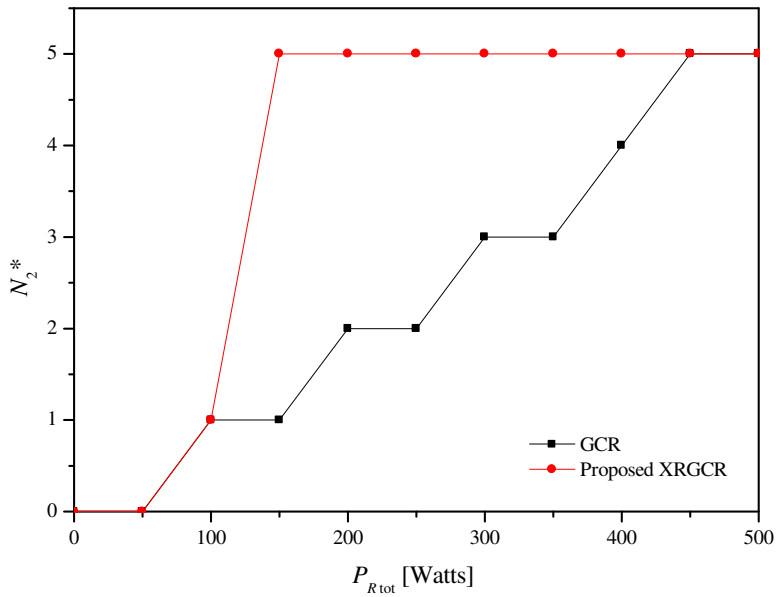

Figure 4.23: Number of relays selected for the RET phase versus total power constraint ($P_{R,\mathrm{tot}}$).

Fig. 4.23, W is fixed at 1000 packets and the power of each relay to retransmit a packet (i.e. P_R) is assumed to be 1 Watt. It can be seen that the proposed XRGCR scheme can utilise all the relays for the RET with a lower $P_{R,\mathrm{tot}}$ (e.g. 150 Watts). However, the GCR scheme requires a much larger $P_{R,\mathrm{tot}}$ (e.g. 450

Watts) if all the relays are used for the retransmission. Thus, for a limited $P_{R,\text{tot}}$ (e.g. from 150 to 400 Watts), the proposed XRGCR scheme is better than the GCR scheme in the sense that all the relays can be used to help the source in the RET phase. This confirms the statement in Remark 4.14 regarding the high power efficiency of the proposed XRGCR scheme.

4.4 Conclusions

This chapter has proposed an NC-based block acknowledgement scheme for multi-relay based cooperative networks. Using the notion of NC, the source and relay nodes can simultaneously determine the data packets to be retransmitted with a reduced number of block ACK packets. This NC-based block ACK scheme can effectively reduce the number of block ACK packets sent from the destination. This reduction results in a lower computational complexity, a more reliable determination of packets to be retransmitted, and a decreased number of data retransmissions at the source and relays compared to the non-NC-based block ACK scheme. Reduced number of retransmissions actually means freeing up more bandwidth and increasing overall network throughput. An error probability analysis for the determination of packets to be retransmitted has been carried out with respect to the SNR of forward and backward links. The derived expression of error probability reflects well the impact of the quality of both the forward and backward links upon the performance of block ACK schemes. General expressions for multi-relay networks have been derived for three asymptotical scenarios of forward links. In addition, simulations have been carried out which have confirmed all the analytical results.

Furthermore, this chapter has proposed a cooperative retransmission scheme for wireless regenerative multi-relay networks based on XOR operations and RC. The XOR combination of block ACK packets at the destination results in a more reliable determination of retransmission and a decreased number of packets to be retransmitted at the source and relays compared to the non-combined-based scheme. The analyses of error probability of the determination

of packets to be retransmitted and the average number of packets to be retransmitted have been carried out with respect to the SNRs of forward, backward and cooperation links. The derived expressions reflect well the impact of RC on the performance of the proposed scheme. Two RS schemes have been then proposed for the multi-relay-based CR based on frame length and total power constraint at the relays. The proposed XRGCR scheme is shown to be power efficient with a lower number of relays required for a small frame length, and a larger number of relays may join in the RET phase for the situation when the total power constraint is limited.

Chapter 5

NC Based Spectrum Sensing

This chapter is concerned with the development and investigation of a new network coding (NC) implementation for cooperative spectrum sensing (CSS) mechanisms in three-hop cognitive wireless relay networks (CWRNs). The data transmission from a source node to a destination node is realized with the aid of two layers of cognitive users (CUs) which are in the transmission coverage of two primary users (PUs). Dealing with the hidden terminal problems, CSS helps the shadowed CUs detect the PUs and improves the sensing reliability at the CUs. Conventionally, the decision of available spectrum at the CUs is carried out based on the global decision at the fusion center (FC). This chapter first proposes a new CSS scheme for a layer of CUs to improve the spectrum sensing performance by exploiting both local decisions at the CUs and global decisions at the FC. Particularly, this chapter derives the probabilities of missed detection and false alarm for a practical scenario where all sensing, reporting and backward channels suffer from Rayleigh fading. The derived expressions not only show that the proposed CSS achieves a better sensing performance than the conventional scheme but also characterise the effects of the fading channels on the sensing reliability. Furthermore, a CSS scheme is proposed for two cognitive radio layers in a three-hop CWRN based on NC. The proposed NC-based CSS scheme helps reduce one phase of sensing for a higher system throughput compared to the conventional scheme which requires eight phases in total to monitor all available spectrums of both PUs.

Finally, simulation results are presented to verify the analytical results and observations.

5.1 Introduction

Along with the significant achievements of cooperative communications in improving data rate and reliability, the large demand of spectrum resources for various wireless applications and services is also taken into consideration since spectrum resources are limited. To cope with the scarcity of spectrum resources, cognitive radio was proposed as an emerging technology to improve spectrum efficiency by providing dynamic spectrum access [152–154]. With cognitive radio technology, when licensed spectrum bands allocated for licensed primary users (PUs) are unused at some specific periods of time, they can be utilized by secondary users, i.e. cognitive users (CUs). When the PUs activate, the CUs should move out of the licensed bands to mitigate any interference to the licensed network. Therefore, in cognitive radio networks, spectrum holes can be opportunistically used by the CUs. In order to detect the occupation and reappearance of a PU, CUs must continuously monitor the spectrum, and thus spectrum sensing is one of the most basic elements in cognitive radio technology. Various well-known signal detection methods have been applied to spectrum sensing technology [155], such as matched filter [156], energy, cyclostationary, wavelet [157] and covariance detection [158]. However, the implementation of these spectrum sensing techniques is not feasible for hidden terminal problems when the CUs suffer from shadowing or severe fading effects while their nearby PUs are active.

Motivated by relaying techniques for cooperative communications, cooperative spectrum sensing (CSS) was proposed not only to help the shadowed CUs detect the PUs but also to improve detection reliability by carrying out spectrum sensing in a cooperative manner [156,159]. A CSS scheme can be divided into three phases, namely the sensing (SS) phase, reporting (RP) phase and backward (BW) phase. These phases can be summarized as follows: Initially,

every CU carries out local spectrum sensing (LSS) in the SS phase to determine locally the existence of the PU. Then, all CUs forward their decisions to a fusion centre (FC), i.e. a common receiver, in the RP phase. Based on the local decisions received from various CUs, the FC makes a global decision on the existence of the PU and then broadcasts this decision to all CUs in the BW phase. Over the wireless medium, the CSS scheme suffers interference and noise from all the SS, RP and BW channels. However, most published work assumes that the RP channels are error-free [160, 161] and that the BW channels are also error-free [159]. Additionally, in practical applications, e.g., in wireless ad hoc or sensor networks, the relay-aided data transmission from the source to the destination node can be realised via various transmission paths or hops. This stimulates to consider a three-hop wireless relay network as a specific model of multi-hop communications[20]. In this model, two layers of relay nodes help the source transmit data to the destination.

This chapter investigates the spectrum sensing in a three-hop cognitive wireless relay network (CWRN) where a source node $\mathcal{S}$ transmits data to a destination node $\mathcal{D}$ via two layers of relay nodes. In a cognitive radio environment, the relay nodes can be regarded as CUs and two layers of relay nodes can be accordingly referred to as two layers of CUs. Each layer of CUs is assumed to be within the coverage of a cognitive radio network corresponding to the transmission range of a PU [162]. Inspired by cooperative spectrum sharing, the CWRN can generate a seamless transmission from $\mathcal{S}$ to $\mathcal{D}$ by exploiting some portions of the spectrum that may not be utilized by the PUs over a period of time. Specifically, a cognitive space-time-frequency coding was proposed in [162] to maximize the spectrum opportunities in the CWRN. However, the cooperative spectrum sharing in the three-hop CWRN poses the question of *how the CUs in two layers can efficiently sense the spectrum holes of both PUs to exploit all the available frequency bands in both cognitive radio networks for cooperative communications.*

[20]The considered model is extendible to a general relay network with more than three hops by changing the operations performed at the FC to adapt to various network configurations.

Dealing with spectrum sensing in three-hop CWRNs, this chapter first considers the CSS for a layer of CUs and then extend to the whole system consisting of two layers of CUs. Specifically, for a cognitive radio layer, a new CSS scheme is proposed to improve the spectrum sensing performance by exploiting both the local and global decisions in spectrum sensing at each CU. The basic idea of the proposed scheme for a cognitive radio layer is that each CU combines its local decision in the SS phase with the global decision of the FC in the BW phase. Also, this chapter takes into account a practical scenario where all the SS, RP and BW channels are characterised by Rayleigh flat fading channels. To the best of the author's knowledge, this has received little attention in the literature. By deriving the expression of the probability of missed detection and false alarm, it is not only shown that the proposed CSS scheme achieves a better CSS performance than the conventional CSS scheme[21] but also evaluate the effects of all the SS, RP and BW channels on the CSS performance.

Extending to the whole system consisting of two layers of CUs in a three-hop CWRN, a total of eight phases is conventionally required to sense the available spectrum of both PUs at each CU, including six phases for the CSS of two cognitive radio layers and two phases at the FC for the exchange of spectrum information between two cognitive radio layers. As the second contribution of the chapter, a new CSS scheme is proposed for three-hop CWRNs based on NC. With the proposed NC-based CSS scheme, the number of phases is reduced by one, and thus the system throughput is improved. The basic idea of the proposed scheme is that the FC combines two decisions of the available spectrum of two PUs and then broadcasts this combination to all the CUs in two layers. Based on the known spectrum information at a CU, the spectrum information of the PU in another layer can be extracted. It can be seen that the signalling number for the spectrum information is reduced by half with a simple XOR operator in the proposed scheme when compared with the con-

[21] The conventional CSS scheme for a cognitive radio layer is defined as the scheme where there is no combination of the local and global decision at the CUs in the BW phase.

ventional scheme[22]. Thus, the system throughput is considerably improved, especially when the number of frequency bands in the wide-band channel is large. This accordingly confirms that the proposed simple XOR operator in the NC-based CSS scheme is efficient.

The rest of the chapter is organized as follows: Section 5.2 describes the implementation of LSS at each CU in a cognitive wireless relay network; The proposed CSS schemes for a cognitive radio layer and for two cognitive radio layers in the three-hop CWRN are presented in Section 5.3; Section 5.4 presents the performance analysis of CSS schemes over Rayleigh flat fading channels; Numerical results are given in Section 5.5, and finally Section 5.6 draws the conclusions from the chapter.

5.2 Local Spectrum Sensing

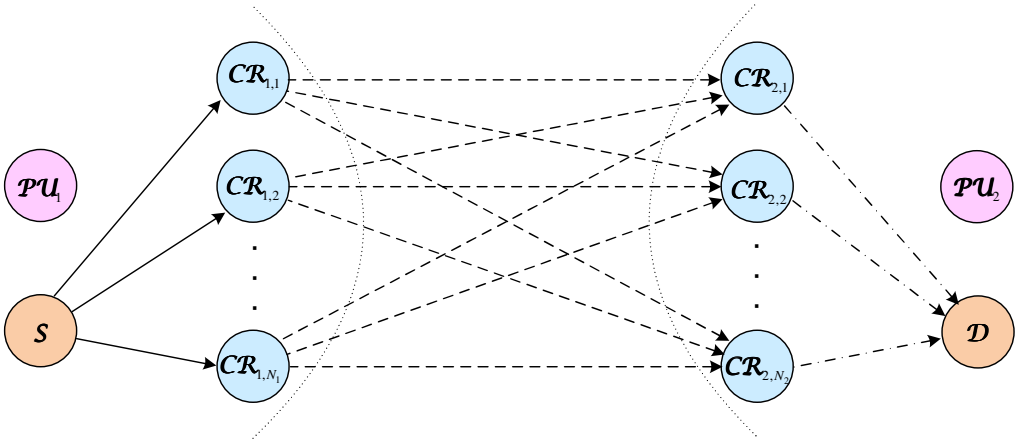

Figure 5.1: System model of three-hop cognitive wireless relay network.

Fig. 5.1 illustrates the system model of the three-hop cognitive wireless relay network under investigation. The data transmission from source node $\mathcal{S}$ to destination node $\mathcal{D}$ is accomplished with the assistance of two layers of relay nodes which are referred to as CUs. It is assumed that there are

[22]The conventional CSS scheme for two cognitive radio layers is defined as the process of eight phases, including six phases for the CSS of two layers and two phases at the FC for the exchange of spectrum information between two layers.

two PUs, namely $\mathcal{PU}_1$ and $\mathcal{PU}_2$, in the network and each CU is within the transmission range of one PU. For convenience, let N_1 and N_2 denote the number of CUs in the first and second layer, respectively. Accordingly, the CUs in two layers can be represented as $\mathcal{CR}^{(N_1)} = \{\mathcal{CR}_{1,1}, \mathcal{CR}_{1,2}, \ldots, \mathcal{CR}_{1,N_1}\}$ and $\mathcal{CR}^{(N_2)} = \{\mathcal{CR}_{2,1}, \mathcal{CR}_{2,2}, \ldots, \mathcal{CR}_{2,N_2}\}$. The two PUs are assumed to operate in a wide-band channel including K non-overlapping frequency bands $f_1, f_2, \ldots, f_K$. A spectrum indicator vector (SIV) of length K (in bits) is used to report the availability of frequency bands in the transmission range of each PU where bits '0' and '1' represent the frequency band being utilized or available, respectively. The CSS of two cognitive radio layers is carried out over a common $\mathcal{FC}$ (see Fig. 5.2). The channels for all links are assumed to be Rayleigh flat fading. The channel gains for the SS links $\mathcal{PU}_i \to \mathcal{CR}_{i,j}$, the RP links $\mathcal{CR}_{i,j} \to \mathcal{FC}$ and the BW links $\mathcal{FC} \to \mathcal{CR}_{i,j}$, $i = 1, 2$, $j = 1, 2, \ldots, N_i$, are denoted by $h_{P_iC_{i,j}}$, $h_{C_{i,j}F}$ and $h_{FC_{i,j}}$, respectively. All the channels are assumed to be time-invariant over the whole transmission of both the data and the SIV, and assumed to be known to all the nodes in the network.

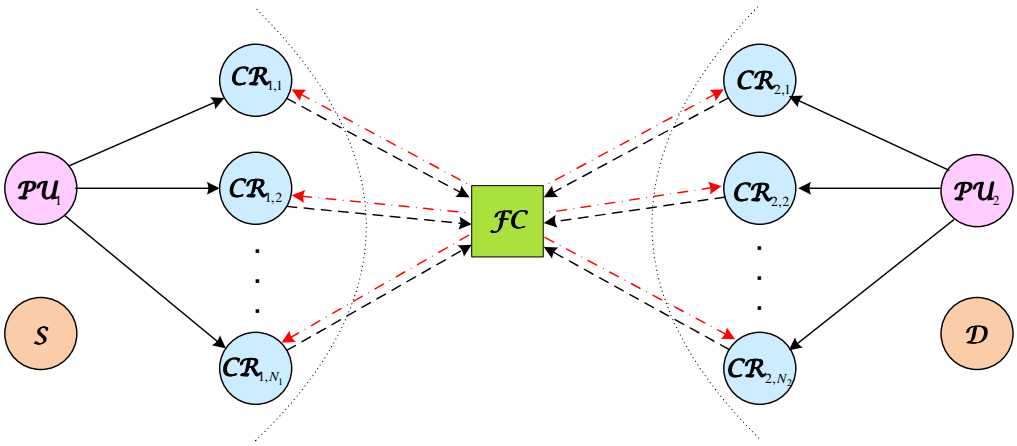

Figure 5.2: Sensing process in cognitive wireless relay network.

Over the SS channel, the received signal at $\mathcal{CR}_{i,j}$, $i = 1, 2$, $j = 1, 2, \ldots, N_i$, can be expressed as

$$\mathbf{r}_{i,j}^{(SS)} = \begin{cases} h_{P_iC_{i,j}}\mathbf{x}_i + \mathbf{n}_{i,j}^{(SS)}, & \mathcal{H}_1^{(\mathcal{PU}_i)}, \\ \mathbf{n}_{i,j}^{(SS)}, & \mathcal{H}_0^{(\mathcal{PU}_i)}. \end{cases} \tag{5.1}$$

where $\mathbf{x}_i$[23] is the transmitted signal from $\mathcal{PU}_i$ and $\mathbf{n}_{i,j}^{(SS)}$ is the independent circularly symmetric complex Gaussian (CSCG) noise vector at $\mathcal{CR}_{i,j}$ over the SS channel. Here, $\mathcal{H}_1^{(\mathcal{PU}_i)} = \{\mathcal{H}_{1,1}^{(\mathcal{PU}_i)}, \mathcal{H}_{1,2}^{(\mathcal{PU}_i)}, \ldots, \mathcal{H}_{1,K}^{(\mathcal{PU}_i)}\}$ and $\mathcal{H}_0^{(\mathcal{PU}_i)} = \{\mathcal{H}_{0,1}^{(\mathcal{PU}_i)}, \mathcal{H}_{0,2}^{(\mathcal{PU}_i)}, \ldots, \mathcal{H}_{0,K}^{(\mathcal{PU}_i)}\}$ denote the hypothesis that the frequency bands are occupied by $\mathcal{PU}_i$ and the hypothesis that the frequency bands are available for CUs, respectively. It is noticed that the vectors in (5.1) have length K which corresponds to the number of frequency bands in the wide-band channel.

Then, following an energy detection rule for unknown signals over fading channels [163], $\mathcal{CR}_{i,j}$ can detect the usage of a k-th frequency band, $k = 1, 2, \ldots, K$, at $\mathcal{PU}_i$ by comparing the energy of the received signal $\mathbf{r}_{i,j}^{(SS)}[k]$ at the k-th frequency band with a corresponding energy threshold $\mathcal{E}_{i,j}[k]$, i.e.

$$E_0\left[\mathbf{r}_{i,j}^{(SS)}[k]\right] \gtrless_{\mathcal{H}_{0,k}^{(\mathcal{CR}_{i,j})}}^{\mathcal{H}_{1,k}^{(\mathcal{CR}_{i,j})}} \mathcal{E}_{i,j}[k], \tag{5.2}$$

where $E_0[.]$ represents the energy measurement of a signal. Here, $\mathcal{H}_{1,k}^{(\mathcal{CR}_{i,j})}$ and $\mathcal{H}_{0,k}^{(\mathcal{CR}_{i,j})}$ denote the estimated hypotheses at $\mathcal{CR}_{i,j}$ that the k-th frequency band is occupied and unoccupied, respectively, by $\mathcal{PU}_i$. Let $\mathbf{s}_{i,j}^{(SS)}$ denote the local SIV estimated at $\mathcal{CR}_{i,j}$ over the SS channel $h_{P_iC_{i,j}}$. The k-th element, $k = 1, 2, \ldots, K$, of $\mathbf{s}_{i,j}^{(SS)}$ can be mathematically formulated as

$$\mathbf{s}_{i,j}^{(SS)}[k] = \begin{cases} 0, & \text{if } E_0\left[\mathbf{r}_{i,j}^{(SS)}[k]\right] \geqslant \mathcal{E}_{i,j}[k], \text{ i.e. } \mathcal{H}_{1,k}^{(\mathcal{CR}_{i,j})}, \\ 1, & \text{otherwise, i.e. } \mathcal{H}_{0,k}^{(\mathcal{CR}_{i,j})}. \end{cases} \tag{5.3}$$

5.3 Cooperative Spectrum Sensing for Cognitive Relay Networks

This section first presents the proposed CSS scheme for a cognitive radio layer in a three-hop CWRN in contrast with the conventional scheme. The spectrum sensing of two cognitive radio layers in the whole system is then taken into consideration with the proposed NC-based CSS scheme for the exchange of spectrum information between two layers of CUs.

[23]Note that a lower-case bold letter will be used to denote a vector throughout this chapter.

5.3.1 Proposed CSS Scheme for A Group of Cognitive Radio Users

For simplicity, this subsection investigates the CSS scheme performed at only one layer of CUs, e.g. $\mathcal{CR}^{(N_1)}$. The CSS scheme for the remaining cognitive radio layer, $\mathcal{CR}^{(N_2)}$, can be similarly obtained[24]. The proposed CSS scheme consists of three phases, which can be described as follows:

Sensing Phase

In the SS phase, each CU carries out the LSS over the SS channel. Specifically, $\mathcal{CR}_{1,j}$, $j = 1, 2, \ldots, N_1$, locally senses the available frequency bands of $\mathcal{PU}_1$ over the SS channel $h_{P_1C_{1,j}}$, and then makes a binary decision in terms of an SIV denoted by $\mathbf{s}_{1,j}^{(SS)}$ (see (5.3)).

Reporting Phase

In the CSS scheme, the spectrum sensing at the CUs is carried out in a cooperative manner with the help of an FC. Over the RP channels, each CU $\mathcal{CR}_{1,j}$, $j = 1, 2, \ldots, N_1$, forwards the local estimated SIV, i.e. $\mathbf{s}_{1,j}^{(SS)}$, to $\mathcal{FC}$[25]. The received signals at $\mathcal{FC}$ from $\mathcal{CR}_{1,j}$ can be written by

$$\mathbf{r}_{1,j}^{(RP)} = \sqrt{\Lambda_{1,j}} h_{C_{1,j}F} \mathbf{x}_{1,j}^{(SS)} + \mathbf{n}_{1,j}^{(RP)}, \tag{5.4}$$

where $\Lambda_{1,j}$ is the transmission power of $\mathcal{CR}_{1,j}$, $\mathbf{x}_{1,j}^{(SS)}$ is the binary phase shift keying (BPSK) modulated version of $\mathbf{s}_{1,j}^{(SS)}$, and $\mathbf{n}_{1,j}^{(RP)}$ is the independent CSCG noise vector at $\mathcal{FC}$ over the RP channel with each entry having zero mean and variance of N_0.

Then, $\mathcal{FC}$ processes to decode the received signals from each $\mathcal{CR}_{1,j}$, $j = 1, 2, \ldots, N_1$. Let $\mathbf{s}_{1,j}^{(RP)}$ denote the decoded SIV at $\mathcal{FC}$ from $\mathcal{CR}_{1,j}$ over the RP channel. Combining all the decoded SIVs $\{\mathbf{s}_{1,j}^{(RP)}\}$ from all the cognitive radio

[24]Note that the CSSs for two layers of CUs can be carried out simultaneously.

[25]Note that specific RP channels are used in the RP phase to avoid collision with PU.

users $\{\mathcal{CR}_{1,j}\}$, $\mathcal{FC}$ makes a global decision using the following OR rule[26]:

$$\mathbf{s}_{FC_1}[k] = \begin{cases} 0, & \text{if } \sum_{j=1}^{N_1} \mathbf{s}_{1,j}^{(RP)}[k] < N_1, \text{ i.e. } \mathcal{H}_{1,k}^{(\mathcal{FC}_1)}, \\ 1, & \text{otherwise, i.e. } \mathcal{H}_{0,k}^{(\mathcal{FC}_1)}, \end{cases} \tag{5.5}$$

where $\mathbf{s}_{FC_1}$ of length K denotes the global SIV estimated at $\mathcal{FC}$ for the first cognitive radio layer, $k = 1, 2, \ldots, K$, and $\mathcal{H}_{1,k}^{(\mathcal{FC}_1)}$ and $\mathcal{H}_{0,k}^{(\mathcal{FC}_1)}$ denote the estimated hypotheses at $\mathcal{FC}$ of the k-th frequency band occupied and unoccupied, respectively, by $\mathcal{PU}_1$. Note that, in (5.5), the decision of the availability of the frequency bands at $\mathcal{FC}$ follows the principle of the OR rule, i.e. $\mathcal{FC}$ decides the k-th frequency band being utilized by $\mathcal{PU}_1$ (i.e. $\mathcal{H}_{1,k}^{(\mathcal{FC}_1)}$) when at least one SIV (i.e. $\mathbf{s}_{1,j}^{(RP)}$) out of N_1 SIVs indicates the k-th frequency band being unavailable (i.e. $\mathcal{H}_{1,k}^{(\mathcal{CR}_{1,j})}$ or $\mathbf{s}_{1,j}^{(RP)}[k] = 0$), and otherwise, $\mathcal{FC}$ decides the k-th frequency band being available.

Backward Phase

In the BW phase, the FC broadcasts the global SIV to all CUs over BW channels. The received signal at $\mathcal{CR}_{1,j}$, $j = 1, 2, \ldots, N_1$, can be written by

$$\mathbf{r}_{1,j}^{(BW)} = \sqrt{\Lambda_{FC}} h_{FC_{1,j}} \mathbf{x}_{FC_1} + \mathbf{n}_{1,j}^{(BW)}, \tag{5.6}$$

where Λ_{FC} is the transmission power of $\mathcal{FC}$, $\mathbf{x}_{FC_1}$ is the BPSK modulated version of $\mathbf{s}_{FC_1}$, and $\mathbf{n}_{1,j}^{(BW)}$ is the independent CSCG noise vector at $\mathcal{CR}_{1,j}$ over the BW channel with each entry having zero mean and variance of N_0. Then, $\mathcal{CR}_{1,j}$ decodes the received signal from $\mathcal{FC}$ as $\mathbf{s}_{1,j}^{(BW)}$.

In the proposed CSS scheme, each CU combines its local SIV determined in the SS phase (i.e. $\mathbf{s}_{1,j}^{(SS)}$) with the global SIV received from the FC in the BW phase (i.e. $\mathbf{s}_{1,j}^{(BW)}$) using the OR rule as follows:

$$\mathbf{s}_{CR_{1,j}}[k] = \begin{cases} 0, & \text{if } \left(\mathbf{s}_{1,j}^{(SS)}[k] + \mathbf{s}_{1,j}^{(BW)}[k]\right) < 2, \text{ i.e. } \bar{\mathcal{H}}_{1,k}^{(\mathcal{CR}_{1,j})}, \\ 1, & \text{otherwise, i.e. } \bar{\mathcal{H}}_{0,k}^{(\mathcal{CR}_{1,j})}, \end{cases} \tag{5.7}$$

[26]The decision of spectrum availability at $\mathcal{FC}$ can follow various rules, such as OR, AND and majority rule. However, the OR rule was shown in [164] to give the best CSS performance compared to the AND and majority rules. Thus, in this chapter, the OR rule is applied to the global detection at $\mathcal{FC}$.

where $\mathbf{s}_{CR_{1,j}}$ denotes the final SIV at $\mathcal{CR}_{1,j}$, $k = 1, 2, \ldots, K$, and $\bar{\mathcal{H}}_{1,k}^{(\mathcal{CR}_{1,j})}$ and $\bar{\mathcal{H}}_{0,k}^{(\mathcal{CR}_{1,j})}$ denote the globally estimated hypotheses at $\mathcal{CR}_{1,j}$, $j = 1, 2, \ldots, N_1$, of the k-th frequency band occupied and unoccupied, respectively, by $\mathcal{PU}_1$, considering both the local and global SIVs.

Remark 5.1 (*Higher Reliability in Spectrum Sensing*). *The proposed CSS scheme can determine the availability of frequency bands more reliably than the conventional scheme. In the conventional CSS scheme, the global SIV received at the CUs from the FC is also the final SIV. This means that the decision at the CUs using the conventional scheme depends totally on the decision at the FC. Instead, in the proposed scheme, the final SIV at the CUs is the combination of two SIVs obtained from the LSS at the CUs and the CSS at the FC. As shown in* (5.7)*, the hypothesis* $\bar{\mathcal{H}}_{0,k}^{(\mathcal{CR}_{1,j})}$ *is decided by* $\mathbf{s}_{CR_{1,j}}[k] = 1$ *if* $\mathbf{s}_{1,j}^{(SS)}[k] = 1$ *and* $\mathbf{s}_{1,j}^{(BW)}[k] = 1$*, which correspond to the hypotheses* $\mathcal{H}_{0,k}^{(\mathcal{CR}_{1,j})}$ *and* $\mathcal{H}_{0,k}^{(\mathcal{FC}_1)}$*. It can be seen that the frequency bands are finally determined to be available at the CUs only if both the LSS and CSS indicate that* $\mathcal{PU}_1$ *does not occupy these frequency bands. Therefore, the probability of missed detection is reduced.*

5.3.2 Proposed NC Based CSS Scheme for Two Groups of Cognitive Radio Users

This subsection investigates a three-hop CWRN consisting of a source node $\mathcal{S}$, a destination node $\mathcal{D}$ and two layers of CUs $\mathcal{CR}^{(N_1)}$ and $\mathcal{CR}^{(N_2)}$, which are in the transmission range of $\mathcal{PU}_1$ and $\mathcal{PU}_2$, respectively (see Fig. 5.1). In order to realize a continuous transmission from $\mathcal{S}$ to $\mathcal{D}$ with the assistance of $\mathcal{CR}^{(N_1)}$ and $\mathcal{CR}^{(N_2)}$ in the three-hop CWRN, the spectrum can be shared in a cooperative manner to efficiently exploit the frequency bands that are not occupied by $\mathcal{PU}_1$ and $\mathcal{PU}_2$. Thus, all the CUs in two layers are required to sense the spectrum holes of both PUs.

The CSS scheme for each cognitive radio layer, as previously presented, consists of three phases to detect the available spectrum in the coverage of the corresponding PU. In order to help two cognitive radio layers know the

spectrum information of each other, the conventional scheme requires two additional phases at $\mathcal{FC}$ to forward the global SIV of a cognitive radio layer to another layer, i.e. $\mathcal{FC}$ sequentially forwards $\mathbf{s}_{FC_1}$ and $\mathbf{s}_{FC_2}$ to $\mathcal{CR}^{(N_2)}$ and $\mathcal{CR}^{(N_1)}$, respectively. Accordingly, this results in a total of eight phases in the conventional CSS scheme for two layers of CUs in the three-hop CWRN. Exploiting the XOR operator, an NC-based CSS scheme is proposed for two cognitive radio layers to reduce the exchange time of the SIVs between $\mathcal{CR}^{(N_1)}$ and $\mathcal{CR}^{(N_2)}$. The proposed CSS scheme for two cognitive radio layers consists of seven phases as follows: SS, RP and BW phases for $\mathcal{CR}^{(N_1)}$; SS, RP and BW phases for $\mathcal{CR}^{(N_2)}$; and an exchange (EX) phase between $\mathcal{CR}^{(N_1)}$ and $\mathcal{CR}^{(N_2)}$.

Following the proposed CSS scheme for each layer of CUs in the first six phases, the final SIV at $\mathcal{CR}_{i,j}$, $i = 1, 2$, $j = 1, 2, \ldots, N_i$, and the global SIV at $\mathcal{FC}$ for the i-th cognitive radio layer are given by $\mathbf{s}_{CR_{i,j}}$ and $\mathbf{s}_{FC_i}$, respectively. In the EX phase of the proposed NC-based CSS scheme, $\mathcal{FC}$ combines the global SIVs determined after two RP phases for two cognitive radio layers, i.e. $\mathbf{s}_{FC_1}$ and $\mathbf{s}_{FC_2}$, as

$$\mathbf{s}_{FC} = \mathbf{s}_{FC_1} \oplus \mathbf{s}_{FC_2}, \tag{5.8}$$

where $\oplus$ denotes the XOR operator and $\mathbf{s}_{FC}$ is the XOR-based combined SIV at $\mathcal{FC}$. Then, $\mathcal{FC}$ forwards $\mathbf{s}_{FC}$ to all CUs in two layers. The received signal at each CU $\mathcal{CR}_{i,j}$, $i = 1, 2$, $j = 1, 2, \ldots, N_i$, can be written as

$$\mathbf{r}_{i,j}^{(EX)} = \sqrt{\Lambda_{FC}} h_{FC_{i,j}} \mathbf{x}_{FC} + \mathbf{n}_{i,j}^{(EX)}, \tag{5.9}$$

where $\mathbf{x}_{FC}$ is the BPSK modulated version of $\mathbf{s}_{FC}$, and $\mathbf{n}_{i,j}^{(EX)}$ is the independent CSCG noise vector at $\mathcal{CR}_{i,j}$ in the EX phase with each entry having zero mean and variance of N_0. Then, $\mathcal{CR}_{i,j}$ decodes the received signal as $\mathbf{s}_{i,j}^{(EX)}$. Note that the decoded signal at $\mathcal{CR}_{i,j}$ of the transmitted signal $\mathbf{s}_{FC_i}$ in the BW phase is given by $\mathbf{s}_{i,j}^{(BW)}$ (see (5.6)). Thus, $\mathcal{CR}_{i,j}$ in the i-th cognitive radio layer can detect the spectrum information of the $\bar{i}$-th cognitive radio layer, $\bar{i} = 1, 2$, $\bar{i} \neq i$, with the XOR operator, i.e.

$$\mathbf{s}_{CR_{i,j}}^{(\bar{i})} = \mathbf{s}_{i,j}^{(EX)} \oplus \mathbf{s}_{i,j}^{(BW)}, \tag{5.10}$$

where $\mathbf{s}_{CR_{i,j}}^{(\bar{i})}$ denotes the global SIV of the $\bar{i}$-th cognitive radio layer estimated at $\mathcal{CR}_{i,j}$.

Remark 5.2 (*Higher System Throughput with NC*). *The proposed NC-based CSS scheme for two cognitive radio layers in the three-hop CWRN achieves a higher system throughput than the conventional CSS scheme. Let* $T_{i,j}^{(SS)}$ *and* $T_{i,j}^{(RP)}$ *denote the local sensing time and reporting time, respectively, for a frequency band at the* j*-th CU in the* i*-th cognitive radio layer,* $i = 1, 2$, $j = 1, 2, \ldots, N_i$. *Also, let* $T^{(BW)}$ *and* $T^{(EX)}$ *denote the backward time and the exchange time, respectively, at FC for a frequency band. It can be seen that the conventional CSS scheme requires a total time of* $[K(\sum_{i=1}^{2}\sum_{j=1}^{N_i} T_{i,j}^{(SS)} + T_{i,j}^{(RP)}) + 2KT^{(BW)} + 2KT^{(EX)}]$ *whilst the total time in the proposed CSS scheme is* $[K(\sum_{i=1}^{2}\sum_{j=1}^{N_i} T_{i,j}^{(SS)} + T_{i,j}^{(RP)}) + 2KT^{(BW)} + KT^{(EX)}]$. *Thus, the proposed NC-based CSS scheme reduces the time of spectrum sensing in the whole system by* $KT^{(EX)}$, *which accordingly results in a higher system throughput.*

5.4 Performance Analysis of CSS

This section investigates two performance metrics for spectrum sensing in CWRNs including the missed detection probability[27] (MDP) and the false alarm probability[28] (FAP). Specifically, this section derives the expressions of MDP and FAP for the proposed CSS scheme over a practical scenario where all the SS, RP and BW channels are characterised by Rayleigh flat fading channels. For convenience, let $P_m^{(A)}$ and $P_f^{(A)}$, $A \in \{\mathcal{CR}_{i,j}, \mathcal{FC}\}$, $i = 1, 2$, $j = 1, 2, \ldots, N_i$, denote the MDP and FAP, respectively, at node A.

For the LSS at a CU $\mathcal{CR}_{i,j}$, $i = 1, 2$, $j = 1, 2, \ldots, N_i$, the average FAP and MDP of the k-th frequency band over the SS channels are given by [163]

$$P_f^{(\mathcal{CR}_{i,j})} = \Pr\left\{\mathcal{H}_{1,k}^{(\mathcal{CR}_{i,j})} | \mathcal{H}_{0,k}^{(\mathcal{PU}_i)}\right\} = \Pr\left\{\mathbf{s}_{i,j}^{(SS)}[k] = 0 | \mathbf{x}_i = 0\right\} = \frac{\Gamma\left(\mu, \frac{\mathcal{E}_{i,j}[k]}{2}\right)}{\Gamma(\mu)}, \quad (5.11)$$

[27] The missed detection probability is defined as the probability that a CU detects an available frequency band given that a PU currently occupies that frequency for transmission.

[28] The false alarm probability is defined as the probability that a CU senses a frequency band occupied by a PU given that the PU does not operate on that frequency band.

$$
\begin{aligned}
P_m^{(\mathcal{CR}_{i,j})} &= \Pr\left\{\mathcal{H}_{0,k}^{(\mathcal{CR}_{i,j})}|\mathcal{H}_{1,k}^{(\mathcal{PU}_i)}\right\} = \Pr\left\{\mathbf{s}_{i,j}^{(SS)}[k]=1|\mathbf{x}_i\neq 0\right\} \\
&= 1 - e^{-\frac{\varepsilon_{i,j}[k]}{2}} \sum_{l=0}^{\mu-2} \frac{\mathcal{E}_{i,j}^{l}[k]}{l!2^l} - \left(\frac{1+\gamma_{P_iC_{i,j}}^{(\mathcal{CR}_{i,j})}}{\gamma_{P_iC_{i,j}}^{(\mathcal{CR}_{i,j})}}\right)^{\mu-1} \\
&\quad \times \left[e^{-\frac{\varepsilon_{i,j}[k]}{2\left(1+\gamma_{P_iC_{i,j}}^{(\mathcal{CR}_{i,j})}\right)}} - e^{-\frac{\varepsilon_{i,j}[k]}{2}} \sum_{l=0}^{\mu-2} \frac{\mathcal{E}_{i,j}^{l}[k](\gamma_{P_iC_{i,j}}^{(\mathcal{CR}_{i,j})})^l}{l!2^l\left(1+\gamma_{P_iC_{i,j}}^{(\mathcal{CR}_{i,j})}\right)^l} \right],
\end{aligned} \tag{5.12}
$$

respectively, where μ is the time-bandwidth product, $\gamma_{P_iC_{i,j}}^{(\mathcal{CR}_{i,j})}$ is the average signal-to-noise ratio (SNR) at $\mathcal{CR}_{i,j}$ over the SS channel $h_{P_iC_{i,j}}$, and $\Gamma[a,b]$ is the upper incomplete gamma function defined as $\Gamma[a,b] \triangleq \int_b^\infty t^{a-1}e^{-t}dt$ [134].

Now, analyse the CSS scheme performed at only one layer of CUs, e.g. $\mathcal{CR}^{(N_1)}$. The analysis of the CSS scheme for the remaining cognitive radio layer, $\mathcal{CR}^{(N_2)}$, can be similarly obtained. In the CSS scheme, each CU forwards the sensing information to FC over the RP channels. The FC then decodes all the received information and makes a global decision based on the OR rule. The FAP and MDP at the FC can be written as

$$
P_f^{(\mathcal{FC}_1)} = \Pr\left\{\mathcal{H}_{1,k}^{(\mathcal{FC}_1)}|\mathcal{H}_{0,k}^{(\mathcal{PU}_1)}\right\} = \Pr\left\{\mathbf{s}_{FC_1}[k]=0|\mathbf{x}_1=0\right\}, \tag{5.13}
$$

$$
P_m^{(\mathcal{FC}_1)} = \Pr\left\{\mathcal{H}_{0,k}^{(\mathcal{FC}_1)}|\mathcal{H}_{1,k}^{(\mathcal{PU}_1)}\right\} = \Pr\left\{\mathbf{s}_{FC_1}[k]=1|\mathbf{x}_1\neq 0\right\}, \tag{5.14}
$$

respectively. From (5.5), (5.13) and (5.14) can be rewritten as

$$
P_f^{(\mathcal{FC}_1)} = 1 - \prod_{j=1}^{N_1} \Pr\left\{\mathbf{s}_{1,j}^{(RP)}[k]=1|\mathbf{x}_1=0\right\}, \tag{5.15}
$$

$$
P_m^{(\mathcal{FC}_1)} = \prod_{j=1}^{N_1} \Pr\left\{\mathbf{s}_{1,j}^{(RP)}[k]=1|\mathbf{x}_1\neq 0\right\}. \tag{5.16}
$$

Thus, if considering an ideal case where the RP channels are error-free, i.e. $\mathbf{s}_{1,j}^{(RP)} = \mathbf{s}_{1,j}^{(SS)}$, from (5.11) and (5.12), the FAP and MDP at the FC can be written as

$$
P_f^{(\mathcal{FC}_1,\text{error-free})} = 1 - \prod_{j=1}^{N_1} \left(1 - P_f^{(\mathcal{CR}_{1,j})}\right), \tag{5.17}
$$

$$
P_m^{(\mathcal{FC}_1,\text{error-free})} = \prod_{j=1}^{N_1} P_m^{(\mathcal{CR}_{1,j})}, \tag{5.18}
$$

respectively. However, the RP channels suffer from fading and noise.

Over a Rayleigh flat fading channel h_{AB}, the bit error rate (BER) for the transmission of BPSK modulated signal is given by [120]

$$P_b(E_{AB}) = \phi(\gamma), \tag{5.19}$$

where γ is the average SNR and $\phi(x) \triangleq \frac{1}{2}\left(1-\sqrt{\frac{x}{1+x}}\right)$. Thus, taking into account the noisy RP channels $\left\{h_{C_{1,j}F}\right\}$, $j = 1, 2, \ldots, N_1$, the FAP and MDP at the FC are given by [159]

$$P_f^{(\mathcal{FC}_1)} = 1 - \prod_{j=1}^{N_1}\left[\left(1-P_f^{(\mathcal{CR}_{1,j})}\right)\left(1-P_b(E_{C_{1,j}F})\right) + P_f^{(\mathcal{CR}_{1,j})}P_b(E_{C_{1,j}F})\right], \tag{5.20}$$

$$P_m^{(\mathcal{FC}_1)} = \prod_{j=1}^{N_1}\left[P_m^{(\mathcal{CR}_{1,j})}\left(1-P_b(E_{C_{1,j}F})\right) + \left(1-P_m^{(\mathcal{CR}_{1,j})}\right)P_b(E_{C_{1,j}F})\right], \tag{5.21}$$

respectively. Here, $P_b(E_{C_{1,j}F}) = \phi(\gamma_{C_{1,j}F}^{(\mathcal{FC})})$ (see (5.19)), where $\gamma_{C_{1,j}F}^{(\mathcal{FC})}$ denotes the SNR at $\mathcal{FC}$ over the RP channel $h_{C_{1,j}F}$.

Then, in order to help each CU decide the availability of the spectrum, the FC needs to forward its decision to all the CUs over the BW channels. In the proposed CSS scheme, $\mathcal{CR}_{1,j}$, $j = 1, 2, \ldots, N_1$, ORs its local SIV with the global SIV received from $\mathcal{FC}$ to make a final decision. Let $P_f^{'(\mathcal{CR}_{1,j})}$ and $P_m^{'(\mathcal{CR}_{1,j})}$ denote the FAP and MDP of the final decision at $\mathcal{CR}_{1,j}$ over the BW channels. Similarly, $P_f^{'(\mathcal{CR}_{1,j})}$ and $P_m^{'(\mathcal{CR}_{1,j})}$ can be derived as

$$P_f^{'(\mathcal{CR}_{1,j})} = \Pr\left\{\bar{\mathcal{H}}_{1,k}^{(\mathcal{CR}_{1,j})} | \mathcal{H}_{0,k}^{(\mathcal{PU}_1)}\right\} = \Pr\left\{\mathbf{s}_{CR_{1,j}}[k] = 0 | \mathbf{x}_1 = 0\right\}, \tag{5.22}$$

$$P_m^{'(\mathcal{CR}_{1,j})} = \Pr\left\{\bar{\mathcal{H}}_{0,k}^{(\mathcal{CR}_{1,j})} | \mathcal{H}_{1,k}^{(\mathcal{PU}_1)}\right\} = \Pr\left\{\mathbf{s}_{CR_{1,j}}[k] = 1 | \mathbf{x}_1 \neq 0\right\}. \tag{5.23}$$

From (5.7), (5.22) and (5.23) can be rewritten as

$$P_f^{'(\mathcal{CR}_{1,j})} = 1 - \Pr\left\{\mathbf{s}_{1,j}^{(SS)}[k] = 1 | \mathbf{x}_1 = 0\right\}\Pr\left\{\mathbf{s}_{1,j}^{(BW)}[k] = 1 | \mathbf{x}_1 = 0\right\}, \tag{5.24}$$

$$P_m^{'(\mathcal{CR}_{1,j})} = \Pr\left\{\mathbf{s}_{1,j}^{(SS)}[k] = 1 | \mathbf{x}_1 \neq 0\right\}\Pr\left\{\mathbf{s}_{1,j}^{(BW)}[k] = 1 | \mathbf{x}_1 \neq 0\right\}. \tag{5.25}$$

In the situation that there is no error in the BW phase, i.e. $\mathbf{s}_{1,j}^{(BW)} = \mathbf{s}_{FC_1}$, substituting (5.11), (5.12), (5.13) and (5.14) into (5.24) and (5.25), the FAP and MDP can be obtained as

$$P_f^{'(\mathcal{CR}_{1,j},\text{error-free})} = 1 - \left(1-P_f^{(\mathcal{CR}_{1,j})}\right)\left(1-P_f^{(\mathcal{FC}_1)}\right), \tag{5.26}$$

$$P_m^{\prime(\mathcal{CR}_{1,j},\text{error-free})} = P_m^{(\mathcal{CR}_{1,j})} P_m^{(\mathcal{FC}_1)}. \tag{5.27}$$

However, in practice, the BW channels also suffer from fading and noise. Thus, the FAP and MDP at $\mathcal{CR}_{1,j}$, $j = 1, 2, \ldots, N_1$, over the noisy BW channels $h_{FC_{1,j}}$ can be written as

$$\begin{aligned} P_f^{\prime(\mathcal{CR}_{1,j})} =& 1 - \left[\left(1 - P_f^{(\mathcal{CR}_{1,j})}\right)\left(1 - P_b(E_{FC_{1,j}})\right) + P_f^{(\mathcal{CR}_{1,j})} P_b(E_{FC_{1,j}})\right] \\ & \times \left[\left(1 - P_f^{(\mathcal{FC}_1)}\right)\left(1 - P_b(E_{FC_{1,j}})\right) + P_f^{(\mathcal{FC}_1)} P_b(E_{FC_{1,j}})\right], \end{aligned} \tag{5.28}$$

$$\begin{aligned} P_m^{\prime(\mathcal{CR}_{1,j})} =& \left[P_m^{(\mathcal{CR}_{1,j})}\left(1 - P_b(E_{FC_{1,j}})\right) + \left(1 - P_m^{(\mathcal{CR}_{1,j})}\right) P_b(E_{FC_{1,j}})\right] \\ & \times \left[P_m^{(\mathcal{FC}_1)}\left(1 - P_b(E_{FC_{1,j}})\right) + \left(1 - P_m^{(\mathcal{FC}_1)}\right) P_b(E_{FC_{1,j}})\right], \end{aligned} \tag{5.29}$$

respectively, where $P_b(E_{FC_{1,j}}) = \phi(\gamma_{FC_{1,j}}^{(\mathcal{CR}_{1,j})})$ and $\gamma_{FC_{1,j}}^{(\mathcal{CR}_{1,j})}$ denotes the SNR at $\mathcal{CR}_{1,j}$ over the BW channel $h_{FC_{1,j}}$.

Corollary 5.1. *For identical SS and RP channels, i.e.* $\gamma_{PC_{1,j}}^{(\mathcal{CR}_{1,j})} \triangleq \gamma_1^{(SS)}$ *and* $\gamma_{C_{1,j}F}^{(\mathcal{FC}_1)} \triangleq \gamma_1^{(RP)}$, $j = 1, 2, \ldots, N_1$, *all CUs achieve the same FAP and MDP in the LSS process, i.e.* $P_f^{(\mathcal{CR}_{1,j})} \triangleq P_f^{(\mathcal{CR}_1)}$ *and* $P_m^{(\mathcal{CR}_{1,j})} \triangleq P_m^{(\mathcal{CR}_1)}$, *and the BERs of all the RP channels are identical, i.e.* $P_b(E_{C_{1,j}F}) \triangleq P_b(E_{C_1F}) = \phi(\gamma_1^{(RP)})$. *Then, the FAP at* $\mathcal{CR}_{1,j}$ *over the BW channels is lower-bounded by* $P_{f,0}^{\prime(\mathcal{CR}_{1,j})}$, *where*

$$\begin{aligned} P_{f,0}^{\prime(\mathcal{CR}_{1,j})} =& 1 - \left(1 - N_1 P_b(E_{C_1F})\right)\left(1 - P_b(E_{FC_{1,j}})\right)^2 \\ & - N_1 P_b(E_{C_1F}) P_b(E_{FC_{1,j}})\left(1 - P_b(E_{FC_{1,j}})\right). \end{aligned} \tag{5.30}$$

Proof. From (5.28), the FAP at $\mathcal{CR}_{1,j}$, $j = 1, 2, \ldots, N_1$, over the BW channels can be rewritten as

$$\begin{aligned} P_f^{\prime(\mathcal{CR}_{1,j})} =& 1 - \left(1 - P_f^{(\mathcal{CR}_{1,j})}\right)\left(1 - P_f^{(\mathcal{FC}_1)}\right)\left(1 - P_b(E_{FC_{1,j}})\right)^2 \\ & - P_b(E_{FC_{1,j}})(1 - P_b(E_{FC_{1,j}}))\left[P_f^{(\mathcal{CR}_{1,j})} + P_f^{(\mathcal{FC}_1)} - 2P_f^{(\mathcal{CR}_{1,j})} P_f^{(\mathcal{FC}_1)}\right] \\ & - P_f^{(\mathcal{CR}_{1,j})} P_f^{(\mathcal{FC}_1)} (P_b(E_{FC_{1,j}}))^2. \end{aligned} \tag{5.31}$$

It can be seen that the FAP of the CSS scheme is lower-bounded if the FAP of the LSS scheme approaches zero. Let $P_{f,0}^{\prime(\mathcal{CR}_{1,j})}$ denote the lower bound of $P_f^{\prime(\mathcal{CR}_{1,j})}$. Then

$$P_{f,0}^{\prime(\mathcal{CR}_{1,j})} = \lim_{P_f^{(\mathcal{CR}_1)} \to 0} P_f^{\prime(\mathcal{CR}_{1,j})}. \tag{5.32}$$

Since $P_f^{(\mathcal{CR}_{1,j})} = P_f^{(\mathcal{CR}_1)}$, $P_m^{(\mathcal{CR}_{1,j})} = P_m^{(\mathcal{CR}_1)}$ and $P_b(E_{C_{1,j}F}) = P_b(E_{C_1F})$, $\forall j = 1, 2, \ldots, N_1$, from (5.20), the FAP at the FC is rewritten by

$$P_f^{(\mathcal{FC}_1)} = 1 - \left[\left(1 - P_f^{(\mathcal{CR}_1)}\right)\left(1 - P_b(E_{C_1F})\right) + P_f^{(\mathcal{CR}_j)} P_b(E_{C_1F})\right]^{N_1}, \quad (5.33)$$

and lower-bounded by

$$P_{f,0}^{(\mathcal{FC}_1)} = \lim_{P_f^{(\mathcal{CR}_1)} \to 0} P_f^{(\mathcal{FC}_1)} = 1 - (1 - P_b(E_{C_1F}))^{N_1} \approx N_1 P_b(E_{C_1F}). \quad (5.34)$$

Thus, from (5.32), $P_{f,0}^{'(\mathcal{CR}_{1,j})}$ can be computed by

$$\begin{aligned} P_{f,0}^{'(\mathcal{CR}_{1,j})} &= 1 - \left(1 - P_{f,0}^{(\mathcal{FC}_1)}\right)\left(1 - P_b(E_{FC_{1,j}})\right)^2 \\ &\quad - P_b(E_{FC_{1,j}})(1 - P_b(E_{FC_{1,j}}))P_{f,0}^{(\mathcal{FC}_1)}. \end{aligned} \quad (5.35)$$

Substituting (5.34) into (5.35), $P_{f,0}^{'(\mathcal{CR}_{1,j})}$ can be obtained as

$$\begin{aligned} P_{f,0}^{'(\mathcal{CR}_{1,j})} &= 1 - (1 - N_1 P_b(E_{C_1F}))\left(1 - P_b(E_{FC_{1,j}})\right)^2 \\ &\quad - N_1 P_b(E_{C_1F}) P_b(E_{FC_{1,j}})\left(1 - P_b(E_{FC_{1,j}})\right). \end{aligned} \quad (5.36)$$

The corollary is proved. □

Remark 5.3 (*Improved MDP and Higher Lower-Bound of FAP with Increased Number of Cognitive Radio Users*). *The proposed CSS scheme improves the MDP at the CUs and increases the lower bound of the FAP when the number of CUs increases. In fact, from* (5.21)*, it can be seen that* $P_m^{(\mathcal{FC}_1)}$ *monotonically decreases over* N_1*. Thus,* $P_m^{'(\mathcal{CR}_{1,j})}$*,* $j = 1, 2, \ldots, N_1$*, given by* (5.29) *is a decreasing function over* N_1*. This means that the MDP at* $\mathcal{CR}_{1,j}$ *is improved as the number of CUs increases. In addition, from* (5.30)*, it can be proved that* $P_{f,0}^{'(\mathcal{CR}_{1,j})}$ *monotonically increases over* N_1*. In other words, the increased number of CUs results in the higher lower bound of the FAP at* $\mathcal{CR}_{1,j}$*. This observation will be confirmed later in the numerical results where the FAP at* $\mathcal{CR}_{1,j}$ *is limited by the lower threshold and the MDP increases quickly to one as the FAP approaches this threshold.*

Remark 5.4 (*Improved Sensing Performance with The Proposed CSS Scheme*). *The proposed CSS scheme at the CUs achieves an improved performance over*

the conventional scheme in terms of MDP. In fact, following the conventional CSS scheme, the final SIV at the CUs is obtained from the global SIV at the FC, which means that $\mathbf{s}_{CR_{1,j}}$, $j = 1, 2, \ldots, N_1$, *depends totally on* $\mathbf{s}_{FC_1}$. *Thus, the MDP of the conventional CSS scheme at* $\mathcal{CR}_{1,j}$ *is given by*

$$P_m^{\prime(\mathcal{CR}_{1,j},conventional)} = P_m^{(\mathcal{FC}_1)}\left(1 - P_b(E_{FC_{1,j}})\right) + \left(1 - P_m^{(\mathcal{FC}_1)}\right) P_b(E_{FC_{1,j}}), \quad (5.37)$$

where $P_m^{(\mathcal{FC}_1)}$ *is given by* (5.21). *Let* G *denote the performance gain achieved with the proposed CSS scheme compared with the conventional scheme.* G *is therefore evaluated as*

$$G \triangleq \frac{P_m^{\prime(\mathcal{CR}_{1,j})}}{P_m^{\prime(\mathcal{CR}_{1,j},conventional)}}. \quad (5.38)$$

From (5.29) *and* (5.37), G *is obtained as*

$$G = P_m^{(\mathcal{CR}_{1,j})}\left(1 - P_b(E_{FC_{1,j}})\right) + \left(1 - P_m^{(\mathcal{CR}_{1,j})}\right) P_b(E_{FC_{1,j}}). \quad (5.39)$$

It can be seen that $G < 1$ *for all* $P_m^{(\mathcal{CR}_{1,j})}$, $P_m^{(\mathcal{FC}_1)}$ *and* $P_b(E_{FC_{1,j}})$. *In other words, independent of the LSS at the CUs, the CSS at the FC, and the quality of the BW channels, the proposed CSS scheme achieves a lower MDP than the conventional scheme. Additionally, a significant gain is achieved with the proposed scheme (i.e. a much lower* G*) when either the BW channels is at high SNR (i.e. a very low* $P_b(E_{FC_{1,j}})$*) or the LSS at the CUs is very reliable (i.e. a very low* $P_m^{(\mathcal{CR}_{1,j})}$*).*

5.5 Numerical and Simulation Results

This section presents numerical and simulation results of the MDP and FAP using various spectrum sensing schemes. The results are obtained by using a Monte Carlo simulation method in MATLAB. Specifically, the relationship between the MDP and the FAP is represented by the complementary receiver operating characteristic (CROC), which is defined as the MDP versus the FAP[29].

[29]The receiver operating characteristic (ROC) is defined as the probability of correct detection versus the probability of false detection, and thus it can be equivalently defined the CROC as the MDP versus the FAP [163].

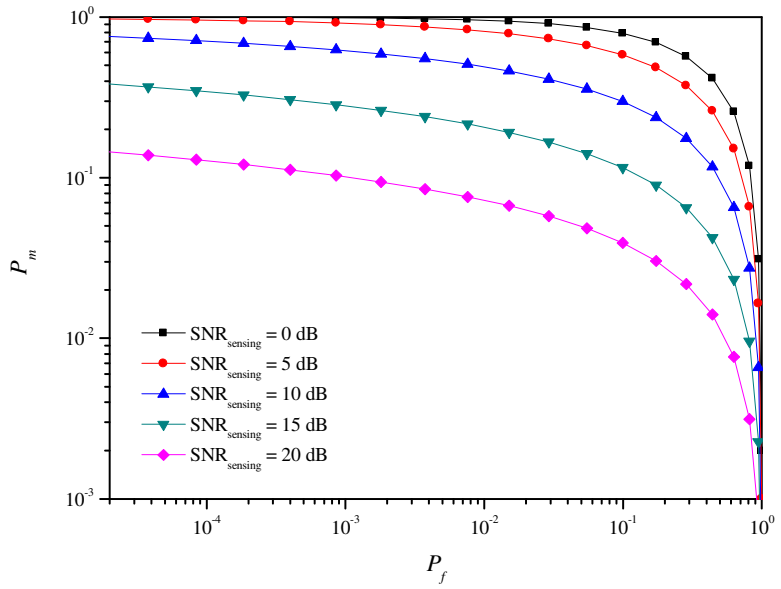

Figure 5.3: Local spectrum sensing performance at a CU ($\mathcal{CR}_{1,1}$) with various SNR values of the SS channel ($\gamma_{P_1C_{1,1}}^{(\mathcal{CR}_{1,1})}$).

Fig. 5.3 shows the CROC curves of the spectrum sensing at a CU with respect to various SNR values of the SS channel. In this figure, LSS is employed at the CU based on energy detection. Without any loss of generality, the first CU in the first cognitive radio layer (i.e. $\mathcal{CR}_{1,1}$) is considered. It is assumed that the time-bandwidth product $\mu = 5$ and the average SNR at $\mathcal{CR}_{1,1}$ over the SS channel $h_{P_1C_{1,1}}$ (i.e. $\gamma_{P_1C_{1,1}}^{(\mathcal{CR}_{1,1})}$) varies in $\{0, 5, 10, 15, 20\}$ dB. It can be seen that the sensing performance deteriorates when $\gamma_{P_1C_{1,1}}^{(\mathcal{CR}_{1,1})}$ decreases. Thus, the LSS at the CU is limited when the SS channel between the PU and the CU suffers severe fading, especially in hidden terminal problems with shadowing.

Now, the CSS for a cognitive radio layer with the assistance of an FC is investigated. In Fig. 5.4, the CROC of the CSS at the FC is plotted for various SNR values of the RP channel. Assume that the CSS is carried out at $\mathcal{FC}$ for the first layer of CUs which includes 2 CUs, i.e. $\mathcal{CR}_{1,1}$ and $\mathcal{CR}_{1,2}$. The SNRs of the SS channels $\gamma_{P_1C_{1,1}}^{(\mathcal{CR}_{1,1})}$ and $\gamma_{P_1C_{1,2}}^{(\mathcal{CR}_{1,2})}$ are assumed to be 10 dB and the SNRs of the RP channels $\gamma_{C_{1,1}F}^{(\mathcal{FC})}$ and $\gamma_{C_{1,2}F}^{(\mathcal{FC})}$ are assumed to be equal and vary in $\{0, 5, 10, 15, 20\}$ dB. It can be observed that improved performance is achieved when the SNR of the RP channels increases. With the same model including

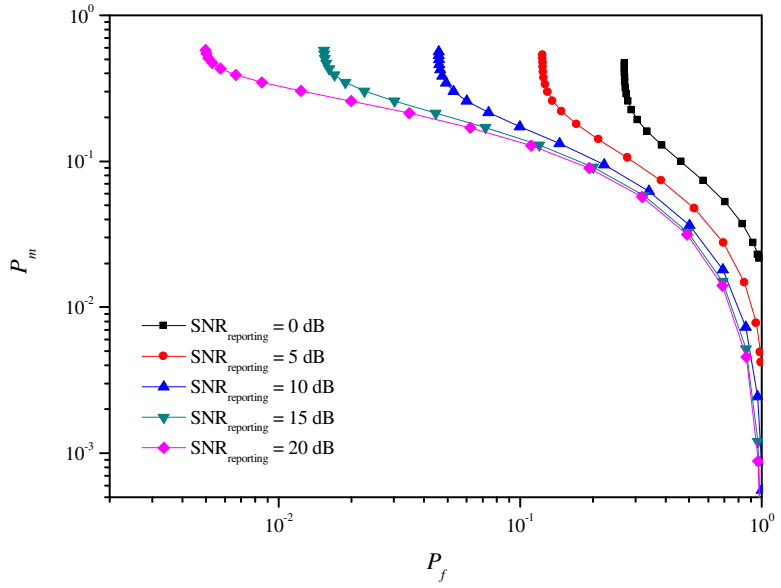

Figure 5.4: Cooperative spectrum sensing performance at FC with 2 CUs, $\gamma_{P_1C_{1,1}}^{(\mathcal{CR}_{1,1})} = \gamma_{P_1C_{1,2}}^{(\mathcal{CR}_{1,2})} = 10$ dB and $\gamma_{C_{1,1}F}^{(\mathcal{FC})} = \gamma_{C_{1,2}F}^{(\mathcal{FC})}$.

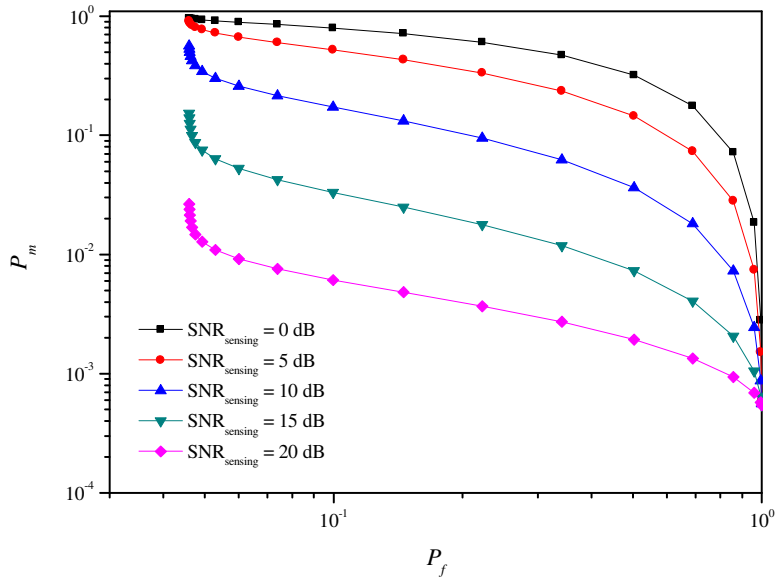

Figure 5.5: Cooperative spectrum sensing performance at FC with 2 CUs, $\gamma_{C_{1,1}F}^{(\mathcal{FC})} = \gamma_{C_{1,2}F}^{(\mathcal{FC})} = 10$ dB and $\gamma_{P_1C_{1,1}}^{(\mathcal{CR}_{1,1})} = \gamma_{P_1C_{1,2}}^{(\mathcal{CR}_{1,2})}$.

2 CUs, the effect of the quality of the SS channels on the CROC at the FC is illustrated in Fig. 5.5 where it is assumed that $\gamma_{C_{1,1}F}^{(\mathcal{FC})} = \gamma_{C_{1,2}F}^{(\mathcal{FC})} = 10$ dB and $\gamma_{P_1C_{1,1}}^{(\mathcal{CR}_{1,1})} = \gamma_{P_1C_{1,2}}^{(\mathcal{CR}_{1,2})} \in \{0, 5, 10, 15, 20\}$ dB. Similarly, it can be seen that improved performance is achieved when the SNR of the SS channels increases.

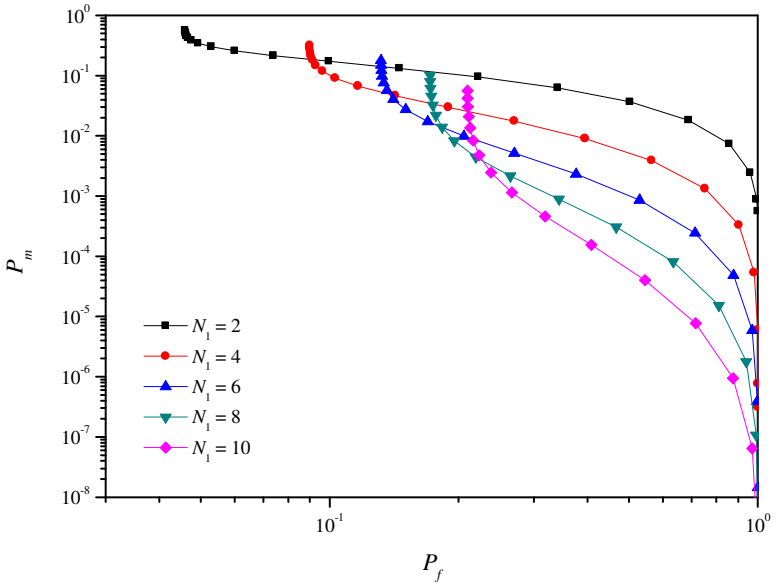

Figure 5.6: Cooperative spectrum sensing performance at FC with $\gamma_{P_1C_{1,j}}^{(\mathcal{CR}_{1,j})} = \gamma_{C_{1,j}F}^{(\mathcal{FC})} = 10$ dB, $j = 1, 2, \ldots, N_1$, and various number of CUs (N_1).

Additionally, Fig. 5.6 considers the effects of the number of cognitive radio users in the first cognitive radio layer on the sensing performance at the FC. The SNRs of the SS and RP channels are assumed to be 10 dB and the number of CUs, i.e. N_1, is assumed to vary in $\{2, 4, 6, 8, 10\}$. It is observed that the sensing performance is improved with increased number of CUs. It is noted that the CROC curves in Figs. 5.4, 5.5 and 5.6 correspond to the sensing performance at the FC in which the SS channels from the PC to the CUs and the RP channels from the CUs to the FC are both assumed to suffer from Rayleigh fading channels. However, in practice, the transmission of the global decision from the FC to the CUs suffers from the fading of the BW channels, that may result in a poor sensing performance at the CUs compared to the sensing performance at the FC.

In Fig. 5.7, the CSS performance at a CU using the proposed scheme is illustrated with respect to various SNR values of the BW channel. It is assumed that there are 2 CUs in the first layer, i.e. $\mathcal{CR}_{1,1}$ and $\mathcal{CR}_{1,2}$ and the CROC curves are corresponding to the sensing performance at $\mathcal{CR}_{1,1}$. The SNRs of the SS and RP channels are assumed to be $\gamma_{C_{1,1}F}^{(\mathcal{FC})} = \gamma_{C_{1,2}F}^{(\mathcal{FC})} = \gamma_{P_1C_{1,1}}^{(\mathcal{CR}_{1,1})} =$

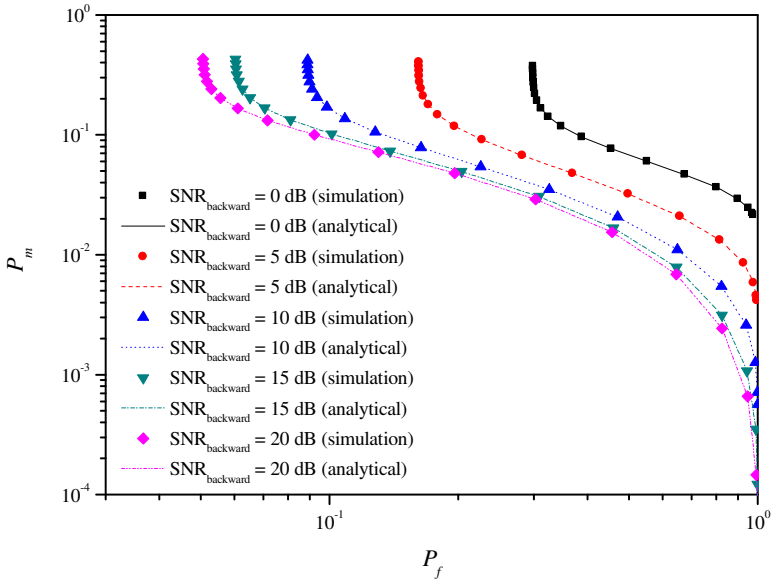

Figure 5.7: Cooperative spectrum sensing performance at a CU ($\mathcal{CR}_{1,1}$) over backward links with 2 CUs, $\gamma_{P_1C_{1,1}}^{(\mathcal{CR}_{1,1})} = \gamma_{P_1C_{1,2}}^{(\mathcal{CR}_{1,2})} = \gamma_{C_{1,1}F}^{(\mathcal{FC})} = \gamma_{C_{1,2}F}^{(\mathcal{FC})} = 10$ dB and various $\gamma_{FC_{1,1}}^{(\mathcal{CR}_{1,1})}$.

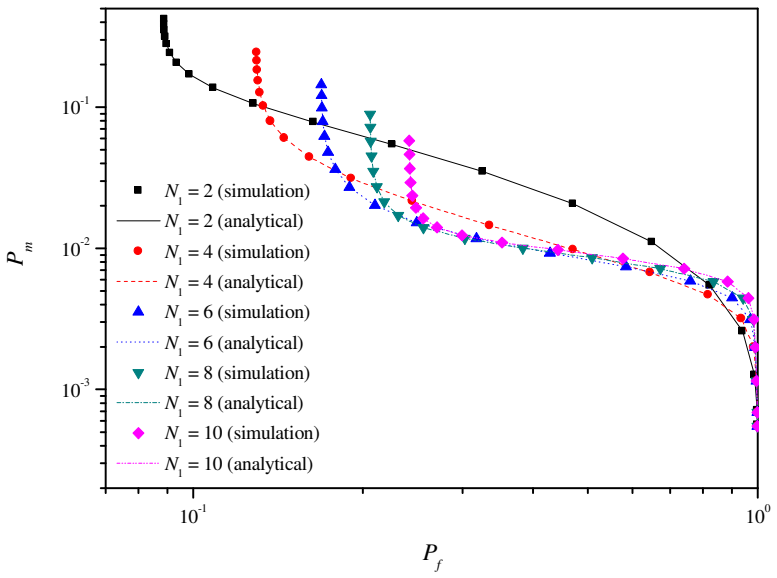

Figure 5.8: Cooperative spectrum sensing performance at a CU ($\mathcal{CR}_{1,1}$) over backward links with $\gamma_{P_1C_{1,j}}^{(\mathcal{CR}_{1,j})} = \gamma_{C_{1,j}F}^{(\mathcal{FC})} = \gamma_{FC_{1,j}}^{(\mathcal{CR}_{1,j})} = 10$ dB, $j = 1, 2, \ldots, N_1$ and various number of CUs (N_1).

$\gamma_{P_1C_{1,2}}^{(\mathcal{CR}_{1,2})} = 10$ dB and the SNR of the BW channel, i.e. $\gamma_{FC_{1,1}}^{(\mathcal{CR}_{1,1})}$, is assumed to vary in $\{0, 5, 10, 15, 20\}$ dB. It can be seen that the sensing performance

at $\mathcal{CR}_{1,1}$ is significantly reduced when $\gamma_{FC_{1,1}}^{(\mathcal{CR}_{1,1})}$ decreases. This observation reflects the effects of the BW channels on the CSS performance. Additionally, the analytical results are shown to match the simulation results. In order to investigate the effects of number of CUs on the CSS performance, Fig. 5.8 illustrates the CROC curves of the CSS at $\mathcal{CR}_{1,1}$ with respect to various numbers of CUs. The SNRs of the SS, RP and BW channels are assumed to be 10 dB and the number of CUs (i.e. N_1) is assumed to be in $\{2, 4, 6, 8, 10\}$. It is observed that the MDP is lower and the lower-bound of FAP is higher when N_1 increases. This observation confirms the statements in Remark 5.3 regarding the improved MDP and higher lower-bound of FAP with the increased number of CUs in the proposed scheme.

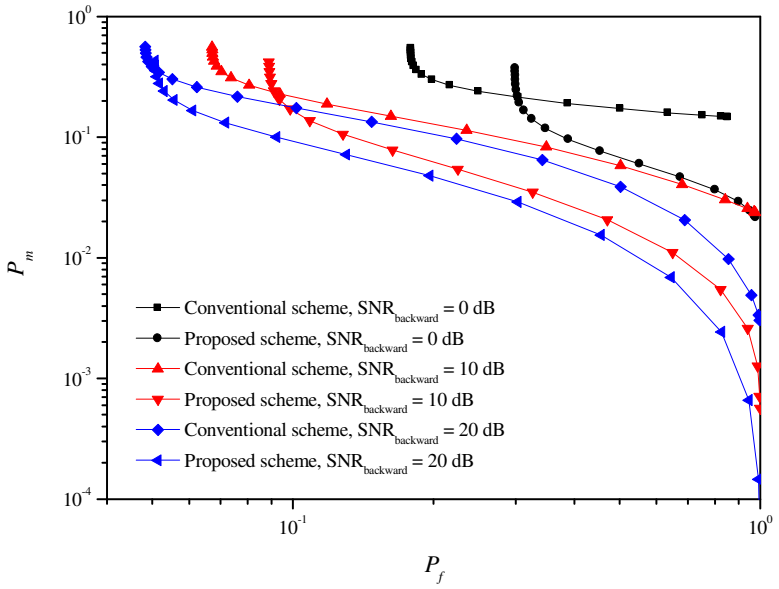

Figure 5.9: Comparison of two cooperative spectrum sensing schemes over backward links with 2 CUs, $\gamma_{P_1C_{1,1}}^{(\mathcal{CR}_{1,1})} = \gamma_{P_1C_{1,2}}^{(\mathcal{CR}_{1,2})} = \gamma_{C_{1,1}F}^{(\mathcal{FC})} = \gamma_{C_{1,2}F}^{(\mathcal{FC})} = 10$ dB and various $\gamma_{FC_{1,1}}^{(\mathcal{CR}_{1,1})}$.

For the comparison between the proposed CSS scheme and the conventional scheme, Fig. 5.9 shows the CROC of both CSS schemes with respect to various SNR values of the BW channel. The CROC curves are plotted for the CSS at $\mathcal{CR}_{1,1}$ in the first cognitive radio layer including 2 CUs, i.e. $\mathcal{CR}_{1,1}$ and $\mathcal{CR}_{1,2}$. The SNRs of the SS, RP and BW channels are assumed as follows: $\gamma_{C_{1,1}F}^{(\mathcal{FC})} =$

$\gamma_{C_{1,2}F}^{(\mathcal{FC})} = \gamma_{P_1C_{1,1}}^{(\mathcal{CR}_{1,1})} = \gamma_{P_1C_{1,2}}^{(\mathcal{CR}_{1,2})} = 10$ dB and $\gamma_{FC_{1,1}}^{(\mathcal{CR}_{1,1})} \in \{0, 10, 20\}$ dB. It can be seen that the proposed CSS scheme achieves improved sensing performance than the conventional scheme for all SNR values of the BW channels. This observation confirms the statements in Remarks 5.1 and 5.4 about the improved reliability of spectrum sensing with the proposed CSS scheme. In fact, in the proposed scheme, the combination of the LSS and CSS at the CU results in better sensing performance at the CUs.

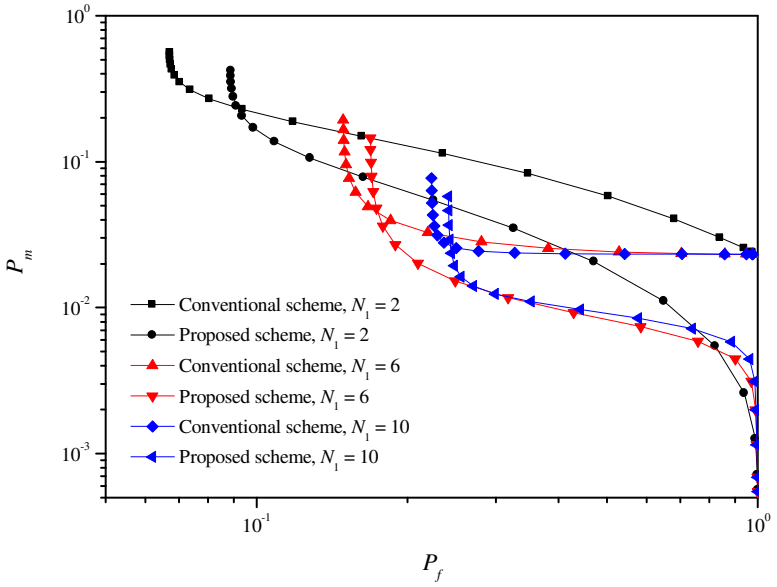

Figure 5.10: Comparison of two cooperative spectrum sensing schemes over backward links with $\gamma_{P_1C_{1,j}}^{(\mathcal{CR}_{1,j})} = \gamma_{C_{1,j}F}^{(\mathcal{FC})} = \gamma_{FC_{1,j}}^{(\mathcal{CR}_{1,j})} = 10$ dB, $j = 1, 2, \ldots, N_1$ and various number of CUs (N_1).

Investigating the effects of the number of CUs on the sensing performance, Fig. 5.10 plots the CROC of both the proposed CSS scheme and the conventional scheme with respect to various number of CUs (i.e. N_1). It is assumed that the SNRs of the SS, RP and BW channels are 10 dB, and N_1 in $\{2, 6, 10\}$. Similarly, it can be observed that the proposed scheme achieves improved performance over the conventional scheme for all values of N_1. This also confirms the statements in Remarks 5.1 and 5.4 about the improved sensing performance with the proposed CSS scheme.

Taking into consideration the MDP, Figs. 5.11 and 5.12 plot the MDP of

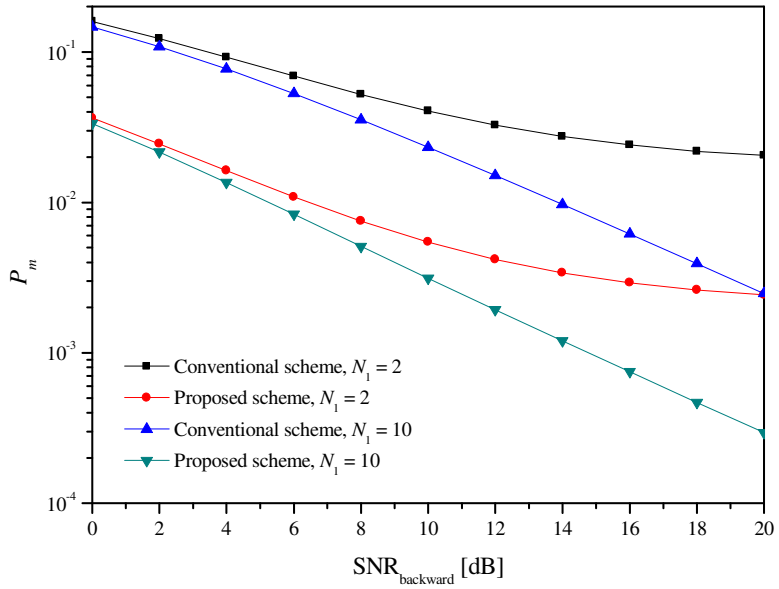

Figure 5.11: MDP of cooperative spectrum sensing over SNR of backward links with $\gamma_{P_1C_{1,j}}^{(\mathcal{CR}_{1,j})} = \gamma_{C_{1,j}F}^{(\mathcal{FC})} = 10$ dB, $j = 1, 2, \ldots, N_1$ and various N_1.

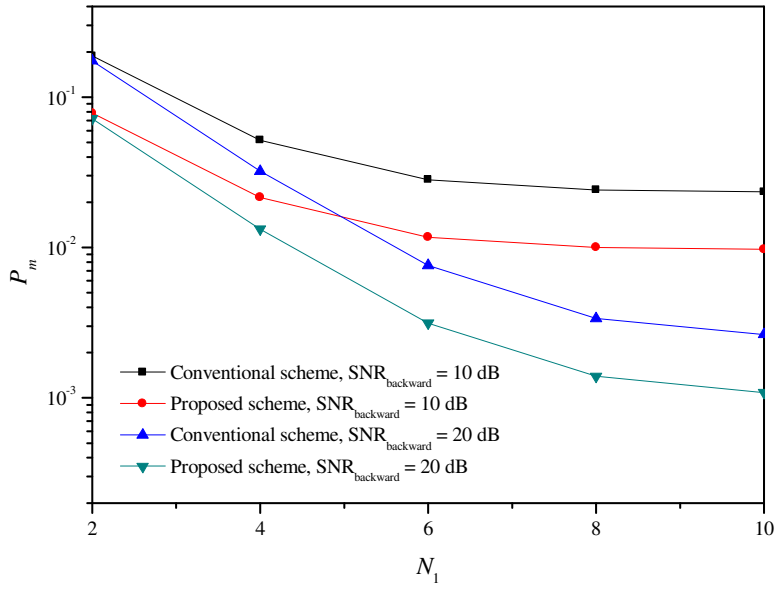

Figure 5.12: MDP of cooperative spectrum sensing over N_1 with $\gamma_{P_1C_{1,j}}^{(\mathcal{CR}_{1,j})} = \gamma_{C_{1,j}F}^{(\mathcal{FC})} = 10$ dB, $j = 1, 2, \ldots, N_1$ and various SNRs of backward links.

various CSS schemes versus SNR of the BW channels and versus number of CUs, respectively. In Fig. 5.11, the SNRs of the SS and RP channels are 10 dB, and N_1 in $\{2, 10\}$. It can be seen that the proposed scheme achieves a much lower MDP than the conventional scheme. For example, an 8 dB improvement

is achieved with the proposed scheme for a MDP of 10^{-2} and $N_1 = 10$. The effectiveness of the proposed scheme is further confirmed in Fig. 5.12 where the MDP of both the proposed CSS scheme and the conventional scheme is plotted over the number of CUs. The SNRs of the SS and RP channels are 10 dB, while the SNRs of the BW channels are in $\{10, 20\}$ dB. It is observed that the MDP of the proposed scheme is improved over that of the conventional scheme for any value of either N_1 or SNR of the BW links. Specifically, for a SNR of BW channels of 20 dB, the proposed scheme achieves an MDP of 10^{-2} with 4 CUs while 6 CUs are required to achieve the same MDP using the conventional scheme. The aforementioned observations from Figs. 5.11 and 5.12 confirm the statements in Remarks 5.1 and 5.4 regarding a better MDP with the proposed CSS scheme.

5.6 Conclusions

This chapter has proposed two CSS schemes for three-hop CWRNs. Exploiting both the local decisions at the CUs and global decisions at the FC, an improved sensing performance is achieved with the first proposed scheme. An analysis of the probabilities of missed detection and false alarm has been carried out with respect to the SNRs of SS, RP and BW channels. The derived expressions reflect well the impact of the quality of the SS, RP and BW links upon the sensing performance and confirm the improvement of sensing reliability with the proposed scheme. Moreover, for the exchange of spectrum information between two cognitive radio layers, an NC-based CSS scheme has been proposed to reduce the number of signallings for a higher system throughput. In addition, simulations have been provided which have confirmed the analytical results.

Chapter 6

Distributed Space-Time-Frequency Block Coding

In previous chapters, network coding has been exploited to reduce the signalling overheads for an improved system throughput in cognitive wireless relay networks (CWRNs). As another approach for high-throughput relay communications, this chapter considers the application of space-time coding to the cooperative transmission in CWRNs over frequency-selective fading channels. A new distributed space-time-frequency block code (DSTFBC) is proposed for a two-hop nonregenerative CWRN, where a primary source node and N secondary source nodes convey information data to their desired primary destination node and N secondary destination nodes via two relay nodes. The proposed DSTFBC is designed to achieve higher data rate, spatial diversity gain and decoupling detection of data blocks at all destination nodes with a low-complexity receiver structure. In the proposed DSTFBC, before forwarding the data received from various sources to the destination nodes, the relay nodes precode the received signals with a precoding matrix, which is effectively formulated to enable cooperative data transmission of all nodes in the CWRN. Furthermore, the pairwise error probability analysis is provided to investigate the achievable diversity gain of the proposed DSTFBC for two channel models including the model where the links from the sources to the relays and from the relays to the destinations are modeled by mixed Rayleigh-Rician fading

and the model where all links are modelled by Rician fading. These two channel models allow to analyse three typical scenarios where the relays are in the neighbourhood of either the sources or the destinations or the midpoint between the source and destination nodes.

6.1 Introduction

Recently, the reliability of wireless communications has been greatly improved by the use of diversity schemes to combat the detrimental effects of fading channels. Space-time block codes (STBCs) [57, 58] are categorised as powerful transmit diversity techniques for multiple-input multiple-output (MIMO) systems. With low-complexity maximum likelihood (ML) decodability and high achievable diversity gain, STBCs are widely used for wireless communications. MIMO technology has gained attention in Long Term Evolution (LTE)-Advanced and Worldwide Interoperability for Microwave Access (WiMAX) wireless networks' standards [3]. Generally, STBCs are designed for co-located antennas, and thus are easily deployed at the base station to improve the performance of downlink transmission in mobile communication systems. For uplink transmission, the realisation of STBCs is challenging due to the constraints on size and hardware complexity in mobile devices. Therefore, in order to adapt the design of STBCs to the uplink transmission of single-antenna devices, another form of diversity, which is known as cooperative diversity or user cooperation, has been proposed in [4–6]. Cooperative diversity allows single-antenna mobile users to share their antennas and cooperate to form a virtual multiple-antenna system. In other words, the uplink communications from the mobile station to the base station is realised in a cooperative manner with cooperating mobile stations, also known as relay stations.

Distributed space-time block codes (DSTBCs) were first introduced in [7] as a distributed implementation of the conventional STBCs for cooperative communications. In [95], a DSTBC scheme was proposed for a two-hop amplify-and-forward (AF) protocol based on the idea of linear dispersion space-time

code [94]. In [97], a distributed orthogonal STBCs was designed to achieve single-symbol ML decodability and full diversity order. DSTBC schemes were mostly specified for flat fading channels [93,95,97,165–167]. However, in many current wireless communications systems, the fading channels are usually regarded as frequency-selective fading channels due to the accommodation of high data-rate transmission. The designs of DSTBC in frequency selective fading channels were investigated in [98] with decode-and-forward (DF) relaying and in [100] with AF relaying for relay networks where there exists one active relay node and a direct communication link between the source and the final destination.

Motivated by relaying and diversity schemes for cooperative communications, cooperative spectrum sensing (CSS) was proposed in [48,156,159] to deal with the hidden terminal problems in cognitive radio networks when the cognitive users (CUs) are shadowed or under severe fading channels while their nearby PUs are active. The CSS scheme not only helps the shadowed CUs detect the PUs but also improves detection reliability. Furthermore, cooperative diversity was incorporated into cognitive networks to construct a cognitive wireless relay network (CWRN) for a seamless transmission by exploiting some portions of the spectrum that may not be utilized by the PUs over a period of time [162, 168–170]. In [168], the CUs perform the role of a relay to assist the data transmission of the PU to increase their opportunities in spectrum access. In [169], a cooperative diversity scheme was proposed for CWRN where the CUs cooperatively send both the signal of the PU and their own signals. In [162], the authors proposed a cognitive space-time-frequency coding to maximize the spectrum opportunities in the CWRN. In [170], a cooperative scheme was proposed to improve the secondary outage probability by optimally selecting the best CU as the relay for the secondary data transmission. In [171–174], various precoding schemes are proposed at the relay to mitigate the interference at the receivers with the assumption that the cognitive relay has non-causal access to the messages of all the transmitters, has channel knowledge of the links between sources and relay and also the forward

links of the relay are perfectly known at the relay.

Most of the literature discussed above on cooperative diversity for CWRN has considered the transmission of either the PU or the CU over frequency-nonselective fading channels for low data-rate communication [162, 168–170, 173]. However, in wide-band communications standards where the system is required to operate at a high data rate, the multipath fading channels become frequency selective. These channels cause severe attenuation in signal strength and unreliable signal detection due to significant inter-symbol interference. In these environments, the cooperative transmission of both the PU and CUs in a CWRN over frequency-selective fading channels for wide-band wireless communications has not previously been investigated. In addition, the diversity gain of cooperative communication in a CWRN for the general frequency-selective fading scenario where the relays are either in the neighborhood of the sources or the destinations or the midpoint of the network has also not been evaluated.

To provide a solution to these problems, this chapter designs a new distributed space-time-frequency block code (DSTFBC) for two-hop CWRNs over frequency-selective fading channels using two active relay nodes with the AF protocol. As shown in [6, 7], the AF relaying protocol is the best option in cooperative communications to achieve the maximum diversity gain. In the proposed DSTFBC, the relays help PU and SUs in the coverage of a CWRN to transmit their own data to their interested destinations. Specifically, the proposed DSTFBC operates as follows (see Fig. 6.1): In the first time slot, primary source $\mathcal{PS}$ and N secondary sources $\{\mathcal{SS}_1, \mathcal{SS}_2, \ldots, \mathcal{SS}_N\}$ send their blocks of information data to two relays $\mathcal{R}_1$ and $\mathcal{R}_2$ using various available frequency bands. In the proposed DSTFBC, one of two relays precodes its received signals before sending to primary destination $\mathcal{PD}$ and N secondary destinations $\{\mathcal{SD}_1, \mathcal{SD}_2, \ldots, \mathcal{SD}_N\}$ in the second time slot. The precoding is designed such that the decoupling detection of each data block is possible at every destination. The main contributions in this chapter can be summarised as follows:

- With the proposed DSTFBC, a data rate of $N + 1/N + 2$ is achieved while the application of distributed space-time block coding (DSTBC) to the considered CWRNs with the employment of repetition code at the source nodes (e.g. [100]) results in a lower rate of 1/3.

- The precoding matrix is proposed at the relays such that decoupling detection of desired data blocks in both the time and frequency domain is possible at $\mathcal{PD}$ and also at $\{\mathcal{SD}_1, \mathcal{SD}_2, \ldots, \mathcal{SD}_N\}$. The design of the precoding matrix is based on the Alamouti scheme [57]. The scheme is effectively modified to provide a solution at the data-block level rather than the data-symbol level to facilitate the cooperative transmission of both the PU and SUs over frequency-selective fading channels in the CWRN context.

- The pairwise error probability (PEP) is analysed to study the achievable diversity gain of the proposed DSTFBC for the general scenario where the relays are located either near the sources or the destinations or the midpoint of the network. For the scenario that the relays are in the neighbour of either the sources or the destinations, the channel model is considered as a mix of Rayleigh and Rician fading, i.e. one of two hops from the sources to the relays or from the relays to the destinations is considered as a line-of-sight (LOS) transmission and the other hop is a non-line-of-sight (NLOS) transmission. For the scenario that the relays are near the network midpoint, all transmission links from the sources to the relay and from the relay to the destinations are regarded as LOS transmissions, which are modelled by Rician fading channels.

The theoretical results prove that the transmission from the sources to the destinations using the proposed scheme achieves the spatial diversity order of $\min(L_{\mathcal{AR}_1}, L_{\mathcal{R}_1\mathcal{B}}) + \min(L_{\mathcal{AR}_2}, L_{\mathcal{R}_2\mathcal{B}})$, where $\mathcal{A} \in \{\mathcal{PS}, \mathcal{SS}_1, \mathcal{SS}_2, \ldots, \mathcal{SS}_N\}$, $\mathcal{B} \in \{\mathcal{PD}, \mathcal{SD}_1, \mathcal{SD}_2, \ldots, \mathcal{SD}_N\}$. Here, $L_{\mathcal{AR}_j}$ and $L_{\mathcal{R}_j\mathcal{B}}$, $j = 1, 2$, are the channel memory lengths for the links from $\mathcal{A}$ to $\mathcal{R}_j$ and from $\mathcal{R}_j$ to $\mathcal{B}$, respectively. The analysis also shows that the fading factor of Rician fading in the LOS

component provides a coding gain to the PEP performance. It means that, as the fading factor increases, an improved performance is observed. Additionally, through the simulation results, it is demonstrated that the proposed DSTFBC scheme achieves a lower bit error rate (BER) when compared with the conventional interference cancellation scheme (e.g. [172]) due to the achievable diversity gain of the proposed DSTFBC method.

The rest of this chapter is organized as follows: Section 6.2 describes the fading channel model in a CWRN. Section 6.3 presents the proposed DSTFBC scheme along with proof of decoupling capability for the proposed DSTFBC in both the time and frequency domains. Performance analysis is presented in Section 6.4. The numerical and simulation results are presented in Section 6.5 and finally Section 6.6 concludes this chapter.

Notation: Bold lower and upper case letters represent vectors and matrices, respectively. The notation used in the chapter is listed as follows:

$(\cdot)^T$; $(\cdot)^*$; $(\cdot)^{\mathcal{H}}$	transpose, complex conjugate and Hermitian transpose
$E(\cdot)$; $\Phi(\cdot)$; $f(\cdot)$	expectation, moment generating and probability density functions
$[\mathbf{x}]_i$; $[\mathbf{A}]_{i,j}$	i-th entry of vector $\mathbf{x}$ and (i,j)-th entry of matrix $\mathbf{A}$
$\|\mathbf{x}\|$	Euclidean norm of vector $\mathbf{x}$
$\mathbf{B} = <\mathbf{A}>^2$	$\mathbf{B} = \mathbf{A}\mathbf{A}^{\mathcal{H}}$
$\mathbf{B} = \mathbf{A}^{1/2}$	a matrix $\mathbf{B}$ such that $\mathbf{B}^2 = \mathbf{A}$
$\otimes$; $\oplus$	matrix direct product and direct sum
$\mathbf{F}_M$	normalised $M \times M$ discrete Fourier transform (DFT) matrix. $[\mathbf{F}_M]_{m,n} = \frac{1}{\sqrt{M}} e^{-j2\pi(m-1)(n-1)/M}$ $\forall$ $1 \leq m, n \leq M$
$\mathbf{0}_{M\times N}$; $\mathbf{I}_N$	all-zero matrix of size $M \times N$ and identity matrix of size $N \times N$.

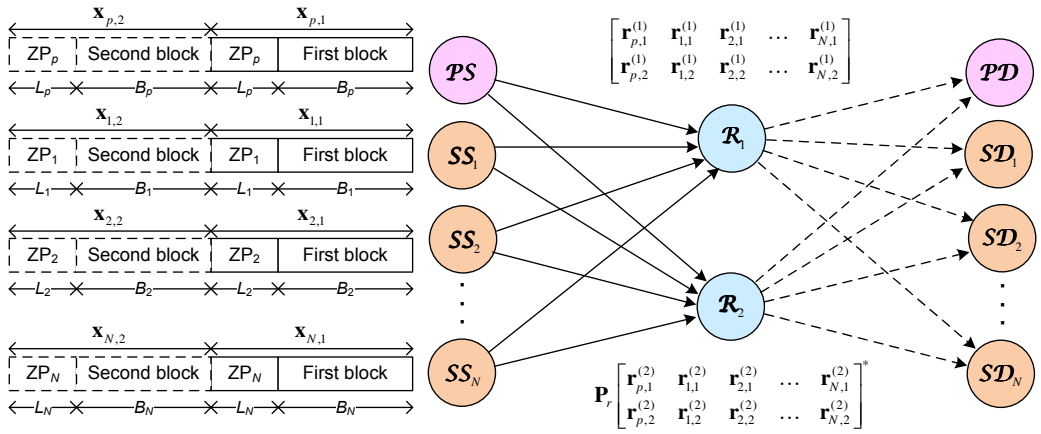

Figure 6.1: System model and data transmission in cognitive wireless relay network with the assistance of two relays.

6.2 Fading Channel Model

Fig. 6.1 illustrates the system model of a cognitive wireless relay network, where the data transmission from primary source $\mathcal{PS}$ and N secondary sources $\{\mathcal{SS}_1, \mathcal{SS}_2, \ldots, \mathcal{SS}_N\}$ to the primary destination $\mathcal{PD}$ and N secondary destinations $\{\mathcal{SD}_1, \mathcal{SD}_2, \ldots, \mathcal{SD}_N\}$ is carried out via a two-hop protocol with the assistance of two relays $\mathcal{R}_1$ and $\mathcal{R}_2$. A half-duplex system is considered where all nodes can either transmit or receive data, but not concurrently. It is assumed that there are no direct links between any pair of source and destination nodes due to either power limitations in each node or distance between nodes, i.e. each source node cannot communicate directly with its intended destination node. The data transmissions of PUs and CUs are assumed to operate in a wide-band channel including K non-overlapping frequency bands. In order to realise simultaneous transmissions, frequency bands are assumed to be properly allocated to all the source and destination nodes as $\{f_p, f_{s_1}, f_{s_2}, \ldots, f_{s_N}\}$ by using various spectrum sensing techniques (e.g. [155, 159]), and thus the number of available frequency bands should satisfy $K \geqslant N + 1$.

This chapter takes into consideration two typical fading models including long-term and short-term fading. In wireless communications, long-term fading is caused by path loss and shadowing effects on the data transmission from source node to destination node, while short-term fading characterises

the frequency selectivity of the wireless channel between these two nodes. Specifically, the long-term and short-term fading between two nodes $\mathcal{A}$ and $\mathcal{B}$, $\mathcal{A},\mathcal{B} \in \{\mathcal{PS}, \mathcal{SS}_1, \mathcal{SS}_2, \ldots, \mathcal{SS}_N, \mathcal{PD}, \mathcal{SD}_1, \mathcal{SD}_2, \ldots, \mathcal{SD}_N, \mathcal{R}_1, \mathcal{R}_2\}$, are characterised by $\xi_{\mathcal{AB}}$ and $\mathbf{h}_{\mathcal{AB}}$, respectively. Here, $\mathbf{h}_{\mathcal{AB}}$ represents a number of independent resolvable paths with an impulse response given by

$$h_{\mathcal{AB}}(\tau) = \sum_{l=1}^{L_{\mathcal{AB}}} h_{\mathcal{AB}}(l)\delta(\tau - \tau_{\mathcal{AB},l}), \tag{6.1}$$

where $L_{\mathcal{AB}}$ is the number of resolvable paths, $h_{\mathcal{AB}}(l)$ denotes the gain of the l-th path which is modelled by a complex Gaussian random variable with zero mean and variance of $\sigma^2_{\mathcal{AB}}(l)$, and τ_l is the relative delay of the l-th path to the first path. Thus, for convenience, denote $\mathbf{h}_{\mathcal{AB}} = [h_{\mathcal{AB}}(1), h_{\mathcal{AB}}(2), \ldots, h_{\mathcal{AB}}(L_{\mathcal{AB}})]^T$. The fading coefficients of the communication channel between two nodes are assumed to be constant over at least two consecutive time slots and vary independently in the next two time slots (i.e. block fading or quasi-static channel model). The total power gain for each link is normalised to be unity, i.e. $E[\|\mathbf{h}_{\mathcal{AB}}\|^2] = \sum_{l=1}^{L_{\mathcal{AB}}} \sigma^2_{\mathcal{AB}}(l) = 1$.

6.3 Proposed DSTFBC and Proofs of Decoupling Capability

This section first introduces the proposed DSTFBC for CWRNs. Then, this section proceeds to prove that the proposed DSTFBC can decouple the detection of two data blocks at each destination node in both the time and frequency domains.

6.3.1 Proposed DSTFBC

Fig. 6.1 briefly illustrates the structure of the transmitted data blocks at $\mathcal{PS}$ and $\{\mathcal{SS}_1, \mathcal{SS}_2, \ldots, \mathcal{SS}_N\}$. Each source node transmits two information-bearing data blocks to its interested destination through the assistance of two relay nodes. Each transmitted data block $\mathbf{x}_{p,i}$, $i = 1, 2$, of length M_p is gener-

ated at $\mathcal{PS}$ by adding a zero-padding (ZP) sequence ZP_p of length L_p to modulated information data block $\mathbf{s}_{p,i}$ of length B_p, which can be expressed as $\mathbf{x}_{p,i} = \left[\mathbf{s}_{p,i}^T, \mathbf{0}_{1\times L_p}\right]^T$ where $\mathbf{s}_{p,i} = \left[[\mathbf{s}_{p,i}]_1, [\mathbf{s}_{p,i}]_2, \ldots, [\mathbf{s}_{p,i}]_{B_p}\right]^T$. To guarantee that the channel matrices $\mathcal{PS} \to \mathcal{R}_1$, $\mathcal{PS} \to \mathcal{R}_2$, $\mathcal{R}_1 \to \mathcal{PD}$ and $\mathcal{R}_2 \to \mathcal{PD}$ are circulant, the length of ZP_p must satisfy $L_p \geqslant \max(L_{\mathcal{PSR}_1}+L_{\mathcal{R}_1\mathcal{PD}}, L_{\mathcal{PSR}_2}+L_{\mathcal{R}_2\mathcal{PD}})$. Similarly, each transmitted data block $\mathbf{x}_{s_i,j}$ at $\mathcal{SS}_i$, $i = 1, \ldots, N$, $j = 1, 2$, of length M_{s_i} is created by adding a ZP_{s_i} of length L_{s_i} to modulated information data block $\mathbf{s}_{s_i,j}$ of length B_{s_i}. Thus, $\mathbf{x}_{s_i,j}$ can be represented as $\mathbf{x}_{s_i,j} = \left[\mathbf{s}_{s_i,j}^T, \mathbf{0}_{1\times L_{s_i}}\right]^T$ where $\mathbf{s}_{s_i,j} = \left[[\mathbf{s}_{s_i,j}]_1, [\mathbf{s}_{s_i,j}]_2, \ldots, [\mathbf{s}_{s_i,j}]_{B_{s_i}}\right]^T$. Also, the length of ZP_{s_i} must satisfy $L_{s_i} \geqslant \max(L_{\mathcal{SS}_i\mathcal{R}_1} + L_{\mathcal{R}_1\mathcal{SD}_i}, L_{\mathcal{SS}_i\mathcal{R}_2} + L_{\mathcal{R}_2\mathcal{SD}_i})$ to assure that the channel matrices $\mathcal{SS}_i \to \mathcal{R}_1$, $\mathcal{SS}_i \to \mathcal{R}_2$, $\mathcal{R}_1 \to \mathcal{SD}_i$ and $\mathcal{R}_2 \to \mathcal{SD}_i$ are circulant.

With proper allocation of available frequency bands $\{f_p, f_{s_1}, f_{s_2}, \ldots, f_{s_N}\}$ for all source and destination nodes, $\{\mathcal{PS}, \mathcal{SS}_1, \mathcal{SS}_2, \ldots, \mathcal{SS}_N\}$ simultaneously transmit two data blocks to both $\mathcal{R}_1$ and $\mathcal{R}_2$ in the first two time slots. In the next $(2N + 2)$ time slots, $\mathcal{R}_1$ amplifies and forwards its $(2N + 2)$ received signals while $\mathcal{R}_2$ precodes its received signals by a precoding matrix before transmitting to all $\{\mathcal{PD}, \mathcal{SD}_1, \mathcal{SD}_2, \ldots, \mathcal{SD}_N\}$. The idea behind the proposed design is that the precoding at $\mathcal{R}_2$ helps enable the decoupling detection of two desired data blocks at every destination. Thus, the following remark can be made:

Remark 6.1 (*Higher data rate*). *A rate of* $N + 1/N + 2$ *is achieved with the proposed DSTFBC. To achieve the same goal in the considered scenario, the source nodes with repetition code (e.g. [100]) which is devised for a one-relay system, must send sequentially two data blocks to two relay nodes during* $(4N + 4)$ *time slots and then both the relay nodes amplify and forward their* $(2N+2)$ *received signals to all the destination nodes in the subsequent* $(2N+2)$ *time slots. Thus, the rate of this scheme is* $1/3$. *Accordingly, the proposed DSTFBC achieves a higher data rate transmission.*

This subsection now proceeds to present the data transmission and precoding process in the proposed DSTFBC for a CWRN. In the first two time

slots, $\mathcal{PS}$ serially transmits $\mathbf{x}_{p,k}$, $k = 1, 2$, to both $\mathcal{R}_1$ and $\mathcal{R}_2$ using its allocated frequency band f_p. In parallel to the primary transmission, each $\mathcal{SS}_i$, $i = 1, 2, \ldots, N$, also serially transmits $\mathbf{x}_{s_i,k}$, $k = 1, 2$, to both $\mathcal{R}_1$ and $\mathcal{R}_2$ using the available frequency f_{s_i}. The received signals at $\mathcal{R}_j$, $j = 1, 2$, from $\mathcal{PS}$ and $\mathcal{SS}_i$ are given by

$$\mathbf{r}_{p,k}^{(\mathcal{R}_j)} = \sqrt{\xi_{\mathcal{PSR}_j}}\mathbf{H}_{\mathcal{PSR}_j}\mathbf{x}_{p,k} + \boldsymbol{\eta}_{p,k}^{(\mathcal{R}_j)}, \tag{6.2}$$

$$\mathbf{r}_{s_i,k}^{(\mathcal{R}_j)} = \sqrt{\xi_{\mathcal{SS}_i\mathcal{R}_j}}\mathbf{H}_{\mathcal{SS}_i\mathcal{R}_j}\mathbf{x}_{s_i,k} + \boldsymbol{\eta}_{s_i,k}^{(\mathcal{R}_j)}, \tag{6.3}$$

respectively, where $\mathbf{H}_{\mathcal{PSR}_j}$ and $\mathbf{H}_{\mathcal{SS}_i\mathcal{R}_j}$ are $M_p \times M_p$ and $M_{s_i} \times M_{s_i}$ circulant channel matrices, and $\boldsymbol{\eta}_{p,k}^{(\mathcal{R}_j)}$ and $\boldsymbol{\eta}_{s_i,k}^{(\mathcal{R}_j)}$ are the white Gaussian noise vectors at $\mathcal{R}_j$ with each entry having zero-mean and variance of $N_0/2$ per dimension. It is noted that for any $M_{\mathcal{AB}} \times M_{\mathcal{AB}}$ circulant matrix $\mathbf{H}_{\mathcal{AB}}$, its (k, l) entry is written as $[\mathbf{H}_{\mathcal{AB}}]_{k,l} = [\mathbf{h}_{\mathcal{AB}}]_{((k-l+1) \bmod M_{\mathcal{AB}})}$. From (6.2) and (6.3), the received signals at $\mathcal{R}_j$, $j = 1, 2$, can be rewritten in vector-matrix form as

$$\mathbf{R}^{(\mathcal{R}_j)} = \begin{bmatrix} \mathbf{r}_{p,1}^{\prime(\mathcal{R}_j)} & \mathbf{r}_{s_1,1}^{\prime(\mathcal{R}_j)} & \mathbf{r}_{s_2,1}^{\prime(\mathcal{R}_j)} & \cdots & \mathbf{r}_{s_N,1}^{\prime(\mathcal{R}_j)} \\ \mathbf{r}_{p,2}^{\prime(\mathcal{R}_j)} & \mathbf{r}_{s_1,2}^{\prime(\mathcal{R}_j)} & \mathbf{r}_{s_2,2}^{\prime(\mathcal{R}_j)} & \cdots & \mathbf{r}_{s_N,2}^{\prime(\mathcal{R}_j)} \end{bmatrix}, \tag{6.4}$$

where $\mathbf{r}_{p,k}^{\prime(\mathcal{R}_j)}$ and $\mathbf{r}_{s_i,k}^{\prime(\mathcal{R}_j)}$, $i = 1, 2, \ldots, N$, $k = 1, 2$, are zero-padded signals after adding ZP sequences to match the length of $M = \max(M_p, M_{s_1}, \ldots, M_{s_N})$. Thus, the size of matrix $\mathbf{R}^{(\mathcal{R}_j)}$ is $2M \times (N + 1)$.

What is new in the proposed DSTFBC is that the received signal at $\mathcal{R}_2$ is conjugated and then precoded by a precoding matrix $\mathbf{P}_{\mathbf{R}}$ as follows:

$$\mathbf{P}_{\mathbf{R}} = \begin{bmatrix} \mathbf{0}_{M\times M} & -\mathbf{P}_M^{(G)} \\ \mathbf{P}_M^{(G)} & \mathbf{0}_{M\times M} \end{bmatrix}, \tag{6.5}$$

where the matrix $\mathbf{P}_M^{(G)}$ is designed as

$$\mathbf{P}_M^{(G)} = \begin{bmatrix} \mathbf{P}_1 & \mathbf{0}_{G\times(M-G)} \\ \mathbf{0}_{(M-G)\times G} & \mathbf{P}_2 \end{bmatrix} = \mathbf{P}_1 \oplus \mathbf{P}_2. \tag{6.6}$$

In (6.6), the matrix $\mathbf{P}_1$ of size $G\times G$ and the matrix $\mathbf{P}_2$ of size $(M-G)\times(M-G)$ have (l, k)-th elements given by

$$[\mathbf{P}_1]_{l,k} = \begin{cases} 1 & \text{if } k = G - l + 1, \\ 0 & \text{otherwise}, \end{cases} \tag{6.7}$$

$$[\mathbf{P}_2]_{l,k} = \begin{cases} 1 & \text{if } k = M - G - l + 1, \\ 0 & \text{otherwise.} \end{cases} \tag{6.8}$$

In order to ensure that, after precoding, at least the last $L_{\mathcal{PSR}_2}$ samples of $-\mathbf{P}_M^{(G)}\mathbf{r}_{p,2}^{'(\mathcal{R}_2)}$ and $\mathbf{P}_M^{(G)}\mathbf{r}_{p,1}^{'(\mathcal{R}_2)}$ and the last $L_{\mathcal{SS}_i\mathcal{R}_2}$, $i = 1, 2, \ldots, N$, samples of $-\mathbf{P}_M^{(G)}\mathbf{r}_{s_i,2}^{'(\mathcal{R}_2)}$ and $\mathbf{P}_M^{(G)}\mathbf{r}_{s_i,1}^{'(\mathcal{R}_2)}$ are all zeros to make the channel matrices $\mathcal{R}_2 \to \mathcal{PD}$ and $\mathcal{R}_2 \to \mathcal{SD}_i$ circulant, it can be chosen $G = \max(B_p,\, B_{s_1},\, B_{s_2},\, \ldots, B_{s_N})$ $+ \max(L_{\mathcal{PSR}_2},\, L_{\mathcal{SS}_1\mathcal{R}_2},\, L_{\mathcal{SS}_2\mathcal{R}_2},\, \ldots, L_{\mathcal{SS}_N\mathcal{R}_2})$. The idea behind the proposed design of precoding matrix in (6.5), (6.6), (6.7) and (6.8) is based on the Alamouti scheme [57]. While the Alamouti scheme was originally proposed at the data-symbol level for direct transmission in MIMO systems, the proposed DSTFBC is specifically designed at the data-block level to assist the cooperative data transmission of the PU and CUs in CWRNs via two relay nodes.

Then, each relay $\mathcal{R}_j$, $j = 1, 2$, normalises its received signals $\mathbf{r}_{p,k}^{(\mathcal{R}_j)}$ and $\mathbf{r}_{s_i,k}^{(\mathcal{R}_j)}$, $i = 1, 2, \ldots, N$, $k = 1, 2$, in (6.2) and (6.3) by factors $\alpha_p^{(\mathcal{R}_j)} = \sqrt{E\left[\left\|\mathbf{r}_{p,k}^{(\mathcal{R}_j)}\right\|^2\right]} = \sqrt{\xi_{\mathcal{PSR}_j} + N_0}$ and $\alpha_{s_i}^{(\mathcal{R}_j)} = \sqrt{E\left[\left\|\mathbf{r}_{s_i,k}^{(\mathcal{R}_j)}\right\|^2\right]} = \sqrt{\xi_{\mathcal{SS}_i\mathcal{R}_j} + N_0}$, respectively, to have unit average energy. Thus, the transmitted signals from $\mathcal{R}_j$, $j = 1, 2$, can be written by

$$\mathbf{X}^{(\mathcal{R}_1)} = \mathbf{R}_0^{(\mathcal{R}_1)}, \tag{6.9}$$

$$\mathbf{X}^{(\mathcal{R}_2)} = \mathbf{P}_{\mathbf{R}}\left[\mathbf{R}_0^{(\mathcal{R}_2)}\right]^*, \tag{6.10}$$

where $\mathbf{R}_0^{(\mathcal{R}_j)}$ is the normalised received signal at $\mathcal{R}_j$, which is given by

$$\mathbf{R}_0^{(\mathcal{R}_j)} = \begin{bmatrix} \frac{1}{\alpha_p^{(\mathcal{R}_j)}}\mathbf{r}_{p,1}^{'(\mathcal{R}_j)} & \frac{1}{\alpha_{s_1}^{(\mathcal{R}_j)}}\mathbf{r}_{s_1,1}^{'(\mathcal{R}_j)} & \frac{1}{\alpha_{s_2}^{(\mathcal{R}_j)}}\mathbf{r}_{s_2,1}^{'(\mathcal{R}_j)} & \cdots & \frac{1}{\alpha_{s_N}^{(\mathcal{R}_j)}}\mathbf{r}_{s_N,1}^{'(\mathcal{R}_j)} \\ \frac{1}{\alpha_p^{(\mathcal{R}_j)}}\mathbf{r}_{p,2}^{'(\mathcal{R}_j)} & \frac{1}{\alpha_{s_1}^{(\mathcal{R}_j)}}\mathbf{r}_{s_1,2}^{'(\mathcal{R}_2)} & \frac{1}{\alpha_{s_2}^{(\mathcal{R}_j)}}\mathbf{r}_{s_2,2}^{'(\mathcal{R}_j)} & \cdots & \frac{1}{\alpha_{s_N}^{(\mathcal{R}_j)}}\mathbf{r}_{s_N,2}^{'(\mathcal{R}_j)} \end{bmatrix}. \tag{6.11}$$

Then, $\mathcal{R}_1$ and $\mathcal{R}_2$ simultaneously forward their messages to $\{\mathcal{PD},\, \mathcal{SD}_1,\, \mathcal{SD}_2,\, \ldots, \mathcal{SD}_N\}$ using $\{f_p,\, f_{s_1},\, f_{s_2},\, \ldots, f_{s_N}\}$ in the subsequent $(2N + 2)$ time

slots[30]. The received signals at $\mathcal{PD}$ over f_p are written by

$$\mathbf{r}_1^{(\mathcal{PD})} = \sqrt{\xi_{\mathcal{R}_1\mathcal{PD}}}\mathbf{H}_{\mathcal{R}_1\mathcal{PD}}\frac{\mathbf{r}_{p,1}^{'(\mathcal{R}_1)}}{\alpha_p^{(\mathcal{R}_1)}} - \sqrt{\xi_{\mathcal{R}_2\mathcal{PD}}}\mathbf{H}_{\mathcal{R}_2\mathcal{PD}}\frac{\mathbf{P}_M^{(G)}\left[\mathbf{r}_{p,2}^{'(\mathcal{R}_2)}\right]^*}{\alpha_p^{(\mathcal{R}_2)}} + \boldsymbol{\eta}_1^{(\mathcal{PD})}, \quad (6.12)$$

$$\mathbf{r}_2^{(\mathcal{PD})} = \sqrt{\xi_{\mathcal{R}_1\mathcal{PD}}}\mathbf{H}_{\mathcal{R}_1\mathcal{PD}}\frac{\mathbf{r}_{p,2}^{'(\mathcal{R}_1)}}{\alpha_p^{(\mathcal{R}_1)}} + \sqrt{\xi_{\mathcal{R}_2\mathcal{PD}}}\mathbf{H}_{\mathcal{R}_2\mathcal{PD}}\frac{\mathbf{P}_M^{(G)}\left[\mathbf{r}_{p,1}^{'(\mathcal{R}_2)}\right]^*}{\alpha_p^{(\mathcal{R}_2)}} + \boldsymbol{\eta}_2^{(\mathcal{PD})}, \quad (6.13)$$

where $\mathbf{H}_{\mathcal{R}_j\mathcal{PD}}$, $j = 1, 2$, is the $M \times M$ circulant channel matrix and $\boldsymbol{\eta}_k^{(\mathcal{PD})}$, $k = 1, 2$, is a white Gaussian noise vector at $\mathcal{PD}$ with each entry having zero-mean and variance of $N_0/2$ per dimension. Similarly, the received signals at $\mathcal{SD}_i$, $i = 1, 2, \ldots, N$, over f_{s_i} are

$$\mathbf{r}_1^{(\mathcal{SD}_i)} = \sqrt{\xi_{\mathcal{R}_1\mathcal{SD}_i}}\mathbf{H}_{\mathcal{R}_1\mathcal{SD}_i}\frac{\mathbf{r}_{s_i,1}^{'(\mathcal{R}_1)}}{\alpha_{s_i}^{(\mathcal{R}_1)}} - \sqrt{\xi_{\mathcal{R}_2\mathcal{SD}_i}}\mathbf{H}_{\mathcal{R}_2\mathcal{SD}_i}\frac{\mathbf{P}_M^{(G)}\left[\mathbf{r}_{s_i,2}^{'(\mathcal{R}_2)}\right]^*}{\alpha_{s_i}^{(\mathcal{R}_2)}} + \boldsymbol{\eta}_1^{(\mathcal{SD}_i)}, \quad (6.14)$$

$$\mathbf{r}_2^{(\mathcal{SD}_i)} = \sqrt{\xi_{\mathcal{R}_1\mathcal{SD}_i}}\mathbf{H}_{\mathcal{R}_1\mathcal{SD}_i}\frac{\mathbf{r}_{s_i,2}^{'(\mathcal{R}_1)}}{\alpha_{s_i}^{(\mathcal{R}_1)}} + \sqrt{\xi_{\mathcal{R}_2\mathcal{SD}_i}}\mathbf{H}_{\mathcal{R}_2\mathcal{SD}_i}\frac{\mathbf{P}_M^{(G)}\left[\mathbf{r}_{s_i,1}^{'(\mathcal{R}_2)}\right]^*}{\alpha_p^{(\mathcal{R}_2)}} + \boldsymbol{\eta}_2^{(\mathcal{SD}_i)}, \quad (6.15)$$

where $\mathbf{H}_{\mathcal{R}_j\mathcal{SD}_i}$, $j = 1, 2$, is the $M \times M$ circulant channel matrix and $\boldsymbol{\eta}_k^{(\mathcal{SD}_i)}$, $k = 1, 2$, is a white Gaussian noise vector at $\mathcal{SD}_i$ with each entry having zero-mean and variance of $N_0/2$ per dimension.

Substituting (6.2) and (6.3) into (6.12), (6.13), (6.14) and (6.15), the received signals at $\mathcal{PD}$ and $\mathcal{SD}_i$, $i = 1, 2, \ldots, N$, can be obtained as

$$\begin{aligned}\mathbf{r}_1^{(\mathcal{PD})} &= \sqrt{\frac{\xi_{\mathcal{PSR}_1}\xi_{\mathcal{R}_1\mathcal{PD}}}{\xi_{\mathcal{PSR}_1} + N_0}}\mathbf{H}_{\mathcal{R}_1\mathcal{PD}}\mathbf{H}_{\mathcal{PSR}_1}\mathbf{x}_{p,1} \\ &\quad - \sqrt{\frac{\xi_{\mathcal{PSR}_2}\xi_{\mathcal{R}_2\mathcal{PD}}}{\xi_{\mathcal{PSR}_2} + N_0}}\mathbf{H}_{\mathcal{R}_2\mathcal{PD}}\mathbf{P}_M^{(G)}\mathbf{H}_{\mathcal{PSR}_2}^*\mathbf{x}_{p,2}^* + \boldsymbol{\eta}_1^{'(\mathcal{PD})},\end{aligned} \quad (6.16)$$

$$\begin{aligned}\mathbf{r}_2^{(\mathcal{PD})} &= \sqrt{\frac{\xi_{\mathcal{PSR}_1}\xi_{\mathcal{R}_1\mathcal{PD}}}{\xi_{\mathcal{PSR}_1} + N_0}}\mathbf{H}_{\mathcal{R}_1\mathcal{PD}}\mathbf{H}_{\mathcal{PSR}_1}\mathbf{x}_{p,2} \\ &\quad + \sqrt{\frac{\xi_{\mathcal{PSR}_2}\xi_{\mathcal{R}_2\mathcal{PD}}}{\xi_{\mathcal{PSR}_2} + N_0}}\mathbf{H}_{\mathcal{R}_2\mathcal{PD}}\mathbf{P}_M^{(G)}\mathbf{H}_{\mathcal{PSR}_2}^*\mathbf{x}_{p,1}^* + \boldsymbol{\eta}_2^{'(\mathcal{PD})},\end{aligned} \quad (6.17)$$

[30]The packets received and transmitted at $\mathcal{R}_1$ and $\mathcal{R}_2$ are assumed to be perfectly synchronised and scheduled.

$$\begin{aligned}\mathbf{r}_1^{(\mathcal{SD}_i)} &= \sqrt{\frac{\xi_{\mathcal{SS}_i\mathcal{R}_1}\xi_{\mathcal{R}_1\mathcal{SD}_i}}{\xi_{\mathcal{SS}_i\mathcal{R}_1}+N_0}}\mathbf{H}_{\mathcal{R}_1\mathcal{SD}_i}\mathbf{H}_{\mathcal{SS}_i\mathcal{R}_1}\mathbf{x}_{s_i,1} \\ &\quad - \sqrt{\frac{\xi_{\mathcal{SS}_i\mathcal{R}_2}\xi_{\mathcal{R}_2\mathcal{SD}_i}}{\xi_{\mathcal{SS}_i\mathcal{R}_2}+N_0}}\mathbf{H}_{\mathcal{R}_2\mathcal{SD}_i}\mathbf{P}_M^{(G)}\mathbf{H}^*_{\mathcal{SS}_i\mathcal{R}_2}\mathbf{x}^*_{s_i,2}+\boldsymbol{\eta}_1^{'(\mathcal{SD}_i)},\end{aligned} \tag{6.18}$$

$$\begin{aligned}\mathbf{r}_2^{(\mathcal{SD}_i)} &= \sqrt{\frac{\xi_{\mathcal{SS}_i\mathcal{R}_1}\xi_{\mathcal{R}_1\mathcal{SD}_i}}{\xi_{\mathcal{SS}_i\mathcal{R}_1}+N_0}}\mathbf{H}_{\mathcal{R}_1\mathcal{SD}_i}\mathbf{H}_{\mathcal{SS}_i\mathcal{R}_1}\mathbf{x}_{s_i,2} \\ &\quad + \sqrt{\frac{\xi_{\mathcal{SS}_i\mathcal{R}_2}\xi_{\mathcal{R}_2\mathcal{SD}_i}}{\xi_{\mathcal{SS}_i\mathcal{R}_2}+N_0}}\mathbf{H}_{\mathcal{R}_2\mathcal{SD}_i}\mathbf{P}_M^{(G)}\mathbf{H}^*_{\mathcal{SS}_i\mathcal{R}_2}\mathbf{x}^*_{s_i,1}+\boldsymbol{\eta}_2^{'(\mathcal{SD}_i)},\end{aligned} \tag{6.19}$$

where $\boldsymbol{\eta}_k^{'(\mathcal{PD})}$ and $\boldsymbol{\eta}_k^{'(\mathcal{SD}_i)}$, $k=1,2$, $i=1,2,\ldots,N$, are effective noise terms including the Gaussian noises at relays and destination, which are defined as

$$\boldsymbol{\eta}_k^{'(\mathcal{PD})}=\sqrt{\frac{\xi_{\mathcal{R}_1\mathcal{PD}}}{\xi_{\mathcal{PSR}_1}+N_0}}\mathbf{H}_{\mathcal{R}_1\mathcal{PD}}\boldsymbol{\eta}_{p,k}^{(\mathcal{R}_1)}+(-1)^k\sqrt{\frac{\xi_{\mathcal{R}_2\mathcal{PD}}}{\xi_{\mathcal{PSR}_2}+N_0}}\mathbf{H}_{\mathcal{R}_2\mathcal{PD}}\boldsymbol{\eta}_{p,k}^{(\mathcal{R}_2)}+\boldsymbol{\eta}_k^{(\mathcal{PD})}, \tag{6.20}$$

$$\boldsymbol{\eta}_k^{'(\mathcal{SD}_i)}=\sqrt{\frac{\xi_{\mathcal{R}_1\mathcal{SD}_i}}{\xi_{\mathcal{SS}_i\mathcal{R}_1}+N_0}}\mathbf{H}_{\mathcal{R}_1\mathcal{SD}_i}\boldsymbol{\eta}_{s_i,k}^{(\mathcal{R}_1)}+(-1)^k\sqrt{\frac{\xi_{\mathcal{R}_2\mathcal{SD}_i}}{\xi_{\mathcal{SS}_i\mathcal{R}_2}+N_0}}\mathbf{H}_{\mathcal{R}_2\mathcal{SD}_i}\boldsymbol{\eta}_{s_i,k}^{(\mathcal{R}_2)}+\boldsymbol{\eta}_k^{(\mathcal{SD}_i)}. \tag{6.21}$$

It can be seen that the received signals at the destination nodes given by (6.16), (6.17), (6.18) and (6.19) consist of both data blocks, which therefore causes interference between them. It should be expected to detect each data block separately for the best performance, i.e. the detection of different data blocks should be decoupled. In the following subsection, the proposed method is presented to detect independently the two data blocks at the destination nodes in both time and frequency domains.

6.3.2 Decoupling in Time and Frequency Domain

For the sake of a fair comparison with other systems, the noise variances of the received signals at $\mathcal{PD}$ and $\mathcal{SD}_i$, $i=1,2,\ldots,N$, to be N_0 are firstly normalised prior to proceeding the data detection. From (6.20) and (6.21), each n-th entry of the effective noise terms $\boldsymbol{\eta}_k^{'(\mathcal{PD})}$ and $\boldsymbol{\eta}_k^{'(\mathcal{SD}_i)}$ at $\mathcal{PD}$ and $\mathcal{SD}_i$, $i=1,2,\ldots,N$

has zero mean and variance of

$$E\left(\left|\left[\boldsymbol{\eta}_k^{'(\mathcal{PD})}\right]_n\right|^2\right) = N_0\left(\frac{\xi_{\mathcal{R}_1\mathcal{PD}}}{\xi_{\mathcal{PSR}_1}+N_0}\sum_{l=1}^{L_{\mathcal{R}_1\mathcal{PD}}}\left|[\mathbf{h}_{\mathcal{R}_1\mathcal{PD}}]_l\right|^2 + \frac{\xi_{\mathcal{R}_2\mathcal{PD}}}{\xi_{\mathcal{PSR}_2}+N_0}\sum_{l=1}^{L_{\mathcal{R}_2\mathcal{PD}}}\left|[\mathbf{h}_{\mathcal{R}_2\mathcal{PD}}]_l\right|^2+1\right), \tag{6.22}$$

$$E\left(\left|\left[\boldsymbol{\eta}_k^{'(\mathcal{SD}_i)}\right]_n\right|^2\right) = N_0\left(\frac{\xi_{\mathcal{R}_1\mathcal{SD}_i}}{\xi_{\mathcal{SS}_i\mathcal{R}_1}+N_0}\sum_{l=1}^{L_{\mathcal{R}_1\mathcal{SD}_i}}\left|[\mathbf{h}_{\mathcal{R}_1\mathcal{SD}_i}]_l\right|^2 + \frac{\xi_{\mathcal{R}_2\mathcal{SD}_i}}{\xi_{\mathcal{SS}_i\mathcal{R}_2}+N_0}\sum_{l=1}^{L_{\mathcal{R}_2\mathcal{SD}_i}}\left|[\mathbf{h}_{\mathcal{R}_2\mathcal{SD}_i}]_l\right|^2+1\right). \tag{6.23}$$

Thus, the received signals at $\mathcal{PD}$ and $\mathcal{SD}_i$ are normalised by factors

$$\alpha^{(\mathcal{PD})}=\sqrt{\frac{\xi_{\mathcal{R}_1\mathcal{PD}}}{\xi_{\mathcal{PSR}_1}+N_0}\sum_{l=1}^{L_{\mathcal{R}_1\mathcal{PD}}}\left|[\mathbf{h}_{\mathcal{R}_1\mathcal{PD}}]_l\right|^2+\frac{\xi_{\mathcal{R}_2\mathcal{PD}}}{\xi_{\mathcal{PSR}_2}+N_0}\sum_{l=1}^{L_{\mathcal{R}_2\mathcal{PD}}}\left|[\mathbf{h}_{\mathcal{R}_2\mathcal{PD}}]_l\right|^2+1}, \tag{6.24}$$

$$\alpha^{(\mathcal{SD}_i)}=\sqrt{\frac{\xi_{\mathcal{R}_1\mathcal{SD}_i}}{\xi_{\mathcal{SS}_i\mathcal{R}_1}+N_0}\sum_{l=1}^{L_{\mathcal{R}_1\mathcal{SD}_i}}\left|[\mathbf{h}_{\mathcal{R}_1\mathcal{SD}_i}]_l\right|^2+\frac{\xi_{\mathcal{R}_2\mathcal{SD}_i}}{\xi_{\mathcal{SS}_i\mathcal{R}_2}+N_0}\sum_{l=1}^{L_{\mathcal{R}_2\mathcal{SD}_i}}\left|[\mathbf{h}_{\mathcal{R}_2\mathcal{SD}_i}]_l\right|^2+1}, \tag{6.25}$$

respectively. Accordingly, the normalised signals at $\mathcal{PD}$ and $\mathcal{SD}_i$ can be written as

$$\mathbf{r}_1^{'(\mathcal{PD})}=\frac{\mathbf{r}_1^{(\mathcal{PD})}}{\alpha^{(\mathcal{PD})}}=\alpha_{p,1}\mathbf{H}_{\mathcal{R}_1\mathcal{PD}}\mathbf{H}_{\mathcal{PSR}_1}\mathbf{x}_{p,1}-\alpha_{p,2}\mathbf{H}_{\mathcal{R}_2\mathcal{PD}}\mathbf{P}_M^{(G)}\mathbf{H}^*_{\mathcal{PSR}_2}\mathbf{x}^*_{p,2}+\boldsymbol{\eta}_1^{''(\mathcal{PD})}, \tag{6.26}$$

$$\mathbf{r}_2^{'(\mathcal{PD})}=\frac{\mathbf{r}_2^{(\mathcal{PD})}}{\alpha^{(\mathcal{PD})}}=\alpha_{p,1}\mathbf{H}_{\mathcal{R}_1\mathcal{PD}}\mathbf{H}_{\mathcal{PSR}_1}\mathbf{x}_{p,2}+\alpha_{p,2}\mathbf{H}_{\mathcal{R}_2\mathcal{PD}}\mathbf{P}_M^{(G)}\mathbf{H}^*_{\mathcal{PSR}_2}\mathbf{x}^*_{p,1}+\boldsymbol{\eta}_2^{''(\mathcal{PD})}, \tag{6.27}$$

$$\mathbf{r}_1^{'(\mathcal{SD}_i)}=\frac{\mathbf{r}_1^{(\mathcal{SD}_i)}}{\alpha^{(\mathcal{SD}_i)}}=\alpha_{s_i,1}\mathbf{H}_{\mathcal{R}_1\mathcal{SD}_i}\mathbf{H}_{\mathcal{SS}_i\mathcal{R}_1}\mathbf{x}_{s_i,1}-\alpha_{s_i,2}\mathbf{H}_{\mathcal{R}_2\mathcal{SD}_i}\mathbf{P}_M^{(G)}\mathbf{H}^*_{\mathcal{SS}_i\mathcal{R}_2}\mathbf{x}^*_{s_i,2}+\boldsymbol{\eta}_1^{''(\mathcal{SD}_i)}, \tag{6.28}$$

$$\mathbf{r}_2^{'(\mathcal{SD}_i)}=\frac{\mathbf{r}_2^{(\mathcal{SD}_i)}}{\alpha^{(\mathcal{SD}_i)}}=\alpha_{s_i,1}\mathbf{H}_{\mathcal{R}_1\mathcal{SD}_i}\mathbf{H}_{\mathcal{SS}_i\mathcal{R}_1}\mathbf{x}_{s_i,2}+\alpha_{s_i,2}\mathbf{H}_{\mathcal{R}_2\mathcal{SD}_i}\mathbf{P}_M^{(G)}\mathbf{H}^*_{\mathcal{SS}_i\mathcal{R}_2}\mathbf{x}^*_{s_i,1}+\boldsymbol{\eta}_2^{''(\mathcal{SD}_i)}, \tag{6.29}$$

where $\boldsymbol{\eta}_k^{''(\mathcal{PD})}$ and $\boldsymbol{\eta}_k^{''(\mathcal{SD}_i)}$, $k=1,2$, are normalised complex Gaussian noise vectors in which each entry has zero mean and variance of $N_0/2$ per dimension. Here, $\alpha_{p,j}$ and $\alpha_{s_i,j}$, $j=1,2$, $i=1,2,\ldots,N$, are defined as

$$\alpha_{p,j}=\sqrt{\frac{\alpha'_{p,n\neq j}\alpha''_{p,j}\xi_{\mathcal{PSR}_j}}{\alpha'_{p,1}\alpha'_{p,2}+\alpha'_{p,2}\alpha''_{p,1}\sum_{l=1}^{L_{\mathcal{R}_1\mathcal{PD}}}\left|[\mathbf{h}_{\mathcal{R}_1\mathcal{PD}}]_l\right|^2+\alpha'_{p,1}\alpha''_{p,2}\sum_{l=1}^{L_{\mathcal{R}_2\mathcal{PD}}}\left|[\mathbf{h}_{\mathcal{R}_2\mathcal{PD}}]_l\right|^2}}, \tag{6.30}$$

$$\alpha_{s_i,j}=\sqrt{\frac{\alpha'_{s_i,n\neq j}\alpha''_{s_i,j}\xi_{\mathcal{SS}_i\mathcal{R}_j}}{\alpha'_{s_i,1}\alpha'_{s_i,2}+\alpha'_{s_i,2}\alpha''_{s_i,1}\sum\limits_{l=1}^{L_{\mathcal{R}_1\mathcal{SD}_i}}\left|[\mathbf{h}_{\mathcal{R}_1\mathcal{SD}_i}]_l\right|^2+\alpha'_{s_i,1}\alpha''_{s_i,2}\sum\limits_{l=1}^{L_{\mathcal{R}_2\mathcal{SD}_i}}\left|[\mathbf{h}_{\mathcal{R}_2\mathcal{SD}_i}]_l\right|^2}}, \quad (6.31)$$

where $n\in\{1,2\}$, $\alpha'_{p,j}=1+\xi_{\mathcal{PSR}_j}/N_0$, $\alpha''_{p,j}=\xi_{\mathcal{R}_j\mathcal{PD}}/N_0$, $\alpha'_{s_i,j}=1+\xi_{\mathcal{SS}_i\mathcal{R}_j}/N_0$ and $\alpha''_{s_i,j}=\xi_{\mathcal{R}_j\mathcal{SD}_i}/N_0$.

For the data decoupling process, both sides of (6.27) and (6.29) are conjugated and then multiplied with $\mathbf{P}_M^{(G)}$. Based on the fact that $\mathbf{P}_M^{(G)}\mathbf{H}^*_{\mathcal{AB}}\mathbf{P}_M^{(G)}=\mathbf{H}^{\mathcal{H}}_{\mathcal{AB}}$ for any $M\times M$ circulant matrix $\mathbf{H}_{\mathcal{AB}}$ [75], the resulting signals are obtained as

$$\mathbf{r}_2^{''(\mathcal{PD})}=\alpha_{p,2}\mathbf{H}^{\mathcal{H}}_{\mathcal{R}_2\mathcal{PD}}\mathbf{H}_{\mathcal{PSR}_2}\mathbf{x}_{p,1}+\alpha_{p,1}\mathbf{H}^{\mathcal{H}}_{\mathcal{R}_1\mathcal{PD}}\mathbf{H}^{\mathcal{H}}_{\mathcal{PSR}_1}\mathbf{P}_M^{(G)}\mathbf{x}^*_{p,2}+\mathbf{P}_M^{(G)}[\boldsymbol{\eta}_2^{''(\mathcal{PD})}]^*, \quad (6.32)$$

$$\mathbf{r}_2^{''(\mathcal{SD}_i)}=\alpha_{s_i,2}\mathbf{H}^{\mathcal{H}}_{\mathcal{R}_2\mathcal{SD}_i}\mathbf{H}_{\mathcal{SS}_i\mathcal{R}_2}\mathbf{x}_{s_i,1}+\alpha_{s_i,1}\mathbf{H}^{\mathcal{H}}_{\mathcal{R}_1\mathcal{SD}_i}\mathbf{H}^{\mathcal{H}}_{\mathcal{SS}_i\mathcal{R}_1}\mathbf{P}_M^{(G)}\mathbf{x}^*_{s_i,2}+\mathbf{P}_M^{(G)}[\boldsymbol{\eta}_2^{''(\mathcal{SD}_i)}]^*. \quad (6.33)$$

From (6.26), (6.28), (6.32) and (6.33), the equations can be grouped in vector-matrix forms as

$$\mathbf{R}^{(\mathcal{PD})}=\begin{bmatrix}\mathbf{r}_1^{'(\mathcal{PD})}\\ \mathbf{r}_2^{''(\mathcal{PD})}\end{bmatrix}=\mathbf{H}_p\begin{bmatrix}\mathbf{x}_{p,1}\\ \mathbf{P}_M^{(G)}\mathbf{x}^*_{p,2}\end{bmatrix}+\begin{bmatrix}\boldsymbol{\eta}_1^{''(\mathcal{PD})}\\ \mathbf{P}_M^{(G)}[\boldsymbol{\eta}_2^{''(\mathcal{PD})}]^*\end{bmatrix}, \quad (6.34)$$

$$\mathbf{R}^{(\mathcal{SD}_i)}=\begin{bmatrix}\mathbf{r}_1^{'(\mathcal{SD}_i)}\\ \mathbf{r}_2^{''(\mathcal{SD}_i)}\end{bmatrix}=\mathbf{H}_{s_i}\begin{bmatrix}\mathbf{x}_{s_i,1}\\ \mathbf{P}_M^{(G)}\mathbf{x}^*_{s_i,2}\end{bmatrix}+\begin{bmatrix}\boldsymbol{\eta}_1^{''(\mathcal{SD}_i)}\\ \mathbf{P}_M^{(G)}[\boldsymbol{\eta}_2^{''(\mathcal{SD}_i)}]^*\end{bmatrix}, \quad (6.35)$$

where

$$\mathbf{H}_p\triangleq\begin{bmatrix}\alpha_{p,1}\mathbf{H}_{\mathcal{R}_1\mathcal{PD}}\mathbf{H}_{\mathcal{PSR}_1} & -\alpha_{p,2}\mathbf{H}_{\mathcal{R}_2\mathcal{PD}}\mathbf{H}^{\mathcal{H}}_{\mathcal{PSR}_2}\\ \alpha_{p,2}\mathbf{H}^{\mathcal{H}}_{\mathcal{R}_2\mathcal{PD}}\mathbf{H}_{\mathcal{PSR}_2} & \alpha_{p,1}\mathbf{H}^{\mathcal{H}}_{\mathcal{R}_1\mathcal{PD}}\mathbf{H}^{\mathcal{H}}_{\mathcal{PSR}_1}\end{bmatrix}, \quad (6.36)$$

$$\mathbf{H}_{s_i}\triangleq\begin{bmatrix}\alpha_{s_i,1}\mathbf{H}_{\mathcal{R}_1\mathcal{SD}_i}\mathbf{H}_{\mathcal{SS}_i\mathcal{R}_1} & -\alpha_{s_i,2}\mathbf{H}_{\mathcal{R}_2\mathcal{SD}_i}\mathbf{H}^{\mathcal{H}}_{\mathcal{SS}_i\mathcal{R}_2}\\ \alpha_{s_i,2}\mathbf{H}^{\mathcal{H}}_{\mathcal{R}_2\mathcal{SD}_i}\mathbf{H}_{\mathcal{SS}_i\mathcal{R}_2} & \alpha_{s_i,1}\mathbf{H}^{\mathcal{H}}_{\mathcal{R}_1\mathcal{SD}_i}\mathbf{H}^{\mathcal{H}}_{\mathcal{SS}_i\mathcal{R}_1}\end{bmatrix}. \quad (6.37)$$

Denote $\boldsymbol{\Omega}_p=[\alpha^2_{p,1}<\mathbf{H}_{\mathcal{PSR}_1}>^2<\mathbf{H}_{\mathcal{R}_1\mathcal{PD}}>^2+\alpha^2_{p,2}<\mathbf{H}_{\mathcal{PSR}_2}>^2<\mathbf{H}_{\mathcal{R}_2\mathcal{PD}}>^2]^{\frac{1}{2}}$ and $\boldsymbol{\Omega}_{s_i}=[\alpha^2_{s_i,1}<\mathbf{H}_{\mathcal{SS}_i\mathcal{R}_1}>^2<\mathbf{H}_{\mathcal{R}_1\mathcal{SD}_i}>^2+\alpha^2_{s_i,2}<\mathbf{H}_{\mathcal{SS}_i\mathcal{R}_2}>^2<\mathbf{H}_{\mathcal{R}_2\mathcal{SD}_i}>^2]^{\frac{1}{2}}$. Then, $\mathbf{H}^{\mathcal{H}}_p\mathbf{H}_p=\mathbf{I}_2\otimes\boldsymbol{\Omega}^2_p$ and $\mathbf{H}^{\mathcal{H}}_{s_i}\mathbf{H}_{s_i}=\mathbf{I}_2\otimes\boldsymbol{\Omega}^2_{s_i}$, which are block-diagonal matrices. Thus, the detection of two data blocks can be decoupled independently by multiplying both sides of (6.34) and (6.35) with the unitary matrices ($\mathbf{I}_2\otimes$

$\mathbf{\Omega}_p^{-1})\mathbf{H}_p^{\mathcal{H}}$ and $(\mathbf{I}_2 \otimes \mathbf{\Omega}_{s_i}^{-1})\mathbf{H}_{s_i}^{\mathcal{H}}$, respectively, as

$$\mathbf{Y}^{(\mathcal{PD})} = \begin{bmatrix} \mathbf{y}_1^{(\mathcal{PD})} \\ \mathbf{y}_2^{(\mathcal{PD})} \end{bmatrix} = (\mathbf{I}_2 \otimes \mathbf{\Omega}_p^{-1})\mathbf{H}_p^{\mathcal{H}}\mathbf{R}^{(\mathcal{PD})} = \begin{bmatrix} \mathbf{\Omega}_p \mathbf{x}_{p,1} \\ \mathbf{\Omega}_p \mathbf{P}_M^{(G)} \mathbf{x}_{p,2}^* \end{bmatrix} + \begin{bmatrix} \bar{\boldsymbol{\eta}}_1^{(\mathcal{PD})} \\ \bar{\boldsymbol{\eta}}_2^{(\mathcal{PD})} \end{bmatrix}, \quad (6.38)$$

$$\mathbf{Y}^{(\mathcal{SD}_i)} = \begin{bmatrix} \mathbf{y}_1^{(\mathcal{SD}_i)} \\ \mathbf{y}_2^{(\mathcal{SD}_i)} \end{bmatrix} = (\mathbf{I}_2 \otimes \mathbf{\Omega}_{s_i}^{-1})\mathbf{H}_{s_i}^{\mathcal{H}}\mathbf{R}^{(\mathcal{SD}_i)} = \begin{bmatrix} \mathbf{\Omega}_{s_i} \mathbf{x}_{s_i,1} \\ \mathbf{\Omega}_{s_i} \mathbf{P}_M^{(G)} \mathbf{x}_{s_i,2}^* \end{bmatrix} + \begin{bmatrix} \bar{\boldsymbol{\eta}}_1^{(\mathcal{SD}_i)} \\ \bar{\boldsymbol{\eta}}_2^{(\mathcal{SD}_i)} \end{bmatrix}, \quad (6.39)$$

where $\bar{\boldsymbol{\eta}}_k^{(\mathcal{PD})}$ and $\bar{\boldsymbol{\eta}}_k^{(\mathcal{SD}_i)}$, $k = 1, 2$, are the Gaussian noise vectors resulting from the decoupling process with each entry having zero mean and variance of $N_0/2$ per dimension.

Remark 6.2 (*Decoupling Capability of Data Blocks*). *From* (6.38) *and* (6.39), *two data blocks transmitted from* $\mathcal{PS}$ *and* $\mathcal{SS}_i$, $i = 1, 2, \ldots, N$, *can be detected independently at* $\mathcal{PD}$ *and* $\mathcal{SD}_i$, *respectively by using general ML detection in the time domain for the best performance. However, general ML detection requires high computational complexity at the destination nodes depending exponentially on the channel memory lengths of all links from the sources to the destinations. Therefore, this chapter introduces a low-complexity decoupling of data blocks at the destination nodes using frequency-domain equalisation.*

It is noted that the circulant matrix $\mathbf{H}_{\mathcal{AB}}$ of size $M \times M$ can be diagonalised as $\mathbf{H}_{\mathcal{AB}} = \mathbf{F}_M^{\mathcal{H}} \mathbf{\Lambda}_{\mathcal{AB}} \mathbf{F}_M$ where $\mathbf{\Lambda}_{\mathcal{AB}}$ is an $M \times M$ diagonal matrix with diagonal entries created by the M-point DFT of the first column of $\mathbf{H}_{\mathcal{AB}}$. Thus, (6.34) and (6.35) can be transformed into the frequency domain by taking the DFT of both sides of the equations, which results in

$$\mathbf{R}_f^{(\mathcal{PD})} = \begin{bmatrix} \mathbf{r}_{f,1}^{(\mathcal{PD})} \\ \mathbf{r}_{f,2}^{(\mathcal{PD})} \end{bmatrix} = \begin{bmatrix} \mathbf{F}_M \mathbf{r}_1^{\prime(\mathcal{PD})} \\ \mathbf{F}_M \mathbf{r}_2^{\prime\prime(\mathcal{PD})} \end{bmatrix} = \mathbf{\Lambda}_p \begin{bmatrix} \mathbf{F}_M \mathbf{x}_{p,1} \\ \mathbf{F}_M \mathbf{P}_M^{(G)} \mathbf{x}_{p,2}^* \end{bmatrix} + \begin{bmatrix} \mathbf{F}_M \boldsymbol{\eta}_1^{\prime\prime(\mathcal{PD})} \\ \mathbf{F}_M \mathbf{P}_M^{(G)} [\boldsymbol{\eta}_2^{\prime\prime(\mathcal{PD})}]^* \end{bmatrix}, \quad (6.40)$$

$$\mathbf{R}_f^{(\mathcal{SD}_i)} = \begin{bmatrix} \mathbf{r}_{f,1}^{(\mathcal{SD}_i)} \\ \mathbf{r}_{f,2}^{(\mathcal{SD}_i)} \end{bmatrix} = \begin{bmatrix} \mathbf{F}_M \mathbf{r}_1^{\prime\mathcal{SD}_i)} \\ \mathbf{F}_M \mathbf{r}_2^{\prime\prime\mathcal{SD}_i)} \end{bmatrix} = \mathbf{\Lambda}_{s_i} \begin{bmatrix} \mathbf{F}_M \mathbf{x}_{s_i,1} \\ \mathbf{F}_M \mathbf{P}_M^{(G)} \mathbf{x}_{s_i,2}^* \end{bmatrix} + \begin{bmatrix} \mathbf{F}_M \boldsymbol{\eta}_1^{\prime\prime(\mathcal{SD}_i)} \\ \mathbf{F}_M \mathbf{P}_M^{(G)} [\boldsymbol{\eta}_2^{\prime\prime(\mathcal{SD}_i)}]^* \end{bmatrix}, \quad (6.41)$$

where

$$\mathbf{\Lambda}_p \triangleq \begin{bmatrix} \alpha_{p,1} \mathbf{\Lambda}_{\mathcal{R}_1 \mathcal{PD}} \mathbf{\Lambda}_{\mathcal{PSR}_1} & -\alpha_{p,2} \mathbf{\Lambda}_{\mathcal{R}_2 \mathcal{PD}} \mathbf{\Lambda}_{\mathcal{PSR}_2}^* \\ \alpha_{p,2} \mathbf{\Lambda}_{\mathcal{R}_2 \mathcal{PD}}^* \mathbf{\Lambda}_{\mathcal{PSR}_2} & \alpha_{p,1} \mathbf{\Lambda}_{\mathcal{R}_1 \mathcal{PD}}^* \mathbf{\Lambda}_{\mathcal{PSR}_1}^* \end{bmatrix}. \quad (6.42)$$

$$\mathbf{\Lambda}_{s_i} \triangleq \begin{bmatrix} \alpha_{s_i,1}\mathbf{\Lambda}_{\mathcal{R}_1\mathcal{SD}_i}\mathbf{\Lambda}_{\mathcal{SS}_i\mathcal{R}_1} & -\alpha_{s_i,2}\mathbf{\Lambda}_{\mathcal{R}_2\mathcal{SD}_i}\mathbf{\Lambda}^*_{\mathcal{SS}_i\mathcal{R}_2} \\ \alpha_{s_i,2}\mathbf{\Lambda}^*_{\mathcal{R}_2\mathcal{SD}_i}\mathbf{\Lambda}_{\mathcal{SS}_i\mathcal{R}_2} & \alpha_{s_i,1}\mathbf{\Lambda}^*_{\mathcal{R}_1\mathcal{SD}_i}\mathbf{\Lambda}^*_{\mathcal{SS}_i\mathcal{R}_1} \end{bmatrix}. \tag{6.43}$$

Denote $\mathbf{\Psi}_p = [\alpha^2_{p,1}<\mathbf{\Lambda}_{\mathcal{PSR}_1}>^2<\mathbf{\Lambda}_{\mathcal{R}_1\mathcal{PD}}>^2 + \alpha^2_{p,2}<\mathbf{\Lambda}_{\mathcal{PSR}_2}>^2<\mathbf{\Lambda}_{\mathcal{R}_2\mathcal{PD}}>^2]^{\frac{1}{2}}$ and $\mathbf{\Psi}_{s_i} = [\alpha^2_{s_i,1}<\mathbf{\Lambda}_{\mathcal{SS}_i\mathcal{R}_1}>^2<\mathbf{\Lambda}_{\mathcal{R}_1\mathcal{SD}_i}>^2 + \alpha^2_{s_i,2}<\mathbf{\Lambda}_{\mathcal{SS}_i\mathcal{R}_2}>^2<\mathbf{\Lambda}_{\mathcal{R}_2\mathcal{SD}_i}>^2]^{\frac{1}{2}}$. It is observed that $\mathbf{\Lambda}^{\mathcal{H}}_p\mathbf{\Lambda}_p = \mathbf{I}_2 \otimes \mathbf{\Psi}^2_p$ and $\mathbf{\Lambda}^{\mathcal{H}}_{s_i}\mathbf{\Lambda}_{s_i} = \mathbf{I}_2 \otimes \mathbf{\Psi}^2_{s_i}$, which are block-diagonal matrices. Thus, by multiplying both sides of (6.40) and (6.41) with the unitary matrix $(\mathbf{I}_2 \otimes \mathbf{\Psi}^{-1}_p)\mathbf{\Lambda}^{\mathcal{H}}_p$ and $(\mathbf{I}_2 \otimes \mathbf{\Psi}^{-1}_{s_i})\mathbf{\Lambda}^{\mathcal{H}}_{s_i}$, respectively, the detection of each data block at $\mathcal{PD}$ and $\mathcal{SD}_i$, $i = 1, 2, \ldots, N$, can be decoupled in the frequency domain as follows:

$$\mathbf{Y}^{(\mathcal{PD})}_f = \begin{bmatrix} \mathbf{y}^{(\mathcal{PD})}_{f,1} \\ \mathbf{y}^{(\mathcal{PD})}_{f,2} \end{bmatrix} = (\mathbf{I}_2 \otimes \mathbf{\Psi}^{-1}_p)\mathbf{\Lambda}^{\mathcal{H}}_p\mathbf{R}^{(\mathcal{PD})}_f = \begin{bmatrix} \mathbf{\Psi}_p\mathbf{F}_M\mathbf{x}_{p,1} \\ \mathbf{\Psi}_p\mathbf{F}_M\mathbf{P}^{(G)}_M\mathbf{x}^*_{p,2} \end{bmatrix} + \begin{bmatrix} \bar{\boldsymbol{\eta}}^{(\mathcal{PD})}_{f,1} \\ \bar{\boldsymbol{\eta}}^{(\mathcal{PD})}_{f,2} \end{bmatrix}, \tag{6.44}$$

$$\mathbf{Y}^{(\mathcal{SD}_i)}_f = \begin{bmatrix} \mathbf{y}^{(\mathcal{SD}_i)}_{f,1} \\ \mathbf{y}^{(\mathcal{SD}_i)}_{f,2} \end{bmatrix} = (\mathbf{I}_2 \otimes \mathbf{\Psi}^{-1}_{s_i})\mathbf{\Lambda}^{\mathcal{H}}_{s_i}\mathbf{R}^{(\mathcal{SD}_i)}_f = \begin{bmatrix} \mathbf{\Psi}_{s_i}\mathbf{F}_M\mathbf{x}_{s_i,1} \\ \mathbf{\Psi}_{s_i}\mathbf{F}_M\mathbf{P}^{(G)}_M\mathbf{x}^*_{s_i,2} \end{bmatrix} + \begin{bmatrix} \bar{\boldsymbol{\eta}}^{(\mathcal{SD}_i)}_{f,1} \\ \bar{\boldsymbol{\eta}}^{(\mathcal{SD}_i)}_{f,2} \end{bmatrix}, \tag{6.45}$$

where $\bar{\boldsymbol{\eta}}^{(\mathcal{PD})}_{f,k}$ and $\bar{\boldsymbol{\eta}}^{(\mathcal{SD}_i)}_{f,k}$, $k = 1, 2$, are the equivalent noise vectors for the k-block at $\mathcal{PD}$ and $\mathcal{SD}_i$, respectively, resulting from the decoupling process in the frequency domain. Since $\mathbf{\Psi}_p$ and $\mathbf{\Psi}_{s_i}$ are diagonal matrices, (6.44) and (6.45) can be decomposed into scalar equations as

$$\left[\mathbf{y}^{(\mathcal{PD})}_{f,1}\right]_n = [\mathbf{\Psi}_p]_{n,n}\left[\mathbf{F}_M\mathbf{x}_{p,1}\right]_n + \left[\bar{\boldsymbol{\eta}}^{(\mathcal{PD})}_{f,1}\right]_n, \tag{6.46}$$

$$\left[\mathbf{y}^{(\mathcal{PD})}_{f,2}\right]_n = [\mathbf{\Psi}_p]_{n,n}\left[\mathbf{F}_M\mathbf{P}^{(G)}_M\mathbf{x}^*_{p,2}\right]_n + \left[\bar{\boldsymbol{\eta}}^{(\mathcal{PD})}_{f,2}\right]_n, \tag{6.47}$$

$$\left[\mathbf{y}^{(\mathcal{SD}_i)}_{f,1}\right]_n = [\mathbf{\Psi}_{s_i}]_{n,n}\left[\mathbf{F}_M\mathbf{x}_{s_i,1}\right]_n + \left[\bar{\boldsymbol{\eta}}^{(\mathcal{SD}_i)}_{f,1}\right]_n, \tag{6.48}$$

$$\left[\mathbf{y}^{(\mathcal{SD}_i)}_{f,2}\right]_n = [\mathbf{\Psi}_{s_i}]_{n,n}\left[\mathbf{F}_M\mathbf{P}^{(G)}_M\mathbf{x}^*_{s_i,2}\right]_n + \left[\bar{\boldsymbol{\eta}}^{(\mathcal{SD}_i)}_{f,2}\right]_n, \tag{6.49}$$

where $n = 1, 2, \ldots, M$. Thus, each of $\left[\mathbf{F}_M\mathbf{x}_{p,1}\right]_n$, $\left[\mathbf{F}_M\mathbf{P}^{(G)}_M\ \mathbf{x}^*_{p,2}\right]_n$, $\left[\mathbf{F}_M\mathbf{x}_{s_i,1}\right]_n$ and $\left[\mathbf{F}_M\mathbf{P}^{(G)}_M\mathbf{x}^*_{s_i,2}\right]_n$ can be independently evaluated using linear equalisation, and then the evaluated outputs are transformed into the time domain to detect $[\mathbf{x}_{p,k}]_n$ and $[\mathbf{x}_{s_i,k}]_n$, $k = 1, 2$, accordingly.

6.4 Performance Analysis

This section derives the PEP expression of the proposed DSTFBC scheme for CWRNs over frequency selective fading channels. Three typical scenarios are taken into consideration, including:

(a) The relay nodes are near the source nodes, i.e. links from $\{\mathcal{PS}, \mathcal{SS}_1, \mathcal{SS}_2, \ldots, \mathcal{SS}_N\}$ to $\{\mathcal{R}_1, \mathcal{R}_2\}$ and from $\{\mathcal{R}_1, \mathcal{R}_2\}$ to $\{\mathcal{PD}, \mathcal{SD}_1, \mathcal{SD}_2, \ldots, \mathcal{SS}_N\}$ experience Rician fading and Rayleigh fading, respectively.

(b) The relays are near the destination nodes, i.e. links from $\{\mathcal{PS}, \mathcal{SS}_1, \mathcal{SS}_2, \ldots, \mathcal{SS}_N\}$ to $\{\mathcal{R}_1, \mathcal{R}_2\}$ and from $\{\mathcal{R}_1, \mathcal{R}_2\}$ to $\{\mathcal{PD}, \mathcal{SD}_1, \mathcal{SD}_2, \ldots, \mathcal{SS}_N\}$ experience Rayleigh fading and Rician fading, respectively.

(c) The relays are near the midpoint, i.e. links from $\{\mathcal{PS}, \mathcal{SS}_1, \mathcal{SS}_2, \ldots, \mathcal{SS}_N\}$ to $\{\mathcal{R}_1, \mathcal{R}_2\}$ and from $\{\mathcal{R}_1, \mathcal{R}_2\}$ to $\{\mathcal{PD}, \mathcal{SD}_1, \mathcal{SD}_2, \ldots, \mathcal{SD}_N\}$ experience Rician fading.

It can be seen that the PEP expression for scenario (b) can be simply obtained from scenario (a) with some interchanged parameters. Thus, it is sufficient to analyse the PEP for scenarios (a) and (c). Also, for the sake of brevity, only the primary transmission is investigated. The PEP analysis for the secondary transmission is straightforward.

Let $\hat{\mathbf{x}}_p$ denote the decoded codeword vector at $\mathcal{PD}$. The conditional PEP is calculated by

$$P(\mathbf{x}_p \to \hat{\mathbf{x}}_p | \mathbf{h}_{\mathcal{PSR}_1}, \mathbf{h}_{\mathcal{PSR}_2}, \mathbf{h}_{\mathcal{R}_1\mathcal{PD}}, \mathbf{h}_{\mathcal{R}_2\mathcal{PD}}) = Q\left(\sqrt{\frac{d^2(\mathbf{x}_p, \hat{\mathbf{x}}_p)}{2N_0}}\right), \tag{6.50}$$

where $Q(\cdot)$ is the Q function and $d(\mathbf{x}_p, \hat{\mathbf{x}}_p)$ is Euclidean distance between $\mathbf{x}_p$ and $\hat{\mathbf{x}}_p$. By applying the Chernoff bound to the Q function [176], the PEP in (6.50) can be upper bounded by

$$P(\mathbf{x}_p \to \hat{\mathbf{x}}_p | \mathbf{h}_{\mathcal{PSR}_1}, \mathbf{h}_{\mathcal{PSR}_2}, \mathbf{h}_{\mathcal{R}_1\mathcal{PD}}, \mathbf{h}_{\mathcal{R}_2\mathcal{PD}}) \leqslant \exp\left(-\frac{d^2(\mathbf{x}_p, \hat{\mathbf{x}}_p)}{4N_0}\right). \tag{6.51}$$

The Euclidean distance in (6.51) is calculated by

$$\begin{aligned} d^2(\mathbf{x}_p, \hat{\mathbf{x}}_p) = {} & \alpha_{p,1}^2 \|\mathbf{H}_{\mathcal{R}_1\mathcal{PD}} \mathbf{H}_{\mathcal{PSR}_1} (\mathbf{x}_{p,1} - \hat{\mathbf{x}}_{p,1})\|^2 \\ & + \alpha_{p,2}^2 \|\mathbf{H}_{\mathcal{R}_2\mathcal{PD}} \mathbf{H}_{\mathcal{PSR}_2} \mathbf{P}_M^{(G)} (\mathbf{x}_{p,2} - \hat{\mathbf{x}}_{p,2})\|^2. \end{aligned} \tag{6.52}$$

(6.52) can be approximated as one of four possible forms as [100]:

$$\begin{aligned} d^2(\mathbf{x}_p, \hat{\mathbf{x}}_p) \approx & \frac{\alpha_{p,1}^2}{M} ||\mathbf{H}_{\mathcal{R}_1\mathcal{PD}}||^2 ||\mathbf{H}_{\mathcal{PSR}_1}\mathbf{e}_1||^2 + \frac{\alpha_{p,2}^2}{M} ||\mathbf{H}_{\mathcal{R}_2\mathcal{PD}}||^2 ||\mathbf{H}_{\mathcal{PSR}_2}\mathbf{e}_2||^2 \\ \approx & \frac{\alpha_{p,1}^2}{M} ||\mathbf{H}_{\mathcal{PSR}_1}||^2 ||\mathbf{H}_{\mathcal{R}_1\mathcal{PD}}\mathbf{e}_1||^2 + \frac{\alpha_{p,2}^2}{M} ||\mathbf{H}_{\mathcal{R}_2\mathcal{PD}}||^2 ||\mathbf{H}_{\mathcal{PSR}_2}\mathbf{e}_2||^2 \\ \approx & \frac{\alpha_{p,1}^2}{M} ||\mathbf{H}_{\mathcal{R}_1\mathcal{PD}}||^2 ||\mathbf{H}_{\mathcal{PSR}_1}\mathbf{e}_1||^2 + \frac{\alpha_{p,2}^2}{M} ||\mathbf{H}_{\mathcal{PSR}_2}||^2 ||\mathbf{H}_{\mathcal{R}_2\mathcal{PD}}\mathbf{e}_2||^2 \\ \approx & \frac{\alpha_{p,1}^2}{M} ||\mathbf{H}_{\mathcal{PSR}_1}||^2 ||\mathbf{H}_{\mathcal{R}_1\mathcal{PD}}\mathbf{e}_1||^2 + \frac{\alpha_{p,2}^2}{M} ||\mathbf{H}_{\mathcal{PSR}_2}||^2 ||\mathbf{H}_{\mathcal{R}_2\mathcal{PD}}\mathbf{e}_2||^2, \end{aligned} \tag{6.53}$$

where $\mathbf{e}_k = \mathbf{x}_{p,k} - \hat{\mathbf{x}}_{p,k}$, $k = 1, 2$. Note that $||\mathbf{H}_{\mathcal{AB}}||^2 = M \sum_{l_{\mathcal{AB}}=1}^{L_{\mathcal{AB}}} |[\mathbf{h}_{\mathcal{AB}}]_{l_{\mathcal{AB}}}|^2$ and $||\mathbf{H}_{\mathcal{AB}}\mathbf{e}_k||^2 = \sum_{l_{\mathcal{AB}}=1}^{L_{\mathcal{AB}}} [\boldsymbol{\lambda}_k]_{l_{\mathcal{AB}}} |[\boldsymbol{\nu}_k]_{l_{\mathcal{AB}}}|^2$, $k = 1, 2$, $\mathcal{A}, \mathcal{B} \in \{\mathcal{PS}, \mathcal{R}_1, \mathcal{R}_2, \mathcal{PD}\}$. Here, $[\boldsymbol{\lambda}_k]_{l_{\mathcal{AB}}}$ denotes the eigenvalue of the codeword difference matrix and $\boldsymbol{\nu}_k$ is a zero-mean complex Gaussian vector with unit variance. In (6.53), each component of the summations of the right hand side can be expressed by either one of two following factors

$$d_1^2 = \sum_{l_{\mathcal{R}_k\mathcal{PD}}=1}^{L_{\mathcal{R}_k\mathcal{PD}}} |[\mathbf{h}_{\mathcal{R}_k\mathcal{PD}}]_{l_{\mathcal{R}_k\mathcal{PD}}}|^2 \sum_{l_{\mathcal{PSR}_k}=1}^{L_{\mathcal{PSR}_k}} [\boldsymbol{\lambda}]_{l_{\mathcal{PSR}_k}} |[\boldsymbol{\nu}]_{l_{\mathcal{PSR}_k}}|^2, \tag{6.54}$$

$$d_2^2 = \sum_{l_{\mathcal{PSR}_k}=1}^{L_{\mathcal{PSR}_k}} |[\mathbf{h}_{\mathcal{PSR}_k}]_{l_{\mathcal{PSR}_k}}|^2 \sum_{l_{\mathcal{R}_k\mathcal{PD}}=1}^{L_{\mathcal{R}_k\mathcal{PD}}} [\boldsymbol{\lambda}]_{l_{\mathcal{R}_k\mathcal{PD}}} |[\boldsymbol{\nu}]_{l_{\mathcal{R}_k\mathcal{PD}}}|^2. \tag{6.55}$$

For simplicity of mathematical formulation, denote $L_{\mathcal{PSR}_k} = L_1$, $L_{\mathcal{R}_k\mathcal{PD}} = L_2$, $\mathbf{h}_{\mathcal{PSR}_k} = \mathbf{h}_1$, $\mathbf{h}_{\mathcal{R}_k\mathcal{PD}} = \mathbf{h}_2$. In the following, the PEP will be analysed for the first and the third scenario of the fading channel models.

6.4.1 Scenario (a): $\mathcal{PS} \to \{\mathcal{R}_1, \mathcal{R}_2\}$: Rician fading, $\{\mathcal{R}_1, \mathcal{R}_2\} \to \mathcal{PD}$: Rayleigh fading

Due to different characteristics of fading channels, there are three cases based on the relationship between L_1 and L_2.

Case 1 ($L_1 < L_2$)

Eq. (6.54) is taken into consideration. Define $Z_1 = d_1^2 = X_1 Y_1$ where $X_1 = \sum_{l_2=1}^{L_2} |[\mathbf{h}_2]_{l_2}|^2$ and $Y_1 = \sum_{l_1=1}^{L_1} [\boldsymbol{\lambda}]_{l_1} |[\boldsymbol{\nu}]_{l_1}|^2$. Applying the Chernoff bound,

the PEP corresponding to d_1^2 is upper bounded by $E_{Z_1}[\exp(-\alpha^2 Z_1/4N_0)] = \Phi_{Z_1}(s)|_{s=-\alpha^2/4N_0}$. Here, α corresponds to α_k, $k=1,2$, if $\mathcal{R}_k$ is considered, and $\Phi_{Z_1}(s)$ can be evaluated as [175], i.e.

$$\Phi_{Z_1}(s) = \int_0^\infty f_{X_1}(x_1)\Phi_{Y_1}(sx_1)dx_1, \tag{6.56}$$

where

$$f_{X_1}(x_1) = \frac{{L_2}^{L_2}}{\Gamma(L_2)}\frac{x_1^{L_2-1}}{e^{L_2 x_1}}, \tag{6.57}$$

$$\Phi_{Y_1}(s) = \prod_{l_1=1}^{L_1}\frac{1+n^2}{1+n^2-s[\boldsymbol{\lambda}]_{l_1}}e^{\frac{n^2 s[\boldsymbol{\lambda}]_{l_1}}{1+n^2-s[\boldsymbol{\lambda}]_{l_1}}}, \tag{6.58}$$

where n is the Nakagami-n or Rician fading parameter and $\Gamma(\cdot)$ represents the Gamma function defined by $\Gamma(k) \triangleq (k-1)!$ for any positive integer k [134].

Substituting (6.57) and (6.58) into (6.56), $\Phi_{Z_1}(s)$ is obtained as

$$\begin{aligned}\Phi_{Z_1}(s)|_{s=-\frac{\alpha^2}{4N_0}} &= \int_0^\infty \frac{{L_2}^{L_2}}{\Gamma(L_2)}\frac{x_1^{L_2-1}}{e^{L_2x_1}}\prod_{l_1=1}^{L_1}\frac{1+n^2}{1+n^2+\frac{\alpha^2}{4N_0}x_1[\boldsymbol{\lambda}]_{l_1}}e^{\frac{-n^2\frac{\alpha^2}{4N_0}x_1[\boldsymbol{\lambda}]_{l_1}}{1+n^2+\frac{\alpha^2}{4N_0}x_1[\boldsymbol{\lambda}]_{l_1}}}dx_1 \\ &= \frac{{L_2}^{L_2}}{\Gamma(L_2)}\int_0^\infty \frac{x_1^{L_2-1}}{e^{L_2x_1}}\prod_{l_1=1}^{L_1}\frac{e^{\frac{-x_1}{\frac{1+n^2}{n^2}}}}{e^{\frac{x_1}{n^2}+\frac{\alpha^2}{4N_0}[\boldsymbol{\lambda}]_{l_1}}}}{\frac{\alpha^2}{4N_0}[\boldsymbol{\lambda}]_{l_1}\left(\frac{x_1}{1+n^2}+\frac{1}{\frac{\alpha^2}{4N_0}[\boldsymbol{\lambda}]_{l_1}}\right)}dx_1.\end{aligned} \tag{6.59}$$

Assuming high signal-to-noise ratio (SNR), i.e. $\alpha^2/4N_0 \gg 1$, and $(1+n^2)/n^2 \approx 1$, (6.59) can be approximated as

$$\Phi_{Z_1}(s)|_{s=-\frac{\alpha^2}{4N_0}} \approx \frac{L_2^{L_2}}{\Gamma(L_2)}\left(\frac{\alpha^2}{4N_0}\right)^{-L_1}\left(\frac{1+n^2}{e^{n^2}}\right)^{L_1}\prod_{l_1=1}^{L_1}\frac{1}{[\boldsymbol{\lambda}]_{l_1}}\int_0^\infty \frac{x_1^{L_2-L_1-1}}{e^{L_2x_1}}dx_1. \tag{6.60}$$

When $L_1 < L_2$, evaluating the integral in (6.60) [134], $\Phi_{Z_1}(s)$ is obtained as

$$\Phi_{Z_1}(s)|_{s=-\frac{\alpha^2}{4N_0}} \approx \left[\frac{L_2(1+n^2)}{e^{n^2}}\right]^{L_1}\frac{\Gamma(L_2-L_1)}{\Gamma(L_2)}\left(\frac{\alpha^2}{4N_0}\right)^{-L_1}\prod_{l_1=1}^{L_1}\frac{1}{[\boldsymbol{\lambda}]_{l_1}}. \tag{6.61}$$

Case 2 ($L_1 > L_2$)

Examine (6.55) and define $Z_2 = d_2^2 = X_2Y_2$ where $X_2 = \sum_{l_1=1}^{L_1}|[\mathbf{h}_1]_{l_1}|^2$ and $Y_2 = \sum_{l_2=1}^{L_2}[\boldsymbol{\lambda}]_{l_2}|[\boldsymbol{\nu}]_{l_2}|^2$. Similarly, applying the Chernoff bound, the PEP corresponding to d_2^2 is upper bounded by $E_{Z_2}[\exp(-\alpha^2 Z_2/4N_0)] = \Phi_{Z_2}(s)|_{s=-\alpha^2/4N_0}$

and $\Phi_{Z_2}(s)$ is computed by

$$\Phi_{Z_2}(s) = \int_0^\infty f_{X_2}(x_2)\, \Phi_{Y_2}(sx_2)\, dx_2, \tag{6.62}$$

where

$$f_{X_2}(x_2) = \frac{L_1^{\frac{3-L_1}{2}}}{n^{L_1-1}} \frac{x_2^{\frac{L_1-1}{2}} I_{L_1-1}[2L_1^{\frac{3}{2}} n x_2^{\frac{1}{2}}]}{e^{L_1^2 n^2 + L_1 x_2}}, \tag{6.63}$$

$$\Phi_{Y_2}(s) = \prod_{l_2=1}^{L_2} \frac{1}{1 - s[\boldsymbol{\lambda}]_{l_2}}. \tag{6.64}$$

Here, $I_\alpha(\beta)$ denotes the modified Bessel function of the first kind, which is defined as $I_\alpha(\beta) \triangleq \left(\frac{\beta}{2}\right)^\alpha \sum_{k=0}^{\infty} \frac{\beta^{2k}}{4^k k! \Gamma(\alpha+k+1)}$, $\alpha \in \mathbb{R}$ [134]. Substituting (6.63) and (6.64) into (6.62), $\Phi_{Z_2}(s)$ is obtained as

$$\Phi_{Z_2}(s)|_{s=-\frac{\alpha^2}{4N_0}} = \int_0^\infty \frac{L_1^{\frac{3-L_1}{2}} x_2^{\frac{L_1-1}{2}}}{n^{L_1-1} e^{L_1^2 n^2 + L_1 x_2}} I_{L_1-1}[2(L_1)^{\frac{3}{2}} n x_2^{\frac{1}{2}}] \prod_{l_2=1}^{L_2} \frac{1}{1 + \frac{\alpha^2}{4N_0} x_2 [\boldsymbol{\lambda}]_{l_2}} dx_2. \tag{6.65}$$

Under the assumption of high SNR (i.e. $\alpha^2/4N_0 \gg 1$), (6.65) can be approximated as

$$\Phi_{Z_2}(s)|_{s=-\frac{\alpha^2}{4N_0}} \approx \left(\frac{\alpha^2}{4N_0}\right)^{-L_2} \frac{L_1^{\frac{3-L_1}{2}}}{n^{L_1-1} e^{L_1^2 n^2}} \prod_{l_2=1}^{L_2} \frac{1}{[\boldsymbol{\lambda}]_{l_2}} \int_0^\infty \frac{x_2^{\frac{L_1-1}{2} - L_2} I_{L_1-1}[2L_1^{\frac{3}{2}} n x_2^{\frac{1}{2}}]}{e^{L_1 x_2}} dx_2. \tag{6.66}$$

Calculating the integral in (6.66) when $L_1 > L_2$, after some mathematical manipulations [134], $\Phi_{Z_2}(s)$ is obtained as

$$\Phi_{Z_2}(s)|_{s=-\frac{\alpha^2}{4N_0}} \approx \frac{L_1^{L_2} \Gamma(L_1 - L_2)}{e^{L_1^2 n^2}} {}_1\tilde{F}_1(L_1 - L_2; L_1; L_1^2 n^2) \left(\frac{\alpha^2}{4N_0}\right)^{-L_2} \prod_{l_2=1}^{L_2} \frac{1}{[\boldsymbol{\lambda}]_{l_2}}, \tag{6.67}$$

where ${}_1\tilde{F}_1(a; b; z)$ is regularized hypergeometric function defined as ${}_1\tilde{F}_1(a; b; z) \triangleq \frac{1}{\Gamma(a)} \sum_{k=0}^{\infty} \frac{\Gamma(a+k)}{\Gamma(b+k)} \frac{z^k}{k!}$ [134].

Case 3 ($L_1 = L_2$)

Considering (6.54), $\Phi_{Z_1}(s)$ can be calculated as:

$$\begin{aligned} \Phi_{Z_1}(s)|_{s=-\frac{\alpha^2}{4N_0}} &= \frac{L_1^{L_1}}{\Gamma(L_1) e^{L_1 n^2}} \left(\frac{\alpha^2}{4N_0}\right)^{-L_1} \prod_{l_1=1}^{L_1} \frac{1}{[\boldsymbol{\lambda}]_{l_1}} \int_0^\infty \frac{x_1^{L_1-1}}{e^{L_1 x_1} \prod_{l_1=1}^{L_1} \left(\frac{x_1}{1+n^2} + \frac{1}{\frac{\alpha^2}{4N_0}[\boldsymbol{\lambda}]_{l_1}}\right)} dx_1 \\ &= \frac{L_1^{L_1} (1+n^2)^{L_1}}{\Gamma(L_1) e^{L_1 n^2}} \left(\frac{\alpha^2}{4N_0}\right)^{-L_1} \prod_{l_1=1}^{L_1} \frac{1}{[\boldsymbol{\lambda}]_{l_1}} \int_0^\infty \frac{x_1^{L_1-1} e^{-L_1(1+n^2)x_1}}{\prod_{l_1=1}^{L_1} \left(x_1 + \frac{1}{\frac{\alpha^2}{4N_0}[\boldsymbol{\lambda}]_{l_1}}\right)} dx_1. \end{aligned} \tag{6.68}$$

By using some mathematical expansions and integral calculations [134], $\Phi_{Z_1}(s)$ is obtained as

$$\Phi_{Z_1}(s)|_{s=-\frac{\alpha^2}{4N_0}}=\left[\frac{L_1(1+n^2)}{e^{n^2}}\right]^{L_1}\left(\frac{\alpha^2}{4N_0}\right)^{-L_1}\sum_{l_1=1}^{L_1}\frac{p_{l_1}}{[\boldsymbol{\lambda}]_{l_1}{}^{L_1}}e^{\frac{L_1(n^2+1)}{\frac{\alpha^2}{4N_0}[\boldsymbol{\lambda}]_{l_1}}}\Gamma\left[1-L_1,\frac{L_1(n^2+1)}{\frac{\alpha^2}{4N_0}[\boldsymbol{\lambda}]_{l_1}}\right], \tag{6.69}$$

where $p_{l_1}\triangleq\prod_{l=1,l\neq l_1}^{L_1}\frac{[\boldsymbol{\lambda}]_{l_1}}{[\boldsymbol{\lambda}]_{l_1}-[\boldsymbol{\lambda}]_l}$ and $\Gamma[\alpha,x]$ is the incomplete Gamma function defined by $\Gamma[\alpha,x]\triangleq\int_x^\infty t^{\alpha-1}e^{-t}dt$ [134].

6.4.2 Scenario (c): $\mathcal{PS}\rightarrow\{\mathcal{R}_1,\mathcal{R}_2\}$ and $\{\mathcal{R}_1,\mathcal{R}_2\}\rightarrow\mathcal{PD}$: Rician fading

Let n_1 and n_2 denote the Rician fading parameters of the links $\mathcal{PS}\rightarrow\{\mathcal{R}_1,\mathcal{R}_2\}$ and $\{\mathcal{R}_1,\mathcal{R}_2\}\rightarrow\mathcal{PD}$, respectively. Similarly, based on the relationship between L_1 and L_2, three cases are investigated.

Case 1 ($L_1<L_2$)

Also, (6.54) is taken into consideration and $\Phi_{Z_1}(s)$ is evaluated where

$$f_{X_1}(x_1)=\frac{L_2^{\frac{3-L_2}{2}}}{n_2^{L_2-1}}\frac{x_1^{\frac{L_2-1}{2}}I_{L_2-1}[2L_2^{\frac{3}{2}}n_2x_1^{\frac{1}{2}}]}{e^{L_2^2n_2^2+L_2x_1}}, \tag{6.70}$$

$$\Phi_{Y_1}(s)=\prod_{l_1=1}^{L_1}\frac{1+n_1^2}{1+n_1^2-s[\boldsymbol{\lambda}]_{l_1}}e^{\frac{n_1^2s[\boldsymbol{\lambda}]_{l_1}}{1+n_1^2-s[\boldsymbol{\lambda}]_{l_1}}}. \tag{6.71}$$

Substituting (6.70) and (6.71) into (6.56), $\Phi_{Z_1}(s)$ is obtained as

$$\begin{aligned}\Phi_{Z_1}(s)|_{s=-\frac{\alpha^2}{4N_0}}=&\int_0^\infty\frac{L_2^{\frac{3-L_2}{2}}}{n_2^{L_2-1}}\frac{x_1^{\frac{L_2-1}{2}}I_{L_2-1}[2L_2^{\frac{3}{2}}n_2x_1^{\frac{1}{2}}]}{e^{L_2^2n_2^2+L_2x_1}}\\&\times\prod_{l_1=1}^{L_1}\frac{1+n_1^2}{1+n_1^2+\frac{\alpha^2}{4N_0}x_1[\boldsymbol{\lambda}]_{l_1}}e^{\frac{-n_1^2\frac{\alpha^2}{4N_0}x_1[\boldsymbol{\lambda}]_{l_1}}{1+n_1^2+\frac{\alpha^2}{4N_0}x_1[\boldsymbol{\lambda}]_{l_1}}}dx_1.\end{aligned} \tag{6.72}$$

Under a high SNR assumption, (6.72) can be approximated as

$$\begin{aligned}\Phi_{Z_1}(s)|_{s=-\frac{\alpha^2}{4N_0}}\approx&\frac{L_2^{\frac{3-L_2}{2}}}{e^{L_2^2n_2^2+L_1n_1^2}}\frac{(1+n_1^2)^{L_1}}{n_2^{L_2-1}}\left(\frac{\alpha^2}{4N_0}\right)^{-L_1}\prod_{l_1=1}^{L_1}\frac{1}{[\boldsymbol{\lambda}]_{l_1}}\\&\times\int_0^\infty\frac{x_1^{\frac{L_2-1}{2}-L_1}}{e^{L_2x_1}}I_{L_2-1}\left[2L_2^{\frac{3}{2}}n_2x_1^{\frac{1}{2}}\right]dx_1.\end{aligned} \tag{6.73}$$

Calculating the integral in (6.60) when $L_1 < L_2$ [134], $\Phi_{Z_1}(s)$ is obtained as

$$\Phi_{Z_1}(s)\big|_{s=-\frac{\alpha^2}{4N_0}} \approx \frac{[L_2(1+n_1^2)]^{L_1}}{e^{L_2^2 n_2^2 + L_1 n_1^2}} \Gamma(L_2 - L_1)\, {}_1\tilde{F}_1\left(L_2 - L_1; L_2; L_2^2 n_2^2\right) \left(\frac{\alpha^2}{4N_0}\right)^{-L_1} \prod_{l_1=1}^{L_1} \frac{1}{[\boldsymbol{\lambda}]_{l_1}}. \tag{6.74}$$

Case 2 ($L_1 > L_2$)

By considering (6.55) with the same approach as case 1, $\Phi_{Z_2}(s)\big|_{s=-\frac{\alpha^2}{4N_0}}$ can be approximated by

$$\Phi_{Z_2}(s)\big|_{s=-\frac{\alpha^2}{4N_0}} \approx \frac{[L_1(1+n_2^2)]^{L_2}}{e^{L_1^2 n_1^2 + L_2 n_2^2}} \Gamma(L_1 - L_2)\, {}_1\tilde{F}_1\left(L_1 - L_2; L_1; L_1^2 n_1^2\right) \left(\frac{\alpha^2}{4N_0}\right)^{-L_2} \prod_{l_2=1}^{L_2} \frac{1}{[\boldsymbol{\lambda}]_{l_2}}. \tag{6.75}$$

Case 3 ($L_1 = L_2$)

(6.72) can be rewritten as

$$\begin{aligned} \Phi_{Z_1}(s)\big|_{s=-\frac{\alpha^2}{4N_0}} &= \frac{L_1^{\frac{3-L_1}{2}}}{n_2^{L_1-1} e^{L_1^2 n_2^2 + L_1 n_1^2}} \left(\frac{\alpha^2}{4N_0}\right)^{-L_1} \prod_{l_1=1}^{L_1} \frac{1}{[\boldsymbol{\lambda}]_{l_1}} \\ &\quad \times \int_0^\infty \frac{x_1^{\frac{L_1-1}{2}} I_{L_1-1}[2L_1^{\frac{3}{2}} n_2 x_1^{\frac{1}{2}}]}{e^{L_1 x_1} \prod_{l_1=1}^{L_1} \left(\frac{x_1}{1+n_1^2} + \frac{1}{\frac{\alpha^2}{4N_0}[\boldsymbol{\lambda}]_{l_1}}\right)} dx_1 \\ &= \frac{L_1^{\frac{3-L_1}{2}}}{n_2^{L_1-1} e^{L_1^2 n_2^2 + L_1 n_1^2}} \left(\frac{\alpha^2}{4N_0}\right)^{-L_1} \prod_{l_1=1}^{L_1} \frac{1}{[\boldsymbol{\lambda}]_{l_1}} \\ &\quad \times \int_0^\infty \frac{x_1^{\frac{L_1-1}{2}} I_{L_1-1}[2L_1^{\frac{3}{2}} n_2 (1+n_1^2)^{\frac{1}{2}} x_1^{\frac{1}{2}}]}{e^{L_1(1+n_1^2)x_1} \prod_{l_1=1}^{L_1} \left(x_1 + \frac{1}{\frac{\alpha^2}{4N_0}[\boldsymbol{\lambda}]_{l_1}}\right)} dx_1. \end{aligned} \tag{6.76}$$

With some mathematical expansions and integral calculations [134], $\Phi_{Z_1}(s)$ can be obtained as

$$\Phi_{Z_1}(s)\big|_{s=-\frac{\alpha^2}{4N_0}} = \frac{L_1^{3-2L_1}}{e^{L_1^2 n_2^2 + L_1 n_1^2}} \frac{1+n_1^2}{n_2^{2L_1-2}} \left(\frac{\alpha^2}{4N_0}\right)^{-L_1} \sum_{l_1=1}^{L_1} \frac{p_{l_1}}{[\boldsymbol{\lambda}]_{l_1}} \left[\Gamma(L_1 - 1, -L_1^2 n_2^2) - \Gamma(L_1 - 1)\right]. \tag{6.77}$$

Remark 6.3 (*Achievable Diversity Gain and Effects of Rician Fading Parameters on Performance*). *From the PEP analysis of fading scenario (a) with Eqs.*

(6.61), (6.67) *and* (6.69) *and fading scenario (c) with Eqs.* (6.74), (6.75) *and* (6.77), *it can be concluded that the diversity gain of the proposed DSTFBC for the primary transmission in all three fading scenarios is* $\min(L_{\mathcal{PSR}_1}, L_{\mathcal{R}_1\mathcal{PD}}) + \min(L_{\mathcal{PSR}_2}, L_{\mathcal{R}_2\mathcal{PD}})$ *by observing the exponential terms of the SNR (i.e.* $\frac{\alpha^2}{4N_0}$*). The PEP analysis for the secondary transmission can be similarly carried out, which results in an achievable diversity gain of* $\min(L_{\mathcal{SS}_i\mathcal{R}_1}, L_{\mathcal{R}_1\mathcal{SD}_i}) + \min(L_{\mathcal{SS}_i\mathcal{R}_2}, L_{\mathcal{R}_2\mathcal{SD}_i})$, $i = 1, 2, \ldots, N$. *Additionally, it can be observed that the Rician fading parameters do not produce any diversity gain, however, they play the part of coding gain, and thus can improve the PEP, which will be confirmed through the numerical and simulation results.*

6.5 Numerical and Simulation Results

This section evaluates the uncoded BER performance of the proposed DSTFBC in a CWRN to justify the analysis of the achievable diversity gain over either mixed Rayleigh-Rician fading channels or both Rayleigh or Rician fading channels. As outlined earlier, Rayleigh flat fading channels represent NLOS transmissions, whilst Rician flat fading channels are modeled for LOS transmissions. The validity of the analysis can be confirmed through the slope of the BER curves since BER is proportional to PEP [176]. The simulation is carried out using quadrature phase shift keying (QPSK) modulation with Gray mapping for random dispersive channels. The fast Fourier transform (FFT) algorithm is exploited for low-complexity data detection. Each transmitted data block consists of 256 symbols including the zero sequence and modulated information-carrying data. A uniform power delay profile and a quasi-static fading channel model[31] are considered in the simulation, where the channel gains are assumed to remain constant over two time slots and change independently in the consecutive two time slots. It is assumed that the destination

[31] It is noted that the channel coefficients may not be constant during two time slots when the FFT block size and/or user velocity increases, and thus it may degrade the BER performance. Dealing with this, several algorithms were proposed for a frequency-domain equaliser, e.g. in [177, 178].

nodes have perfect channel state information. The results are obtained in MATLAB by using Monte Carlo simulation method.

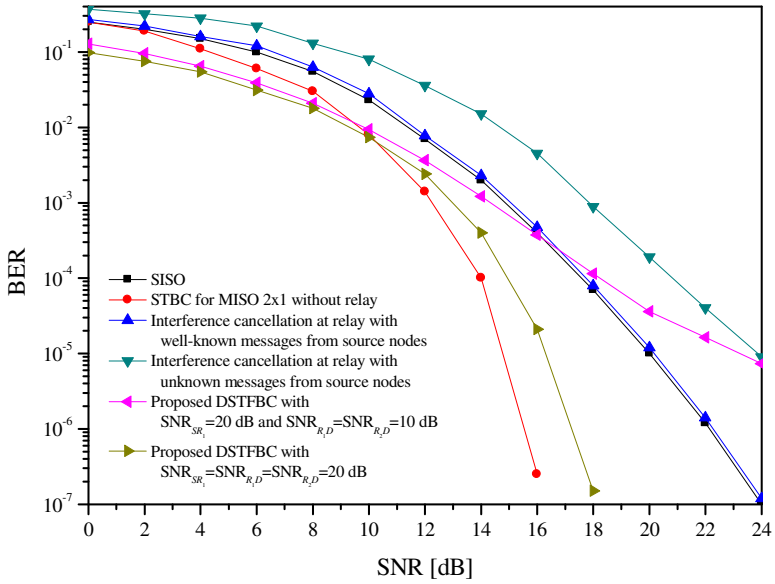

Figure 6.2: Performance comparison of various transmission schemes in CWRN over Rayleigh frequency selective fading channels with $L_{\mathcal{PSR}_1} = 5$, $L_{\mathcal{PSR}_2} = 7$, $L_{\mathcal{R}_1\mathcal{PD}} = 5$, $L_{\mathcal{R}_2\mathcal{PD}} = 7$.

Fig. 6.2 shows the BER performance comparison of the primary transmission using the proposed DSTFBC, single-input single-output (SISO) (e.g. [179]), STBC (e.g. [180]) and interference cancellation at relay (ICR) (e.g. [172]). The fading of links $\mathcal{PS} \to \{\mathcal{R}_1, \mathcal{R}_2\}$ and $\{\mathcal{R}_1, \mathcal{R}_2\} \to \mathcal{PD}$ are assumed to be frequency-selective Rayleigh fading where the channel memory lengths are $L_{\mathcal{PSR}_1} = 5$, $L_{\mathcal{PSR}_2} = 7$, $L_{\mathcal{R}_1\mathcal{PD}} = 5$ and $L_{\mathcal{R}_2\mathcal{PD}} = 7$. It is assumed that the value of $\xi_{\mathcal{PSR}_1}/N_0$ is fixed at 20 dB, $\xi_{\mathcal{R}_1\mathcal{PD}} = \xi_{\mathcal{R}_2\mathcal{PD}} = \xi_{\mathcal{RPD}}$. The BER curves are plotted as a function of SNR. The STBC scheme refers to the classical STBC devised for co-located antennas without relay nodes, where $\mathcal{PS}$ is assumed to be equipped with two antennas, $\mathcal{PD}$ with single antenna, and each path from one antenna from $\mathcal{PS}$ to $\mathcal{PD}$ has 6 taps (i.e. $L_{\mathcal{PSPD}} = 5$). The performance of STBC for no-relay scenario is presented as a benchmark to compare with the other schemes. The ICR scheme refers to the scheme where the cognitive relay helps a primary and multiple secondary users de-

code, precode and forward their messages to the respective primary receiver and secondary receivers using a precoding scheme at the relay for interference compensation. Here, the ICR scheme with known messages and the ICR scheme with unknown messages from the source nodes are both taken into consideration. In Fig. 6.2, SNR is referred to $\xi_{\mathcal{PSPD}}/N_0$ for the direct transmission scenario without relay assistance, while SNR is referred to $\xi_{\mathcal{PSR}_2}/N_0$ for the relaying scenario. Additionally, the ICR scheme with known messages and the ICR scheme with unknown messages from the source nodes are both taken into investigation. The performance of STBC is regarded as a benchmark. It can be observed that the ICR scheme with unknown messages from the sources nodes shows the worst BER performance. The SISO and ICR systems perform better than the DSTFBC in the high-SNR region due to the existence of an error floor when $\xi_{\mathcal{RPD}}$ is small. At high $\xi_{\mathcal{RPD}}/N_0$, the BER performance curves of the DSTFBC and conventional STBC schemes have the same slope, reflecting the same diversity order. As proved in the PEP analysis, the diversity gain of the proposed DSTFBC for the primary transmission is $\min(L_{\mathcal{PSR}_1}, L_{\mathcal{R}_1\mathcal{PD}}) + \min(L_{\mathcal{PSR}_2}, L_{\mathcal{R}_2\mathcal{PD}}) = 12$, which is also the maximum diversity gain of $(2 \times L_{\mathcal{PSPD}}) = 12$ achieved by STBC [75].

Figs. 6.3 and 6.4 show the BER performances of the primary and secondary transmissions as a function of $\xi_{\mathcal{PSR}_2}/N_0$ and $\xi_{\mathcal{SS}_1\mathcal{R}_2}/N_0$, respectively, using the proposed DSTBC for various combinations of channel lengths. For simplicity, the transmission of $\mathcal{SS}_1$ is studied only. The performance of the transmission of other CR users can be similarly obtained. All fading channels are Rayleigh fading. It is assumed that $\xi_{\mathcal{PSR}_1}/N_0 = 20$ dB, $\xi_{\mathcal{SS}_1\mathcal{R}_1}/N_0 = 15$ dB, $\xi_{\mathcal{R}_1\mathcal{PD}} = \xi_{\mathcal{R}_2\mathcal{PD}} = \xi_{\mathcal{RPD}} = 10$ dB and $\xi_{\mathcal{R}_1\mathcal{SD}} = \xi_{\mathcal{R}_2\mathcal{SD}} = \xi_{\mathcal{RSD}} = 5$ dB. For the primary and secondary transmissions, the BERs for the following cases are compared:

- Case 1: $L_{\mathcal{PSR}_1} = L_{\mathcal{PSR}_2} = L_{\mathcal{R}_1\mathcal{PD}} = L_{\mathcal{R}_2\mathcal{PD}} = 2$, $L_{\mathcal{SS}_1\mathcal{R}_1} = L_{\mathcal{SS}_1\mathcal{R}_2} = L_{\mathcal{R}_1\mathcal{SD}_1} = L_{\mathcal{R}_2\mathcal{SD}_1} = 2 \rightarrow$ diversity order $= 4$;

- Case 2: $L_{\mathcal{PSR}_1} = 2$; $L_{\mathcal{PSR}_2} = 3$, $L_{\mathcal{R}_1\mathcal{PD}} = 2$, $L_{\mathcal{R}_2\mathcal{PD}} = 3$, $L_{\mathcal{SS}_1\mathcal{R}_1} = 2$, $L_{\mathcal{SS}_1\mathcal{R}_2} = 3$, $L_{\mathcal{R}_1\mathcal{SD}_1} = 2$, $L_{\mathcal{R}_2\mathcal{SD}_1} = 3 \rightarrow$ diversity order $= 5$;

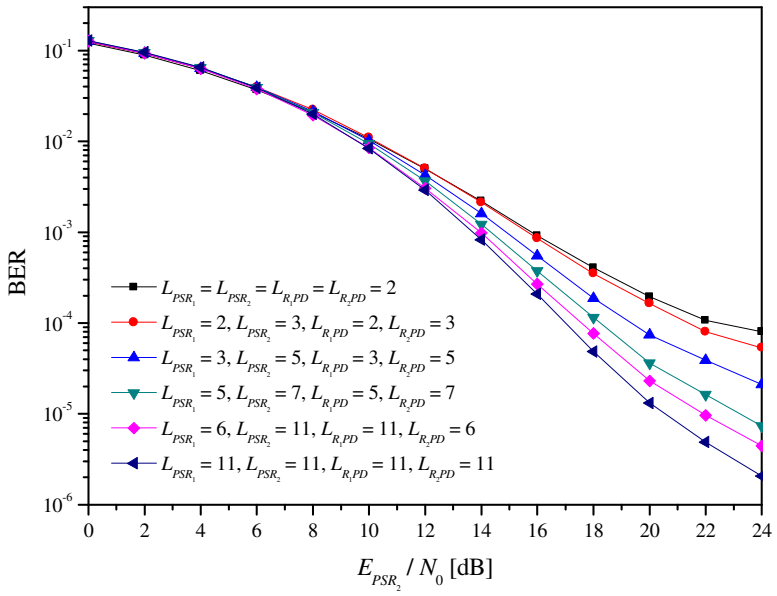

Figure 6.3: BER performance of the primary transmission over Rayleigh frequency selective fading channels with various combinations of channel memory order.

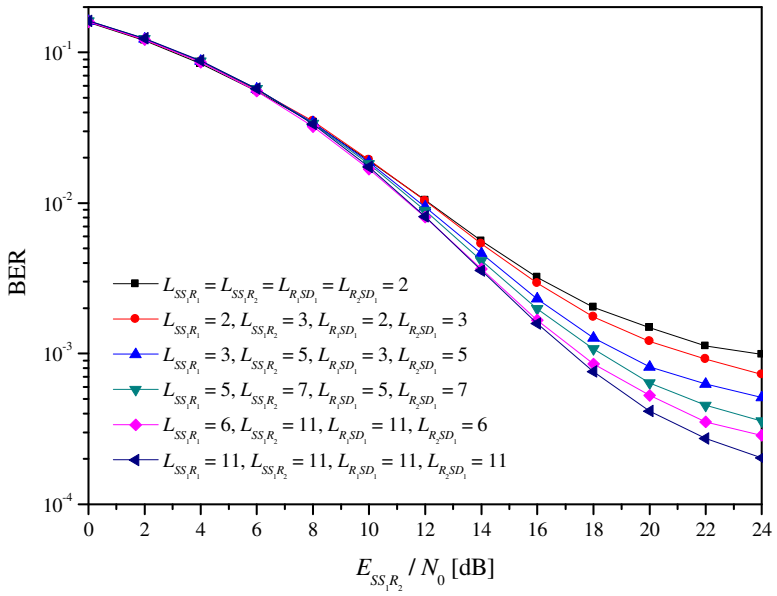

Figure 6.4: BER performance of the secondary transmission over Rayleigh frequency selective fading channels with various combinations of channel memory order.

- Case 3: $L_{\mathcal{PSR}_1} = 3$, $L_{\mathcal{PSR}_2} = 5$, $L_{\mathcal{R}_1\mathcal{PD}} = 3$, $L_{\mathcal{R}_2\mathcal{PD}} = 5$, $L_{\mathcal{SS}_1\mathcal{R}_1} = 3$, $L_{\mathcal{SS}_1\mathcal{R}_2} = 5$, $L_{\mathcal{R}_1\mathcal{SD}_1} = 3$, $L_{\mathcal{R}_2\mathcal{SD}_1} = 5 \rightarrow$ diversity order $= 8$;

- Case 4: $L_{\mathcal{PSR}_1} = 5$, $L_{\mathcal{PSR}_2} = 7$, $L_{\mathcal{R}_1\mathcal{PD}} = 5$, $L_{\mathcal{R}_2\mathcal{PD}} = 7$, $L_{\mathcal{SS}_1\mathcal{R}_1} = 5$, $L_{\mathcal{SS}_1\mathcal{R}_2} = 7$, $L_{\mathcal{R}_1\mathcal{SD}_1} = 5$, $L_{\mathcal{R}_2\mathcal{SD}_1} = 7 \rightarrow$ diversity order $= 12$;
- Case 5: $L_{\mathcal{PSR}_1} = 6$, $L_{\mathcal{PSR}_2} = 11$, $L_{\mathcal{R}_1\mathcal{PD}} = 11$, $L_{\mathcal{R}_2\mathcal{PD}} = 6$, $L_{\mathcal{SS}_1\mathcal{R}_1} = 6$, $L_{\mathcal{SS}_1\mathcal{R}_2} = 11$, $L_{\mathcal{R}_1\mathcal{SD}_1} = 11$, $L_{\mathcal{R}_2\mathcal{SD}_1} = 6 \rightarrow$ diversity order $= 12$;
- Case 6: $L_{\mathcal{PSR}_1} = 11$, $L_{\mathcal{PSR}_2} = 11$, $L_{\mathcal{R}_1\mathcal{PD}} = 11$, $L_{\mathcal{R}_2\mathcal{PD}} = 11$, $L_{\mathcal{SS}_1\mathcal{R}_1} = 11$, $L_{\mathcal{SS}_1\mathcal{R}_2} = 11$, $L_{\mathcal{R}_1\mathcal{SD}_1} = 11$, $L_{\mathcal{R}_2\mathcal{SD}_1} = 11 \rightarrow$ diversity order $= 22$.

Through the BER performance of the above six cases, it can be observed that the diversity gain is improved with increased number of channel memory taps, which results in steeper BER curves. Explicitly, in Figs. 6.3 and 6.4, the curve for case 1 has the smallest slope while the steepest curve correspond to case 6 since case 1 and case 6 achieve the lowest and highest diversity gain, respectively. Also, it is observed that the curves for case 4 and case 5 have the same slope at high SNR with the same achievable diversity order. These facts confirm the conclusion in Remark 6.3 regarding the achievable diversity gain of the proposed DSTFBC.

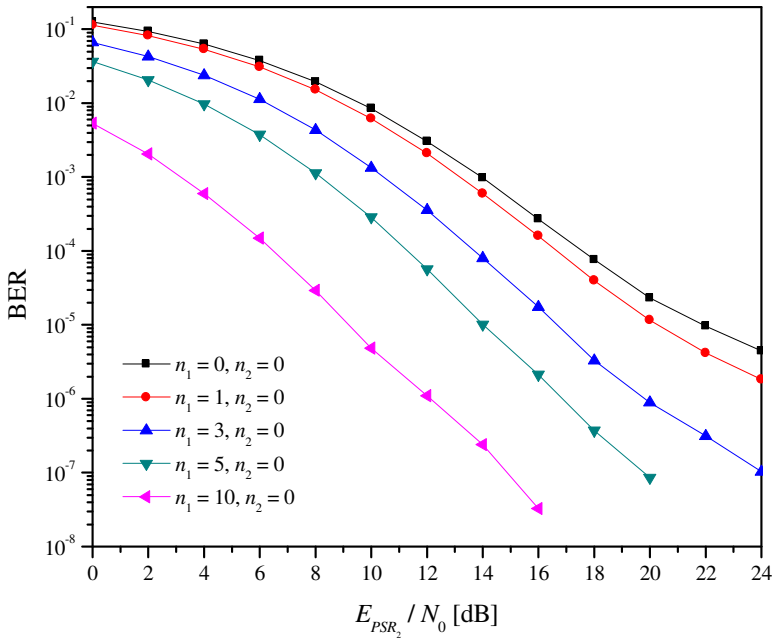

Figure 6.5: BER performance of the primary transmission over mixed Rician-Rayleigh frequency selective fading channels with various Rician fading factors.

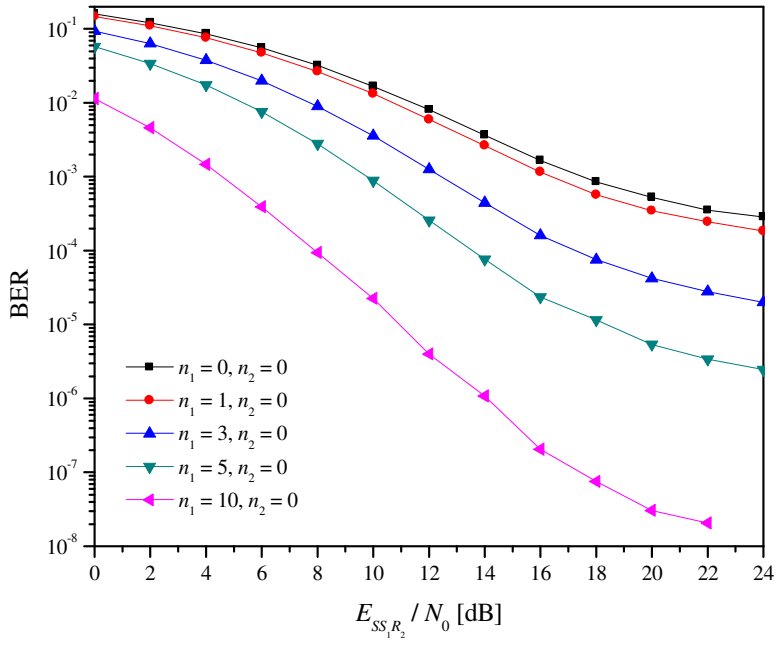

Figure 6.6: BER performance of the secondary transmission over mixed Rician-Rayleigh frequency selective fading channels with various Rician fading factors.

The performance of the proposed DSTFBC for both the primary and secondary transmissions over wireless fading channels where the relays are located near the source nodes is drawn in Figs. 6.5 and 6.6. For this situation, the communication links $\{\mathcal{PS}, \mathcal{SS}_1\} \rightarrow \{\mathcal{R}_1, \mathcal{R}_2\}$ and $\{\mathcal{R}_1, \mathcal{R}_2\} \rightarrow \{\mathcal{PD}, \mathcal{SD}_1\}$ are assumed to be LOS and NLOS, respectively, and thus the fading channels $\{\mathcal{PS}, \mathcal{SS}_1\} \rightarrow \{\mathcal{R}_1, \mathcal{R}_2\}$ are considered as Rician distributions and $\{\mathcal{R}_1, \mathcal{R}_2\} \rightarrow \{\mathcal{PD}, \mathcal{SD}_1\}$ as Rayleigh distributions. The channel memory orders of fading channels $\{\mathcal{PS}, \mathcal{SS}_1\} \rightarrow \{\mathcal{R}_1, \mathcal{R}_2\}$ and $\{\mathcal{R}_1, \mathcal{R}_2\} \rightarrow \{\mathcal{PD}, \mathcal{SD}_1\}$ are assumed to be $L_{\mathcal{PSR}_1} = 6$, $L_{\mathcal{PSR}_2} = 11$, $L_{\mathcal{R}_1\mathcal{PD}} = 11$, $L_{\mathcal{R}_2\mathcal{PD}} = 6$, $L_{\mathcal{SS}_1\mathcal{R}_1} = 6$, $L_{\mathcal{SS}_1\mathcal{R}_2} = 11$, $L_{\mathcal{R}_1\mathcal{SD}_1} = 11$ and $L_{\mathcal{R}_2\mathcal{SD}_1} = 6$. In Figs. 6.5 and 6.6, the BER performances of the primary and secondary transmissions are plotted as a function of $\xi_{\mathcal{PSR}_2}/N_0$ and $\xi_{\mathcal{SS}_1\mathcal{R}_2}/N_0$, respectively, with different values of Rician fading factor. Specifically, n_1 is varied in $\{0, 1, 3, 5, 10\}$ while $n_2 = 0$ since links $\{\mathcal{R}_1, \mathcal{R}_2\} \rightarrow \{\mathcal{PD}, \mathcal{SD}_1\}$ are Rayleigh fading. The SNR values of the other links are similarly set as in Figs. 6.3 and 6.4. It can be seen that an improved performance is achieved as n_1 increases. However, the

slopes of the BER curves are almost the same at high SNR, which means that they achieve the same diversity gain. This can be explained as the influence of the LOS component on the BER gain through all ranges of SNR values where the Rician fading parameter only produces coding gain to the PEP as it can be seen in the analysis. This also confirms the conclusion about the achievable diversity gain mentioned in Remark 6.3, which is independent of Rician fading factor. Additional results, which are omitted for brevity, also show the same observations of achievable diversity gain and the same effects of Rician fading factor on the performance of the proposed DSTFBC if the relays are located near the destination nodes, i.e. the channels $\{\mathcal{PS}, \mathcal{SS}_1\} \rightarrow \{\mathcal{R}_1, \mathcal{R}_2\}$ and $\{\mathcal{R}_1, \mathcal{R}_2\} \rightarrow \{\mathcal{PD}, \mathcal{SD}_1\}$ are characterised by Rayleigh and Rician distributions, respectively.

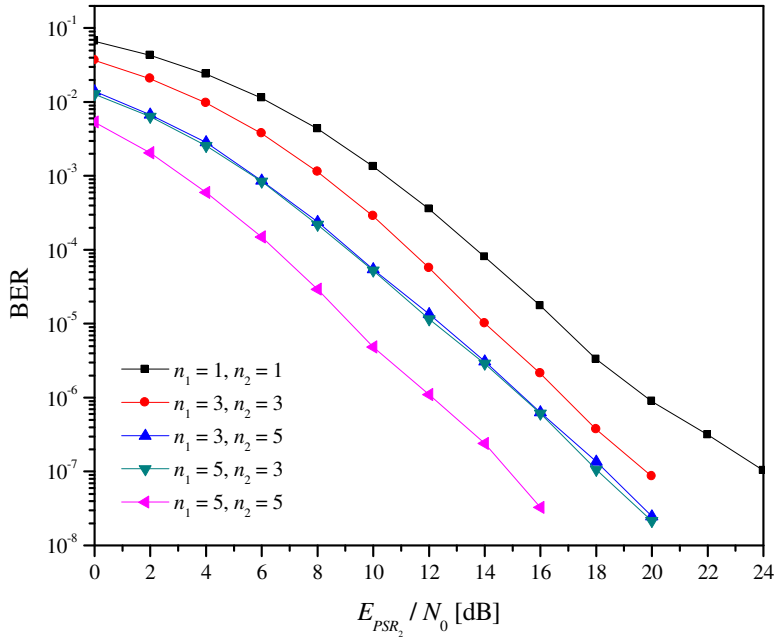

Figure 6.7: BER performance of the primary transmission over Rician frequency selective fading channels with various Rician fading factors.

The scenario where the relays are located near the midpoint is now investigated. In this situation, all links $\{\mathcal{PS}, \mathcal{SS}_1\} \rightarrow \{\mathcal{R}_1, \mathcal{R}_2\}$ and $\{\mathcal{R}_1, \mathcal{R}_2\} \rightarrow \{\mathcal{PD}, \mathcal{SD}_1\}$ are assumed to be LOS, and thus they are all characterised by Rician fading. The BER performance of the proposed DSTFBC for both pri-

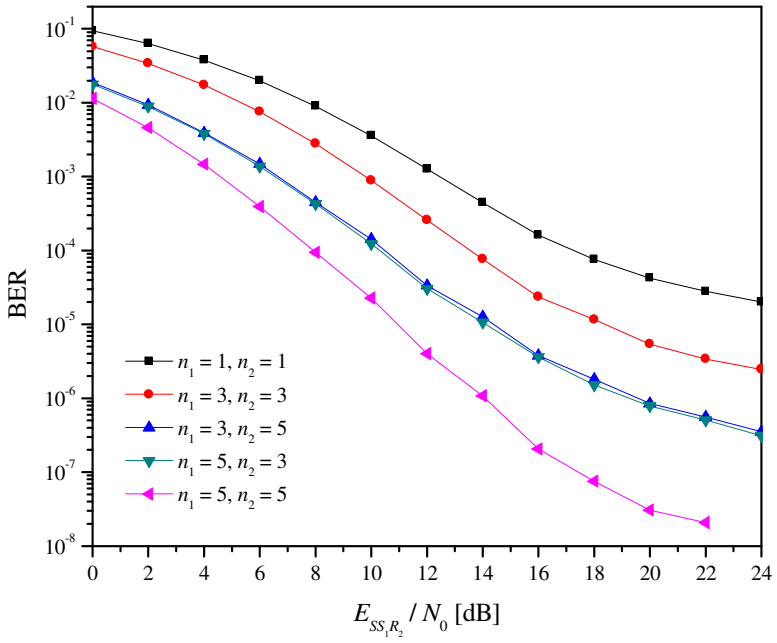

Figure 6.8: BER performance of the secondary transmission over Rician frequency selective fading channels with various Rician fading factors.

mary and secondary transmissions is plotted in Figs. 6.7 and 6.8 as a function of $\xi_{\mathcal{PSR}_2}/N_0$ and $\xi_{\mathcal{SS}_1\mathcal{R}_2}/N_0$, respectively, with respect to various Rician fading values and with the same assumptions of SNR values as in Figs. 6.3 and 6.4. Specifically, five cases $\{n_1 = 1, n_2 = 1\}$, $\{n_1 = 3, n_2 = 3\}$, $\{n_1 = 3, n_2 = 5\}$, $\{n_1 = 5, n_2 = 3\}$ and $\{n_1 = 5, n_2 = 5\}$ are considered. The channel memory orders of fading channels $\{\mathcal{PS}, \mathcal{SS}_1\} \to \{\mathcal{R}_1, \mathcal{R}_2\}$ and $\{\mathcal{R}_1, \mathcal{R}_2\} \to \{\mathcal{PD}, \mathcal{SD}_1\}$ are assumed as in Figs. 6.5 and 6.6. Similarly, it can be observed that the BER curves have the same slopes at high SNR and a reduced BER is always achieved when either n_1 or n_2 increases. Specifically, the BER curves are only shifted down with the same slope if either n_1 or n_2 increases. This means that they achieve the same diversity gain, however, the increased Rician fading factor provides further coding gain to the BER performance. This again confirms the statement in Remark 6.3 regarding the achievable diversity gain, which depends only on the channel memory lengths.

6.6 Conclusions

In this chapter, a new DSTFBC scheme has been proposed to facilitate the cooperative transmission of both PU and SUs over frequency-selective fading channels in two-hop cognitive wireless relay systems. The proposed DSTFBC can achieve a data rate of $N+1/N+2$ and spatial diversity order of $\min(L_{\mathcal{PSR}_1}, L_{\mathcal{R}_1\mathcal{PD}}) + \min(L_{\mathcal{PSR}_2}, L_{\mathcal{R}_2\mathcal{PD}})$ for primary transmission and $\min(L_{\mathcal{SS}_i\mathcal{R}_1}, L_{\mathcal{R}_1\mathcal{SD}_i}) + \min(L_{\mathcal{SS}_i\mathcal{R}_2}, L_{\mathcal{R}_2\mathcal{SD}_i})$, $i = 1, 2, \ldots, N$, for secondary transmission. Particularly, using the proposed DSTFBC design, data detection at both primary and secondary destinations can be decoupled in the frequency domain for a low-complexity receiver. The data rate of the proposed DSTFBC has been proved to be higher than that of repetition code which only achieves a maximum data rate of 1/3 for a two-relay system. Furthermore, the PEP performance has been analysed for various scenarios of relay location represented by a mixed Rayleigh and Rician frequency-selective fading channel model. The analysis and simulation results have validated the theoretically derived diversity order and have shown that the LOS component in Rician fading effectively improves the error rate performance at the destination nodes.

Chapter 7

Conclusions and Future Work

7.1 Summary of Original Work

This dissertation has addressed issues of data throughput in various wireless relay network models with the main objective to improve the data throughput in these networks. This objective has been tackled through various means of achieving high-throughput relay communications by proposing and evaluating new implementations of network coding (NC) and space-time coding (STC) techniques. Specifically, this thesis has designed new automatic repeat request, channel quality indicator reporting, acknowledgement, retransmission, spectrum sensing and diversity coding schemes in the context of wireless relay channels. The original work in this thesis can be summarised as follows:

Chapter 1 summarised the motivation and main contributions of the thesis. The concepts of diversity and MIMO techniques were briefly summarised along with the basic principles and specific protocols of cooperative communications to indicate several physical layer issues and aspects of various relaying techniques. Distributed STC was investigated to improve bandwidth efficiency in cooperative communications and physical layer NC was thoroughly examined for an improved throughput in different relay network models.

Chapter 2 proposed various automatic repeat request (ARQ) retransmission protocols for wireless two-way single-relay networks (TWSRNs) and multi-source multidestination single-relay networks (MMSRNs) based on NC. Firstly,

two improved NC-based ARQ schemes were developed for TWSRNs to reduce the number of retransmissions. The combination of an improved NC-based selective repeat ARQ scheme in the broadcast phase and a traditional selective repeat ARQ scheme in the multiple access phase was shown to achieve the highest throughput efficiency compared to other combinations of ARQ schemes. Secondly, to cope with the delay latency issue when applying the basic ARQ protocols to MMSRN, a new reliable ARQ transmission protocol was proposed for MMSRNs over mixed fading channels. In this new ARQ protocol, two packet-combination algorithms for retransmissions at the relay and sources were developed to efficiently retransmit all lost packets. Mathematical formulation of transmission bandwidth was also derived to show the superior performance of this new NC-based ARQ protocol compared with some other ARQ protocols. Two typical fading scenarios were considered where the relay is located in the neighbourhood of either the sources or the destinations to demonstrate the improved performance.

Chapter 3 was concerned with channel quality indicator (CQI) reporting for data exchange in two-way multi-relay networks (TWMRNs). Two efficient CQI reporting schemes were proposed based on NC via XOR and superposition coding to allow two terminals to simultaneously estimate the CQI of the distant terminal-relay link without incurring additional overhead. With these proposed schemes, the transmission time for CQI feedback at the relays is reduced by half while the increase in complexity and the loss of performance are negligible. Therefore, a system throughput improvement of 16.7% is achieved. In order to study performance behaviour of the proposed schemes, upper and lower bounds of the mean square error (MSE) of the estimated CQI were derived to show that the MSE of the estimated CQI increases proportionally with the square of the cardinality of CQI level sets, though an increased number of CQI levels would eventually lead to a higher data-rate transmission. Furthermore, a low-complexity relay selection (RS) scheme was proposed based on the derived bounds to significantly reduce the complexity by at least three times for the case of a large number of relays.

Chapter 4 proposed a new solution to deal with the problems of block acknowledgement (ACK) and retransmission in wireless regenerative multi-relay networks. Specifically, a block ACK scheme was firstly proposed based on NC to significantly reduce the acknowledgement overheads and reduce the computational operators. The error probability of the determination of the packets to be retransmitted at the source and relays was analysed to demonstrate that the NC-based scheme also improves the reliability of block ACK transmissions. Secondly, this chapter considered cooperative retransmission (CR) with the assistance of all available relays. A CR scheme was proposed based on relay cooperation and binary XOR operations to significantly reduce the number of packets retransmitted to produce a more power efficient system with non-overlapped retransmissions. The error probability of retransmission decisions at the source and relays was also derived to realise the improved reliability of the retransmissions with the proposed CR scheme. Furthermore, this chapter derived the average number of packets to be retransmitted at the source and relays, not only to demonstrate that the proposed CR scheme reduces the number of retransmissions and removes overlapped retransmitted packets, but also to determine the optimised number of relays used for the retransmission phase.

Chapter 5 investigated cooperative spectrum sensing (CSS) mechanisms in three-hop cognitive wireless relay networks (CWRNs) where the data transmission from a source node to a destination node is realized with the aid of two layers of cognitive users (CUs) in the transmission coverage of two primary users (PUs). A new CSS scheme was firstly proposed for a layer of CUs to improve the spectrum sensing performance by exploiting both local decisions at the CUs and global decisions at the fusion centre (FC). Additionally, the probabilities of missed detection and false alarm were analysed for a practical scenario where all sensing, reporting and backward channels suffer from Rayleigh fading. Through the derived expressions, it was not only shown that the proposed CSS scheme achieves an improved sensing performance over the conventional scheme but also characterised the effects of the fading channels

on the sensing reliability. Furthermore, in this chapter, a CSS scheme was proposed for two cognitive radio layers in a three-hop CWRN based on NC via the binary XOR operator to help reduce one phase of sensing for a higher system throughput compared to the conventional scheme which requires eight phases in total to monitor all available spectrums of both PUs.

Chapter 6 proposed a new distributed space-time-frequency block code (DSTFBC) for a two-hop nonregenerative CWRN over frequency-selective fading channels to achieve higher data rate of $N + 1/N + 2$, spatial diversity gain and permit decoupling detection of data blocks at all destination nodes with a low-complexity receiver structure. In the proposed new DSTFBC, the relay nodes precode the received signals with a proper precoding matrix prior to forwarding the data received from various sources to the destination nodes. The precoding matrix was effectively formulated to enable cooperative data transmission of all nodes in the CWRN. Furthermore, the pairwise error probability analysis was provided to investigate the achievable diversity gain of the proposed DSTFBC for three typical scenarios where the relays are in the neighbourhood of either the sources or the destinations or the midpoint. The proposed DSTFBC was shown to achieve spatial diversity order of $\min(L_{\mathcal{PSR}_1}, L_{\mathcal{R}_1\mathcal{PD}}) + \min(L_{\mathcal{PSR}_2}, L_{\mathcal{R}_2\mathcal{PD}})$ for primary transmission and $\min(L_{\mathcal{SS}_i\mathcal{R}_1}, L_{\mathcal{R}_1\mathcal{SD}_i}) + \min(L_{\mathcal{SS}_i\mathcal{R}_2}, L_{\mathcal{R}_2\mathcal{SD}_i})$, $i = 1, 2, \ldots, N$, for secondary transmission.

7.2 Future Work

Besides various proposals and designs presented in this dissertation, there are still many potential issues that need to be investigated. Here, several current challenges and possible extensions are provided as motivation for future work.

Most of the previous and recent research literature has been dedicated to investigating distributed space-time block codes (DSTBCs) for one-way relay networks considering either flat fading channels for narrowband communications or frequency-selective fading channels for broadband communications.

The DSTBCs for NC-based two-way relay networks over various fading channels are still unknown. The question of how the relays in two-way relay networks combine the signals received from two end nodes in an efficient way to achieve both the benefits of improved diversity gain and enhanced throughput by using both DSTBC and NC techniques requires to be investigated. Considering frequency-selective fading channels in two-way relay networks, other related issues are the design of equalizers and the extraction method at an end node for the required information based on the combined signal received from the relay. In addition, methods of effective channel estimation at an end node in the context of two-way relay networks over frequency-selective fading channels also need to be investigated.

Another issue that affects the application of NC to practical wireless relay networks is the requirement of symbol synchronisation at the relays. In fact, the synchronisation of received symbol at the relays is assumed in most of studies related to NC. A significantly improved throughput of 100 % (i.e. with only two time slots for data exchange) is only achieved with NC implementations when the relays receive simultaneously the data from two sources so as to combine and then forward back to two sources. This means that the data synchronisation is required at two sources. Thus, possible research topics could include the synchronisation and scheduling of data transmission in wireless two-way relay networks using NC. For example, the relays only perform NC combination if they receive data from two sources at the same time, otherwise they could help one source forward the data to another source after a short time-out period instead of waiting for the simultaneous transmissions from two sources. These research topics could be later extended to the scenario of data retransmission where the synchronisation is also strictly required. As pointed out in previous work [37], the retransmission of the lost packets in two-way relay networks can be carried out in an effective way using NC. However, in this work, it has been assumed that the packets received at the relay are well synchronised and scheduled. Similarly, an efficient NC-based acknowledgement of the lost packets was proposed for one-way relay networks

in [44] to reduce the number of required signaling transmissions, i.e. block ACK packets, and also to improve the reliability of the retransmission with the assumption of perfect scheduling of data and block ACK packets at all nodes in the network. Another approach of the scheduling investigation is the data retransmission in multisource multidestination relay networks in [39, 40] where an NC-based ARQ protocol was proposed to significantly reduce the transmission bandwidth with an implied assumption of well scheduling in the whole network for both data and reporting channels. In fact, the imperfect synchronisation and scheduling of the data and signaling information may result in the delay of the NC-based combination techniques proposed above. The data acknowledgement and retransmission may be carried out using the conventional non-NC-based schemes if certain synchronisation and scheduling conditions are not satisfied. Therefore, new efficient acknowledgement and retransmission mechanisms taking into account various synchronisation and scheduling scenarios require to be developed and investigated.

For multi-relay networks, orthogonal relaying is often assumed to guarantee that there is no correlation of the received signals at different relays. In this case, one relay transmits data independently and could not overhear the data transmitted from the other relays. For non-orthogonal relaying, the overhearing and interference of packets at the relay should be taken into consideration. The interference could cause the reduction of performance in terms of error probability but the overheard data could be helpful in increasing the data throughput for a better spectral efficiency. Thus, interesting topics could be evaluating and quantifying the trade-off between the reliability and throughput in non-orthogonal relaying scenarios.

An important question in multi-user scenario is how users are managed and share their resources. Interestingly, cognitive radio has been proposed in [152] to provide an efficient use of limited spectrum resources by allowing secondary users to exploit the licensed bands when the primary or licensed users are not in operation. The unused frequency bands are now utilized by the secondary users, and thus the spectrum utilization is significantly improved.

Two concepts, cooperative spectrum sensing and cooperative spectrum sharing, were presented as new robust sensing and sharing techniques. To cope with the issues of these two techniques, cooperative spectrum sensing was proposed in [48] based on NC to enhance the probability of detection of the primary users and improve the system throughput. DSTFBC was also designed in Chapter 6 for cooperative spectrum sharing to improve the throughput and reliability of the data transmission in CWRNs. Inspired by these research areas, well-known cooperative techniques could be further investigated for cooperative sensing and sharing, where both flat and frequency-selective fading channels could be taken into account. Additionally, the impacts of channel coding on the performance of the proposed schemes in the thesis in terms of both reliability and throughput could be interesting topics to be investigated.

References

[1] G. J. Foschini and M. J. Gans, "On limits of wireless communications in a fading environment when using multiple antennas," *Wireless Pers. Commun.*, vol. 6, pp. 311–335, Mar. 1998.

[2] E. Telatar, "Capacity of multi-antenna gaussian channels," *Eur. Trans. Telecommun*, vol. 10, no. 6, pp. 585–596, Nov. 1999.

[3] Q. Li, G. Li, W. Lee, M. il Lee, D. Mazzarese, B. Clerckx, and Z. Li, "MIMO techniques in WiMAX and LTE: A feature overview," *IEEE Commun. Mag.*, vol. 48, no. 5, pp. 86–92, May 2010.

[4] A. Sendonaris, E. Erkip, and B. Aazhang, "User cooperation diversity - Part I. System description," *IEEE Trans. Commun.*, vol. 51, no. 11, pp. 1927–1938, Nov. 2003.

[5] A. Sendonaris, E. Erkip, and B. Aazhang, "User cooperation diversity - Part II. Implementation aspects and performance analysis," *IEEE Trans. Commun.*, vol. 51, no. 11, pp. 1939–1948, Nov. 2003.

[6] J. Laneman, D. Tse, and G. Wornell, "Cooperative diversity in wireless networks: Efficient protocols and outage behavior," *IEEE Trans. Inf. Theory*, vol. 50, no. 12, pp. 3062–3080, Dec. 2004.

[7] J. Laneman and G. Wornell, "Distributed space-time-coded protocols for exploiting cooperative diversity in wireless networks," *IEEE Trans. Inf. Theory*, vol. 49, no. 10, pp. 2415–2425, Oct. 2003.

[8] K. Loa, C.-C. Wu, S.-T. Sheu, Y. Yuan, M. Chion, D. Huo, and L. Xu, "IMT-advanced relay standards [WiMAX/LTE update]," *IEEE Commun. Mag.*, vol. 48, no. 8, pp. 40–48, Aug. 2010.

[9] Y. Yang, H. Hu, J. Xu, and G. Mao, "Relay technologies for WiMax and LTE-advanced mobile systems," *IEEE Commun. Mag.*, vol. 47, no. 10, pp. 100–105, Oct. 2009.

[10] I. Garcia, K. Sakaguchi, and K. Araki, "Cell planning for cooperative transmission," in *Proc. IEEE WCNC'08*, Las Vegas, USA, Mar. 2008, pp. 1769–1774.

[11] Z. Sheng, K. Leung, and Z. Ding, "Cooperative wireless networks: From radio to network protocol designs," *IEEE Commun. Mag.*, vol. 49, no. 5, pp. 64–69, May 2011.

[12] S. Moh, "Two cooperation models and their optimal routing for cooperative diversity in wireless ad hoc networks," in *Proc. IEEE ISWCS'08*, Reykjavik, Iceland, Oct. 2008, pp. 57–61.

[13] S. Sharma, Y. Shi, Y. Hou, and S. Kompella, "An optimal algorithm for relay node assignment in cooperative ad hoc networks," *IEEE/ACM Trans. Netw.*, vol. 19, no. 3, pp. 879–892, Jun. 2011.

[14] L. Sun, T. Zhang, L. Lu, and H. Niu, "Cooperative communications with relay selection in wireless sensor networks," *IEEE Trans. Consum. Electron.*, vol. 55, no. 2, pp. 513–517, May 2009.

[15] M. Elhawary and Z. Haas, "Energy-efficient protocol for cooperative networks," *IEEE/ACM Trans. Netw.*, vol. 19, no. 2, pp. 561–574, Apr. 2011.

[16] Y. Chen, J. Teo, J. Lai, E. Gunawan, K. S. Low, C. B. Soh, and P. Rapajic, "Cooperative communications in ultra-wideband wireless body area networks: Channel modeling and system diversity analysis," *IEEE J. Sel. Areas Commun.*, vol. 27, no. 1, pp. 5–16, Jan. 2009.

[17] R. D'Errico, R. Rosini, and M. Maman, "A performance evaluation of cooperative schemes for on-body area networks based on measured time-variant channels," in *Proc. IEEE ICC 2011*, Kyoto, Japan, Jun. 2011, pp. 1–5.

[18] A. Dimakis, V. Prabhakaran, and K. Ramchandran, "Decentralized erasure codes for distributed networked storage," *IEEE Trans. Inf. Theory*, vol. 52, no. 6, pp. 2809–2816, Jun. 2006.

[19] A. Dimakis, K. Ramchandran, Y. Wu, and C. Suh, "A survey on network codes for distributed storage," *Proc. of the IEEE*, vol. 99, no. 3, pp. 476–489, Mar. 2011.

[20] R. Ahlswede, N. Cai, S.-Y. Li, and R. Yeung, "Network information flow," *IEEE Trans. Inf. Theory*, vol. 46, no. 4, pp. 1204–1216, Jul. 2000.

[21] R. Koetter and M. Medard, "An algebraic approach to network coding," *IEEE/ACM Trans. Netw.*, vol. 11, no. 5, pp. 782–795, Oct. 2003.

[22] S. Katti, D. Katabi, W. Hu, H. Rahul, and M. Medard, "The importance of being opportunistic: Practical network coding for wireless environments," in *Proc. Allerton'05*, Montecillo, Illinois, USA, Sep. 2005.

[23] S. Zhang, S. C. Liew, and P. P. Lam, "Hot topic: Physical-layer network coding," in *Proc. ACM MobiCom'06*, Los Angeles, CA, USA, Sep. 2006, pp. 358–365.

[24] S. Katti, S. Gollakota, and D. Katabi, "Embracing wireless interference: Analog network coding," in *Proc. ACM SIGCOMM'07*, Kyoto, Japan, Aug. 2007, pp. 397–408.

[25] S. Katti, H. Rahul, W. Hu, D. Katabi, M. Medard, and J. Crowcroft, "XORs in the air: Practical wireless network coding," *IEEE/ACM Trans. Netw.*, vol. 16, no. 3, pp. 497–510, Jun. 2008.

[26] J. Zhang, K. Ben Letaief, P. Fan, and K. Cai, "Network-coding-based signal recovery for efficient scheduling in wireless networks," *IEEE Trans. Veh. Technol.*, vol. 58, no. 3, pp. 1572–1582, Mar. 2009.

[27] R. Louie, Y. Li, and B. Vucetic, "Practical physical layer network coding for two-way relay channels: Performance analysis and comparison," *IEEE Trans. Wireless Commun.*, vol. 9, no. 2, pp. 764–777, Feb. 2010.

[28] M. Ju and I.-M. Kim, "Error performance analysis of BPSK modulation in physical-layer network-coded bidirectional relay networks," *IEEE Trans. Commun.*, vol. 58, no. 10, pp. 2770–2775, Oct. 2010.

[29] J. M. Park, S.-L. Kim, and J. Choi, "Hierarchically modulated network coding for asymmetric two-way relay systems," *IEEE Trans. Veh. Technol.*, vol. 59, no. 5, pp. 2179–2184, Jun. 2010.

[30] D. Nguyen, T. Tran, T. Nguyen, and B. Bose, "Wireless broadcast using network coding," *IEEE Trans. Veh. Technol.*, vol. 58, no. 2, pp. 914–925, Feb. 2009.

[31] C. Fragouli, J. Widmer, and J.-Y. Le Boudec, "Efficient broadcasting using network coding," *IEEE/ACM Trans. Netw.*, vol. 16, no. 2, pp. 450–463, Apr. 2008.

[32] Y. Chen and S. Kishore, "On the tradeoffs of implementing randomized network coding in multicast networks," *IEEE Trans. Commun.*, vol. 58, no. 7, pp. 2107–2115, Jul. 2010.

[33] P. Fan, C. Zhi, C. Wei, and K. Ben Letaief, "Reliable relay assisted wireless multicast using network coding," *IEEE J. Sel. Areas Commun.*, vol. 27, no. 5, pp. 749–762, Jun. 2009.

[34] Y. Liu, W. Chen, J. Ji, and J. Zhang, "Network-coded cooperation for multi-unicast with non-ideal source-relay channels," in *Proc. IEEE ICC 2010*, Cape Town, South Africa, May 2010, pp. 1–5.

[35] J. Liu, D. Goeckel, and D. Towsley, "Bounds on the throughput gain of network coding in unicast and multicast wireless networks," *IEEE J. Sel. Areas Commun.*, vol. 27, no. 5, pp. 582–592, Jun. 2009.

[36] Q.-T. Vien, L.-N. Tran, and H. X. Nguyen, "Network coding-based ARQ retransmission strategies for two-way wireless relay networks," in *Proc. IEEE SoftCOM 2010*, Split, Croatia, Sep. 2010, pp. 180–184.

[37] Q.-T. Vien, L.-N. Tran, and H. X. Nguyen, "Efficient ARQ retransmission schemes for two-way relay networks," *J. Commun. Software and Systems*, vol. 7, no. 1, pp. 9–15, Mar. 2011.

[38] Q.-T. Vien, B. G. Stewart, H. Tianfield, H. X. Nguyen, and J. Choi, "An efficient network coded ARQ for multisource multidestination relay networks

over mixed flat fading channels," *Elsevier AEU Int. J. Electron. Commun.*, Sep. 2012, DOI 10.1016/j.aeue.2012.08.013.

[39] Q.-T. Vien, H. Tianfield, B. G. Stewart, H. X. Nguyen, and J. Choi, "An efficient retransmission strategy for multisource multidestination relay networks over Rayleigh flat fading channels," in *Proc. IEEE WPMC 2011*, Brest, France, Oct. 2011, pp. 171–175.

[40] Q.-T. Vien, L.-N. Tran, and E.-K. Hong, "Network coding-based retransmission for relay aided multisource multicast networks," *EURASIP J. Wireless Commun. Net.*, vol. 2011, Article ID 643920, 10 pages, 2011.

[41] Q.-T. Vien and H. X. Nguyen, "Network coding-based channel quality indicator reporting for two-way multi-relay networks," *Wiley J. Wireless Commun. and Mobile Computing*, Sep. 2012, DOI 10.1002/wcm.2296.

[42] Q.-T. Vien and H. X. Nguyen, "CQI reporting strategies for nonregenerative two-way relay networks," in *Proc. IEEE WCNC 2012*, Paris, France, Apr. 2012, pp. 974–979.

[43] Q.-T. Vien, H. X. Nguyen, J. Choi, B. G. Stewart, and H. Tianfield, "Network coding-based block acknowledgement scheme for wireless regenerative relay networks," *IET Commun.*, Sep. 2012, DOI 10.1049/iet-com.2011.0681.

[44] Q.-T. Vien, H. X. Nguyen, J. Choi, B. G. Stewart, and H. Tianfield, "Network coding-based block ACK for wireless relay networks," in *Proc. IEEE VTC 2011-Spring*, Budapest, Hungary, May 2011, pp. 1–5.

[45] Q.-T. Vien, B. G. Stewart, H. Tianfield, and H. X. Nguyen, "Cooperative retransmission for wireless regenerative multi-relay networks," *IEEE Trans. Veh. Technol.*, Oct. 2012, DOI 10.1109/TVT.2012.2224393.

[46] Q.-T. Vien, B. G. Stewart, H. Tianfield, and H. X. Nguyen, "An efficient cooperative retransmission for wireless regenerative relay networks," in *Proc. IEEE GLOBECOM 2012*, Anaheim, California, USA, Dec. 2012, pp. 4622–4627.

[47] Q.-T. Vien, B. G. Stewart, H. Tianfield, and H. X. Nguyen, "Efficient cooperative spectrum sensing for three-hop cognitive wireless relay networks," to appear in *IET Communications*, Nov. 2012.

[48] Q.-T. Vien, H. Tianfield, and B. G. Stewart, "Efficient cooperative spectrum sensing for cognitive wireless relay networks over Rayleigh flat fading channels," in *Proc. IEEE VTC 2012-Spring*, Yokohama, Japan, May 2012, pp. 1–5.

[49] L. Zheng and D. N. C. Tse, "Diversity and multiplexing: A fundamental tradeoff in multiple antenna channels," *IEEE Trans. Inf. Theory*, vol. 49, no. 5, pp. 1073–1096, May 2003.

[50] C.-E. Sundberg and N. Seshadri, "Digital cellular systems for North America," in *Proc. IEEE GLOBECOM'90*, San Diego, CA, USA, Dec. 1990, pp. 533–537.

[51] P. Balaban and J. Salz, "Dual diversity combining and equalization in digital cellular mobile radio," *IEEE Trans. Veh. Technol.*, vol. 40, no. 2, pp. 342–354, May 1991.

[52] J. Winters, J. Salz, and R. Gitlin, "The impact of antenna diversity on the capacity of wireless communication systems," *IEEE Trans. Commun.*, vol. 42, no. 234, pp. 1740–1751, Feb./Mar./Apr. 1994.

[53] V. Tarokh, N. Seshadri, and A. Calderbank, "Space-time codes for high data rate wireless communication: performance criterion and code construction," *IEEE Trans. Inf. Theory*, vol. 44, no. 2, pp. 744–765, Mar. 1998.

[54] J.-C. Guey, M. Fitz, M. Bell, and W.-Y. Kuo, "Signal design for transmitter diversity wireless communication systems over Rayleigh fading channels," *IEEE Trans. Commun.*, vol. 47, no. 4, pp. 527–537, Apr. 1999.

[55] N. Seshadri, V. Tarokh, and A. Calderbank, "Space-time codes for wireless communication: Code construction," in *Proc. IEEE VTC'97*, vol. 2, Phoenix, AZ, USA, May 1997, pp. 637–641.

[56] Z. Safar and K. Liu, "Systematic space-time trellis code construction for correlated Rayleigh fading channels," *IEEE Trans. Inf. Theory*, vol. 50, no. 11, pp. 2855–2865, Nov. 2004.

[57] S. Alamouti, "A simple transmit diversity technique for wireless communications," *IEEE J. Sel. Areas Commun.*, vol. 16, no. 8, pp. 1451–1458, Oct. 1998.

[58] V. Tarokh, H. Jafarkhani, and A. Calderbank, "Space-time block codes from orthogonal designs," *IEEE Trans. Inf. Theory*, vol. 45, no. 5, pp. 1456–1467, Jul. 1999.

[59] G. Ganesan and P. Stoica, "Space-time block codes: a maximum SNR approach," *Information Theory, IEEE Transactions on*, vol. 47, no. 4, pp. 1650–1656, May 2001.

[60] O. Tirkkonen and A. Hottinen, "Square-matrix embeddable space-time block codes for complex signal constellations," *IEEE Trans. Inf. Theory*, vol. 48, no. 2, pp. 384–395, Feb. 2002.

[61] O. Tirkkonen, A. Boariu, and A. Hottinen, "Minimal non-orthogonality rate 1 space-time block code for 3+ Tx antennas," in *Proc. IEEE ISSSTA'00*, vol. 2, Parsippany, NJ, USA, Sep. 2000, pp. 429–432.

[62] H. Jafarkhani, "A quasi-orthogonal space-time block code," *IEEE Trans. Commun.*, vol. 49, no. 1, pp. 1–4, Jan. 2001.

[63] W. Su and X.-G. Xia, "Signal constellations for quasi-orthogonal space-time block codes with full diversity," *IEEE Trans. Inf. Theory*, vol. 50, no. 10, pp. 2331–2347, Oct. 2004.

[64] B. Hochwald and W. Sweldens, "Differential unitary space-time modulation," *IEEE Trans. Commun.*, vol. 48, no. 12, pp. 2041–2052, Dec. 2000.

[65] B. Hughes, "Differential space-time modulation," *IEEE Trans. Inf. Theory*, vol. 46, no. 7, pp. 2567–2578, Nov. 2000.

[66] B. Hochwald and T. Marzetta, "Unitary space-time modulation for multiple-antenna communications in Rayleigh flat fading," *IEEE Trans. Inf. Theory*, vol. 46, no. 2, pp. 543–564, Mar. 2000.

[67] B. Hochwald, T. Marzetta, T. Richardson, W. Sweldens, and R. Urbanke, "Systematic design of unitary space-time constellations," *IEEE Trans. Inf. Theory*, vol. 46, no. 6, pp. 1962–1973, Sep. 2000.

[68] M. Damen, K. Abed-Meraim, and J.-C. Belfiore, "Diagonal algebraic space-time block codes," *IEEE Trans. Inf. Theory*, vol. 48, no. 3, pp. 628–636, Mar. 2002.

[69] P. Fan, "Design of diagonal algebraic space time codes with 8-star-PSK signals," in *Proc. IEEE PIMRC'03*, vol. 2, Beijing, China, Sep. 2003, pp. 1036–1040.

[70] V. Tarokh, A. Naguib, N. Seshadri, and A. Calderbank, "Combined array processing and space-time coding," *IEEE Trans. Inf. Theory*, vol. 45, no. 4, pp. 1121–1128, May 1999.

[71] J. Du and Y. Li, "Parallel detection of groupwise space-time codes by predictive soft interference cancellation," *IEEE Trans. Commun.*, vol. 54, no. 12, pp. 2150–2154, Dec. 2006.

[72] H. Nguyen, J. Choi, and T. Le-Ngoc, "High-rate groupwise STBC using low-complexity SIC based receiver," *IEEE Trans. Wireless Commun.*, vol. 8, no. 9, pp. 4677–4687, Sep. 2009.

[73] E. Lindskog and A. Paulraj, "A transmit diversity scheme for channels with intersymbol interference," in *IEEE ICC'00*, vol. 1, New Orleans, LA, USA, Jun. 2000, pp. 307–311.

[74] N. Al-Dhahir, "Single-carrier frequency-domain equalization for space-time block-coded transmissions over frequency-selective fading channels," *IEEE Commun. Lett.*, vol. 5, no. 7, pp. 304–306, Jul. 2001.

[75] S. Zhou and G. Giannakis, "Space-time coding with maximum diversity gains over frequency-selective fading channels," *IEEE Signal Process. Lett.*, vol. 8, no. 10, pp. 269–272, Oct. 2001.

[76] D. Agrawal, V. Tarokh, A. Naguib, and N. Seshadri, "Space-time coded OFDM for high data-rate wireless communication over wideband channels," in *Proc. IEEE VTC'98*, vol. 3, Ottawa, Canada, May 1998, pp. 2232–2236.

[77] B. Lu and X. Wang, "Space-time code design in OFDM systems," in *Proc. IEEE GLOBECOM'00*, vol. 2, San Francisco, USA, Nov. 2000, pp. 1000–1004.

[78] R. Blum, Y. G. Li, J. Winters, and Q. Yan, "Improved space-time coding for MIMO-OFDM wireless communications," *IEEE Trans. Commun.*, vol. 49, no. 11, pp. 1873–1878, Nov. 2001.

[79] Y. Gong and K. Letaief, "An efficient space-frequency coded wideband OFDM system for wireless communications," in *Proc. IEEE ICC'02*, vol. 1, New York, USA, Apr. 2002, pp. 475–479.

[80] W. Su, Z. Safar, M. Olfat, and K. Liu, "Obtaining full-diversity space-frequency codes from space-time codes via mapping," *IEEE Trans. Signal Process.*, vol. 51, no. 11, pp. 2905–2916, Nov. 2003.

[81] W. Su, Z. Safar, and K. Liu, "Full-rate full-diversity space-frequency codes with optimum coding advantage," *IEEE Trans. Inf. Theory*, vol. 51, no. 1, pp. 229–249, Jan. 2005.

[82] Y. Gong and K. Letaief, "Space-frequency-time coded OFDM for broadband wireless communications," in *Proc. IEEE GLOBECOM'01*, vol. 1, San Antonio, Texas, USA, Nov. 2001, pp. 519–523.

[83] Z. Liu, Y. Xin, and G. Giannakis, "Space-time-frequency coded OFDM over frequency-selective fading channels," *IEEE Trans. Signal Process.*, vol. 50, no. 10, pp. 2465–2476, Oct. 2002.

[84] B. Lu, X. Wang, and K. Narayanan, "LDPC-based space-time coded OFDM systems over correlated fading channels: Performance analysis and receiver design," *IEEE Trans. Commun.*, vol. 50, no. 1, pp. 74–88, Jan. 2002.

[85] A. Molisch, M. Win, and J. Winters, "Space-time-frequency (STF) coding for MIMO-OFDM systems," *IEEE Commun. Lett.*, vol. 6, no. 9, pp. 370–372, Sep. 2002.

[86] E. C. van der Meulen, "Three-terminal communication channels," *Adv. Appl. Probab.*, vol. 3, pp. 120–154, 1971.

[87] T. Cover and A. Gamal, "Capacity theorems for the relay channel," *IEEE Trans. Inf. Theory*, vol. 25, no. 5, pp. 572–584, Sep. 1979.

[88] G. Kramer, M. Gastpar, and P. Gupta, "Cooperative strategies and capacity theorems for relay networks," *IEEE Trans. Inf. Theory*, vol. 51, no. 9, pp. 3037–3063, Sep. 2005.

[89] T. Hunter and A. Nosratinia, "Cooperation diversity through coding," in *Proc. IEEE ISIT'02*, Lausanne, Switzerland, Jun. 2002, p. 220.

[90] T. Hunter and A. Nosratinia, "Diversity through coded cooperation," *IEEE Trans. Wireless Commun.*, vol. 5, no. 2, pp. 283–289, Feb. 2006.

[91] R. Nabar and H. Bolcskei, "Space-time signal design for fading relay channels," in *Proc. IEEE GLOBECOM'03*, vol. 4, San Francisco, USA, Dec. 2003, pp. 1952–1956.

[92] R. Nabar, H. Bolcskei, and F. Kneubuhler, "Fading relay channels: Performance limits and space-time signal design," *IEEE J. Sel. Areas Commun.*, vol. 22, no. 6, pp. 1099–1109, Aug. 2004.

[93] S. Yiu, R. Schober, and L. Lampe, "Distributed space-time block coding," *IEEE Trans. Commun.*, vol. 54, no. 7, pp. 1195–1206, Jul. 2006.

[94] B. Hassibi and B. Hochwald, "High-rate codes that are linear in space and time," *IEEE Trans. Inf. Theory*, vol. 48, no. 7, pp. 1804–1824, Jul. 2002.

[95] Y. Jing and B. Hassibi, "Distributed space-time coding in wireless relay networks," *IEEE Trans. Wireless Commun.*, vol. 5, no. 12, pp. 3524–3536, Dec. 2006.

[96] Y. Jing and H. Jafarkhani, "Using orthogonal and quasi-orthogonal designs in wireless relay networks," *IEEE Trans. Inf. Theory*, vol. 53, no. 11, pp. 4106–4118, Nov. 2007.

[97] Z. Yi and I.-M. Kim, "Single-symbol ML decodable distributed STBCs for cooperative networks," *IEEE Trans. Inf. Theory*, vol. 53, no. 8, pp. 2977–2985, Aug. 2007.

[98] G. Scutari and S. Barbarossa, "Distributed space-time coding for regenerative relay networks," *IEEE Trans. Wireless Commun.*, vol. 4, no. 5, pp. 2387–2399, Sep. 2005.

[99] P. Anghel and M. Kaveh, "Relay assisted uplink communication over frequency-selective channels," in *Proc. IEEE Workshop SPAWC'03*, Rome, Italy, Jun. 2003, pp. 125–129.

[100] H. Mheidat, M. Uysal, and N. Al-Dhahir, "Equalization techniques for distributed space-time block codes with amplify-and-forward relaying," *IEEE Trans. Signal Process.*, vol. 55, no. 5, pp. 1839–1852, May 2007.

[101] B. Rankov and A. Wittneben, "Spectral efficient protocols for half-duplex fading relay channels," *IEEE J. Sel. Areas Commun.*, vol. 25, no. 2, pp. 379–389, Feb. 2007.

[102] P. Popovski and H. Yomo, "Physical network coding in two-way wireless relay channels," in *Proc. IEEE ICC'07*, Glasgow, Scotland, Jun. 2007, pp. 707–712.

[103] B. Nazer and M. Gastpar, "Computation over multiple-access channels," *IEEE Trans. Inf. Theory*, vol. 53, no. 10, pp. 3498–3516, Oct. 2007.

[104] S. Zhang and S.-C. Liew, "Channel coding and decoding in a relay system operated with physical-layer network coding," *IEEE J. Sel. Areas Commun.*, vol. 27, no. 5, pp. 788–796, Jun. 2009.

[105] R. Zhang, Y.-C. Liang, C. C. Chai, and S. Cui, "Optimal beamforming for two-way multi-antenna relay channel with analogue network coding," *IEEE J. Sel. Areas Commun.*, vol. 27, no. 5, pp. 699–712, Jun. 2009.

[106] L. Song, G. Hong, B. Jiao, and M. Debbah, "Joint relay selection and analog network coding using differential modulation in two-way relay channels," *IEEE Trans. Veh. Technol.*, vol. 59, no. 6, pp. 2932–2939, Jul. 2010.

[107] S. Yao and M. Skoglund, "Analog network coding mappings in Gaussian multiple-access relay channels," *IEEE Trans. Commun.*, vol. 58, no. 7, pp. 1973–1983, Jul. 2010.

[108] A. Argyriou and A. Pandharipande, "Cooperative protocol for analog network coding in distributed wireless networks," *IEEE Trans. Wireless Commun.*, vol. 9, no. 10, pp. 3112–3119, Oct. 2010.

[109] H.-M. Wang, X.-G. Xia, and Q. Yin, "A linear analog network coding for asynchronous two-way relay networks," *IEEE Trans. Wireless Commun.*, vol. 9, no. 12, pp. 3630–3637, Dec. 2010.

[110] D. To and J. Choi, "Convolutional codes in two-way relay networks with physical-layer network coding," *IEEE Trans. Wireless Commun.*, vol. 9, no. 9, pp. 2724–2729, Sep. 2010.

[111] S. Verdu, *Multiuser Detection.* UK: Cambridge University Press, 1998.

[112] C. Shannnon, "Two-way communication channels," in *Proc. 4th Berkeley Symp. Math. Statist. Probab.*, vol. 1, 1961, pp. 611–644.

[113] S. S. L. Chang, "Theory of information feedback systems," *IEEE Trans. Inf. Theory*, vol. 2, no. 3, pp. 29–40, Sep. 1956.

[114] J. Kumar Sundararajan, D. Shah, and M. Medard, "ARQ for network coding," in *Proc. IEEE ISIT'08*, Toronto, Canada, Jul. 2008, pp. 1651–1655.

[115] Y. Liu and A. Petropulu, "Cooperative beamforming in multi-source multi-destination relay systems with SINR constraints," in *Proc. IEEE ICASSP 2010*, Dallas, Texas, USA, Mar. 2010, pp. 2870–2873.

[116] W.-J. Huang, Y.-W. Hong, and C.-C. Kuo, "Relay-assisted decorrelating multiuser detector (RAD-MUD) for cooperative CDMA networks," *IEEE J. Sel. Areas Commun.*, vol. 26, no. 3, pp. 550–560, Apr. 2008.

[117] R. Lupas and S. Verdu, "Linear multiuser detectors for synchronous code-division multiple-access channels," *IEEE Trans. Inf. Theory*, vol. 35, no. 1, pp. 123–136, Jan. 1989.

[118] A. Duel-Hallen, "Decorrelating decision-feedback multiuser detector for synchronous code-division multiple-access channel," *IEEE Trans. Commun.*, vol. 41, no. 2, pp. 285–290, Feb. 1993.

[119] P. Patel and J. Holtzman, "Analysis of a simple successive interference cancellation scheme in a DS/CDMA system," *IEEE J. Sel. Areas Commun.*, vol. 12, no. 5, pp. 796–807, Jun. 1994.

[120] M. K. Simon and M.-S. Alouini, *Digital Communication over Fading Channels*, 2nd ed. John Wiley & Sons, 2005.

[121] B. Jiang, F. Gao, X. Gao, and A. Nallanathan, "Channel estimation and training design for two-way relay networks with power allocation," *IEEE Trans. Wireless Commun.*, vol. 9, no. 6, pp. 2022–2032, Jun. 2010.

[122] H. Gacanin, T. Sjödin, and F. Adachi, "On channel estimation for analog network coding in a frequency-selective fading channel," *EURASIP J. Wireless Commun. Net.*, vol. 2011, Article ID 980430, 12 pages, 2011.

[123] I. Prodan, T. Obara, F. Adachi, and H. Gacanin, "Pilot-assisted channel estimation without feedback for bi-directional broadband ANC," in *Communications (APCC), 2011 17th Asia-Pacific Conference on*, Sabah, Malaysia, Oct. 2011, pp. 157–162.

[124] *IEEE Standard for Local and Metropolitan Area Networks - Part 16: Air Interface for Broadband Wireless Access Systems*, IEEE Std. 802.16Ź-2009, May 2009.

[125] R. Schoenen, D. Bultmann, and Z. Xu, "Channel quality indication for adaptive resource scheduling in multihop OFDMA systems," in *Proc. EW'09*, Aalborg, Denmark, May 2009, pp. 58–62.

[126] Z. Yong, L. Jun, X. Youyun, and C. Yueming, "An adaptive non-orthogonal cooperation scheme based on channel quality information," in *Proc. WiCom'07*, Shanghai, China, Sep. 2007, pp. 988–991.

[127] J.-B. Kim and D. Kim, "Comparison of two SNR-based feedback schemes in multiuser dual-hop amplify-and-forward relaying networks," *IEEE Commun. Lett.*, vol. 12, no. 8, pp. 557–559, Aug. 2008.

[128] H. Yomo and E. de Carvalho, "A CSI estimation method for wireless relay network," *IEEE Commun. Lett.*, vol. 11, no. 6, pp. 480–482, Jun. 2007.

[129] W. Xu, X. Dong, and Y. Huang, "Asymptotic achievable rate analysis for selection strategies in amplify-and-forward MIMO two-hop networks with feedback," *IEEE Trans. Veh. Technol.*, vol. 59, no. 7, pp. 3662–3668, Sep. 2010.

[130] H. Wu, Y. Wang, G. Wei, and D. Yang, "A relay selection scheme for the downlink of cellular networks," in *Proc. IEEE WiCom'09*, Beijing, China, Sep. 2009, pp. 1–4.

[131] F. Brouwer, I. de Bruin, J. Silva, N. Souto, F. Cercas, and A. Correia, "Usage of link-level performance indicators for HSDPA network-level simulations in E-UMTS," in *Proc. IEEE ISSSTA'04*, Sydney, Australia, Aug. 2004, pp. 844–848.

[132] K. Freudenthaler, A. Springer, and J. Wehinger, "Novel SINR-to-CQI mapping maximizing the throughput in HSDPA," in *Proc. IEEE WCNC'07*, Hong Kong, China, Mar. 2007, pp. 2231–2235.

[133] F. Tsuzuki and T. Ohtsuki, "Channel estimation with selective superimposed pilot sequences under fast fading environments," in *Proc. IEEE VTC 2004-Fall*, vol. 1, Los Angeles, CA, USA, Sep. 2004, pp. 62–66.

[134] I. S. Gradshteyn and I. M. Ryzhik, *Table of Integrals, Series, and Products*, 7th ed. Academic Press, 2007.

[135] H. A. David and H. N. Nagaraja, *Order Statistics*, 3rd ed. Wiley, 2003.

[136] Y. Kim, S. Choi, K. Jang, and H. Hwang, "Throughput enhancement of IEEE 802.11 WLAN via frame aggregation," in *Proc. IEEE VTC'04-Fall*, vol. 4, Los Angeles, CA, USA, Sep. 2004, pp. 3030–3034.

[137] I. Tinnirello and S. Choi, "Efficiency analysis of burst transmissions with block ACK in contention-based 802.11e WLANs," in *Proc. IEEE ICC'05*, vol. 5, Seoul, Korea, May 2005, pp. 3455–3460.

[138] Y. Chen, S. Emeott, and R. Choudhury, "An analytical model of block acknowledgement and selective retransmission in an 802.11e WLAN network," in *Proc. IEEE GLOBECOM'06*, San Francisco, California, USA, Nov. 2006, pp. 1–5.

[139] O. Cabral, A. Segarra, and F. Velez, "Implementation of IEEE 802.11e block acknowledgement policies based on the buffer size," in *Proc. EW'08*, Prague, Czech Republic, Jun. 2008, pp. 1–7.

[140] O. Cabral, A. Segarra, F. Velez, A. Mihovska, and N. Prasad, "Optimization of multi-service IEEE802.11e block acknowledgement," in *Proc. IEEE RWS'09*, San Diego, CA, USA, Jan. 2009, pp. 380–383.

[141] Y. Xiao, "Packing mechanisms for the IEEE 802.11n wireless LANs," in *Proc. IEEE GLOBECOM'04*, vol. 5, Dallas, Texas, USA, Nov. 2004, pp. 3275–3279.

[142] T. Nakajima, Y. Utsunomiya, Y. Nishibayashi, T. Tandai, T. Adachi, and M. Takagi, "Compressed Block Ack, an efficient selective repeat mechanism for IEEE802.11n," in *Proc. IEEE PIMRC'05*, vol. 3, Berlin, Germany, Sep. 2005, pp. 1479–1483.

[143] T. Nakajima, T. Nabetani, Y. Utsunomiya, T. Adachi, and M. Takagi, "A simple and efficient selective repeat scheme for high throughput WLAN, IEEE802.11n," in *Proc. IEEE VTC'07-Spring*, Dublin, Ireland, Apr. 2007, pp. 1302–1306.

[144] *IEEE Standard for Local and Metropolitan Area Networks - Part 11: Wireless LAN Medium Access Control (MAC) and Physical Layer (PHY) Specifications - Amendment 5: Enhancements for Higer Throughput*, IEEE Std. 802.11nŹ-2009, Oct. 2009.

[145] Y. Liu, "A low complexity protocol for relay channels employing rateless codes and acknowledgement," in *Proc. IEEE ISIT'06*, Seattle, Washington, USA, Jul. 2006, pp. 1244–1248.

[146] K. Nagao, Y. Kadowaki, and Y. Yamao, "Multi-hop transmission performance of cognitive temporary bypassing for wireless ad hoc networks," in *Proc. IEEE CCNC'09*, Las Vegas, Nevada, USA, Jan. 2009, pp. 1–5.

[147] K. Lu, S. Fu, and Y. Qian, "Increasing the throughput of wireless LANs via cooperative retransmission," in *Proc. IEEE GLOBECOM'07*, Washington, DC, USA, Nov. 2007, pp. 5231–5235.

[148] S. S. Ikki and M. H. Ahmed, "On the performance of cooperative-diversity networks with the Nth best-relay selection scheme," *IEEE Trans. Commun.*, vol. 58, no. 11, pp. 3062–3069, Nov. 2010.

[149] V. Shah, N. Mehta, and R. Yim, "The relay selection and transmission trade-off in cooperative communication systems," *IEEE Trans. Wireless Commun.*, vol. 9, no. 8, pp. 2505–2515, Aug. 2010.

[150] B.-G. Choi, S. J. Bae, K. yul Cheon, A.-S. Park, and M. Y. Chung, "Relay selection and resource allocation schemes for effective utilization of relay zones in relay-based cellular networks," *IEEE Commun. Lett.*, vol. 15, no. 4, pp. 407–409, Apr. 2011.

[151] L. Fan, X. Lei, and W. Li, "Exact closed-form expression for ergodic capacity of amplify-and-forward relaying in channel-noise-assisted cooperative networks with relay selection," *IEEE Commun. Lett.*, vol. 15, no. 3, pp. 332–333, Mar. 2011.

[152] I. Mitola, J. and J. Maguire, G.Q., "Cognitive radio: Making software radios more personal," *IEEE Pers. Commun.*, vol. 6, no. 4, pp. 13–18, Aug. 1999.

[153] S. Haykin, "Cognitive radio: Brain-empowered wireless communications," *IEEE J. Sel. Areas Commun.*, vol. 23, no. 2, pp. 201–220, Feb. 2005.

[154] J. Wang, M. Ghosh, and K. Challapali, "Emerging cognitive radio applications: A survey," *IEEE Commun. Mag.*, vol. 49, no. 3, pp. 74–81, Mar. 2011.

[155] T. Yucek and H. Arslan, "A survey of spectrum sensing algorithms for cognitive radio applications," *IEEE Commun. Surveys and Tutorials*, vol. 11, no. 1, pp. 116–130, first quarter 2009.

[156] D. Cabric, S. Mishra, and R. Brodersen, "Implementation issues in spectrum sensing for cognitive radios," in *Proc. ACSSC'04*, vol. 1, Pacific Grove, CA, USA, Nov. 2004, pp. 772–776.

[157] Z. Tian and G. B. Giannakis, "A wavelet approach to wideband spectrum sensing for cognitive radios," in *Proc. CROWNCOM'06*, Mykonos Island, Greece, Jun. 2006, pp. 1–5.

[158] Y. Zeng and Y.-C. Liang, "Covariance based signal detections for cognitive radio," in *Proc. IEEE DySPAN'07*, Dublin, Ireland, Apr. 2007, pp. 202–207.

[159] W. Zhang and K. Letaief, "Cooperative spectrum sensing with transmit and relay diversity in cognitive radio networks," *IEEE Trans. Wireless Commun.*, vol. 7, no. 12, pp. 4761–4766, Dec. 2008.

[160] G. Ganesan and Y. Li, "Cooperative spectrum sensing in cognitive radio, part I: Two user networks," *IEEE Trans. Wireless Commun.*, vol. 6, no. 6, pp. 2204–2213, Jun. 2007.

[161] S. Mishra, A. Sahai, and R. Brodersen, "Cooperative sensing among cognitive radios," in *Proc. IEEE ICC'06*, vol. 4, Istanbul, Turkey, Jun. 2006, pp. 1658–1663.

[162] K. Ben Letaief and W. Zhang, "Cooperative communications for cognitive radio networks," *Proc. of the IEEE*, vol. 97, no. 5, pp. 878–893, May 2009.

[163] F. F. Digham, M.-S. Alouini, and M. K. Simon, "On the energy detection of unknown signals over fading channels," *IEEE Trans. Commun.*, vol. 55, no. 1, pp. 21–24, Jan. 2007.

[164] A. Ghasemi and E. S. Sousa, "Opportunistic spectrum access in fading channels through collaborative sensing," *J. Commun.*, vol. 2, no. 2, pp. 71–82, Mar. 2007.

[165] P. Anghel, G. Leus, and M. Kavehl, "Multi-user space-time coding in cooperative networks," in *Proc. IEEE ICASSP '03*, vol. 4, Hong Kong, April 2003, pp. IV–73–76.

[166] J. Harshan and B. Rajan, "High-rate, single-symbol ML decodable precoded DSTBCs for cooperative networks," *IEEE Trans. Inf. Theory*, vol. 55, no. 5, pp. 2004–2015, May 2009.

[167] G. Rajan and B. Rajan, "Multigroup ML decodable collocated and distributed space-time block codes," *IEEE Trans. Inf. Theory*, vol. 56, no. 7, pp. 3221–3247, Jul. 2010.

[168] O. Simeone, Y. Bar-Ness, and U. Spagnolini, "Stable throughput of cognitive radios with and without relaying capability," *IEEE Trans. Commun.*, vol. 55, no. 12, pp. 2351–2360, Dec. 2007.

[169] Y. Han, A. Pandharipande, and S. Ting, "Cooperative decode-and-forward relaying for secondary spectrum access," *IEEE Trans. Wireless Commun.*, vol. 8, no. 10, pp. 4945–4950, Oct. 2009.

[170] Y. Zou, J. Zhu, B. Zheng, and Y.-D. Yao, "An adaptive cooperation diversity scheme with best-relay selection in cognitive radio networks," *IEEE Trans. Signal Process.*, vol. 58, no. 10, pp. 5438–5445, Oct. 2010.

[171] M. Sarkar, T. Ratnarajah, and M. Sellathurai, "On the mutual information of cognitive relay assisted Rayleigh fading MIMO channel," in *Proc. UKIWCWS 2009*, India, Dec. 2009, pp. 1–5.

[172] M. Sarkar, T. Ratnarajah, and M. Sellathurai, "On the outage behavior of cognitive relay assisted MIMO multiple access channel," in *Proc. IEEE PIMRC'09*, Tokyo, Japan, Sep. 2009, pp. 1–6.

[173] M. Sarkar, T. Ratnarajah, and M. Sellathurai, "Outage performance of MIMO multiple access interference channel with cognitive relay," in *Proc. IEEE ICC 2010*, Cape Town, South Africa, May 2010, pp. 1–5.

[174] C. Masouros and T. Ratnarajah, "Utilization of primary-secondary cross-interference via adaptive precoding in cognitive relay assisted MIMO wireless systems," in *Proc. IEEE ICC 2011*, Kyoto, Japan, Jun. 2011, pp. 1–5.

[175] A. Stuart and J. K. Ord, *Kendall's advanced theory of statistics*, 5th ed. C. Griffin, London, U.K., 1987.

[176] J. G. Proakis, *Digital Communications*, 4th ed. McGraw Hill, 2001.

[177] B. Ng and D. Falconer, "A novel frequency domain equalization method for single-carrier wireless transmissions over doubly-selective fading channels," in *IEEE GLOBECOM '04*, vol. 1, Dallas, TX, USA, Nov.-3 Dec. 2004, pp. 237–241.

[178] P. Schniter and H. Liu, "Iterative frequency-domain equalization for single-carrier systems in doubly-dispersive channels," in *Proc. the 38th Asilomar Conference on Signals, Systems, and Computers*, vol. 1, Pacific Grove, Calif, USA, Nov. 2004, pp. 667–671.

[179] N. Benvenuto and S. Tomasin, "Block iterative DFE for single carrier modulation," *IEE Electro. Lett.*, vol. 39, no. 19, pp. 1144–1145, Sep. 2002.

[180] Y. Zhu and K. Letaief, "Single-carrier frequency-domain equalization with decision-feedback processing for time-reversal space-time block-coded systems," *IEEE Trans. Commun.*, vol. 53, no. 7, pp. 1127–1131, Jul. 2005.